Identification of Chemical Mediators that Regulate the Specialized Metabolism in *Nostoc punctiforme*

Abstract

Specialized metabolites, so-called natural products, are produced by a variety of different organisms, including bacteria and fungi. Due to their wide range of different biological activities, including pharmaceutical relevant properties, microbial natural products are an important source for drug development. They are encoded by biosynthetic gene clusters (BGCs), which are a group of locally clustered genes. By screening genomic data for genes encoding typical core biosynthetic enzymes, modern bioinformatical approaches are able to predict a wide range of BGCs. To date, only a small fraction of the predicted BGCs have their associated products identified.

The phylum of the cyanobacteria has been shown to be a prolific, but largely untapped source for natural products. Especially multicellular cyanobacterial genera, like *Nostoc*, harbor a high amount of BGCs in their genomes.
A main goal of this study was to develop new concepts for the discovery of natural products in cyanobacteria. Due to its diverse setup of orphan BGCs and its amenability to genetic manipulation, *Nostoc punctiforme* PCC 73102 (*N. punctiforme*) appeared to be a promising candidate to be established as a model organism for natural product discovery in cyanobacteria. By utilizing a combination of genome-mining, bioactivity-screening, variations of culture conditions, as well as metabolic engineering, not only two new polyketides were discovered, but also first-time insights into the regulation of the specialized metabolism in *N. punctiforme* were gained during this study.

The cultivation of *N. punctiforme* to very high densities by utilizing increasing light intensities and CO_2 levels, led to an enhanced metabolite production, causing rather complex metabolite extracts. By utilizing a library of CFP reporter mutant strains, each strain reporting for one of the predicted BGCs, it was shown that eight out of 15 BGCs were upregulated under high density (HD) cultivation conditions. Furthermore, it could be demonstrated that the supernatant of an HD culture can increase the expression of four of the influenced BGCs, even under conventional cultivation conditions. This led to the hypothesis that a chemical mediator encoded by one of the affected BGCs is accumulating in the HD supernatant and is able to increase the expression of other BGCs as part of a cell-density dependent regulatory circuit. To identify which of the BGCs could be a main trigger of the presumed regulatory circuit, it was tried to activate four BGCs (*pks1*, *pks2*, *ripp3*, *ripp4*) selectively by overexpression of putative pathway-specific regulatory

genes that were found inside the gene clusters. Transcriptional analysis of the mutants revealed that only the mutant strain targeting the *pks1* BGC, called AraC_PKS1, was able to upregulate the expression of its associated BGC. From an RNA sequencing study of the AraC_PKS1 mutant strain, it was discovered that beside *pks1*, the orphan BGCs *ripp3* and *ripp4* were also upregulated in the mutant strain. Furthermore, it was observed that secondary metabolite production in the AraC_PKS1 mutant strain is further enhanced under high-light and high-CO_2 cultivation conditions. The increased production of the *pks1* regulator NvlA also had an impact on other regulatory factors, including sigma factors and the RNA chaperone Hfq. Analysis of the AraC_PKS1 cell and supernatant extracts led to the discovery of two novel polyketides, nostoclide and nostovalerolactone, both encoded by the *pks1* BGC. Addition of the polyketides to *N. punctiforme* WT demonstrated that the *pks1*-derived compounds are able to partly reproduce the effects on secondary metabolite production found in the AraC_PKS1 mutant strain. This indicates that both compounds are acting as extracellular signaling factors as part of a regulatory network. Since not all transcriptional effects that were found in the AraC_PKS1 mutant strain could be reproduced by the *pks1* products, it can be assumed that the regulator NvlA has a global effect and is not exclusively specific to the *pks1* pathway.

This study was the first to use a putative pathway specific regulator for the specific activation of BGC expression in cyanobacteria. This strategy did not only lead to the detection of two novel polyketides, it also gave first-time insights into the regulatory mechanism of the specialized metabolism in *N. punctiforme*. This study illustrates that understanding regulatory pathways can aid in the discovery of novel natural products. The findings of this study can guide the design of new screening strategies for bioactive compounds in cyanobacteria and help to develop high-titer production platforms for cyanobacterial natural products.

Zusammenfassung

Sekundärmetabolite, auch Naturstoffe genannt, werden von einer Vielzahl an Organismen, darunter Bakterien und Pilzen, hergestellt. Aufgrund ihrer Vielzahl an verschiedenen Bioaktivitäten, einschließlich pharmakologisch relevanter Wirkungen, sind mikrobielle Naturstoffe eine wichtige Grundlage für die Arzneimittelentwicklung. Naturstoffe werden durch eine Ansammlung lokal gruppierter Gene, sogenannten Biosynthese-Genclustern (BGC), im Genom kodiert. Moderne bioinformatische Methoden durchsuchen Genom-Daten nach Genen, die typische biosynthetische Enzyme kodieren. Auf Grundlage dessen können verschiedenste BGCs vorhergesagt werden. Bislang konnte allerdings nur für einen kleinen Teil der vorhergesagten BGCs das dazugehörige Produkt identifiziert und charakterisiert werden.

Cyanobakterien sind nachweislich eine reichhaltige, aber weitestgehend unerschlossene Quelle für Naturstoffe. Insbesondere mehrzellige Gattungen, wie *Nostoc*, tragen eine Vielzahl an BGCs in ihren Genomen.
Ein Hauptziel dieser Studie war es, neue Konzepte für die Entdeckungen von Naturstoffen in Cyanobakterien zu entwickeln. *Nostoc punctiforme* PCC 73102 (*N. punctiforme*) erwies sich als besonders geeigneter Stamm für diese Aufgabe, da er eine Vielzahl weitestgehend ununtersuchter Gencluster besitzt und zugänglich für genetische Modifikationen ist. Eine Kombination aus Genome Mining, Bioaktivitäts-Screening, verschiedenen Kultivierungsbedingungen und Metabolic Engineering führte zur Entdeckung zweier neuer Polyketide und gewährte im Verlauf der Studie erstmals Einblicke in den spezialisierten Metabolismus von *N. punctiforme*.

Die Kultivierung von *N. punctiforme* in sehr hohen Zelldichten, ermöglicht durch sehr hohe Lichtintensitäten und erhöhte CO_2-Verfügbarkeit, führte zu einer verstärkten Metabolitproduktion und komplexen Metabolitextrakten. Unter Verwendung einer Bibliothek von CFP-Reportermutanten, bei der jede Mutante eines der vorhergesagten BGCs repräsentiert, konnte gezeigt werden, dass 8 von 15 BGCs unter Hochzelldichte-Kultivierungsbedingungen hochreguliert wurden. Zudem zeigte sich, dass der Überstand einer dichten Kultur, auch unter konventionellen Kultivierungsbedingungen, vier der regulierten BGCs beeinflussen kann. Dies lässt vermuten, dass sich unter Hochzelldichte-Kultivierungsbedingungen ein chemischer Mediator, welcher von einem der beeinflussten BGCs produziert wird, im Überstand anhäuft und die Expression anderer BGCs als Teil eines zelldichte-abhängigen

Regelkreises kontrollieren kann. Um herauszufinden, welches der BGCs ein Hauptauslöser des vermuteten Regelkreises sein könnte, wurde versucht die Expression von vier BGCs (*pks1*, *pks2*, *ripp3*, *ripp4*) mittels Überexpression von potentiell biosynthese-spezifischen regulatorischen Genen zu aktivieren. Eine transkriptionelle Analyse der Mutanten ergab, dass nur der Stamm, welcher das *pks1* BGC aktivieren sollte (AraC_PKS1), einen positiven Effekt auf die Expression des zu erwartenden BGCs hatte. Eine RNA-Sequenzierungsstudie ergab, dass in der AraC_PKS1 Mutante neben dem *pks1* BGC auch die kryptischen BGCs *ripp3* und *ripp4* eine erhöhte Transkription aufwiesen. Zudem wurde beobachtet, dass sich die Sekundärmetabolitproduktion in der Mutante durch Kultivierung unter erhöhten Licht-Intensitäten und CO_2-Leveln erweitern lässt. Unabhängig von den Kultivierungsbedingungen, hat die erhöhte Produktion des *pks1* Regulators NvlA in der Mutante einen Einfluss auf andere regulatorische Faktoren, wie Sigma-Faktoren und das RNA-Chaperon Hfq. Die Analyse des Zell- und Überstandsextrakts der AraC_PKS1 Mutante führte zur Entdeckung zweier neuer Polyketide, Nostoclid und Nostovalerolacton, welche beide vom *pks1* BGC codiert werden. Die Zugabe dieser Polyketide zum *N. punctiforme* Wildtyp zeigte, dass diese in der Lage sind einen Teil der Sekundärmetabolit-Effekte der AraC_PKS1 Mutante zu reproduzieren. Dies lässt darauf schließen, dass beide Polyketide als Signalstoffe innerhalb eines regulatorischen Netzwerks agieren. Da nicht alle transkriptionellen Effekte der AraC_PKS1 Mutante durch die Zugabe der *pks1* Produkte reproduziert werden konnten, ist anzunehmen, dass der Regulator NvlA einen globalen Effekt hat und nicht ausschließlich die *pks1* Biosynthese reguliert.

Diese Studie war die erste, welche einen potentiell biosynthese-spezifischen Regulator für die gezielte Aktivierung von BGC-Expression in Cyanobakterien verwendet hat. Diese Strategie führte neben der Entdeckung zweier neuer Polyketide, zu ersten Einblicken in den regulatorischen Mechanismus, der den spezialisierten Metabolismus in *N. punctiforme* kontrolliert. Diese Studie veranschaulicht, dass das Verstehen regulatorischer Mechanismen für die Entdeckung neuer Naturstoffe hilfreich sein kann. Die Studien-Ergebnisse können die Entwicklung neuer Screening-Strategien für bioaktive Metabolite in Cyanobakterien anregen und können dabei helfen Hochtiter-Produktions-plattformen für cyanobakterielle Naturstoffe zu entwickeln.

Contents

List of Figures

List of Tables

xxi

List of Abbreviations

A domain	adenylation domain
ACAD	acyl-CoA dehydrogenase
ACP	acyl carrier protein
AHL	N-acyl-homoserine lactone
AIP	autoinducing polypeptide
AMP	adenosinmonophosphat
AntiSMASH	antibiotics and secondary metabolite analysis shell
approx.	approximately
APS	ammonium persulfate
apt	anabaenopeptin
AT domain	acyltransferase domain
B. subtilis	*Bacillus subtilis*
BGC	biosynthetic gene cluster
bom	basis of mobility
bp	base pairs
C domain	condensation domain
C. reinhardtii	*Chlamydomonas reinhardtii* SAG 73.72
CBB	coomassie brilliant blue
cDNA	complementary DNA
CDS	CFP coding sequence
CFP	cyan fluorescent protein
CoA	coenzym A
COG	cluster of orthologous groups
C_t	cycle threshold
CTAB	cetyltrimethylammonium bromide
DAR	dialkylresorcinol
DEPC	diethylpyrocarbonat
DH domains	dehydratase
DMSO	dimethyl sulfoxide
DNA	deoxyribonucleic acid
dNTP	desoxynucleoside triphosphate

DTT	dithiothreitol
E. coli	*Escherichia coli*
ebo	eustigmatophyte/bacterial operon
EDTA	ethylenediaminetetraacetic acid
FAAL	fatty acyl-AMP ligase
GBL	γ-butyrolactone
gDNA	genomic DNA
HCCA	α-Cyano-4-hydroxycinnamic acid
HD	high density
His-Tag	polyhistidine-Tag
HIV	human immunodeficiency virus
HL/HC	high-light/high-carbon
HPLC	high performance liquid chromatography
KR domain	ketoreductase domain
KS domain	ketosynthase domain
LB	lysogeny broth
LC-MS	liquid chromatography–mass spectrometry
LC-HRMS	liquid chromatography– high resolution mass spectrometry
MALDI-TOF	matrix-assisted laser desorption/ionization - time of flight
Mb	mega base
MCS	multiple cloning site
MM	master mix
MOPS	3-morpholinopropanesulfonic acid
MS	mass spectrometry
MS/MS	tandem mass spectrometry
mvd	microviridin
N. punctiforme	*Nostoc punctiforme* PCC 73102
NAD	nicotinamide adenine dinucleotide
Ncl	nostoclide
Ni-NTA-agarose	nickel nitrilotriacetic acid agarose
NMR	nuclear magnetic resonance
nos	nostopeptolide
NosA	nostamide A
NRP	nonribosomal peptide
NRPS	nonribosomal peptide synthase
Nvl	nostovalerolactone
OD	optical density
ori	origin of replication

OSMAC	one strain many compounds
PCP domain	peptidyl carrier protein domain
PCR	polymerase chain reaction
PEG	polyethylene glycol
PK	polyketide
PKS	polyketide synthase
PMSF	phenylmethylsulfonyl fluoride
Ppan	4′-phosphopantetheine
PPY	Photopyrone
PTM	post-translational modifications
qPCR	quantitative PCR
RiPP	ribosomally synthesized and post-translationally modified peptides
RNA	ribonucleic acid
rpm	round per minute
rRNA	ribosomal ribonucleic acid
RT-qPCR	real-time quantitative PCR
scy	Scytonemin
SDS	sodium dodecyl sulfate
SDS-PAGE	sodium dodecyl sulfate polyacrylamide gel electrophoresis
SMGC	secondary metabolite biosynthetic gene cluster
SN	supernatant
T domain	thiolation domain
TAE	tris-acetate-EDTA
TAP	tris-acetate-phosphate
TBS-T	tris-buffered saline with Tween20
TE	tris-EDTA
TFA	trifluoroacetic acid
Tris	tris(hydroxymethyl)aminomethane
SOC	super optimal broth with catabolite repression
UV	ultraviolet
WT	wild type
YPSII	photosystem II quantum yield

Chapter 1

Introduction

1.1 Diversity of Specialized Metabolites

Specialized metabolites are small molecules that are produced naturally by a biological source. They are also called secondary metabolites or natural products [1]. Those molecules show a diverse setup of different biological activities. These include ecological activities such as involvement in cell differentiation, symbiosis and defense mechanisms against other organisms or stress response [2]. Specialized metabolites also feature pharmaceutical relevant properties like anticancer, antibiotic or immunosuppressant activities [3]. The biosynthetic pathway for the production of specialized metabolites is typically encoded by a locally clustered group of genes, called biosynthetic gene cluster (BGC) or secondary metabolite biosynthetic gene cluster (SMGC) [4]. The expression of a BGC is often regulated in response to the ecological function of the related natural product [5]. For example, the expression of a BGC encoding the cyanobacterial sunscreen scytonemin is induced by UV-A (380–315 nm) radiation [6] and the BGC of bikaverin found in *Fusarium* is expressed to protect itself against its antagonist *Ralstonia solanacearum* [7].

According to their chemical structure and their synthesis pathway, natural products can be categorized into different compound classes. The most prevalent classes are alkaloids, terpenoids, polyketides, non-ribosomal peptides, as well as ribosomally synthesized and post-translationally modified peptides (RiPPs) [8].

Specialized metabolites are produced by a variety of different organisms, including bacteria, fungi, plants and animals. A major source for natural products with biotechnological or pharmaceutical relevant bioactivities are microorganisms. Besides the well-known antibiotic agent penicillin [9], fungi are able to produce plenty of specialized metabolites with diverse

bioactivities. Cyclosporin A, produced by *Tolypocladium inflatum*, is used for example as a immunosuppressor, but it has also other pharmaceutical relevant activities, such as anti-inflammatory, fungicidal and antiparasitic activities [10]. Strobilurins are fungicides, originally isolated from *Strobilurus tenacellus*, that have been widely used in agriculture [11]. *Fusarium moniliforme* is able to produce gibberellin, a so-called phytohormon, which can regulate plant growth [12]. Other prolific producers of natural products belong to the phylum of actinobacteria. Especially the *Streptomyces* genus is well-known for its biosynthetic potential. Streptomycetes produce around two thirds of pharmaceutically relevant antibics, including streptomycin produced by *Streptomyces griseus*, neomycin produced by *Streptomyces fradiae* and tetracyclines produced by *Streptomyces rimosus* [13, 14].
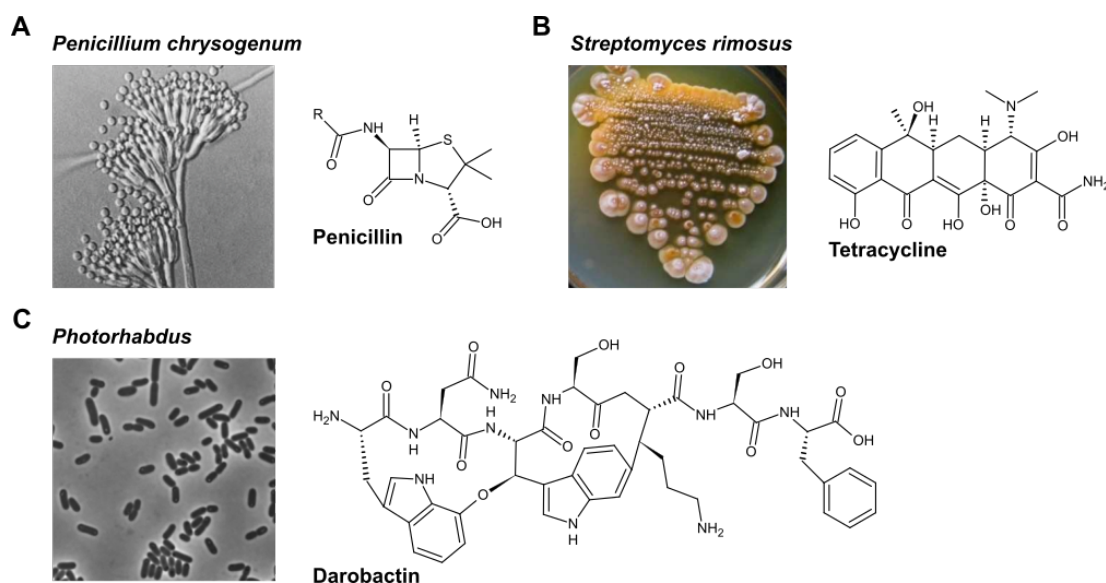
FIGURE 1.1: **Examples of specialized metabolites and their producers**
(A) Basic chemical structure of penicillin, which was discovered in *Penicillium chrysogenum*. (Picture source: Harris et al. 2006 [15]); **(B)** Chemical structure of tetracycline, which is produced by *Streptomyces rimosus*. (Picture source: Singh et al. 2012 [16]); **(C)** Chemical structure of darobactin, which was recently isolated from *Photorhabdus* isolates. (Picture source: da Silva et al. 2013 [17])

Other bacteria that show a large biosynthetic potential, which has not been comprehensively explored so far, include cyanobacteria and proteobacteria, like *Photorhabdus*, *Burkholderia* and *Pseudomonas* [18]. Recently, a new promising antibiotic, called darobactin, which is acting against gram-negative bacteria, was discovered in *Photorhabdus* isolates [19].

1.1.1 RiPPs - Ribosomally Synthesized and Post-Translationally Modified Peptides

RiPPs have been recently considered as a major class of natural products [20]. The ribosomally synthesized precursor peptides undergo extensive post-translationally modifications (PTM), leading to a high degree of chemical and structural diversity, although ribosomal peptides are restricted to the canonical amino acids, which are directly encoded in the genetic code [20, 21]. According to their structural features and biosynthetic machinery, ribosomal peptides are divided into different compound classes [20, 22]. Major classes are, among others, lanthipeptides [20, 23], cyanobactins [20, 24], lasso peptides [20, 25] and thiopeptides [20, 26]. A schematic overview of ribosomal peptide synthesis is depicted in **Figure 1.2**.
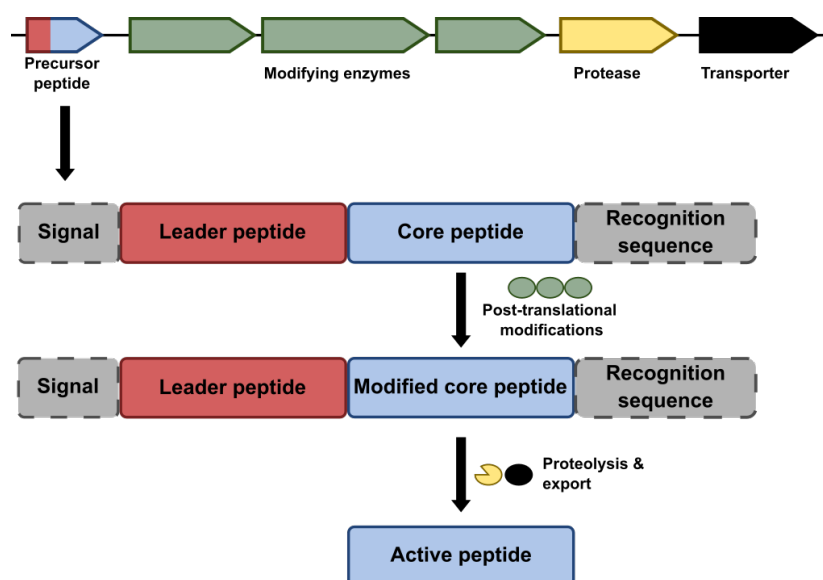
FIGURE 1.2: **Ribosomal peptide synthesis**
Organization of a RiPP gene cluster and schematic overview of ribosomal peptide synthesis.

Precursor peptides can be divided into two regions, an N-terminal leader-peptide region and a C-terminal core peptide region [27]. The core peptide undergoes extensive PTMs and is cleaved of from the leader peptide to become a smaller, but active fragment [20, 21]. In some cases, further modifications will be installed after separation from the leader peptide [20]. The leader peptide contains directing sequences for the recruitment of modifying enzymes, leading to the implementation of various PTMs, like macrocyclization, lacton formation or lanthionine synthesis, in the core region [21, 22]. The genes that encode modifying enzymes are often clustered around

the precursor peptide encoding genes [21]. Furthermore, the leader peptide contains at least one proteolytic cleavage site for secretion of the active peptide [20, 21]. In some cases, leader peptides also assist in folding or stabilization of the precursor peptide [27].

Due to their relatively short biosynthetic pathways and the direct connection between precursor gene and the final product, RiPPs are well suited for genome mining for new compounds, a technique for the prediction of natural products based on genomic data [8].

1.1.2   Polyketides and Nonribosomal Peptides

Polyketides (PK) and nonribosomal peptides (NRP) are two additional major classes of natural products [28]. Both are characterized by a broad spectrum of biological activities and remarkable structural variety [29–31]. PKs and NRPs are synthesized on large enzyme complexes, called nonribosomal peptide synthetases (NRPS) and polyketide synthases (PKS), respectively [28]. Type I PKS and NRPS enzymes share a typical modular organization. The arrangement and number of modules often determines the number and order of monomer components of the final product [31]. A variety of natural products show features of both NRPs and PKs. Those hybrids are assembled by a combination of PKS and NRPS modules [31]. A recent genome mining study reported that approximately one third of the newly discovered gene clusters are hybrid PKS/NRPS cluster [28].

1.1.2.1   NRPs - Nonribosomal Peptides

NRPs derive from NRPS enzyme complexes, which are composed of an array of catalytic modules that are able to assemble complex natural products [32]. Unlike ribosomally synthesized peptides, NRPs are not restricted to the proteinogenic amino acids [31]. They are capable to process a variety of different monomers, including noncanonical and nonproteinogenic amino acids, fatty acids and heterocycles, among other moieties [32, 33].
Each so-called elongation module contains at least three essential domains: an adenylation (A) domain, a peptidyl carrier protein (PCP) domain, also referred to as thiolation (T) domain, and a condensation (C) domain [32]. The A domain is responsible for selection and activation of amino acid substrates [31, 33]. The adenylated substrate is transferred to the PCP domain, where it is covalently attached to the 4′-phosphopantetheine (Ppan) cofactor via a thioester bond. Subsequently, the C domain catalyzes a peptide bond formation between

two adjacent PCP domains loaded with their respective substrates [32]. The resulting peptide chain is either extended further, undergoes additional modification steps or is released due to the catalytic activity of the thioesterase (TE) domain [32, 34]. Besides the essential domains, several auxiliary domains, like epimerization domains, methylation domains and cyclization domains, can be integrated into the NRP assembly line for modifications of the peptide chain [33]. An overview of the assembly line of NRPs is depicted in **Figure 1.3**.
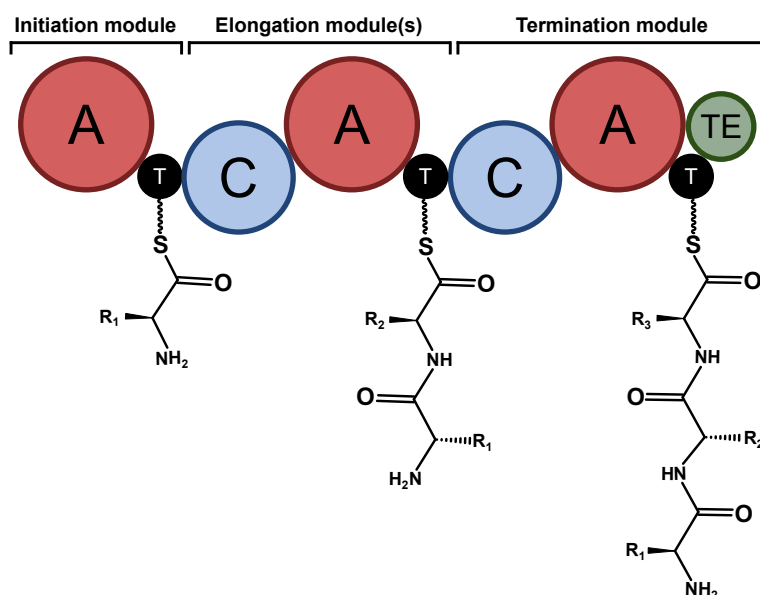
FIGURE 1.3: **Nonribosomal peptide synthesis**
Schematic overview of an NRP assembly line.
A - adenylation domain, T - thiolation domain,
C - condensation domain, TE - Thioesterase

Despite the common modular organization of NRPS systems, also nonmodular stand-alone PCP [35], A and C domains [36] can be found.

1.1.2.2 PKs - Polyketides

Polyketide synthetases (PKSs) catalyze the biosynthesis of polyketides from acyl coenzym A (CoA) precursors [30]. According to their organization and effect mechanism, PKSs are typically differentiated into three distinct types [37]. Type I PKSs are multidomain enzymes characterized by their modular organization. Similar to an NRPS module, a type I PKS module contains at least three catalytic domains, a ketosynthase (KS) domain, an acyltransferase (AT) domain and an acyl carrier protein (ACP) domain that are responsible for selection, activation and elongation of the growing polyketide chain [37]. Auxiliary modifying domains, like ketoreductase (KR) domains or

dehydratase (DH) domains, are found between AT and ACP domains [37, 38]. The assembly line for type I polyketides is shown in **Figure 1.4**.
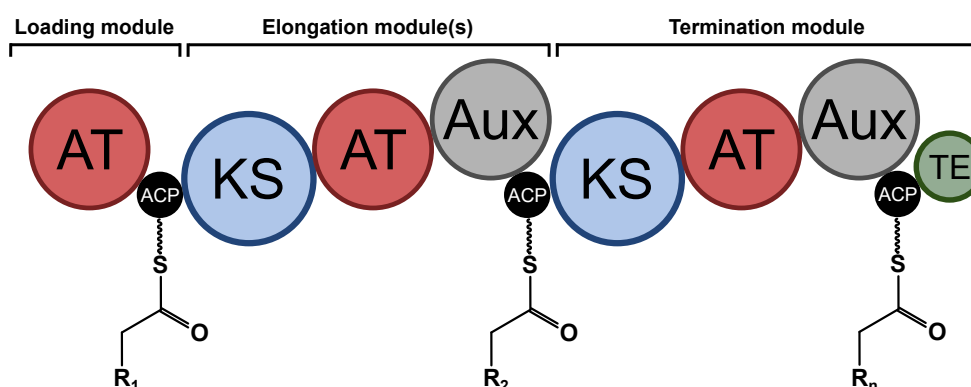
FIGURE 1.4: **Polyketide synthesis**
Schematic overview of a type I polyketide assembly line. Possible auxiliary domains are ketoreductase (KR) domains or dehydratase (DH) domains. AT - acyltransferase domain, ACP - acyl carrier protein domain, KS - ketosynthase domain, Aux - auxiliary domains, TE - Thioesterase

Type II PKS multienzyme complexes contain only a single set of iteratively acting catalytic domains. Like type I PKSs, they depend on an ACP domain for activation of acyl CoA substrates [30]. However, type III PKSs are independent from an ACP domain and act directly on the acyl CoA substrate [30].

1.2   Natural Product Discovery

Natural products, especially from plants and microbes, have been an important source for pharmaceutically relevant compounds, including antibiotic, fungicidal, antiproliferative, immunosuppressive, herbicidal and insecticidal drugs [39, 40]. During the "golden era" of drug discovery (1940-1970), brute force screening of microbes from soil samples led to the discovery of a plethora of new drugs, effective against various ailments [13, 41]. Especially the introduction of antibiotics strongly contributed to the expansion of the human life span [41]. With a globally rising life expectancy, the occurrence of life-threatening chronic diseases, such as cancer, cardio-vascular diseases and chronic respiratory diseases, are increasing [42]. With emerging chronic diseases and the spreading development of drug resistance mechanisms in human pathogens, the demand for new drugs is growing [41, 43]. However, traditional screening approaches for the discovery of new natural products are not profitable anymore, as these methods tend to rediscover already known compounds rather than new ones

[18]. To overcomes these problems genome-based approaches, combining bioinformatics-assisted methods with metabolic engineering, were developed [13, 43].

1.2.1 Traditional Natural Product Discovery Strategies

The "golden era" of drug discovery started in the 1940s with the development of penicillin and the discovery of streptomycin, actinomycin and streptothricin by systematic screening of actinomycetes from soil samples [18, 40]. These findings encouraged pharmaceutical companies to start screening microbe extracts for pharmaceutical useful compounds, focusing on antibiotic or antifungal activities [44]. The microorganisms for screening were acquired mostly from soil samples and later on also from freshwater samples [44]. After fermentation, a phenotype screening is conducted to search for relevant activities of the fermentation broth against a cell line of interest [18]. Since screening approaches were designed to have simple read-outs, such as cell death or cell inhibition, no prior knowledge about the compound's mechanism of action is needed [44]. If a desired effect occurs, the screening process is followed by compound isolation, purification and characterization for clinical development and lastly commercialization of the compound as a drug [18, 44]. For several decades only minor changes, including screening refinements and improvements in mass spectrometry and nuclear magnetic resonance, were implemented into the screening process [44]. Until the 1980s, this was a very profitable procedure for the discovery of novel natural products, leading to the development of a multitude of new drugs [40], for example erythromycin A [45], nystatin [46] and seromycin [47]. Due to high rediscovery rates and the absence of new technologies, the discovery of new and useful compounds slowed down fundamentally [18, 40]. Since natural product discovery was no longer profitable, most of the major companies withdrew from active research on this topic [18, 40]. However, due to improvements and increased affordability of genome sequencing methods, it was revealed that only a minor fraction of potentially available natural products has actually been discovered so far. In recent years, this development has led to a reinduced interest in natural product discovery [18, 47, 48].

1.2.2   Modern Natural Product Discovery Strategies

1.2.2.1   Genome Mining

Prediction of natural products based on genomic data is the basic concept of genome mining [49]. This idea was initiated by the sequencing of the complete genome of *Streptomyces coelicolor* [50] and *Streptomyces avermitilis* [51]. It was revealed that the genome sequences have the potential to produce approximately ten times more secondary metabolites than known from experimental studies [18, 49]. These observations in supposedly well-studied strains led to the expansion of the genome mining concept to other microbes, such as cyanobacteria, myxobacteria and anaerobes [49]. Nowadays, genome sequencing data of a great number of microbial strains are available. To handle such huge amounts of data, computerized methods, like BAGEL [52], CLUSEAN [53] and AntiSMASH [54], were developed, with AntiSMASH as the most comprehensive one [22]. In general, those tools are able to detect biosynthetic gene clusters by screening the genomic data for conserved genes or domains, typically involved in known biosynthetic pathways, such as PKS or NRPS domains [49, 55]. This is a very effective and reliable method to detect BGCs of already described compound classes [55].

For the prediction and detection of BGCs encoding novel compound classes other methods are necessary, but the development of appropriate tools have only recently begun [55]. One of those tools is the ClusterFinder algorithm [56], which is based on hidden markov models. Instead of searching for specific signature genes, this algorithm is looking for broad gene function patterns to detect novel gene cluster types [55, 56]. However, the resulting data must be interpreted very cautiously, as this method gives a lot of false-positive predictions [54]. The recently developed tool DeepBGC [57] reduces false-positive predictions rates and improves novel gene cluster detection through the combination of different machine learning algorithms. Other methods like EvoMining [58] are based on phylogeny and the idea that all enzymes involved in the secondary metabolism are evolved from enzymes of the primary metabolism. Although computerized genome mining is an evolving field, there is already a large gap between identified gene clusters and known specialized metabolites [59]. A large fraction of the BGCs identified by genome mining tools are cryptic [59]. For the identification and characterization of the corresponding specialized metabolites, synthetic biology approaches, aiming to activate a desired gene cluster, and appropriate detection methods, like mass spectrometry, are necessary [18, 60]. A typical

workflow for genome-based natural product discovery is depicted in **Figure 1.5**.
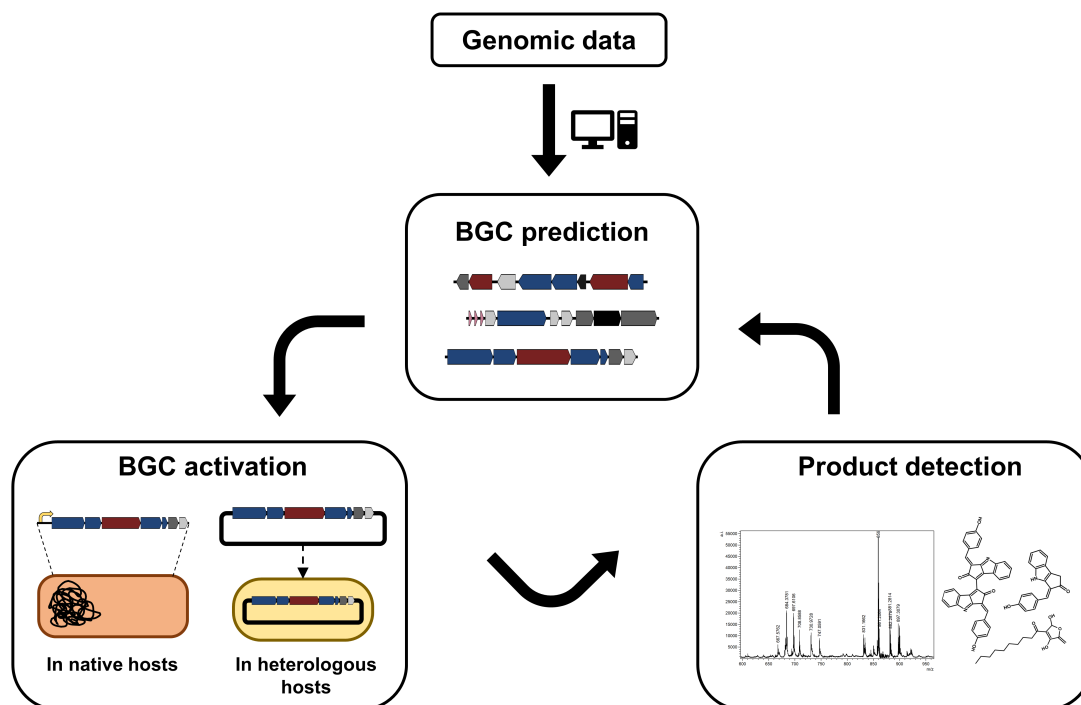
FIGURE 1.5: **Typical workflow of genome-based natural product discovery**

Nevertheless, the analysis of genome sequencing data by bioinformatical tools is a efficient strategy to prioritize BGCs of interest and guide laboratory-based efforts to identify the corresponding natural products [59].

1.2.2.2   Activation of Silent Biosynthetic Gene Clusters

The production of specialized metabolites is often tightly regulated and specific environmental conditions are needed to activate related biosynthetic pathways in the native organism [43]. Therefore, a large fraction of BGCs, identified by genome mining tools, is not or only poorly expressed under conventional laboratory cultivation conditions [43]. The activation and expression of a BGC of interest can be challenging. Therefore, several approaches have been developed to either trigger gene cluster expression in the native organism or express the BGC heterologously in a model organism to identify the corresponding natural product [18, 61].

If the native organism is amenable to genetic manipulation, metabolic engineering approaches focused on optimizing biosynthetic pathway processes can be used [61, 62]. When potential pathway-specific regulators

have already been detected in-silico, a commonly used approach is to
overexpress positive regulatory genes and to delete negative regulatory
genes to enhance gene cluster expression [43, 63]. Previously characterized
cluster-situated regulatory genes from related strains can also be used to
activate silent BGCs in the native producer [64]. Another way to activate
BGC expression is to improve the supply of necessary precursors from the
primary metabolism by either overexpressing the corresponding genes or by
shutting down competing pathways [62, 63]. Introducing a strong promoter
upstream of the BGC can also initiate gene cluster expression [43]. Duplication
of important biosynthetic genes or the whole BGC can enhance natural product
production as well [18, 62]. Alternatively, secondary metabolite production
can also be activated by methods based on the "one strain many compounds"
(OSMAC) framework [65], which covers induction of gene expression through
a variety of different environmental cultivation conditions, variations in
medium composition, co-cultivation with other microbial strains and the
addition of chemical elicitors [66, 67]. These methods are also suitable for
organisms that are not amenable to genetic manipulation [66].

In cases where cultivation of the native organism is too laborious or not
possible at all, the BGC of interest can be expressed heterologously [43]. This
means expression of the desired BGC in a non-native, but well-studied model
organism. For the most commonly used heterologous hosts, such as *E. coli* or
Saccharomyces cerevisiae, direct cloning approaches have been developed that
are able to handle large DNA fragments [13, 43]. As a result, these approaches
are suitable for cloning large BGCs such as NRPS or PKS clusters. Typical
cloning tools are TAR [68, 69] and RecET [70], which are based on homologous
recombination, Gibson assembly [71] and CRISPR-Cas9 [72, 73]. To enhance
BGC expression in the heterologous host, it is often advisable to replace certain
native regulatory elements of the BGC, such as promoters, terminators or
ribosomal binding sites by regulatory elements that are already approved to
work properly in the heterologous host [62, 73].

Independent from the expression approach used, BGC products are detected
and identified by mass spectrometry-based methods, like MS/MS or LC-MS
[43].

1.2.2.3   Quorum Sensing as a Tool for BGC Activation

A naturally occurring regulation system of the secondary metabolome
in microorganisms is quorum sensing. Quorum sensing is a cell-to-cell
communication strategy that regulates gene expression in a cell density-

dependent manner. It regulates a wide range of processes, such as biofilm formation, bioluminescence, sporulation and the production of virulence factors, as well as specialized metabolites including antibiotics and toxins.

The quorum sensing system is based on small signaling molecules, so-called autoinducers, which are released into the environment. Thereby, the concentration of the autoinducers is proportional to the cell density. When the concentration reaches a certain threshold, the signaling molecule interacts with a cognate receptor protein, triggering a coordinated alteration in gene expression. The major classes of signaling molecules that are related to quorum sensing are *N*-acyl-homoserine lactones (AHLs) in gram-negative bacteria, structurally diverse autoinducing polypeptides (AIPs) in gram-positive bacteria and boron-furan-derived signaling molecules (autoinducer-2, AI-2), which are used by gram-positive and gram-negative bacteria [74]. Besides these, there are further small signaling molecules that have been found to be involved in quorum sensing systems, such as γ-butyrolactones (GBLs) in *Streptomcyes* [75], dialkylresorcinols (DARs) in *Photorhabdus asymbiotica* [76], photopyrones (PPYs) in *Photorhabdus luminescens* [77] and diffusible signal factors in *Xanthomonas campestris* [78].

Quorum sensing was found to be involved in the production of several bioactive specialized metabolites, like the lantibiotics nisin and subtilin [79], the antifungal compound pyrrolnitrin [80] and the polyketide antibiotic mupirocin [81]. In *Burkholderia thailandensis*, genetic manipulation of a quorum sensing regulator, induced the activation of the thailandamide BGC and led to the discovery of a novel polyketide, called thailandamide lactone [82].

Due to the involvement in secondary metabolite production, targeted activation or manipulation of the quorum sensing machinery by metabolic engineering or cultivation-based approaches is a promising strategy to activate silent BGCs.

1.3 Cyanobacteria

Cyanobacteria are oxygenic, photosynthetically active prokaryotes. They are often described as gram-negative bacteria, although they combine characteristics that are typical for both, gram-negative and gram-positive bacteria [83].

Cyanobacteria are ancient organisms, existing at least for 2.7 billion years [84]. Their photosynthetic activities are considered to have had a major impact on the oxygenation of the earths atmosphere, enabling the evolution of higher life

forms [84, 85].

Historically, they had been termed as blue-green algae, due to their bluish green color, some morphological similarities to algae and their aquatic environment [86]. Once the fundamental differences between prokaryotes and eukaryotes were defined in the 1960s, it became apparent that blue-green algae have typical prokaryotic features in terms of their cellular properties. Supported by these findings, they were reclassified as cyanobacteria, forming a new bacterial phylum [87].

Cyanobacteria show a large diversity in terms of their morphology. They are found in the form of single cells, filaments or colonies. The size of cells ranges between 0.5 μm to 100 μm in diameter [85, 88]. Cyanobacteria are native throughout various habitats and can be found in terrestrial as well as freshwater environments [89]. Some species are adapted to extreme environments like saline lakes [90] or hot springs [91]. Even in Antarctica cyanobacteria can be found [86].
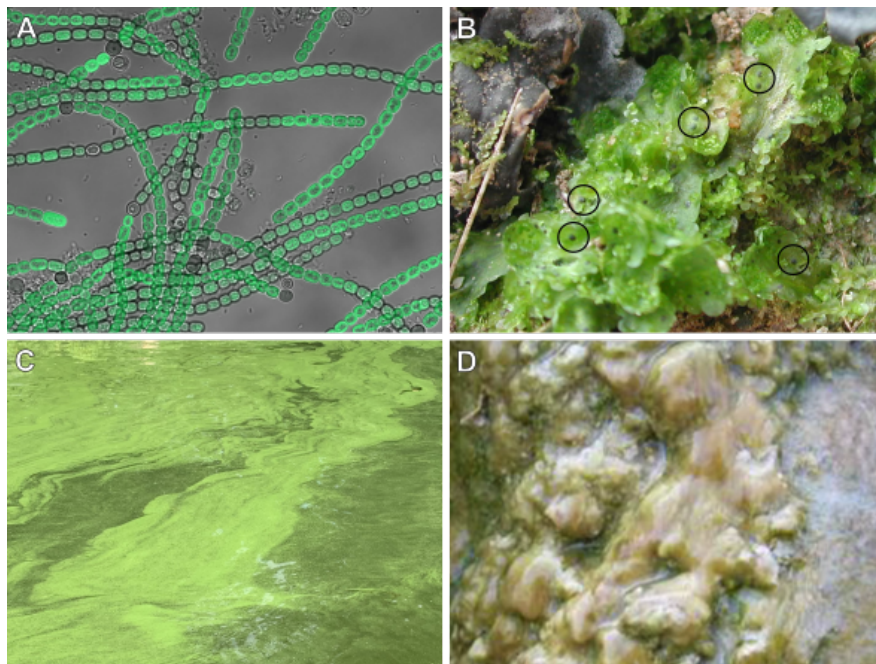
FIGURE 1.6: **Diverse appearances of cyanobacteria**
(**A**) Filaments of *N. punctiforme* PCC 73102 (picture by Julia Krumbholz); (**B**) Symbiosis between the liverwort *Blasia pusilla L.* and *Nostoc*. Symbiotic cavities harboring *Nostoc* are indicated by black circles. (picture by Anton Liaimer); (**C**) *Microcystis* bloom in a freshwater lake in Potsdam, Germany (picture by Julia Krumbholz); (**D**) Cyanobacterial mat in an Algerian hot spring (Picture source: Amarouche-Yala et al. 2014 [92])

Some cyanobacterial species are able to live in symbiotic relationships with eukaryotic hosts, including plants, fungi and sponges [93]. Entering such relationships can protect cyanobacteria from environmental extremes or predation [93]. In contrast, there are also cyanobacterial strains that can be harmful to surrounding organisms. Under conditions like high temperatures, strong light intensities or increased nutrient availability, several aquatic cyanobacteria, like *Microcystis aeruginosa*, are able to rapidly increase their population size, which is also called cyanobacterial bloom [94]. Often these blooms produce toxic specialized metabolites, known as cyanotoxins, which can be harmful to other organisms, including humans [88, 94].

1.3.1 Cyanobacterial Specialized Metabolites

Based on their ubiquitous occurrence in nature and their unique interactions with other organisms, cyanobacteria have developed complex genetic pathways for the production of secondary metabolites [88]. Although these metabolites are not essential for the organism, they can be the key advantage in terms of interspecies competition or defense mechanism against environmental stress [95]. Due to the high degree of structural variety and an enormous spectrum of bioactivities, including anti-cancer, antibiotic, anti-inflammatory, anti-viral and anti-fungal activities, cyanobacterial metabolites show a strong potential for utilization in drug development and other biotechnological applications [96, 97].

It was shown that the cyanotoxin microcystin has not only health threatening properties, but also the potential to be used as a targeted cancer therapeutic for pancreatic cancer, when modified properly [98]. The polysaccharides spirulan and Ca-spirulan, produced by *Spirulina* sp., show strong activity against several enveloped viruses, including HIV and influenza viruses [99]. The alkaloid pigment scytonemin can be found in a variety of different cyanobacterial species. It protects the organism from dangerous UV radiation [100] and is also able to repress cell proliferation [101]. Therefore, it is a promising candidate for the development of sunscreen agents and anti-cancer therapeutics [96].

Comprehensive genome mining studies of cyanobacteria have discovered a high number of BGCs for which the corresponding products are unknown [102, 103]. These BGCs are also referred to as orphan BGCs. Especially multicellular cyanobacterial genera with a complex morphology, like *Nostoc*, frequently show a high amount of BGCs including NRPS, PKS and RiPP

BGCs [103]. Unfortunately, the systematic exploration of cyanobacterial metabolites is strongly hampered due to the fact that most of the specialized metabolite producing strains are non-model organisms. This can make handling, cultivation and possibly required genetic manipulation to activate gene cluster expression rather challenging [104].

1.3.2 *Nostoc punctiforme* PCC 73102

Nostoc punctiforme PCC 73102 (from here on *N. punctiforme*) is a terrestrial filamentous cyanobacterium, belonging to the order *Nostocales*. *N. punctiforme* has a complex life cycle and it can develop a variety of different cell types (see **Figure 1.7**), which enables adaptation to changing environmental conditions [105].
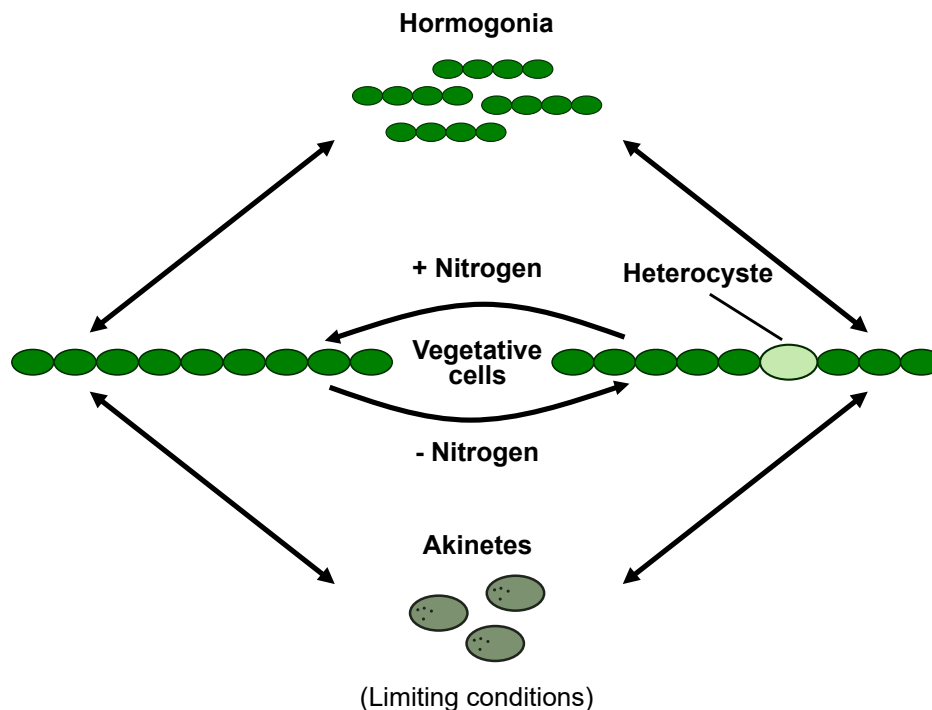
FIGURE 1.7: **Schematic overview of the life cycle of *N. punctiforme* PCC 73102**
N. punctiforme grows as vegetative filaments. In absence of a combined nitrogen source, a fraction of the cells differentiate into heterocysts, which are able to fix nitrogen. Under limiting conditions akinetes are formed. Hormogonia are motile filaments, which are essential for the initiation of symbiotic interactions.

In absence of combined nitrogen, vegetative cells can differentiate into so-called heterocysts. These cells are able to fix nitrogen from dinitrogen (N_2) in the air, in order to supply the remaining vegetative cells of the filament with nitrogen. However, heterocysts are no longer able to perform photosynthesis and therefore rely on the supply with carbohydrates from the surrounding

vegetative cells [105]. Under nutrient-limiting conditions, vegetative cells differentiate into spore-like akinetes [106]. These cells are resistant to unfavorable environmental impacts, like aridity or cold, and remain viable over long time periods. Once environmental conditions improve, akinetes can differentiate back into vegetative cells [106]. In response to environmental signals, vegetative cells can also differentiate into motile filaments, called hormogonia [107]. Besides their function as dispersal units, hormogonia are also essential for the initiation of symbiotic interactions of *N. punctiforme* with plants or fungi [93, 107]. The intensity of the symbiotic interactions strongly depends on the symbiotic host. On one hand, there are relatively lose interactions, were the infectious cyanobacteria (cyanobionts) are housed outside host cells or in specialized cavities, like in liverworts. On the other hand, it also appears that cyanobionts are housed intracellular in symbiotic organs, as in *Gunnera* sp. [93, 107].

1.3.2.1 The Genome of *N. punctiforme*

The genome of *N. punctiforme* was one of the first cyanobacterial genomes that has been completely sequenced [105]. With 9.06 Mb it is one of the largest genomes that can be found in cyanobacteria. It comprises of the bacterial chromosome with a size of 8.23 Mb and 5 plasmides (pNPUN01-05) [105, 108]. An extraordinary high number of BGCs is encoded in the genome of *N. punctiforme*, including gene clusters for the production of polyketides, nonribosomal peptides, as well as ribosomally synthesized peptides [109, 110]. So far, five BGCs have been assigned to their corresponding natural product, including heterocyst glicolipids [111], the terpene geosmin [112], the NRPs anabaenopeptin [113] and nostopeptolide [114] and the RiPP microviridin [115]. Still, the majority of BGCs in *N. punctiforme* remains orphan.

Nostopeptolide   **Anabaenopeptin**

Nostopeptolide 1052:   R = H
Nostopeptolide A: R = CH₂CH₃

Nostamide A: R = H
AP NZ857:   R = OH
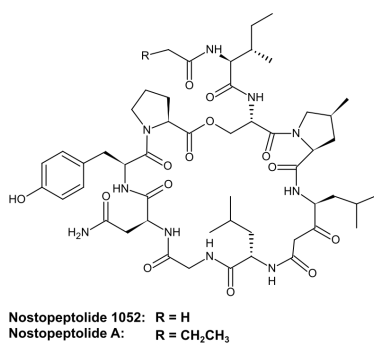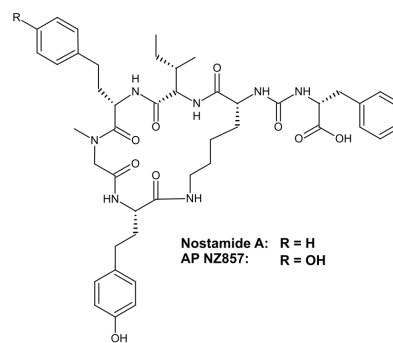
Microviridin
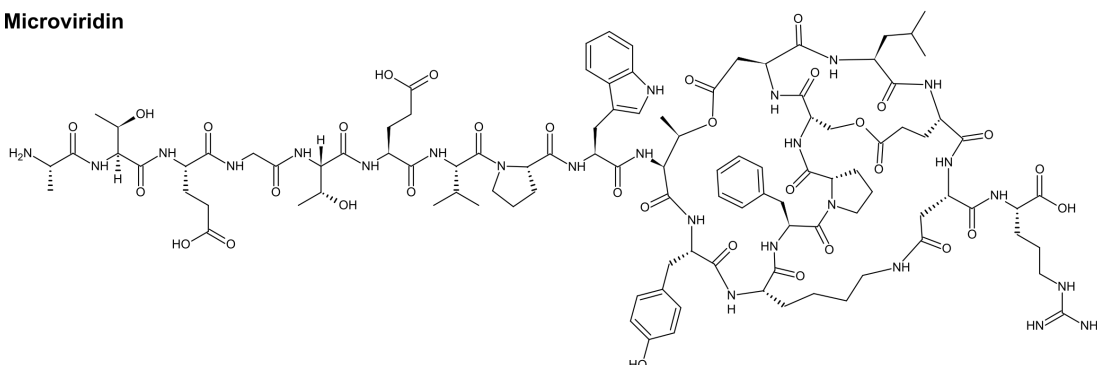
FIGURE 1.8: **Specialized metabolites found in *N. punctiforme* PCC 73102**

The large number of unexplored BGCs and an accessibility for genetic manipulation make *N. punctiforme* a suitable organism for the development and establishment of new natural product discovery strategies in cyanobacteria. A recent transcriptional study [110] revealed that the cultivation of *N. punctiforme* at very high cell densities leads to an upregulated expression of several BGCs. Although there are currently no reports on cell density dependent factors that control gene cluster expression, the data of the study strongly suggests extracellular signals as a major trigger of gene cluster expression [110].

1.4   Aim of the Study

Cyanobacteria are a prolific, but largely untapped source of new natural products. Due to their tight regulation, natural product BGCs are often only poorly expressed or silent under standard cultivation conditions. Therefore, elucidation of triggering factors and development of BGC activation strategies are necessary for the discovery of new natural compounds.
A major goal of this study was to establish a filamentous cyanobacterial strain as a model organism for natural product discovery in cyanobacteria. Due to

its large number of orphan BGCs and its amenability to genetic manipulation, *N. punctiforme* was identified as a promising organism for this purpose.

By utilizing a combination of genome mining, bioactivity-screening, as well as cultivation-based and metabolic engineering approaches, new concepts for natural product discovery in cyanobacteria should be developed. The impact of abiotic and biotic factors on BGC expression should be analzyed, with particular emphasis on the effects of high cell density cultivation. It should be investigated whether alterations in BGC expression are caused by a cell density-dependent signaling pathway. Therefore, potential chemical mediators that are encoded by formerly silent BGCs and possibly involved in such a pathway, should be identified and structurally elucidated. Furthermore, the impact of the potential cell density dependent chemical mediators on the expression of other BGCs should be analyzed in detail, to provide further insights into a potential signaling network, regulating a specialized metabolism.

The understanding of regulatory pathways, controlling a specialized metabolism in *N. punctiforme*, can guide the design of screening strategies for the systematic exploration of new bioactive compounds in other cyanobacteria. Additionally, this knowledge can help to establish a high-titer production of bioactive compounds in the native producer.

Chapter 2

Material and Methods

2.1 Material

2.1.1 Bacterial Strains

2.1.1.1 Common and Wild-type Strains

Escherichia coli Xl-1 Blue	Agilent Technologies, Waldbronn, Germany
Escherichia coli J53 (RP4)	AG Leister, LMU Munich, Germany
Escherichia coli B	Sigma-Aldrich, St. Louis, MO, USA
Bacillus subtilis ATCC 6633	Sigma-Aldrich, St. Louis, MO, USA
Nostoc punctiforme PCC 73102	Pasteur Culture Collection, Institut Pasteur, Paris, France
Anabaena sp. PCC 7120	Pasteur Culture Collection, Institut Pasteur, Paris, France
Nostoc sp. KVJ2	Anton Liaimer, UiT, Tromsø, Norway [107]
Nostoc sp. KVJ20	Anton Liaimer, UiT, Tromsø, Norway [107]

2.1.1.2 *Nostoc punctiforme* PCC 73102 Reporter Mutant Strains

NRPS1-CFP (pDD003)	Daniel Dehm, AG Dittmann, University of Potsdam, Germany [115]
PKS2-CFP (pDD004)	Daniel Dehm, AG Dittmann, University of Potsdam, Germany [115]

PKS4-CFP (pDD007)   Daniel Dehm, AG Dittmann, University
                                     of Potsdam, Germany [115]

NRPS2-CFP (pDD009)   Daniel Dehm, AG Dittmann, University
                                     of Potsdam, Germany [115]

RiPP4-CFP (pDD011)   Daniel Dehm, AG Dittmann, University
                                     of Potsdam, Germany [115]

RiPP1b-CFP (F3224-CFP)   Daniel Dehm, AG Dittmann, University
                                     of Potsdam, Germany [115]

Ripp1a-CFP (pDD025)   Daniel Dehm, AG Dittmann, University
                                     of Potsdam, Germany [115]

RiPP3-CFP (pDD027)   Daniel Dehm, AG Dittmann, University
                                     of Potsdam, Germany [115]

PKS5-CFP (pDD031)   Daniel Dehm, AG Dittmann, University
                                     of Potsdam, Germany [115]

PKS1-CFP (pDD032)   Daniel Dehm, AG Dittmann, University
                                     of Potsdam, Germany [115]

PKS3-CFP (pDD033)   Daniel Dehm, AG Dittmann, University
                                     of Potsdam, Germany [115]

MVD-CFP (pDD045)   Daniel Dehm, AG Dittmann, University
                                     of Potsdam, Germany [115]

Apt-CFP (P-aptA-CFP)   Arthur Guljamow, AG Dittmann,
                                     University of Potsdam, Germany [110]

Nos-CFP (P-nosA-CFP)   Anton Liaimer, UiT, Tromsø, Norway
                                     [116]

2.1.2   Media

LB-agar   Carl Roth, Karlsruhe, Germany

LB-broth   Carl Roth, Karlsruhe, Germany

SOC media   2% (w/v) tryptone, 0.5% (w/v) yeast extract,
                                     10 mM NaCl, 2.5 mM KCl, 10 mM $MgCl_2$,
                                     10 mM $MgSO_4$, 20 mM Glucose

$BG-11_0$ as described by Rippka *et al.* 1979 [117]

BG-11   as described by Rippka *et al.* 1979 [117]

Bacto agar   BD Difco, Sparks, USA

2.1.3   Antibiotics

Streptomycin   Carl Roth, Karlsruhe, Germany

Chloramphenicol   Carl Roth, Karlsruhe, Germany

2.1.4   Plasmids

pDD012   Daniel Dehm, AG Dittmann, University of Potsdam, Germany

pRL1049   provided by lab of Prof. Dr. John C. Meeks, University of California, USA [118]

pRL271   provided by lab of Prof. Dr. John C. Meeks, University of California, USA [119]

pSK008   Stella Scholz, AG Dittmann, University of Potsdam, Germany

pSK009   Stella Scholz, AG Dittmann, University of Potsdam, Germany

2.1.5   Primer

All Primers were manufactured by Sigma Aldrich Chemie GmbH (Steinheim, Germany).

2.1.5.1   Primers for Gibson DNA Assembly

TABLE 2.1: **List of primers for Gibson DNA Assembly**

Name	Sequence (5' to 3')	Description
J013_FW	acaactactggtgaggaagttaaagagcgctGATCGCTGCTGGTTTGCTTA	homologous region (upstream) for *NPUN_RS25520* knockout
J014_RV	gatcaccaaggtagtcggcaaataaTCGCTGCTAAAATCCCAACG	homologous region (upstream) for *NPUN_RS25520* knockout

J015_FW	acttcggcgatcaccgcttccctcaCGCC TCAGTTGTGCTTTTCT	homologous region (downstream) for *NPUN_RS25520* knockout
J016_RV	ctgcaggcatgcaagctttcgcggcgccA TCCGACCTAAGTTGCCACA	homologous region (downstream) for *NPUN_RS25520* knockout
J056_FW	tcgatgataagctgtcaaacatgagAAG TACTTAGTATTATATTGCAG TCAATAAA	*NPUN_RS16340* promoter region
J057_RV	cgcaagaggccctttcgtcttcaagaattcC TTTTTCTCCTATTGGATTGGC TAATATGAC	*NPUN_RS16340* promoter region
J058_FW	tagccaatccaataggagaaaaaggTCT TGCCATGCCTAAAGAGC	*NPUN_RS25500/25505*, *ripp4* regulatory gene
J059_RV	cgcaagaggccctttcgtcttcaagaattcA AACTAAAGGGCAACCAGCA	*NPUN_RS25500/25505*, *ripp4* regulatory gene
J092_FW	tagccaatccaataggagaaaaaggCA AGAGTGCCATTATGAACAG AAAG	*NPUN_RS25505*, *ripp4* regulatory gene
J063_FW	cgcaagaggccctttcgtcttcaagaattcT GTATCAAGCCTTCCACTCCT	*NPUN_RS16765*, *ripp3* regulatory gene
J064_RV	tagccaatccaataggagaaaaaggGCT ACAACTCCTACGCGGC	*NPUN_RS16765*, *ripp3* regulatory gene
J072_FW	cgcaagaggccctttcgtcttcaagaattcT GTTTTAAACTAGCACCAAA ATCCT	*NPUN_RS10525*, *pks1* regulatory gene
J073_RV	tagccaatccaataggagaaaaaggTG AGAGATGCTAGATGTATTC GC	*NPUN_RS10525*, *pks1* regulatory gene
J074_FW	tagccaatccaataggagaaaaaggTCA ATATGACCTATGAAACCAA AAGA	*NPUN_RS16090*, *pks2* regulatory gene
J075_RV	cgcaagaggccctttcgtcttcaagaattcG TTTGCCCTGGGGTTGGTTAC	*NPUN_RS16090*, *pks2* regulatory gene

J110_FW	actagagtagtggaggttactagggATG AGAGGATCGCATCACC	*NPUN_RS25510, ripp4* precursor
J111_RV	ggactgagctagccgtcaaggcgcgTTA TCTCGTTGGACAGTCGTTA	*NPUN_RS25510, ripp4* precursor
J112_RV	ggactgagctagctgtcaaggcgcgTTA TCTCGTTGGACAGTCGTTA	*NPUN_RS25510, ripp4* precursor

2.1.5.2 Primers for RT-qPCR

TABLE 2.2: **List of primers for RT-qPCR**

Name	Sequence (5' to 3')	Target
C3_FW	CGTGGTTGACTGGAGA TGCT	*NPUN_RS10475, pks1*
C3_RV	AAGCCTCTCGTGCCGT TTTA	*NPUN_RS10475, pks1*
D132_FW	GCGGACTAGCTCATCA GACC	*NPUN_RS15970, pks2*
D133_RV	GTACCATCCCCACAAC CCAT	*NPUN_RS15970, pks2*
D136_FW	AGAACGGGCGCTACTC TTTT	*NPUN_RS17005, pks3*
D137_RV	TTTCTTGGTGGATAGGC GGG	*NPUN_RS17005, pks3*
D138_FW	ACTCTCAGGCGAATGT TCCA	*NPUN_RS17455, pks4*
D139_RV	CCTGAAATTGACGCGC AGAT	*NPUN_RS17455, pks4*
C21_FW	GGGGAATGGAAAGCA TGGGA	*NPUN_RS33540, pks5*
C21_RV	ATTAACGCCCCTTCCCT GTG	*NPUN_RS33540, pks5*
C8_FW	AGCGGCAACATATTCC CCAA	*NPUN_RS15385, nrps1*

C8_RV	ACGCCCAACCTGCTCT ATTC	*NPUN_RS15385, nrps1*
Cp_FW	CTCATGTCGGGTGCAG CTTA	*NPUN_CR074, nrps2*
Cp_RV	CCTCAATCCAAGTCAG GCGT	*NPUN_CR074, nrps2*
C10L_FW	GGCAGAATTGGGAGG ACGAA	*NPUN_RS16255, ripp1a*
C10L_RV	TCCCAAACCCATCATT GAGCA	*NPUN_RS16255, ripp1a*
D134_FW	CGAAAGAAGCAGTCAT CAAA	*NPUN_RS16310, ripp1b*
D135_RV	TTGCTTTTCTTGCATCA CTG	*NPUN_RS16310, ripp1b*
C11a_FW	AGCAGACATCATAGCT CCACT	*NPUN_RS16795, ripp3*
C11a_RV	GGGTGCAGAAAAGGG CTACA	*NPUN_RS16795, ripp3*
D140_FW	GCGATCTCTCAAATGC TGGC	*NPUN_RS25510, ripp4*
D141_RV	CGTGTGATTCAGAGAC GGCT	*NPUN_RS25510, ripp4*
D150_FW	GCTAGGAGCTACTGAG AACA	*NPUN_AF077, ripp5*
D151_RV	AGCATCTACCTCCTGA ATCG	*NPUN_AF077, ripp5*
apt_RT_FW	GAAATTGAGGCGCTTT TGAG	*NPUN_RS12350, apt*
apt_RT_RV	GGCTAGTGACGCTCAC ATCA	*NPUN_RS12350, apt*
NosA_RT_FW	GTTTGCCCTCTCTGCTG AAC	*NPUN_RS1097), nos*

NosA_RT_RV	GCGGTAAAGCAGGGT ATCAA	*NPUN_RS10970, nos*
J093_FW	ATGCCTACAAACACAG TCAAA	*NPUN_RS38845, mvd*
J094_RV	GGAACCTCTGTTCCTTC AGTAG	*NPUN_RS38845, mvd*
rnpB_RT3_FW	GCGGTTGCAGATCAGT CATA	*NPUN_RS38010, rnpB*
rnpB_RT3_RV	TCTGTGGCACTATCCTC ACG	*NPUN_RS38010, rnpB*
J097_FW	GCATGAATTTAGGTGC AGATG	*NPUN_RS10525, pks1* regulatory gene
J098_RV	GGTGATTGCCGCTGAT TA	*NPUN_RS10525, pks1* regulatory gene
J099_FW	CAGAAGAAGGCGCTC ATAG	*NPUN_RS16090, pks2* regulatory gene
J0100_RV	CTGCGATCGCTGCTAA A	*NPUN_RS16090, pks2* regulatory gene
J0101_FW	CAAGGGAAGTTGGGC AATTA	*NPUN_RS16765, ripp3* regulatory gene
J0102_RV	CGATCGTTCCTAATGG GTATTG	*NPUN_RS16765, ripp3* regulatory gene

2.1.5.3   Primers for Sequencing

TABLE 2.3: **List of primers for sequencing**

Name	Sequence (5′ to 3′)	Target
D021_S1	AGGATGACGATGAGCGCATT	pRL 1049
D022_S2	CGGCACTCGACAGAATTGGC	pRL 1049
D064_S7	AGTAACCGGCAAAATCGC	Streptomycin resistance cassette
D064_S8	ATTGAAGATGAGGAGCGAT	Streptomycin resistance cassette

| J095_FW | TTGCCGGGAAGCTAGAGTAA | pRL 271 |
| J096_RV | GTTCGAAGAACTGCCGATGT | pRL 271 |

2.1.6   Markers and Dyes

GeneRuler™ 1kb DNA Ladder	Thermo Fisher Scientific, Waltham, MA, USA
GeneRuler™ Low Range DNA Ladder	Thermo Fisher Scientific, Waltham, MA, USA
Pageruler™ Prestained Protein Ladder	Thermo Fisher Scientific, Waltham, MA, USA
$6\times$ DNA loading dye	Thermo Fisher Scientific, Waltham, MA, USA
$2\times$ RNA loading dye	Thermo Fisher Scientific, Waltham, MA, USA
$5\times$ SDS loading dye	250 mM Tris-Cl pH 6.8, 0.1% (w/v) Bromophenol blue, 10% (w/v) SDS, 50% (v/v) Glycerol, 500 mM β-Mercaptoethanol

2.1.7   Enzymes

Maxima™ Hot Start Green $2\times$ PCR Master Mix	Thermo Fisher Scientific, Waltham, MA, USA
$2\times$ Blue S'Green qPCR Mix Seperate ROX	Biozym Scientific, Hessisch Oldendorf, Germany
Phusion™ High-Fidelity DNA Polymerase	Thermo Fisher Scientific, Waltham, MA, USA
S7 Fusion Polymerase™	Mobidiag, Espoo, Finland
RNase A/T1 mix	Thermo Fisher Scientific, Waltham, MA, USA
T5 Exonuclease	New England Biolabs, Ipswich, MA, USA

FastDigest restriction enzymes	Thermo Fisher Scientific, Waltham, MA, USA
Lysozym	VWR, Radnor, PA, USA
Proteinase K	Thermo Fisher Scientific, Waltham, MA, USA
FastAP Thermosensitive Alkaline Phosphatase	Thermo Fisher Scientific, Waltham, MA, USA

2.1.8   Antibodies

Monoclonal Anti-polyHistidine antibody (mouse)	Sigma-Aldrich, St. Louis, MO, USA
Anti-Mouse IgG-Peroxidase antibody (rabbit)	Sigma-Aldrich, St. Louis, MO, USA

2.1.9   Chemicals

β-Mercaptoethanol	Ferak, Berlin, Germany
Acetic acid	Carl Roth, Karlsruhe, Germany
Acetonitrile	VWR, Radnor, PA, USA
Agarose	Biozym Scientific, Hessisch Oldendorf, Germany
Aluminium sulfate	Sigma-Aldrich, St. Louis, MO, USA
APS	Carl Roth, Karlsruhe, Germany
BisTris	Carl Roth, Karlsruhe, Germany
Bromophenol blue	Carl Roth, Karlsruhe, Germany
Chloroform	Carl Roth, Karlsruhe, Germany
CBB - Coomassie Brilliant Blue (G250)	Thermo Fisher Scientific, Waltham, MA, USA
CTAB	Carl Roth, Karlsruhe, Germany
DEPC	Carl Roth, Karlsruhe, Germany

dNTP mix, 10 mM each	Thermo Fisher Scientific, Waltham, MA, USA
DTT	Carl Roth, Karlsruhe, Germany
EDTA	Carl Roth, Karlsruhe, Germany
Ethanol	VWR, Radnor, PA, USA
Ethidium bromide	Sigma-Aldrich, St. Louis, MO, USA
Glycerol	Carl Roth, Karlsruhe, Germany
Glycin	Carl Roth, Karlsruhe, Germany
Hydrochloride acid 37%	Carl Roth, Karlsruhe, Germany
Hydrogen peroxide 30%	Carl Roth, Karlsruhe, Germany
Imidazol	Carl Roth, Karlsruhe, Germany
Immersion oil	Carl Roth, Karlsruhe, Germany
Isopropanol	VWR, Radnor, PA, USA
Lithium chloride	Carl Roth, Karlsruhe, Germany
Magnesium chloride	Carl Roth, Karlsruhe, Germany
Methanol	VWR, Radnor, PA, USA
Monosodium phosphate	Carl Roth, Karlsruhe, Germany
MOPS	Carl Roth, Karlsruhe, Germany
NAD	Carl Roth, Karlsruhe, Germany
Ni-NTA-agarose	Qiagen, Hilden, Germany
PEG-8000	Carl Roth, Karlsruhe, Germany
Phenol solution	Sigma-Aldrich, St. Louis, MO, USA
Phenol:Chloroform:Isoamyl alcohol	Sigma-Aldrich, St. Louis, MO, USA
Phosphoric acid	Carl Roth, Karlsruhe, Germany
PMSF	Carl Roth, Karlsruhe, Germany

Potassium carbonate | VWR, Radnor, PA, USA

Potassium bicarbonate | VWR, Radnor, PA, USA

Powdered milk | Carl Roth, Karlsruhe, Germany

Rotiphorese® Gel 40 (19:1) | Carl Roth, Karlsruhe, Germany

SDS | SERVA Electrophoresis GmbH, Heidelberg, Germany

Sodium acetate | Sigma-Aldrich, St. Louis, MO, USA

Sodium chloride | Carl Roth, Karlsruhe, Germany

Sodium citrate | Merck KGgA, Darmstadt, Germany

Temed | Carl Roth, Karlsruhe, Germany

Tris | Carl Roth, Karlsruhe, Germany

Trifluoroacetic acid | Thermo Fisher Scientific, Waltham, MA, USA

TRIzol | Life Technologies, Carlsbad, CA, USA

Tween 20 | Carl Roth, Karlsruhe, Germany

Urea | Carl Roth, Karlsruhe, Germany

2.1.10   Buffers and Solutions

Buffer B | 8 M Urea, 100 mM NaH_2PO_4, 10 mM Tris, pH 8.0 (HCl)

Coomassie staining solution | 5% (w/v) aluminium sulfate, 10% (v/v) ethanol, 0.02% (w/v) CBB, 2% (v/v) phosphoric acid

Destainer | 2% (v/v) phosphoric acid, 10% (v/v) ethanol

10× FastDigest buffer | Thermo Fisher Scientific, Waltham, MA, USA

Homogenization buffer	100 mM Tris (pH 8-9.0), 5 mM EDTA (pH 8.0), 100 mM NaCl, 0.5% SDS
2× Hot Fusion Master Mix	40% (v/v) 5× ISO buffer, 4 U T5-Exonuclease, 25 U Phusion™ High-Fidelity polymerase
5× ISO buffer	500 mM Tris, 50 mM MgCl$_2$, dNTPs (1 mM each), 50 mM DTT, 25% (w/v) PEG-8000, 5 mM NAD
20× MOPS Running buffer	1 M MOPS, 1 M Tris, 70 mM SDS, 7 mM EDTA
Lysis buffer (protein extraction)	100 mM Tris-HCl, 150 mM NaCl, 10% (v/v) Glycerol
5× Phusion GC buffer (green)	Thermo Fisher Scientific, Waltham, MA, USA
5× SDS Gel buffer	1.8 M Bis-Tris, pH 6.5-6.8 (HCl)
1× TAE buffer	40 mM Tris, 1 mM EDTA, 0.12% (v/v) acetic acid
TBS-T buffer	50 mM Tris, 150 mM NaCl, 0.1% (v/v) Tween20, pH 7.4 (HCl)
TE buffer	10 mM Tris, 1 mM EDTA, pH 8.0
1× Transfer buffer	192 mM glycine, 25 mM Tris, 20% (v/v) methanol

2.1.11   Commercial Kits

GenElute™ Plant Genomic DNA Miniprep Kit	Sigma-Aldrich, St. Louis, MO, USA
GeneJET Gel Extraction Kit	Thermo Fisher Scientific, Waltham, MA, USA
GeneJET PCR Purification Kit	Thermo Fisher Scientific, Waltham, MA, USA
GeneJET Plasmid Miniprep Kit	Thermo Fisher Scientific, Waltham, MA, USA

Maxima™ H Minus cDNA Synthesis Kit	Thermo Fisher Scientific, Waltham, MA, USA
NEBuilder® HiFi DNA Assembly MM	New England Biolabs, Ipswich, MA, USA
RNeasy® Mini Kit	Qiagen, Hilden, Germany
SERVA*Light* Polaris Chemiluminescence Kit	SERVA Electrophoresis GmbH, Heidelberg, Germany
Turbo DNA-*free*™ Kit	Invitrogen, Waltham, MA, USA

2.1.12 Membranes, Cartridges, Filters, Cuvettes

Acrodisc® syringe filters (4 mm)	Pall, New York, USA
Electroporation cuvette (2 mm)	PEQLAB, Erlangen, Germany
Immobilon Transfer membrane, HATF, 85 mm	Merck Millipore, Darmstadt, Germany
Protan™ NC Blotting membrane, 0.45 µm	GE Healthcare Life Science, Little Chalfont, UK
Rotilabo® inserts 100, borosilic gl.	Carl Roth, Karlsruhe, Germany
Sep-Pak C18 Plus Short cartridge	Waters, Milford, MA, USA
Septa PTFE/Silicone	Carl Roth, Karlsruhe, Germany
Whatman 3mm paper	Whatman GmbH, Maidstone, UK

2.1.13 Technical Devices

Agarose gel electrophoresis chamber	PEQLAB, Erlangen, Germany
ChemiDoc XRS $^+$	Bio-Rad, Hercules, CA, USA
Centrifuges	
Perfect Spin 24	PEQLAB, Erlangen, Germany
Micro Star 17R	VWR, Radnor, PA, USA

Heraeus Multifuge 1S-R	Thermo Fisher Scientific, Waltham, MA, USA
Sigma 6-16K	Sigma, Osterode am Harz, Germany
Sigma 6-16KS	Sigma, Osterode am Harz, Germany

Concentrator RVC 2-25 CDplus with CT 02-50	Martin Christ Gefriertrocknungsanlagen, Osterode am Harz, Germany
Electroporator Micropuls™	Bio-Rad, Hercules, CA, USA
Fluorescence microscope Zeiss LSM 780	Carl Zeiss Microscopy GmbH, Jena, Germany

Axio Observer Z1 with diode laser (405 nm), HeNe laser (633 nm)

AxioCam digital microscope camera

PlanApo 1.4/63× oil immersion objective

ZEN Software

HPLC System	Shimadzu Europa, Duisburg, Germany

Auto injector SIL-20AC

Column oven CTO-10AS

Communications bus module CBM-20A

Degasser DGU-20A5

Diode array detector SPD-M20A

Fraction collector FRC 10A

Liquid chromatograph LC-10A

SymmetryShield RP18 column (3.5 µm, 4.6 mm × 100 mm)

SymmetryShield Sentry Guard column (3.5 µm, 3.9 mm × 20 mm)

Microflex™ LRF with FlexAnalysis Software	Bruker, Billerica, MA, USA
Mini-PROTEAN® Electrophoresis Cell	Bio-Rad, Hercules, CA, USA
Nanodrop™ 2000 Spectrophotometer	Thermo Fisher Scientific, Waltham, MA, USA
PCR system Mastercycler® nexus X2	Eppendorf AG, Hamburg, Germany
PowerPac™ Basic power supply	Bio-Rad, Hercules, CA, USA
RT PCR system Light Cycler® 96	Roche, Basel, Switzerland
Ultrasonic homogenizer Sonoplus HD	Bandelin electronic, Berlin, Germany
Novaspec III spectrophotometer	Amersham Bioscience, Little Chalfont, UK

2.2 Methods

2.2.1 Microbiological Methods

2.2.1.1 Cultivation of *E. coli*

Liquid *Escherichia coli* cultures were grown overnight in LB-media under standard cultivation conditions at 37 °C and 220 rpm. Transformation mixtures were cultivated overnight at 37 °C on solid agar plates (1.5% agar). For plasmid selection and maintaining, a certain amount of antibiotic (see table **2.4**) was added to liquid LB media or LB agar plates.

TABLE 2.4: **Antibiotic concentrations**
Depending on vector specific antibiotic resistances, LB media was supplemented with a certain concentration of antibiotics.

Vector	Antibiotic	Concentrations [µg/ml]
pRL1049	Streptomycin	20
pRL271	Chloramphenicol	12.5
pDD012	Streptomycin / Chloramphenicol	20 / 12.5

For all cloning procedures *E. coli* Xl-1 blue cells were used.

2.2.1.2 Cryopreservation of *E. coli*

Frozen stocks for all *E. coli* strains were prepared by adding $1\times$ volume of LB media with 50% (v/v) glycerol to a *E. coli* culture. The stocks were stored at -80 °C.

2.2.1.3 Cultivation of *N. punctiforme*

2.2.1.3.1 Conventional Cultivation

N. punctiforme cultures were cultivated under diazotrophic conditions in liquid $BG11_0$ [117] media under continuous white light illumination (fluorescent tube) with an intensity of 30 µmol photons $m^{-2}\,s^{-1}$ at 23 °C. For transformation approaches and maintenance, solid $BG11_0$ agar plates containing 1.2 % bacto agar were used for cultivation. Mutant strains were cultivated in selective media containing 2 µg/ml streptomycin.

2.2.1.3.2 High Density Cultivation

For high density (HD) cultivation of *N. punctiforme*, 100 ml HD cultivation vessels were used together with an HDC 1.100B platform (CellDeg GmbH, Berlin, Germany). The lower vessel of the system was filled with 200 ml bicarbonate buffer. The buffer was obtained by mixing 3 M $KHCO_3$ and 3 M K_2CO_3 solutions at ratios of 1:1, 4:1 and 9:1, providing CO_2 partial pressures of 5, 32 and 90 mbar, respectively. Cultures were shaken at 100–250 rpm and illuminated with a dimmable full-spectrum LED-panel (HYG05-D100*3W-W, RoHS). A schematic overview of an HD cultivation setup is depicted in **Figure 2.1**.
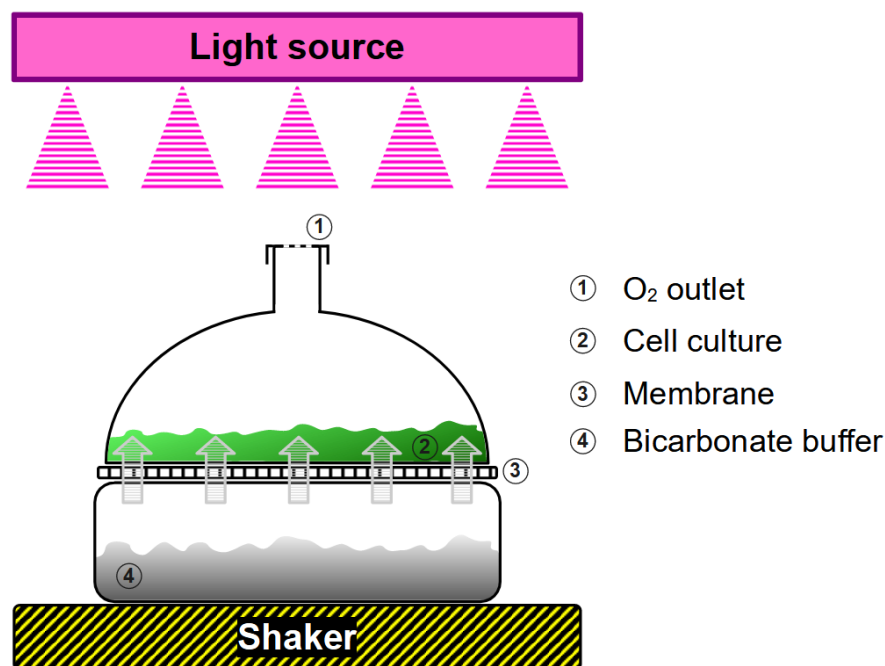
FIGURE 2.1: **High density cultivation setup**
Schematic overview of the high density cultivation system with the HDC 1.100B platform from the CellDeg company. Scheme adapted from Lippi et al. 2018 [120].

The bicarbonate buffer was exchanged every 72–120 h. Usually, a cultivation was started with a light intensity of 60 µmol photons $m^{-2}\,s^{-1}$ and a bicarbonate buffer providing a partial pressure of 32 mbar. After initial growth, the light intensity was increased to 100 µmol photons $m^{-2}\,s^{-1}$ and the 90 mbar bicarbonate buffer was used. After that, the light intensity was increased regularly every 72–120 h, depending on culture growth, until the cultivation was stopped or the maximum light intensity of 800 µmol photons $m^{-2}\,s^{-1}$ has been reached. To monitor the growth of the cultures, cells were pelleted at 3000 $\times$ g for 10 min and weighed to determine the wet weight of the culture.

Additionally, samples of the culture supernatant were taken and kept for further analysis. *N. punctforme* wild-type (WT) HD cultures were grown for 20–70 days and then analyzed by HPLC (see **Section 2.2.4.1**).

For HD cultivation of *N. punctiforme* reporter mutant strains, 10 ml HD cultivation vessels were used together with an HDC 9.10B platform. The cultivation was usually started with a light intensity of 60 µmol photons $m^{-2} s^{-1}$ and a 5 mbar bicarbonate buffer. After 10–14 days the light intensity was set to 100 µmol photons $m^{-2} s^{-1}$ and the 32 mbar bicarbonate buffer was used. The bicarbonate buffer was exchanged every 72–120 h. After 10 and 20 days of cultivation, a small portion of fresh media was added to the culture. Reporter mutant strains were cultivated over a time period of 30 days and analyzed by confocal fluorescence microscopy after 10, 20 and 30 days.

To obtain large amounts of HD cell pellets and supernatants of *N. punctiforme* WT, the cultivation was carried out by the CellDeg company. They used a 1.5 l HD cultivation vessel with the HDC 1.1500 platform, directly linked to a CO_2 compartment. Cultures were illuminated by two LED-panels (AP673L, Valoya, Finnland) and shaken at 100 rpm. CO_2 concentrations and light intensities were controlled by a growth control unit. Cultures were grown for 18–24 days in $BG11_0$ media without medium exchange.

The HDC 1.100B platform for 100 ml cultivation vessels was later replaced by an HDC 9.100 universal platform. This platform is directly connected to a CO_2 compartment. For illumination, a high-power LED light source (RX400, AP673L, Valoya, Finnland) was used. Light intensity and CO_2 partial pressure were monitored and controlled by a growth control unit (CellDeg GmbH, Berlin, Germany). This platform was mainly used for high-light/high-CO_2 (HL/HC) cultivation approaches of the *N. punctiforme* AraC_PKS1 mutant and WT. HL/HC cultivation approaches were started with a light intensity of 70 µmol photons $m^{-2} s^{-1}$ and a concentration of 3% CO_2. After cultivation for 7–10 days, the light intensity was increased to 120 µmol photons $m^{-2} s^{-1}$ and the CO_2 concentration was set to 6 %. The cultures were harvested after 20 days of cultivation.

2.2.1.3.3   Conventional Cultivation with High Density Supernatant

Conventionally grown *N. punctiforme* mutant reporter strains (see **Section 2.1.1.2**) were centrifuged for 5 min at 3,000 × g. The pellet was resuspended in 15 ml of HD culture supernatant from a 20 days old *N. punctiforme* WT high density cultivation. The cell suspension was supplemented with 2 µg/ml

streptomycin and transferred into a 35 ml cultivation flask. In parallel, the same strains were cultivated in $BG11_0$ media, supplemented with 2 µg/ml streptomycin as a control. After 1, 2 and/or 7 days of cultivation, all cultures were analyzed by confocal fluorescence microscopy.

2.2.1.3.4 Bioactivity-guided Assay

To analyze the influence of certain metabolites on *N. punctiforme* cultures, HPLC peaks were fractionated (see **Section 2.2.4.1**) and added to a target culture. Therefore, a metabolite amount equal to the volume of the target culture was collected, dried in a vacuum concentrator and dissolved in 80 µl of 60% methanol.

Reporter mutant strains were prepared by transferring 4 ml of a culture supplemented with fresh $BG11_0$ containing 2 µg/ml streptomycin into a 12-well plate. The cells were grown for 3–5 days under conventional cultivation conditions (see **Section 2.2.1.3.1**) on a rotary shaker (45 rpm). Then, the metabolite solution was added to the culture. As a control, 80 µl of 60% methanol were added to an additional culture. Cultures were analyzed by confocal fluorescence microscopy after 1, 2, 4 and/or 7 days.

N. punctiforme WT cultures were prepared by transferring 15 ml of a culture supplemented with fresh $BG11_0$ into a 35 ml cultivation flask. The cultures were grown for 3–5 days under conventional cultivation conditions (see **Section 2.2.1.3.1**) on a rotary shaker (45 rpm). Then, the metabolite solution was added to the culture. As a control, 80 µl of 60% methanol were added to an additional culture. After 1, 2, 4 and/or 7 days cultures were analyzed by HPLC analysis (see **Section 2.2.4.1**) and RT-qPCR (see **Section 2.2.2.16**), respectively.

2.2.1.4 Cryopreservation of *N. punctiforme*

Frozen stocks of all *N. punctiforme* strains were prepared by adding 5% (v/v) filter sterilized DMSO to a dense culture in a sterile manner. Afterwards, 1 ml of the prepared culture was added to a freezing vial. The stocks were stored at -80 °C.

2.2.1.5 Allelopathy Assay

2.2.1.5.1 Influence of Autocrine Factors on Cyanobacteria

N. punctiforme, the *Nostoc* strains KVJ2 and KVJ20 and/or *Anabaena sp.* PCC 7120 were used as indicator strains. Those were prepared by homogenization

in liquid $BG11_0$ media using a syringe. The cells were spread on a $BG11_0$ plate (1.2% bacto agar). Once the cell lawn had dried, a thin layer of semi-solid $BG11_0$ (0.7% bacto agar) agar was poured on top. Paper disks (5 mm) soaked in methanolic extracts (see **Section 2.2.3.1**) from pellet and supernatant of a *N. punctiforme* high density culture were placed on top of the agar. Alternatively, isolated metabolites, dissolved in 60% methanol, were tested. A paper disk with 10 µg streptomycin served as an antibiotic control and a disk soaked in 60% methanol served as a negative control. Plates were grown under standard cultivation conditions for 2–3 weeks.

To characterize a potential allelopathic effect of the AraC_PKS1 mutant against cyanobacteria, an alternative approach was used. Small culture droplets of the indicator strains (*N. punctiforme*, *Nostoc* KVJ2, *Nostoc* KVJ20, *Anabaena sp.* PCC 7120) were placed in close vicinity to droplets of the AraC_PKS1 mutant strain on a $BG11_0$ plate. The plates were grown under standard cultivation conditions for two weeks to visualize potential growth effects. Plates with single droplets of each culture served as a control. All samples were tested in triplicates.

2.2.1.5.2 Influence of Nostoclides N1 and N2 on Green Algae

The influence of the nostoclides N1 and N2 on the eukaryotic alga *Chlamydomonas reinhardtii* SAG 73.72 (*C. reinhardtii*) was tested in cooperation with the working group of Severin Sasso (University of Leipzig, Institute for Biology, Department of Plant Physiology, Leipzig, Germany).
A *C. reinhardtii* culture (from the SAG culture collection, Göttingen University, Germany) was cultivated for 2 days at 20 °C in tris-acetate-phosphate (TAP) medium [121]. Under continuous illumination with an intensity of 50 µmol photons m^{-2} s^{-1}, the culture was shaken at 200 rpm on an orbital shaker. The cell concentration was measured with a Coulter counter (Multisizer 4e, Beckmann Coulter, Brea CA, United States) equipped with a 30 µm capillary. A size range of 3.5–13 µm was used for the analysis. The culture was transferred to a 24-well plate (Greiner CELLSTAR, Kremsmünster, Austria) and each well was filled with 1 ml with an initial concentration of 2×10^6 cells/ml. *C. reinhardtii* cultures were treated with the nostoclides N1 and N2, dissolved in ethanol. Treated cultures had a final nostoclide concentration of 10 µM. A sample treated with ethanol only and an untreated sample served as controls. Cell concentrations were measured again after 24 h of incubation.

2.2.1.6 Chlorophyll Fluorescence Measurements

Chlorophyll fluorescence measurements of *C. reinhardtii* and *N. punctiforme* treated with the nostoclides N1 and N2 were done in cooperation with the working group of Severin Sasso (University of Leipzig, Institute for Biology, Department of Plant Physiology, Leipzig, Germany).

C. reinhardtii cultures were prepared as described in **Section 2.2.1.5.2**. A *N. punctiforme* pre-culture was mixed thoroughly before transferring the cultures to a 24-well plate (1 ml per well). The cell concentration of *N. punctiforme* could not be measured due to its filamentous growth.

C. reinhardtii cultures and *N. punctiforme* cultures were treated with the nostoclides N1 and N2 (final concentration: 10 µM). After 24 h, chlorophyll fluorescence was determined with a Pulse-amplitude modulated (PAM) fluorometer (PAM101/103, Walz, Effeltrich, Germany) following the saturating pulse method [122]. Saturating pulses with a light intensity of 3500 µmol photons $m^{-2}\,s^{-1}$ and a duration of 800 ms were applied. Samples were diluted with 500 µl of their respective media and were placed in the dark for 5 min. Subsequently, the maximum quantum yield of photosystem II (PSII; Fv/Fm) was measured. Then, the samples were illuminated with 700 µmol photons $m^{-2}\,s^{-1}$ for 3 min, followed by another illumination step with 2000 µmol photons $m^{-2}\,s^{-1}$ for 3 min. Afterwards, the effective PSII quantum yield (Fv′/Fm′) was measured. The software GraphPad Prism 9 was used for statistical analyses.

2.2.1.7 Confocal Fluorescence Microscopy

N. punctiforme reporter mutant strains, expressing CFP, were observed alive. A sample of 15 µl was directly pipetted onto a glass slide and cloaked with a cover slide. Confocal microscopy was performed on a Zeiss LSM 780 (see **Section 2.1.13**). A PlanApo 1.4/63× oil immersion objective and filter presets for eCFP and chlorophyll α (excitation at 405/633 nm, detection at 450–550 nm / 650–725 nm) were used. For operating the microscope and image acquisition, the Zen software (version 2.3) was used. The Zen blue edition software (version 2.3, lite) was used for image processing.

2.2.2 Molecular Biological Methods

2.2.2.1 Isolation of Genomic DNA from *N. punctiforme*

To isolate genomic DNA from *N. punctiforme*, 20 ml of a dense, but healthy culture were harvested by centrifugation at 1,000 × g for 5 min at room temperature. For the removal of polysaccharides, the cell pellet was washed twice with 5 M NaCl. Then, the pellet was resuspended in 1 ml TE buffer. A spatula tip full of lysozyme was added. The suspension was mixed by inverting the tube gently several times and incubated at 37 °C for 1 h. During that time, the mixture was inverted periodically. After incubation, 500 µl 0.5 M EDTA, 1 ml of a Proteinase K solution (2 mg/ml in TE buffer) and 100 µl 20% SDS were added and the suspension was mixed by inverting the tube gently. The mixture was incubated for another hour at 37 °C and inverted periodically during that time. Then, 1/6 × Vol of 5 M NaCl and 1/8 × Vol CTAB solution (10% (v/v) CTAB, 0.7 M NaCl in ultrapure water) were mixed into the suspension. After an incubation step at 65 °C for 10 min, the suspension was centrifuged at 13,000 × g for 5 min at room temperature to pellet the cell debris. The supernatant was transferred into a new tube and extracted once with 1 × volume of chloroform. For the precipitation of DNA, 2 × Vol 95 % ethanol was added and the mixture was incubated overnight at -20 °C.

On the next day, the mixture was centrifuged at 13,000 × g for 5 min at 4 °C. The resulting DNA pellet was resolubilized in 500 µl TE buffer and transferred into a micro centrifuge tube. The DNA was extracted with 1 × Vol Phenol:Chloroform (1:1), followed by a centrifugation step at 13,000 × g for 2 min. The extraction of the aqueous phase was repeated until the phase was clear. The DNA was precipitated by adding 1/10 × Vol 3 M sodium acetate and 2 × Vol 95% ethanol to the aqueous phase, followed by centrifugation at 13,000 × g for 2 min at 4 °C. The DNA pellet was washed twice with 70% ethanol. Afterwards, the ethanol was removed and the dried DNA pellet was dissolved in 50 µl of ultrapure water. For RNA removal, 1 µl of RNase A/T1 mix was added to the DNA and incubated for 1 h at 37 °C. The dissolved DNA was stored at 4 °C.

2.2.2.2 PCR - Polymerase Chain Reaction

To amplify desired DNA fragments, a PCR was performed. A typical PCR reaction mixture contained:

0.02 U/µl	DNA polymerase
20–50 ng	Template
0.5 µM	Reverse primer
0.5 µM	Forward primer
200 µM each	10 mM dNTPs
10 (4) µl	5× Phusion GC buffer (green)
up to 50 (20) µl	Ultrapure water

Either genomic DNA or plasmid DNA was used as template. PCR reaction mixtures were placed into a thermal cycler and the following PCR protocol was executed:

TABLE 2.5: **PCR cycling conditions**
A typical PCR program consists of five consecutive reaction steps, each with a certain temperature, duration and number of cycles.

Step	Temperature [°C]	Time [min]	Cycles
Initial denaturation	98	3	1
Denaturation	98	0.5	
Annealing	Primer dependent	0.5	35
Extension	72	0.5 per kb	
Final extension	72	10	1
Storage	12	∞	1

To validate and purify the amplified DNA fragments, a agarose gel electrophoresis (see **Section 2.2.2.3**) was performed.

Colony PCR was used for rapid detection of positive clones after transformation of *E. coli* (see **Section 2.2.2.7**). Therefore, a small fraction of an *E. coli* colony was used as template for the PCR. The Maxima™ Hot Start Green 2× PCR Master Mix was used and 10 µl PCR reaction mixtures were prepared as follows:

5 µl	Maxima™ Master Mix
1	*E. coli* colony (picked from plate)
0.5 µM	Reverse primer
0.5 µM	Forward primer
up to 10 µl	Ultrapure water

For the colony PCR, the temperature of the denaturation steps was lowered to 95 °C and the initial denaturation step was prolonged to 10 min. The PCR was validated by agarose gel electrophoresis.

2.2.2.3   Agarose Gel Electrophoresis

DNA and RNA fragments were separated regarding their size by using agarose gel electrophoresis. Depending on the fragment size, an appropriate agarose concentration between 1% to 2% was chosen. The desired amount of agraose was dissolved in $1\times$ TAE buffer by boiling up in a microwave oven. To visualize nucleic acids by UV-illumination after electrophoresis, ethidium bromide was added to the dissolved agarose with a final concentration of 0.05 mg/ml. Solidified agarose gels were immersed in $1\times$ TAE buffer and then loaded with nucleic acid samples. If not already included due to prior experiments, a loading dye (see **Section 2.1.6**) was mixed into the samples. As a size standard a DNA ladder (see **Section 2.1.6**) was used. Agarose gels were run for 20–30 min at constant voltage between 100–120 V, depending on the gel size. After electrophoresis, the ChemiDoc XRS+ was used in combination with Image Lab™ (version 5.2, Bio-Rad laboratories) for signal visualization and image processing.

2.2.2.4   DNA Extraction from Agarose Gels

DNA extraction from agarose gels was carried out using the GeneJET Gel Extraction Kit (see **Section 2.1.11**) according to manufacturer's instructions. The extracted DNA was eluted with 30 µl ultrapure water.

2.2.2.5   Restriction Digestion

For DNA cleavage, FastDigest restriction enzymes were used. A typical reaction mixture contained:

1 µg–3µg	Plasmid DNA
1 µl	FastDigest restriction enzyme
3 µl	$10\times$ FastDigest buffer
up to 30 µl	Ultrapure water

If the cleaved DNA was to be used in an assembly reaction (see **Section 2.2.2.6**), 1 µl of FastAP was added to the reaction mixture to prevent recirculization of the cleaved plasmid DNA during the assembly reaction. The reaction mixture

was incubated for 1 h at 37 °C. Afterwards, the digested DNA was visualized on an agarose gel (see **Section 2.2.2.3**) and extracted (see **Section 2.2.2.4**).

2.2.2.6   DNA Assembly

To prepare cloning vectors containing a desired gene sequence, either the NEBuilder® HiFi DNA Assembly or the Hot Fusion assembly method (see **Section 2.1.10**, [123]) was used. Both methods are based on homologous recombination. Therefore, DNA fragments with overlapping vector sequences at their ends (at least 25 bp) are needed. Appropriate primers were designed with the "Primer3web" software (version 4.1.0, [124]). PCR products were visually validated by agarose gel electrophoresis (see **Section 2.2.2.3**) and extracted from the gel afterwards (see **Section 2.2.2.4**). A linearized vector, the DNA fragments (inserts) and one of the assembly master mixes were put together in one reaction tube. A typical mixture contained:

50 ng	Linearized vector
3–10× equimolar amount of vector	Insert
5 µl	2× Assembly MM (Hot Fusion/HiFi)
up to 10 µl	Ultrapure water

The tubes were incubated at 50 °C for 50 min in a thermocycler. The assembled DNA was directly used for transformation.

2.2.2.7   Transformation of *E. coli*

Transformation was performed by using chemically competent *E. coli* Xl-1 blue cells. Therefore, an aliquot of 50 µl cell suspension was thawed on ice. Afterwards, half the volume of an assembly mixture (see **Section 2.2.2.6**) or 1 µl of an already ligated plasmid was added to the cells. The suspension was mixed by inverting the tube carefully. After keeping the mixture on ice for 30 min, a heat-shock at 42°C for 1 min in a water bath was carried out. Then, 500 µl SOC medium (see **Section 2.1.2**) was added and the cell suspension was incubated for 1 h at 37 °C and 220 rpm. Cells were spread on selective plates (see **Section 2.2.1.1**) and incubated overnight at 37 °C. On the next day, a colony PCR (see **Section 2.2.2.2**) was performed. Potentially positive colonies were picked and cultivated overnight in 5 ml selective LB media (see **Section 2.2.1.1**) at 37 °C.

For further validation, transformed plasmids were isolated (see **Section 2.2.2.8**) and sequenced (see **Section 2.2.2.10**).

2.2.2.8 Plasmid Isolation from *E. coli*

The isolation of plasmid DNA from *E. coli* cultures was carried out using the GeneJet Plasmid Mini Prep Kit (see **Section 2.1.11**) according to manufacturer's instructions. The isolated plasmid DNA was eluted with 40 µl ultrapure water.

2.2.2.9 DNA and RNA Quantification

The concentrations of DNA and RNA in aqueous solutions were measured using the Nanodrop™ 2000 spectrophotometer (see **Section 2.1.13**) as instructed by the manufacturer.

2.2.2.10 DNA Sequencing

Sequencing of DNA was conducted by GATC Biotech (Cologne, Germany) or LGC Genomics (Berlin, Germany). DNA samples were prepared as instructed by the different companies.

2.2.2.11 Transformation of *N. punctiforme*

2.2.2.11.1 Electroporation

To introduce pre-assembled plasmid-constructs, such as (over)expression plasmids, into *N. punctiforme*, electroporation was performed as described below.

A sufficient amount of a dense, but healthy *N. punctiforme* culture was harvested by centrifugation at 2,000 $\times$ g for 5 min. The cells were washed four times with sterile water. Afterwards, cells were resuspended in 400 µl ultrapure water per planned transformation sample and held on ice until needed. Tubes, containing 10 µg of desired plasmid DNA, were prepared on ice. To each tube, 400 µl of *N. punctiforme* cell suspension was added and mixed by pipetting. Subsequently, the mixture of one tube was transferred into a precooled electroporation cuvette. The electroporation was performed with an electroporator (Micropulser™, Bio Rad) by using the following conditions: 4 ms, 1.5 kV, 1 puls. Cells were spread on filter-covered $BG11_0$ (+5 mM $NaHCO_3$) plates and placed under low light (10 μE $m^{-2}s^{-1}$) for 2 days. Typically, every electroporation sample was prepared in triplicates together with an additional negative control, carrying no plasmid. Afterwards, the plates were placed under standard light conditions (30 μE $m^{-2}s^{-1}$) for 5–7 days until cell growth was visible. For selection of mutants, the filters were

transferred onto selective $BG11_0$ (+5 mM $NaHCO_3$) plates containing 2 µg/ml streptomycin. After 2–3 weeks, the cellular background of the non-resistant cells died off and resistant colonies appeared on the plate. For further growth, those colonies were transferred into liquid $BG11_0$ media. The genotype of the potential mutants was tested by isolation of total DNA by using the GenElute™ Plant Genomic DNA Miniprep Kit with a subsequent PCR amplification. To confirm the presence of a replicating plasmid (pRL1049 as plasmid backbone), the primer pair D021_S1/D022_S2 (see **Section 2.1.5**) was used.

2.2.2.11.2   Triparental Conjugation

Triparental conjugation is another method for the introduction of genetic material into *N. punctiforme*. This method is preferred when genomic DNA needs to be modified by gene replacement, knockout or integration of genetic material.

One day before the triparental conjugation, an appropriate amount of *N. punctiforme* was sonicated briefly ($2\times$ [pulse on: 6 sec, pulse off: 3 sec, 20% amplitude]). The cells were washed once with fresh $BG11_0$ media. The culture regenerated overnight in fresh $BG11_0$ media.
Additionally, donor *E. coli* strains, containing the desired plasmid, and the *E. coli* mobilizer strain J53 (RP4) were grown separately overnight in selective LB media.

On the next day, all *E. coli* cultures were diluted (1:40) with fresh LB media. *E. coli* cells were grown until reaching an OD_{600nm} of 0.7–0.8. Then, cells were centrifuged at 1,000 $\times$ g for 10 min and washed once with plain LB media. The supernatant was removed and *E. coli* cell pellets were resuspended to an OD_{600nm} of 9–10 with fresh LB media. Equal amounts (250 µl) of donor and mobilizer cells were combined in a microcentrifuge tube, gently mixed and incubated for 90 min at 30 °C in the dark.
The regenerated *N. punctiforme* culture was centrifuged for 10 min at 1,000 $\times$ g. The cell pellet was resuspended in 500 µl fresh $BG11_0$ media per planned conjugation sample. To each tube containing the already incubated *E. coli* mixture, 500 µl of *N. punctiforme* cell suspension was added. The cell suspension was mixed gently by inverting the tubes and centrifuged for 30 sec at 8,000 $\times$ g. Half of the supernatant was removed and the cell pellet was resuspended in the remaining supernatant. Cells were spread on filter-covered $BG11_0$ (with 0.5% LB media and 5 mM $NaHCO_3$) plates and incubated at low

light (10 µE $m_{600nm}s^{-1}$) for 2 days. Afterwards, filters were transferred to
$BG11_0$ (5 mM $NaHCO_3$) plates and placed under standard light conditions
(30 µE $m^{-2}s^{-1}$) for 5–7 days until cell growth was visible. For selection of
mutants, the filters were transferred onto selective $BG11_0$ (+ 5 mM $NaHCO_3$)
plates containing 2 µg/ml streptomycin. After 2–3 weeks, the background
died off and resistant colonies appeared on the plate. For further growth,
those colonies were transferred into liquid $BG11_0$ media. The genotype
of the potential mutants was tested by isolation of total DNA by using
the GenElute™ Plant Genomic DNA Miniprep Kit and a subsequent PCR
amplification. To confirm the presence of a replicating plasmid, (pRL1049 as
plasmid backbone) the primer pair D021_S1/D022_S2 (see **Section 2.1.5**) was
used. In case of a knockout, the primer pair D064_S7/D064_S8, amplifying the
streptomycin resistance cassette, was used.

2.2.2.12   TRIzol RNA Extraction from *N. punctiforme*

For RNA extraction with TRIzol, 100–200 mg (wet weight) of a freshly
harvested *N. punctiforme* culture were used. Pelleted cells were dissolved in
1 ml TRIzol. The mixture was flash frozen in liquid nitrogen, subsequently
the samples were incubated at 65 °C for 20 min at 1400 rpm. Then, 200 µl
chloroform was added to each sample and the mixture was incubated for 4 min
at 65 °C and 1400 rpm. For phase separation, samples were centrifuged at
11,000 × g for 15 min at 4 °C. The aqueous phase was transferred to a fresh
tube and mixed with 0.35 × Vol isopropanol and 0.35 × Vol salt solution (0.8 M
sodium citrate, 1.2 M NaCl). The samples were incubated for 30–60 min at
room temperature. Afterwards, the samples were centrifuged at 11,000 × g
for 10 min at 4 °C. The supernatant was discarded and the pellet was washed
with 1 ml 80% ethanol. After centrifugation at 7500 × g for 5 min at 4 °C, the
supernatant was discarded and the remaining pellet was dried for 10–15 min
at room temperature. The pellet was dissolved in 40 µl autoclaved and
DEPC-treated ultrapure water. For complete resuspension, the samples were
incubated for 10 min at 55 °C and 850 rpm.

2.2.2.13   RNA Quality Control and Purification

A control PCR was performed to make sure that no genomic DNA remained
in the RNA samples. The control PCR was conducted analogous to the
colony PCR setup (see **Section 2.2.2.2**), with the exception that 20 ng of crude
RNA was used as template. The primer pair rnpB_RT3_FW/rnpB_RT3_RV,

amplifying the housekeeping gene *RnpB*, was used. The results of the PCR were visualized by an agarose gel electrophoresis (see **Section 2.2.2.3**). If genomic DNA was still present in the samples, either the RNeasy™ Mini Kit or the Turbo DNA-*free*™ Kit was used according to the respective instructions of the manufacturer to remove gDNA and purify the RNA isolates. Afterwards, the purity of the samples was tested again by PCR. Purified gDNA-free RNA was stored at -80 °C.

2.2.2.14   RNA Sequencing

Whole RNA sequencing, including RNA quality control and rRNA depletion, was conducted by Novogene (Cambridge, United Kingdom). RNA samples were prepared as instructed by the company. Novogene performed the RNA sequencing on an Illumina Novaseq 6000 with a PE150 platform. For data processing of the raw sequencing data, the tools provided by the Galaxy web platform and its public server [125] (usegalaxy.eu) were utilized. To map paired-end reads from the raw sequencing DNA to the *N. punctiforme* reference genome (Genbank GCA_000020025.1; RefSeq GCF_000020025.1), the HISAT method (version 2.1.0) [126] was used. Unmapped reads and reads smaller than 20 bp were removed from the mapped reads by using a BAM filter (version 0.5.9). With HTSeq (version 0.9.1) [127] the filtered reads were counted. The counted reads were further processed outside the Galaxy web platform by using the R (version 4.02) [128] package DESeq2 (version 1.30.1) [129]. The package was used to normalize the data and to calculate $\log_2$ fold changes and p-values.

2.2.2.15   cDNA Synthesis

The synthesis of cDNA from RNA samples was carried out using the Maxima™ H Minus cDNA synthesis kit (see **Section 2.1.11**) according to the instructions of the manufacturer. For the cDNA synthesis, up to 1.5 µg of RNA was used. If not used immediately for PCR or RT-qPCR, the cDNA was stored at -80 °C.

For validation of the cDNA synthesis, a PCR (see **Section 2.2.2.2**) with primers for the housekeeping gene *rnpB* and 1 µl of the synthesized cDNA was performed. Afterwards, the PCR products were loaded on a 2% (w/v) agarose gel and visually validated by gel electrophoresis (see **Section 2.2.2.3**).

2.2.2.16   RT-qPCR - Real-Time Quantitative PCR

For semi-quantitative analysis of gene expression levels, a real-time quantitative PCR (RT-qPCR) was performed. For each gene that was to be tested, specific primer pairs were designed. Those had a melting temperature of around 60 °C and amplified an amplicon with a size between 100–150 bp. All RT-qPCR primers are listed in **Table 2.1.5.2**. For the reaction, cDNA (see **Section 2.2.2.15**) was used as template. A typical 10 µl RT-qPCR reaction mixture contained:

5 µl	2× Blue S'Green qPCR mix
0.5 µM	Forward primer
0.5 µM	Reverse primer
1 ng	cDNA
up to 10 µl	Ultrapure water

Initially, a cDNA-water mixture was loaded into a 96 well plate. Then, the Blue S'Green qPCR mix was premixed with prepared primer solutions and the mixture was added to the corresponding well, already containing cDNA. All steps involving the dye containing Blue S'Green qPCR mix were performed in darkness, to reduce light exposure prior to the RT-qPCR. The final plates were sealed with an adhesive optical film (BZO Seal Film, Biozym, Germany), to reduce contamination and evaporation of the samples. For each biological sample, three replicates were prepared. The RT-qPCR was performed by using the RT-qPCR system LightCycler®96 with the following protocol:

TABLE 2.6: **RT-qPCR cycling conditions**

Step	Temperature [°C]	Time [sec]	Cycles
Initial denaturation	95	120	1
Denaturation	95	5	
Annealing/Extension	60	20	45
	95	10	
Melting	65	60	1
	97	1	
Storage	37	∞	1

The results of the RT-qPCR were analyzed with the LightCycler®96 application software (version 1.1.0.1320, 2011) and fold changes were calculated and visualized with R [128] (see **Section 2.2.2.18**).

2.2.2.17 Calculation of RT-qPCR Primer Efficiencies

The accumulation of a fluorescence signal is used to quantify the DNA during RT-qPCR. Therefore, C_t (cycle threshold) values are used, which indicate the number of PCR cycles required to exceed the background fluorescence level. Here, the amount of DNA is inversely proportional to the C_t values, i.e. the lower the C_t values in the sample the higher is the amount of DNA in the sample.

To calculate reasonable log-fold changes using the $\Delta\Delta C_t$ method, primer pairs, used in the respective RT-qPCR, need to have an amplification efficiency between 90% and 110%. Primer efficiencies were determined by running a series of different cDNA amounts, including 0.1 ng, 1 ng and 10 ng, in an otherwise regular RT-qPCR analysis. Each primer pair, which should be used for subsequent transcriptional analysis, was tested against all mentioned cDNA amounts. Each sample was tested in technical triplicates. After performing the regular RT-qPCR protocol (see **Section 2.2.2.16**), the corresponding C_t values were determined by the LightCycler®96 application software (version 1.1.0.1320, 2011). The C_t values for each primer pair were plotted against the $\log_{10}$ (cDNA amount) and the slope m of the corresponding linear regression curve was calculated. Finally, primer efficiencies were calculated by using the following equation:

$$Efficiency\,[\%] = (10^{\frac{-1}{m}} - 1) \times 100$$

All primer pairs with efficiencies between 90% and 110% were accepted for transcriptional analysis.

2.2.2.18 Calculation of Fold Changes utilizing the $\Delta\Delta C_t$ Method

The $\Delta\Delta C_t$ method is used to calculate fold changes from the C_t values of the RT-qPCR. A fold change is the ratio of gene expression between two conditions and it is standardly used to visualize transcriptional differences between a sample and a control group. Beside the C_t values of the target gene, the C_t values of a housekeeping gene are needed, for every condition tested. In this study the housekeeping gene *RnpB* was used. The corresponding C_t

values were used as a reference to calculate ΔC_t values for every target gene under every condition, respectively.

$$\Delta C_{t\,target\,gene} = C_{t\,refernce\,gene} - C_{t\,target\,gene}$$

The ΔC_t values are used to calculate the differences between sample and control group, utilizing the following equation:

$$\Delta\Delta C_{t\,target\,gene} = \Delta C_{t\,target\,gene\,sample} - \Delta C_{t\,target\,gene\,control}$$

$\Delta\Delta C_t$ values represent the $\log_2$ fold changes between sample and control group. Hereby, the values of the control group are used as a reference. Therefore, values greater than zero indicate an upregulation and values less than zero indicate a downregulation of the transcription level in the sample group. $\Delta\Delta C_t$ values with absolute values of 1, indicate a doubling or halving of the transcript level. Usually, the threshold of $\pm$ 1 is used to define meaningful changes in the transcription level. To obtain fold changes instead of $\log_2$ fold changes the antilogarithm of the $\Delta\Delta C_t$ values is taken, as described beneath:

$$fold\,change\ = 2^{\Delta\Delta C_{t\,target\,gene}}$$

By taking the antilogarithm, the base level of the transcription level changes from 0 to 1. Therefore, fold changes with a value bigger than 1 indicate an upregulation and values between 1 and 0 indicate a downregulation in terms of the transcription in the sample group.

The standard deviation s of every ΔC_t value was calculated by using the standard deviation of the target and reference gene C_t values, calculated by the LightCycler®96 application software (version 1.1.0.1320, 2011), with the following equation:

$$s = \sqrt{(s_{target\,gene})^2 + (s_{reference\,gene})^2}$$

These values were used to define a confidence interval.

2.2.2.19   DNA synthesis

DNA synthesis of the modified and His-tagged precursor gene *RS25510* was conducted by the ProteoGenix company (Schiltigheim, France). DNA data and vector samples (pRL1049) were prepared as instructed by the company.

2.2.3 Biochemical Methods

2.2.3.1 *N. punctiforme* Sample Preparation for HPLC

N. punctiforme cells were harvested by centrifugation at 3,000 × g for 10 min. Culture supernatant and cell pellet were separated and both prepared for HPLC analysis.

The culture supernatant was purified using a Sep-Pak® Plus C18 cartridge (Waters GmbH). The cartridge was equilibrated with 2 ml 100% methanol and washed with 2 ml ultrapure water. Then, the culture supernatant was loaded onto the cartridge and washed once with 5% methanol. Matrix-bound metabolites were eluted with 100% methanol. The methanolic extract was dried in a vacuum concentrator. Dried extracts were dissolved in 200 µl 60% methanol, centrifuged and filtered with Acrodisc® Syringe filters (Pall GmbH). The cell pellet was resuspended in 10 ml ultrapure water. Cells were lysed on ice by sonification for 10 min (pulse on: 2 sec, pulse off: 3 sec, 60% amplitude). The cell debris was pelleted by centrifugation at 10,000 × g for 10 min. The cell pellet supernatant was purified using the same methods as for the culture supernatant.

2.2.3.2 Extraction and Purification of His-tagged Proteins from *N. punctiforme*

N. punctiforme cells were harvested by centrifugation at 3,000 × g for 10 min at room temperature. The resulting cell pellet was resuspended in 10 ml 1 M Tris-HCl (pH 7.5) and centrifuged again for 10 min at 3,000 × g. The supernatant was removed and the cell pellet was resuspended in 15 ml lysis buffer (see **Section 2.1.10**). Imidazol with a final concentration of 10 mM was added to the mixture. Additionally, PMSF with a final concentration of 1 mM was added to prevent protein degradation. Cells were lysed by sonification for 15 min (pulse on: 2 sec, pulse off: 2 sec, 65% amplitude), followed by a centrifugation step for 20 min at 10,000 × g and 4 °C. In the meantime, nickel(Ni)-NTA-agarose was prepared. For that, 1 ml of Ni-NTA-agarose was centrifuged at 13,000 × g for 1 min. The resulting agarose pellet was washed twice with 1 M Tris HCl (pH 7.5). Finally, the Ni-NTA-agarose pellet was resuspended in lysis buffer (1:1). The supernatant and pellet of the lysed cells were separated and treated individually.
The supernatant was mixed with 1/50 × Vol Ni-NTA-agarose and rotated for 1 h at 4 °C to bind His-tagged proteins to the agarose. Afterwards, the

mixture was centrifuged for 5 min at 4600 $\times$ g and 4 °C. The supernatant was transferred into a fresh tube and the pellet was washed twice with 5 ml lysis buffer containing 20 mM imidazol. Again, supernatants were transferred into fresh tubes. The pellet was eluted twice with 200 µl lysis buffer containing 250 mM imidazol and a third time with 200 µl lysis buffer containing 500 mM imidazol. Again, the supernatants were transferred into fresh tubes. The tubes were stored at 4 °C, until analyzed by SDS-page (see **Section 2.2.3.3**).

The pellet of the cell debris was resuspended in 1 ml of buffer B (see **Section 2.1.10**) and incubated for 1 hour at room temperature. The suspension was centrifuged for 5 min at 13,000 $\times$ g at room temperature. The supernatant was transferred into a fresh tube and stored at 4 °C, until analyzed by SDS-PAGE (see **Section 2.2.3.3**).

2.2.3.3   SDS-PAGE - SDS Polyacrylamide Gel Electrophoresis

Proteins and peptides were separated with respect to their size by SDS polyacrylamide gel electrophoresis (SDS-PAGE). Usually a 15% SDS-PAGE gel containing the following ingredients was prepared:

TABLE 2.7: **Composition of SDS-PAGE gels**
An SDS-PAGE gel consists of a running gel with a stacking gel on top.

	Running gel	Stacking gel
5$\times$ SDS gel buffer	1 ml	0.4 ml
40% Acrylamide	1.9 ml	0.25 ml
Ultrapure water	2.1 ml	1.35 ml
10% APS	50 µl	20 µl
Temed	5µl	5µl

Before loaded onto the gel, the protein samples were prepared by adding 5$\times$ SDS loading dye (see **Section 2.1.6**), followed by an incubation at 95 °C for 5 min. A protein ladder (see **Section 2.1.6**) was used as a size standard. SDS-PAGE gels were completely immersed in MOPS running buffer (see **Section 2.1.10**) and ran for 40 min at a constant voltage of 200 V in a Mini-PROTEAN® electrophoresis cell. Gels were either stained or kept for further analysis.

For the visualization of protein signals, the gels were stained. The gels were washed once with water and boiled up twice while floating in water to get

rid of the SDS. The gels were stained with Coomassie staining solution (see **Section 2.1.10**) for several hours or overnight. Then, the gels were washed with water and destained with destainer (see **Section 2.1.10**) for 1 hour.

2.2.3.4 Western Blot

To verify the presence of desired His-tagged proteins, a western blot analysis was performed. After accomplishing an SDS-PAGE, proteins were transferred from the SDS-PAGE gels onto a nitrocellulose membrane for immunodetection. The blotting was performed using the Mini Trans-Blot® Cell system and the blot sandwich was prepared according to the instructions of the manufacturer. Blots were run at a constant voltage of 80 V for 1 hour. After transfer, the membrane was blocked in 5% (w/v) powdered milk in TBS-T for 30 min at 4 °C. During the blocking the membrane was gently shaken. The membrane was rinsed twice with TBS-T. Primary antibodies (Anti-polyHistidine, see **Section 2.1.8**) were diluted 1:10,000 in TBS-T. The membrane was covered in primary antibody solution and gently shaken overnight at 4 °C. On the next day, the membrane was washed twice with TBS-T for 10 min at 4 °C. Secondary antibodies (Anti-mouse, see **Section 2.1.8**) were diluted 1:10,000 in TBS-T. The membrane was incubated in secondary antibody solution for 1 hour at room temperature. Finally, the membrane was washed four times with TBS-T for 5 min. Visualization of band signals was performed using the SERVA*Light* Polaris Chemiluminescence Kit according to manufacturer's instructions in combination with a ChemiDoc XRS$^+$ imaging system.

2.2.4 Chemical Analyses

2.2.4.1 HPLC Analysis

The HPLC analysis was carried out by using a Shimadzu HPLC system (see **Section 2.1.13**). A sample volume of 20–50 µl was injected and loaded on a SymmetryShield RP18 column (3.5 µm, 4.6 mm × 100 mm) and a SymmetryShield Sentry Guard column (3.5 µm, 3.9 mm × 20 mm). As mobile phases, 0.05% TFA in ultrapure water (solvent A) and 0.05% TFA in acetonitrile (solvent B), were used. The following gradient conditions were used at a flow rate of 1 ml/min: equilibration with 20% solvent B for 1 min, linear gradient to 60% solvent B in 35 min, followed by a linear gradient to 100% solvent B in 1 min, finally solvent B was reduced to 20% in 4 min. For a stronger separation of hydrophilic compounds, the following gradient conditions were used at

a flow rate of 1 ml/min: equilibration with 2% solvent B for 1 min, linear gradient to 60% solvent B in 40 min, followed by a linear gradient to 100% solvent B in 2 min and holding 100% solvent B for 3 min, finally solvent B was reduced to 2% in 5 min. Absorption spectra were recorded simultaneously at $\lambda = 199$ nm and $\lambda = 350$ nm.

For peak sampling, one of the gradient conditions was chosen based on polarity of the desired compound. Usually, a sample volume of 50 µl was used. Fractionated compounds were either analyzed by MALDI-TOF mass spectrometry (see **Section 2.2.4.2**) or added to a *N. punctiforme* culture to analyze the transcriptional influence (see **Section 2.2.1.3.4**).

Preparative HPLC of the AraC_PKS1 mutant strain was conducted by Keishi Ishida (Leibniz Institute for Natural Product Research and Infection Biology, Hans Knöll Institute, Jena, Germany) using the settings described below.

For preparative HPLC, a Shimadzu preparative HPLC system (Shimadzu, Jena, Germany) was used. Samples were loaded onto a Symmetry C18 column (5 µm, 3.9 mm $\times$ 150 mm, Waters GmbH, Eschborn, Germany). As mobile phases, ultrapure water (solvent A) and acetonitrile (solvent B) were used with the following gradient conditions at a flow rate of 1 ml/min: equilibration with 5% solvent B for 10 min, followed by a linear gradient to 99 % solvent B in 30 min. The concentration of 99% solvent B was kept for 1 min. UV spectra were recorded by a Shimadzu UV-1800 spectrophotometer (Shimadzu, Jena, Germany)

2.2.4.2   MALDI-TOF MS

Peak samples were dried in a vacuum concentrator and resuspended in 2 µl acetonitrile and 8 µl 0.1% TFA. As a matrix solution, 3 mg/ml HCCA, dissolved in 84% acetonitrile, 13% ethanol, 3% ultrapure water and 0.1% TFA was used. For MS analysis, 0.3 µl of the sample solution was spotted onto the stainless steel MALDI target plate and mixed with an equal amount of matrix solution. Dried samples were analyzed with the Microflex™LRF MALDI-TOF MS system in positive ionization mode. The laser power was set to 30%. Resulting data was recorded with the FlexControl software (version 3.0; Bruker, Billerica, MA, USA) and analyzed with the mMass software (version 5.5.0, [130]).

2.2.4.3 Isolation of Nostoclides (N1, N2), Nostovalerolactone, 9-Dehydronostovalerolactone and Prescytonemin

The following isolation and purification of the compounds, found in the supernatant and cell pellet of the AraC_PKS1 mutant strain, was conducted by Keishi Ishida (Leibniz Institute for Natural Product Research and Infection Biology, Hans Knöll Institute, Jena, Germany) as described below.

All purification steps were performed on a Shimadzu preparative HPLC system (Shimadzu, Jena, Germany). UV spectra were recorded by a Shimadzu UV-1800 spectrophotometer (Shimadzu, Jena, Germany).

Cell pellets (wet weight 9 g) from the AraC_PKS1 mutant strain, cultivated under HL/HC cultivation conditions (see **Section 2.2.1.3.2**), were resuspended in 200 ml 80 % methanol. The resuspended cells were lysed by sonification (BANDELIN SONOPULS HD2200 with sonotrode MS73 (BANDELIN electronic, Berlin, Germany)) for 2 min at 50% amplitude and room temperature. Afterwards, the extracts were centrifuged at 9000 × g for 15 min at 15 °C. The obtained cell pellet supernatant was extracted twice with 200 ml methanol. The methanolic extracts were dried in a vaccum concentrator. Dried extracts were dissolved in 200 ml 90% methanol and washed with 200 ml hexane. The obtained aquatic phase was further purified by flash column chromatography (2.5 × 6.0 cm, LiChroprep C18, 40–63 µm, Merck, Darmstadt, Germany). Extracts were eluted in multiple steps with 200 ml 20% methanol, 100 ml 50% methanol, 100 ml 100% methanol and 100 ml dichloromethane, respectively. The fraction eluted with 100% methanol was further purified by flash column chromatography (2.5 × 6.0 cm, LiChroprep C18, 40–63 µm, Merck, Darmstadt, Germany). Compounds were again eluted in multiple steps with 100 ml of 50% methanol, 70% methanol, 80% methanol and 100% methanol, respectively. The fraction eluted with 80% methanol was further purified by reversed-phase HPLC (Nucleosil 100-7 C18, 21.2 × 250 mm, Machery-Nagel, Düren, Germany). For that, 0.1% TFA in ultrapure water (solvent A) and 83 % acetonitrile (solvent B) were used as mobile phases. The following gradient conditions were used at a flow-rate of 16 ml/min: equilibration with 20% solvent B for 10 min, linear gradient up to 100% solvent B within 40 min, finally this concentration was kept for 10 min. The compounds nostoclide N1 and N2 were fractionated and the fractions were further purified by reversed-phase HPLC (Nucleosil 100-7 C18, 10 × 250 mm) using an isocratic mobile phase and a flow-rate of 6 ml/min. The mobile phase contained equal amounts of 83 % acetonitrile and 0.1% TFA in ultrapure water.

From this final purification step, the compounds nostoclide N1 (530 µg) and nostoclide N2 (930 µg) were obtained.

Culture supernatant (500 ml) from the AraC_PKS1 mutant strain, cultivated under HL/HC cultivation conditions (see **Section 2.2.1.3.2**), was loaded on Amberlite XAD4 beads (3.0 × 7.0 cm, Sigma-Aldrich, Taufkirchen, Germany). The beads were washed with 150 ml ultrapure water and bound metabolites were eluted with 300 ml methanol, followed by 150 ml acetone. Both elutions and the nostovalerolactone-containing fraction from the cell pellet extraction were purified by reversed-phase HPLC (LiChroSpher WP300 RP-18, 10 × 250 mm, Merck, Darmstadt, Germany). For that, ultrapure water (solvent A) and acetonitril (solvent B) were used as mobile phases. The following gradient conditions were used at a flow-rate of 6 ml/min: equilibration with 5% solvent B for 10 min, linear gradient up to 45% solvent B within 20 min, finally the concentration of solvent B was increased to 100% within 10 min. From this purification step, the compound nostovalerolactone (16.8 mg) was obtained. Another fraction contained 9-dehydronostovalerolactone, which was further purified by reversed-phase HPLC (LiChroSpher WP300 RP-18, 10 × 250 mm). A mixture of 50 mM sodium phosphate (pH 7.5) and 50 mM Na_2SO_4 (solvent A) and acetonitril (solvent B) were used as mobile phases. The following gradient conditions were used at a flow-rate of 5 ml/min: equilibration with 20% solvent B for 10 min, followed by a linear gradient up to 100% solvent B within 40 min. Extracts were subjected to a SPE column (C18 ec, 1 g, Chromabond, Machery-Nagel) to obtain a small amount of 9-dehydronostovalerolactone (200 µg).

During the purification process of nostovalerolactone, a fraction containing the compound prescytonemin was obtained. This fraction was purified by reversed-phase HPLC (Nucleodur HTec, 10 × 250 mm, Machery-Nagel). An isocratic mobile phase containing 83% acetonitrile and 0.1% TFA in ultrapure water at a ratio of 55:45 and a flow-rate of 6 ml/min was used. From this purification step, the compound prescytonemin (200 µg) was obtained.

The obtained compounds were further analyzed by nuclear magnetic resonance (NMR) spectroscopy (see **Section 2.2.4.5**).

2.2.4.4   Isolation of Nostovalerolactone from 1-^{13}C and 1,2-[13]C$_2$ Sodium Acetate fed AraC_PKS1 Cultures

AraC_PKS1 mutant cultures with a volume of 100 ml were fed with 1-^{13}C and 1,2-[13]C$_2$ labeled sodium acetates (8 mg), respectively. Therefore, the cultures

were cultivated under HL/HC cultivation conditions (see **Section 2.2.1.3.2**). The cultures were fed with equal amounts of a 1:1 mixture of labeled and unlabeled sodium acetate (2 mg, each) on the 12th, 16th, 18th and 21st after inoculation. The cultures were harvested after 24 days.

The following compound purification by preparative HPLC was conducted by Keishi Ishida (Leibniz Institute for Natural Product Research and Infection Biology, Hans Knöll Institute, Jena, Germany).

The supernatants of the fed mutant cultures were loaded onto Amberlite XAD4 beads (2.0×7.0). The beads were washed with 75 ml ultrapure water and bound compounds were eluted in two steps with 150 ml methanol and 150 ml acetone, respectively. The methanol eluted fractions were purified by reversed phase HPLC (LiChroSpher WP300 RP-18, 10×250 mm). Ultrapure water (solvent A) and acetonitrile (solvent B) were used as mobiles phases. The following gradient conditions were used at a flow-rate of 6 ml/min: equilibration with 10% solvent B for 10 min, followed by a linear gradient up to 100% solvent B in 30 min. From this purification step, 1-^{13}C acetate labeled nostovalerolactone (9.3 mg) and 1,2-$^{13}C_2$ acetate labeled nostovalerolactone (5.9 mg) were obtained.

The obtained compounds were further analyzed by nuclear magnetic resonance (NMR) spectroscopy (see **Section 2.2.4.5**).

2.2.4.5   Structural Elucidation

The structural elucidation of the compounds found in the supernatant and cell pellet of the AraC_PKS1 mutant strain was conducted by Keishi Ishida (Leibniz Institute for Natural Product Research and Infection Biology, Hans Knöll Institute, Jena, Germany) as described below.

NMR spectroscopy data of the compounds found in AraC_PKS1 were recorded on an AVANCE III 500 MHz or 600 MHz spectrometer (Bruker Biospin, Rheinstetten, Germany). Obtained spectra were referenced to the residual solvent peak. As residual solvents, deuterated dimethyl sulfoxide (DMSO-d6), pyridine-d5 or methanol-d4 were used. Liquid chromatography - high resolution mass spectrometry (LC-HRMS) measurements were carried out on an Exactive or Q Exactive Orbitrap high performance benchtop device with an electrospray ion source and an Accela HPLC system (Thermo Fisher Scientific, Bremen, Germany). The used HPLC system consists of an autosampler with a column oven, a PDA detector and a 1250 pump (max. pressure = 1250 bar).

2.2.5 In Silico Analyses

2.2.5.1 Identification of Biosynthetic Gene Clusters

For identification and localization of biosynthtic gene clusters in the genome of *N. punctiforme*, the bioinformatic tool AntiSMASH (version 5.1.1, [54]) was utilized.

2.2.5.2 Nucleotide and Protein Sequence Analysis

Nucleotide and protein sequences were received from the NCBI database (National Center for Biotechnology Information, 2020 [131]). Nucleotide and protein sequences were analyzed with SnapGene® Viewer software (version 5.0.8, from Insightful Science; available at snapgene.com), ApE (version, 2.0.61, by M. Wayne Davis) and the software tools of NCBI BLAST [132, 133].

2.2.5.3 Design of Chemical Structures

Chemical structures were drawn with the ACD/ChemSketch software (freeware, version 12.01; Advanced Chemistry Development (ACD/Labs), Toronto, Canada).

2.2.6 Experimental Workflow

2.2.6.1 Detection of New Secondary Metabolites

To detect and identify new secondary metabolites, *N. punctiforme* WT and overexpression mutants were cultivated under different cultivation conditions, including conventional, high light and high carbon (HL/HC) and in case of the WT, also high density (HD) cultivation conditions. The cultures were analyzed as shown in **Figure 2.2**.
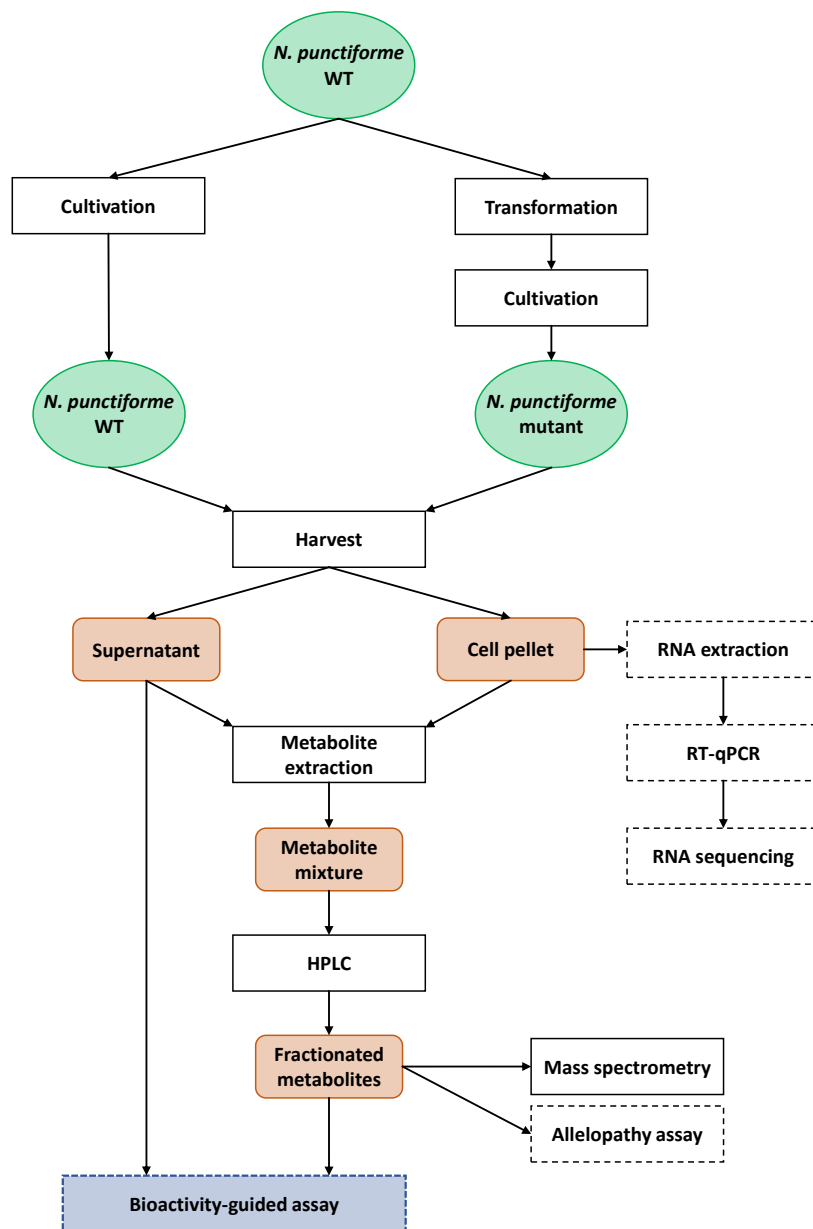
FIGURE 2.2: **Workflow for the detection of new secondary metabolites**
Dashed lines indicate experiments conducted only for selected samples.

2.2.6.2 Characterization of Potential Signaling Factors

Potential signaling factors were analyzed for further characterization like shown in the scheme (**Figure 2.3**) below:
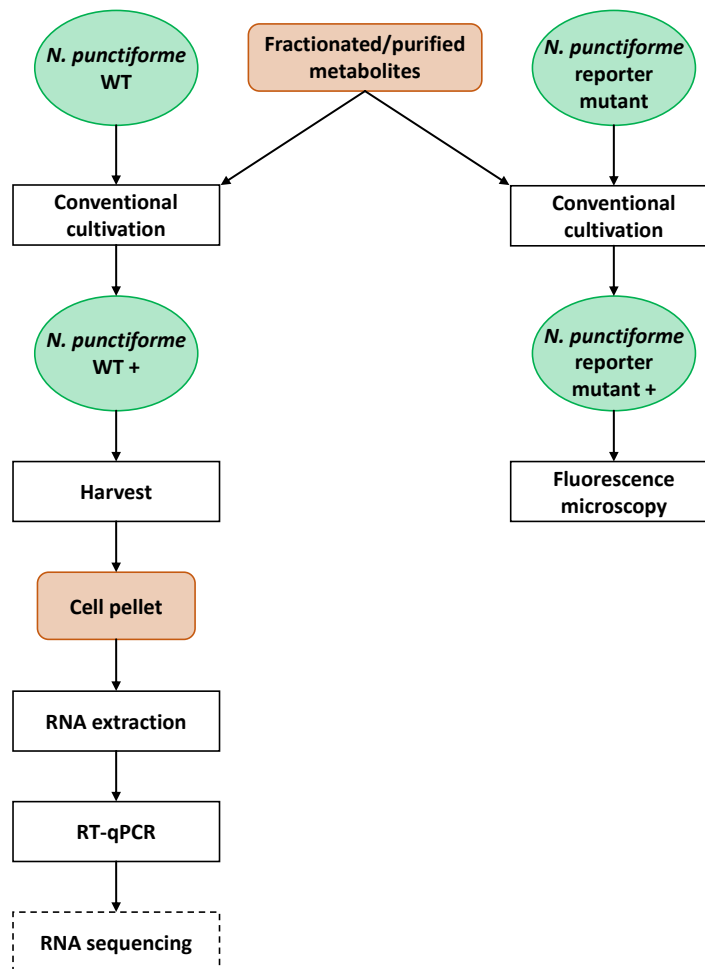
FIGURE 2.3: **Workflow for the analysis of newly detected secondary metabolites**
Dashed lines indicate experiments conducted only for selected samples.

2.2.6.3 Influence of High Density Cultivation on Gene Cluster Expression

To analyze the impact of high density cultivation on gene cluster expression, a set of reporter mutant strains, each reporting for one of the gene clusters, was utilized (see **Figure 2.4**).
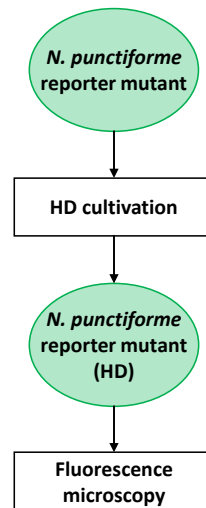
FIGURE 2.4: **Workflow to analyze the influence of HD cultivation by utilizing reporter mutant strains**

Chapter 3

Results

3.1 Mining the Genome of *N. punctiforme* for Biosynthetic Gene Clusters

Although the genome of *N. punctiforme* shows a large capability for the production of diverse secondary metabolites, information on its secondary metabolism is rather limited. However, the presence of a diverse setup of potential biosynthetic gene clusters (BGCs) and its amenability to genetic manipulation makes *N. punctiforme* a promising candidate for the establishment of new strategies for natural product discovery in cyanobacteria. To gain a comprehensive overview about *N. punctiformes* genetic potential, the genome (BioProject: PRJNA216; GenBank assembly accession: GCA_000020025.1, 2008) was mined for the presence of BGCs utilizing the web version of the genome mining platform AntiSMASH (version 4.1.0., later 5.1.2) [54, 134, 135]. AntiSMASH predicted a total number of 24 BGC regions located on chromosomal or plasmid DNA, including 15 BGCs belonging to the NRPS, PKS, NRPS-PKS hybrid or RIPP type, respectively. Predicted, but orphan BGCs were named arbitrarily.

A total of three PKS BGCs were identified (see **Figure 3.1**) by AntiSMASH. These gene clusters are referred to as *pks1* (genes: *NPUN_RS10390 – NPUN_RS10535*), *pks2* (genes: *NPUN_RS15970 – NPUN_RS16090*) and *pks3* (genes: *NPUN_RS17005 – NPUN_RS17085*).

PKS BGCs
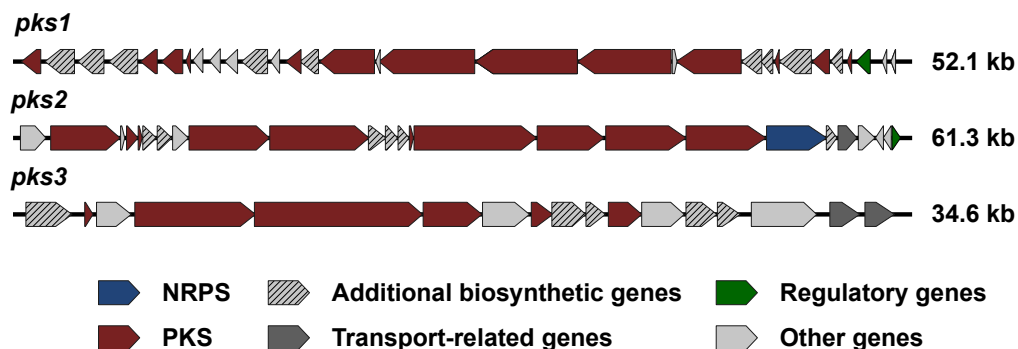
FIGURE 3.1: **PKS biosynthetic gene clusters detected in**
N. punctiforme **by AntiSMASH**

Additionally, four BGCs of the NRPS type were detected (see **Figure 3.2**), this included the already known gene clusters of anabaenopeptin (*apt*, genes: *NPUN_RS12350 – NPUN_RS12380*) and nostopeptolide (*nos*, genes: *NPUN_RS38830 – NPUN_RS11005*), as well as two cryptic gene clusters named *nrps1* (genes: *NPUN_RS15360 – NPUN_RS37610*) and *nrps2* (genes: *NPUN_RS36790 – NPUN_RS38145*). Unlike all other NRPS BGCs, *nrps2* is located on one of the endogenous plasmids of *N. punctiforme*.

NRPS BGCs
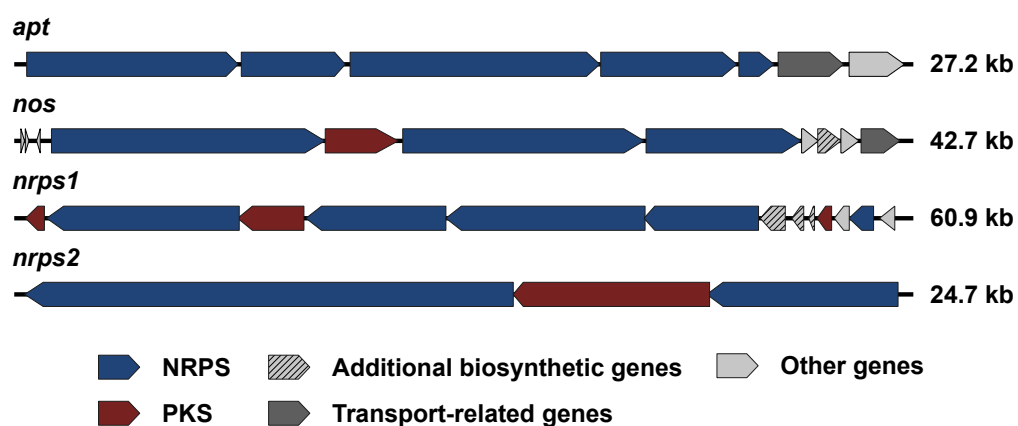
FIGURE 3.2: **NRPS biosynthetic gene clusters detected in**
N. punctiforme **by AntiSMASH**

Furthermore, AntiSMASH detected two hybrid BGCs, encoding genes for NRPSs and PKSs (see **Figure 3.4**). These gene clusters are referred to as *pks4* (genes: *NPUN_RS17290 – NPUN_RS17455*) and *pks5* (genes: *NPUN_RS33505 – NPUN_RS40215*).

NRPS-PKS hybrid BGCs
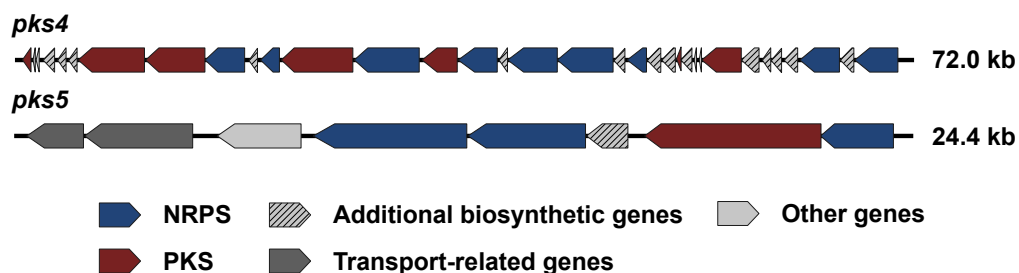
FIGURE 3.3: **NRPS-PKS hybrid biosynthetic gene clusters detected in *N. punctiforme* by AntiSMASH**

Finally, six BGCs of the RiPP type were predicted by AntiSMASH (see **Figure 3.4**), including the gene cluster of Microviridin (*mvd*, genes: *NPUN_RS38845 – NPUN_RS11030*) and five cryptic gene clusters that were named *ripp1a* (genes: *NPUN_RS16205 – NPUN_RS16255*), *ripp1b* (genes: *NPUN_RS16310 – NPUN_RS16355*), *ripp3* (genes: *NPUN_RS16780 – NPUN_RS40840*), *ripp4* (genes: *NPUN_RS25500 – NPUN_RS25545*) and *ripp5* (genes: *NPUN_RS34125 – NPUN_RS34155*). The BGCs of *ripp1a*, *ripp3*, *ripp4* and *ripp5* encode potential lanthipeptides, since all of them containing a gene that encodes the lanthipeptide synthetase LanM. The *ripp5* BGC is not located on the chromosome, but on one of the native plasmids.

Ripp BGCs
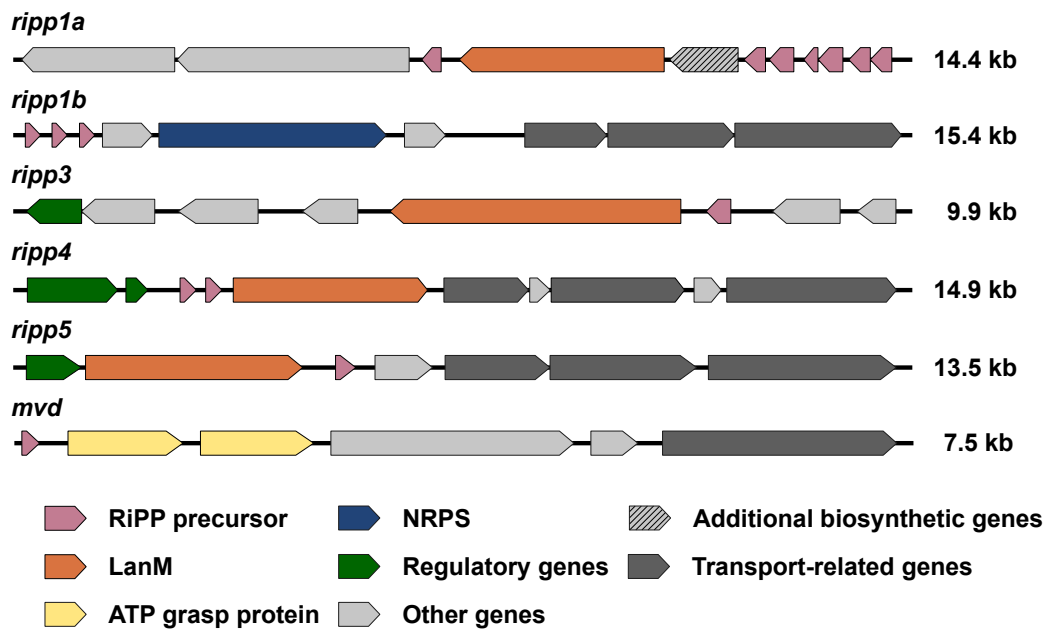
FIGURE 3.4: **RiPP biosynthetic gene clusters detected in**
N. punctiforme **by AntiSMASH**

3.2 Influences of High Cell Density on *N. punctiforme*

Cyanobacteria are typically considered as slow-growing organisms under conventional laboratory conditions, especially when compared to commonly used model organisms such as *E. coli* or yeast [136]. The growth of photoautotrophic organisms depends on light and inorganic carbon, but the sufficient supply and distribution of those within a the culture is complicated. In a conventionally grown dense culture, light attenuation is a major problem. Most of the light is absorbed by a thin surface layer, thus the majority of the culture is light-limited [137]. Another problem in dense cultures is the insufficient supply with inorganic carbon. Unfortunately, this problem cannot be solved by using media buffered with HCO_3^-, because this can result in an increased and therefore toxic pH level [137].

To overcome these problems and to optimize the growth of photoautotrophic organisms, a high density (HD) cultivation system for photoautotrophic organisms was recently developed [137]. By turbulent mixing of the culture and adjustable light intensities, light attenuation is prevented [137]. Sufficient amounts of inorganic carbon are provided by a membrane-mediated CO_2 supply [137]. This was achieved either by using an external CO_2 source or a bicarbonate buffer, releasing CO_2 from a separate compartment [120, 137]. The different cultivation setups that are used for cyanobacteria are depicted in **Figure 3.5**.
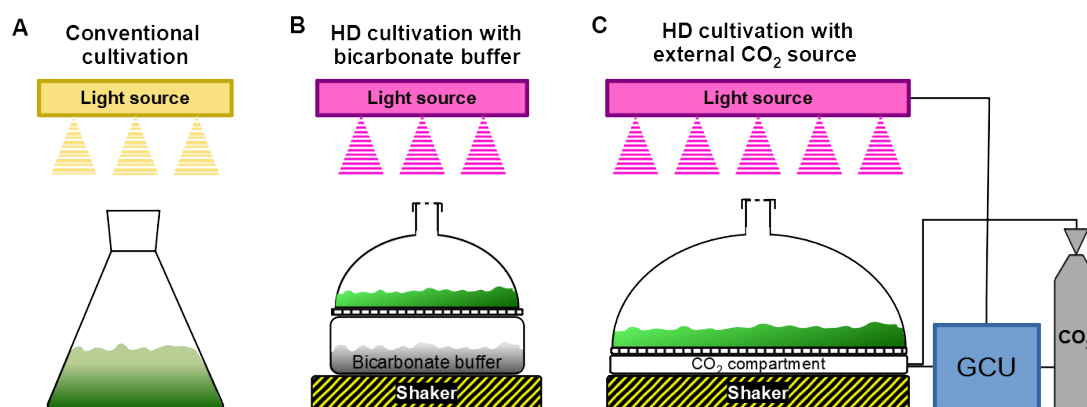
FIGURE 3.5: **Different cultivation setups for cyanobacteria**
(A) Conventional cultivation setup. A fluorescent tube with white light illumination is used as a light source. **(B)** High density (HD) cultivation setup using a bicarbonate buffer as CO_2 source. To maintain CO_2 supply the buffer has to be changed regularly. The setup uses a dimmable LED panel, with a growth-optimized light spectrum, as a light source. **(C)** High density cultivation (HD) setup using an external CO_2 source. The setup uses a dimmable LED panel, with a growth-optimized light spectrum, as a light source. The CO_2 concentration and the light intensity can be controlled and monitored by the Growth Control Unit (GCU). Schemes adapted from Lippi et al. 2018 [120].

A recent study by Guljamow et al. [110] showed that the cultivation of *N. punctiforme* at high cell densities has a strong influence on the expression of biosynthetic gene clusters. Additionally, this study revealed that small molecule natural products, accumulating in the supernatant of a high density (HD) culture, are able to trigger BGC expression, even under conventional growth conditions. This data strongly suggested that a cell density dependent signaling pathway could be involved in the regulation of BGC expression. To investigate these observations in more detail, several high density cultivation approaches were conducted and metabolic changes were analyzed by HPLC. To visualize transcriptional changes caused by high density cultivation, a reporter mutant strain library was utilized.

3.2.1   High Density Cultivation of *N. punctiforme* WT

In order to reproduce the findings described in Guljamow et al. [110], two high density cultivation approaches, referred to as HD1 and HD2, were conducted, utilizing a further developed culture vessel system of the CellDeg company (CellDeg GmbH, Berlin, Germany). Cultures were grown as described in **Section 2.2.1.3.2** with periodic exchange of the BG11$_0$ medium. The growth of the cultures was monitored by regular determination of the wet weight (see **Figure 3.6A**). The cultivation sample HD1 had an initial wet weight

of 0.7 g. Steady growth of the culture was observed until stagnation after 54 days. After increasing the light intensity from 600 µmol photons $m^{-2}\,s^{-1}$ to 800 µmol photons $m^{-2}\,s^{-1}$ on day 66, growth could be detected again. Further details on light intensities and CO_2 buffers used are summarized in **Appendix Table B.1**. The culture was harvested on day 69 with a final wet weight of 13.5 g.

The HD2 cultivation sample was inoculated with a cell mass of 4.8 g. After an initial stationary phase with no detectable growth, the culture showed strong growth from day 17 until day 45. Then, the detected cell mass decreased. After increasing the light intensity from 600 µmol photons $m^{-2}\,s^{-1}$ to 800 µmol photons $m^{-2}\,s^{-1}$ on day 52, growth was visible again. Further details on light intensities and CO_2 buffers used are shown in **Appendix Table B.2**. The culture was harvested on day 55 with a final wet weight of 24.3 g. Although HD2 has grown 14 days less than HD1, the cultures final wet weight was almost twice as big as the HD1 wet weight. This shows that the amount of cell mass used for the inoculation is not only influencing the growth behavior at the beginning of the cultivation, but also over a long period of time.
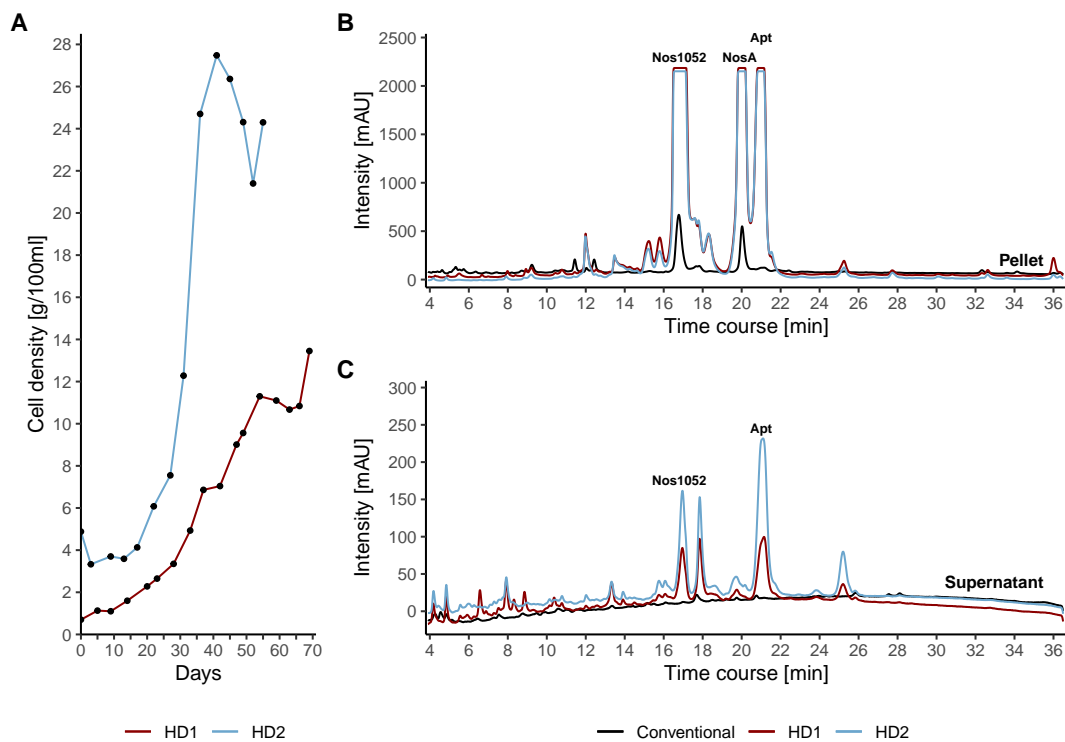
FIGURE 3.6: **Analysis of high density cultivation approaches of *N. punctiforme* with media exchange**
(A) Growth curves of HD1 and HD2. **(B)** HPLC profiles of cell pellet extracts. **(C)** HPLC profiles of supernatant extracts.
A conventionally grown *N. punctiforme* culture was used as a control. HPLC profiles are shown at a wavelength of 199 nm. Known metabolite peaks are labeled (Nos1052: nostopeptolide 1052, NosA: nostopeptolide A, Apt: nostamid A).

Pellet and supernatant of the harvested cultures were further analyzed by HPLC. Despite the differences in cell density, both cultures, HD1 and HD2, showed very similar HPLC chromatograms (see **Figure 3.6B, C**). Besides an increased production of anabaenopeptin (Apt) and nostopeptolide (Nos1052, NosA), which are metabolites commonly found in *N. punctiforme*, several small additional peaks were found in the chromatograms of the cell pellet and supernatant of both HD cultures. The presence of additional peaks that were not detectable in the conventionally grown control culture hints towards an upregulation of metabolite production caused by HD cultivation conditions, confirming the findings of Guljamow et al. [110].

To obtain larger amounts of *N. punctiforme* grown under HD conditions, a large scale fermentation was carried out by the CellDeg company as described in **Section 2.2.1.3.2**. The HD cultivation setup they used is depicted in **Figure**

3.5C. They attempted to optimize growth conditions in terms of metabolite production and accumulation by rapidly increasing the light intensity (up to 620 µmol photons m^{-2} s^{-1}, see **Appendix Table B.3–B.4**) and not replacing the cultivation media. This type of cultivation resulted in rather complex extracts (see **Appendix Figure A.1**).

In order to further investigate the impact of media exchange and strong light intensities during HD cultivation on metabolite production, two more cultivation approaches were conducted. Similar to the cultivations carried out by the CellDeg company, the cultivation media was not exchanged during the cultivation. One of the cultures (HD noME) was grown with light intensities up to 350 µmol photons m^{-2} s^{-1} over a time period of 27 days (see **Appendix Table B.5**). Whereas the other culture (HD noME + LS) was grown over a time period of 56 days with light intensities up to 800 µmol photons m^{-2} s^{-1} (see **Appendix Table B.6**) to initiate light stress. Despite the strong light intensities, the culture remained green and healthy looking throughout the whole cultivation. The growth of both cultures was rather limited compared to the HD cultures with regular exchange of the BG11$_0$ medium, only reaching a final wet weight of around 8 g per 100 ml. For a stronger separation of hydrophilic compounds, gradient conditions, different from the HD1 and HD2 conditions, were used for the HPLC analysis, starting with an acetonitrile concentration of 2% instead of 20% (see **Section 2.2.4.1**). HPLC profiles of both cultivation samples are shown in **Figure 3.7**.
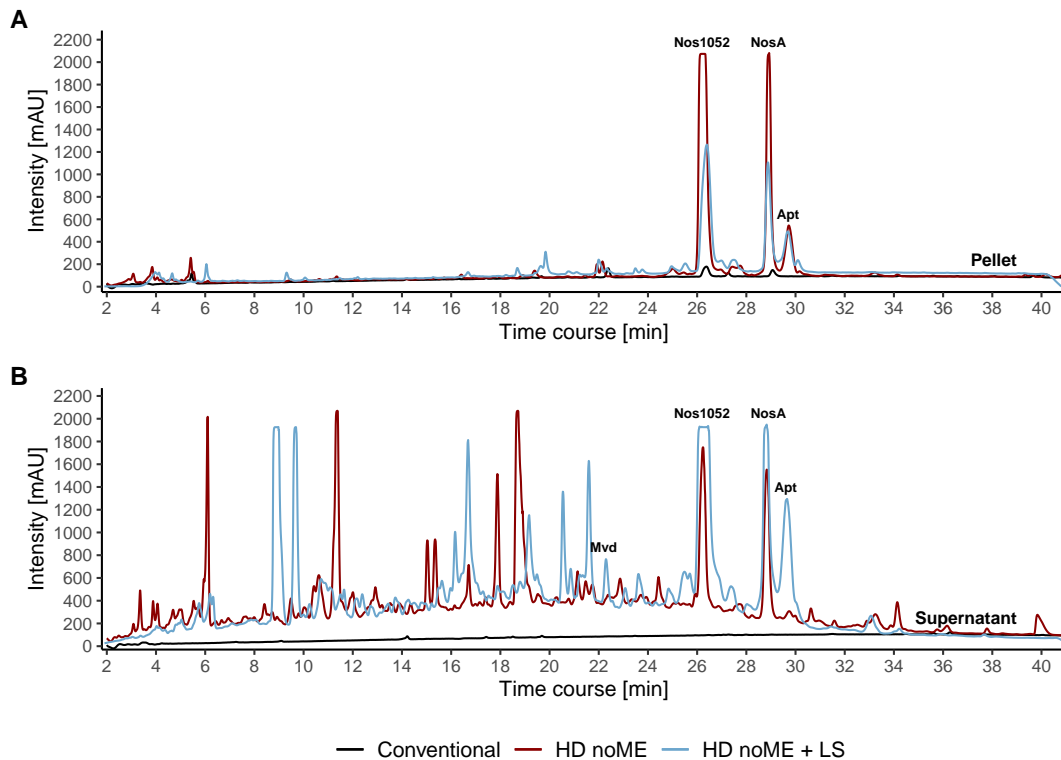
FIGURE 3.7: **HPLC analysis of a high density cultivation approach of**
N. punctiforme **without media exchange and with & without light stress**
(A) HPLC profiles of cell pellet extracts. **(B)** HPLC profiles of supernatant extracts.
HD noME was grown without media exchange and with light intensities up to
$300\ \mu\text{mol photons m}^{-2}\ \text{s}^{-1}$. HD noME + LS was grown without media exchange
and with light intensities up to $800\ \mu\text{mol photons m}^{-2}\ \text{s}^{-1}$. A conventionally
grown *N. punctiforme* culture was used as a control. HPLC profiles are shown at a
wavelength of 199 nm. Known metabolite peaks are labeled (Mvd: microviridin,
Nos1052: nostopeptolide 1052, NosA: nostopeptolide A, Apt: nostamid A).

Similar to all other HD cultivation approaches, the production of
anabaenopeptin and nostopeptolide was strongly increased compared to
the conventionally grown control culture. Interestingly, anabaenopeptin
did not accumulate in the supernatant of the HD noME + LS sample.
Both pellet extracts showed only a small amount of additional, but rather
small peaks. However, HPLC analysis of supernatant extracts showed
an enormous amount of new, not characterized peaks, but not all peaks
appearing in HD noME were also present in HD noME + LS and vice
versa. This indicates that light intensity and stress have a strong impact on
metabolite production. Furthermore, without media exchange potentially
density-dependent metabolites can accumulate in the supernatant, which can
also have an impact on the production of other metabolites.

In order to find and identify new compounds, the HD extracts were analyzed by several mass spectrometric techniques as part of a cooperative study led by Martin Baunach (University of Potsdam, Potsdam, Germany) and Vincent Wiebach (Technische Universität Berlin, Berlin Germany). For compound identification and potential assignment to an associated BGC, MS/MS-based analyses were performed. These are especially suitable for the detection of RiPPs, because the basic amino acid sequence can be deduced from the precursor gene sequence. During this study, only a new microviridin variant was found and structurally elucidated (further described by Dehm et al. [115], [138]). Unfortunately, none of the other peaks could be assigned to one of the orphan BGCs by MS/MS analyses. As an alternative for MS/MS analyses, NMR spectroscopy can be used, which is also a suitable method for the characterization of polyketides and NRPs. However, large amounts of an already purified compound are required for NMR analysis.

In summary, the HPLC analysis of the different HD cultivation samples indicates that not cell density alone, but also light intensity plays a major role in activation of metabolite production. Without regular media exchange, not only secreted metabolites, but also by-products and degradation products strongly accumulate in the supernatant, resulting in very complex extracts, difficult and laborious to analyze.

3.2.2 Transcriptional Reporter Studies

Although, high density cultivation of *N. punctiforme* have led to an enormous increase of new, uncharacterized compound peaks in HPLC analysis, the complexity of the metabolite extracts complicates the assignment of these peaks to the predicted orphan BGCs. To narrow down the pool of potential new metabolites and facilitate identification, the transcriptional activity of each BGC should be analyzed in the context of high density cultivation. By giving initial clues about which BGCs may be involved in a potential cell density-dependent signaling network, this approach should help to prioritize BGCs of interest.

To track the transcriptional activity of the predicted BGCs, a library of reporter mutant strains, generated by Daniel Dehm (University of Potsdam, Potsdam, Germany) [115, 138], was utilized. Each of the strains reports for one of the 15 BGCs predicted by AntiSMASH. The mutant strains were created by introducing a cyanobacterial reporter plasmid into *N. punctiforme*. These plasmid were constructed based on the pRL1049 vector and contained a CFP

coding sequence (CDS) fused to a 5′ untranslated potential promoter region (5′UTR) of a representative gene of the desired BGC. As a representative gene, the first (precursor) gene of a given BGC was chosen. If the representative gene is transcribed then also the CFP located on the introduced plasmid should be transcribed, resulting in a detectable fluorescence signal. A strain containing a plasmid carrying a CFP gene but no promoter region served as a negative control (see **Appendix Figure A.2**). The control did not show an unspecific CFP signal or a phenotype.

TABLE 3.1: **List of selected *N. punctiforme* genes used for reporter strain construction**

Biosynthetic gene cluster	5′UTR target gene
Anabaenopeptin (*apt*)	*RS12350*
Microviridin (*mvd*)	*RS10970*
Nostopeptolide (*nos*)	*RS38845*
nrps1	*RS42520*
nrps2	*RS38145*
pks1	*RS10525*
pks2	*RS15970*
pks3	*RS17005*
pks4	*RS17455*
pks5	*RS40215*
ripp1a	*RS16255*
ripp1b	*RS16310*
ripp3	*RS16795*
ripp4	*RS25510*
ripp5	*RS38030*

To evaluate the impact of high density cultivation on BGC expression, each reporter strain was cultivated under HD cultivation conditions, as described in **Section 2.2.1.3.2**, and analyzed by confocal fluorescence microscopy (see Section **2.2.1.7**). As a control, every reporter strain was also grown under conventional cultivation conditions and analyzed microscopically.

From the three PKS clusters found by AntiSMASH, two clusters, namely *pks1* and *pks2*, showed an increased expression after 30 days of HD cultivation when compared to a conventionally grown culture (see **Figure 3.8**).

When grown conventionally, the *pks1* reporter strain did not show any fluorescence signal. Presumably, the representative gene was not transcribed under this conditions and the whole gene cluster was not expressed. Cultivation under HD conditions activated the expression of the *pks1* BGC, indicated by a clear CFP signal visible in a fraction of the cells. However, induced expression results in atypical cell shapes and short filaments, especially in case of cells showing a fluorescence signal, which could be an indicator of increased cell stress. Similar to the *pks1* reporter strain, the *pks2* reporter strain showed almost no fluorescence under conventional cultivation conditions, but the CFP was clearly increased when the strain was cultivated under HD conditions, indicating the expression of the *pks2* BGC. The *pks3* BGC was already expressed under conventional cultivation conditions, displayed by a strong CFP signal in nearly all cells of the reporter strain. The CFP signal was not influenced by HD cultivation.
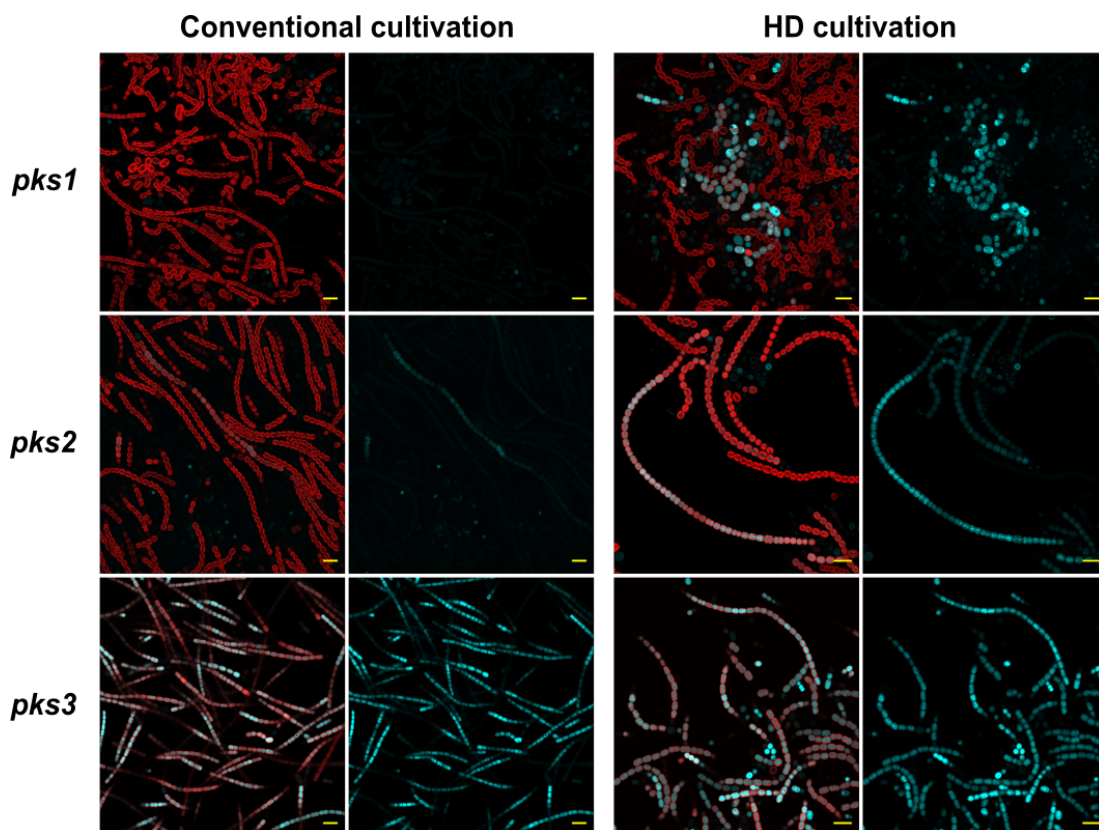
FIGURE 3.8: **Fluorescence micrographs of PKS BGC reporter strains cultivated conventionally and under HD conditions**
Cultures were grown for 30 days under both cultivation conditions. CFP fluorescence signal (blue) indicates promoter activity of the respective BGCs. Chlorophyll-α autofluorescence (red) indicates living vegetative cells. Respective left images show merged CFP/Chlα channels. Respective right images show only the CFP channels. Yellow scale bars indicate 10 µm.

The influence of HD cultivation conditions on the expression of NRPS BGCs is depicted in **Figure 3.9**. The *apt* BGC was the only NRPS gene cluster showing an upregulated expression upon HD cultivation, indicated by the enhanced CFP signal in small segments of the filaments in the corresponding reporter mutant strain. Since the fluorescence signal detected in the reporter strains of *nos*, *nrps1*, and *nrps2* looked similar under both cultivaton conditions, the expression of these clusters seemed to be unaffected by HD cultivation.
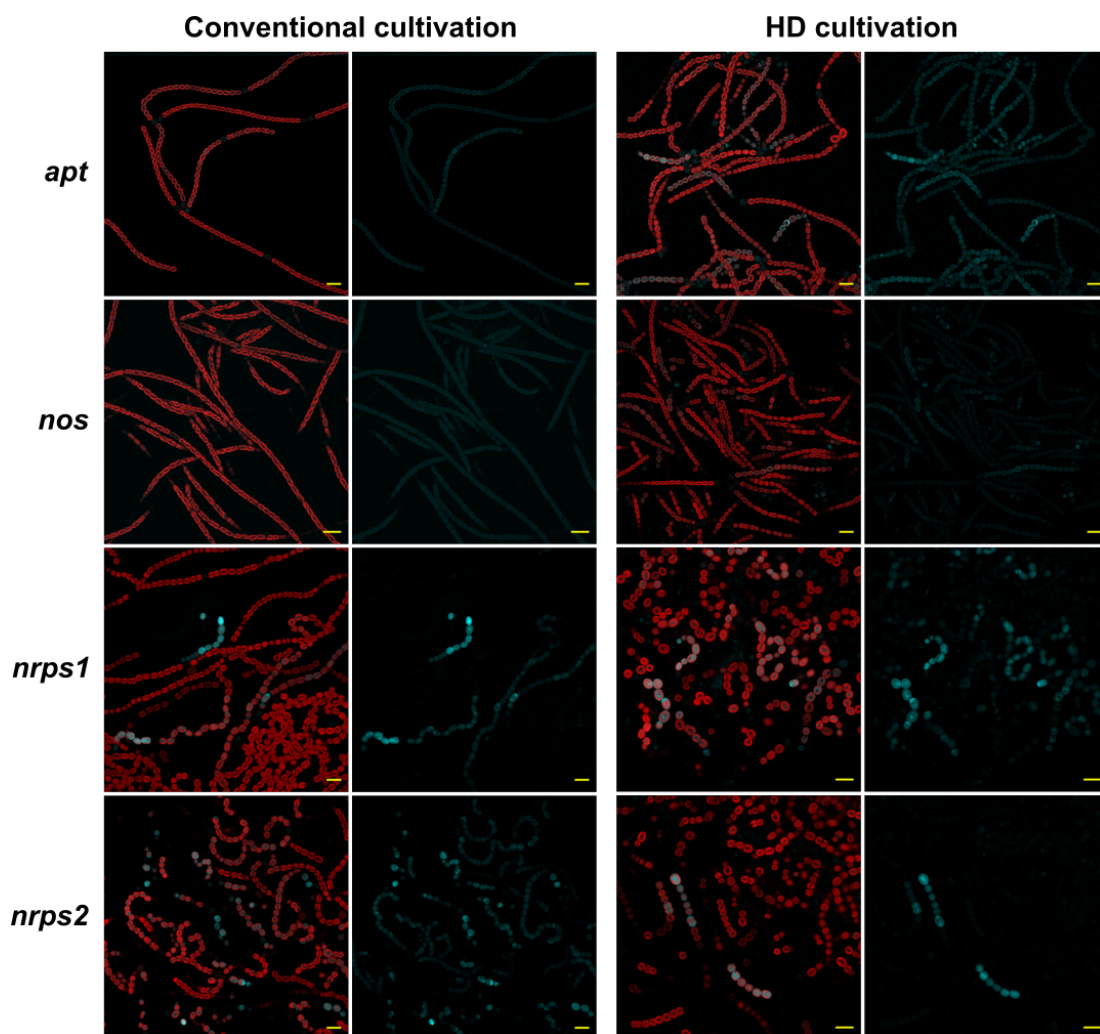
FIGURE 3.9: **Fluorescence micrographs of NRPS BGC reporter strains cultivated conventionally and under HD conditions**
Cultures were grown for 30 days under both cultivation conditions. CFP fluorescence signal (blue) indicates promoter activity of the respective BGCs. Chlorophyll-α autofluorescence (red) indicates living vegetative cells. Respective left images show merged CFP/Chlα channels. Respective right images show only the CFP channels. Yellow scale bars indicate 10 μm.

From the NRPS-PKS hybrid BGCs only the expression of the *pks4* BGC was influenced upon HD cultivation conditions (see **Figure 3.10**). When the

pks4 reporter strain was grown conventionally, the fluorescence signal was restricted to single cells or very short filament segments. Upon HD cultivation, the CFP signal was broader distributed throughout the whole culture with some filaments showing a stronger signal. The fluorescence signal in the *pks5* reporter strain was not influenced upon HD cultivation. Upon both cultivation conditions, a distinct CFP signal was visible, indicating that the transcription of the representative gene (*RS40215*) was not influenced by the different cultivation conditions.
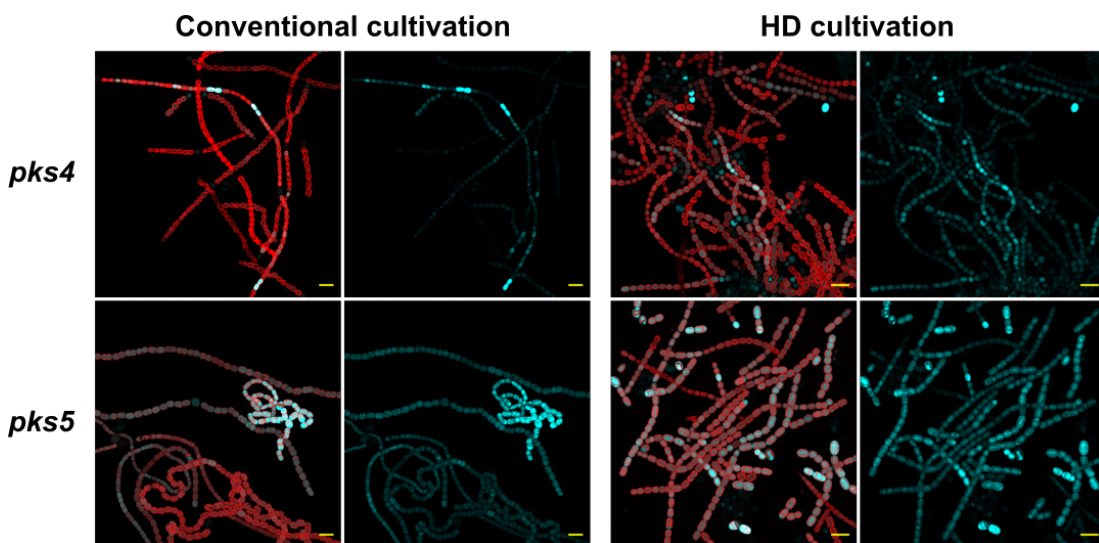
FIGURE 3.10: **Fluorescence micrographs of NRPS-PKS hybrid BGC reporter strains cultivated conventionally and under HD conditions**
Cultures were grown for 30 days under both cultivation conditions. CFP fluorescence signal (blue) indicates promoter activity of the respective BGCs. Chlorophyll-α autofluorescence (red) indicates living vegetative cells. Respective left images show merged CFP/Chlα channels. Respective right images show only the CFP channels. Yellow scale bars indicate 10 μm.

High density cultivation of all six RiPP BGC reporter strains revealed that the expression of four RiPP BGCs, namely *mvd*, *ripp1a*, *ripp1b* and *ripp4*, are influenced by HD cultivation, as can be seen in **Figure 3.11**. Upon conventional cultivation, the CFP signal of the *mvd* reporter strain was restricted to single filaments, whereas under HD conditions the CFP signal was widely distributed throughout the whole culture. Based on the presence of atypical cells and filaments, cell stress is assumed to result from increased *mvd* expression. The CFP signals detected in the *ripp1a* and *ripp1b* reporter strains were limited to short filament segments, when the strains were cultivated conventionally. Upon HD conditions, the fluorescence signals were widely distributed throughout the respective cultures. Additionally, the signal strength of the *ripp1a* reporter strain became stronger. The observations

indicate an increased expression of the *ripp1a* and *ripp1b* BGCs. For the *ripp4* BGC the expression was restricted to small filament fractions under conventional cultivation conditions. Similar to the other influenced RiPP reporter strains, the *ripp4* reporter strain showed an increased and widely distributed CFP signal when grown under HD conditions. The CFP signals detected in the *ripp3* and *ripp5* reporter strains did not change upon HD cultivation.
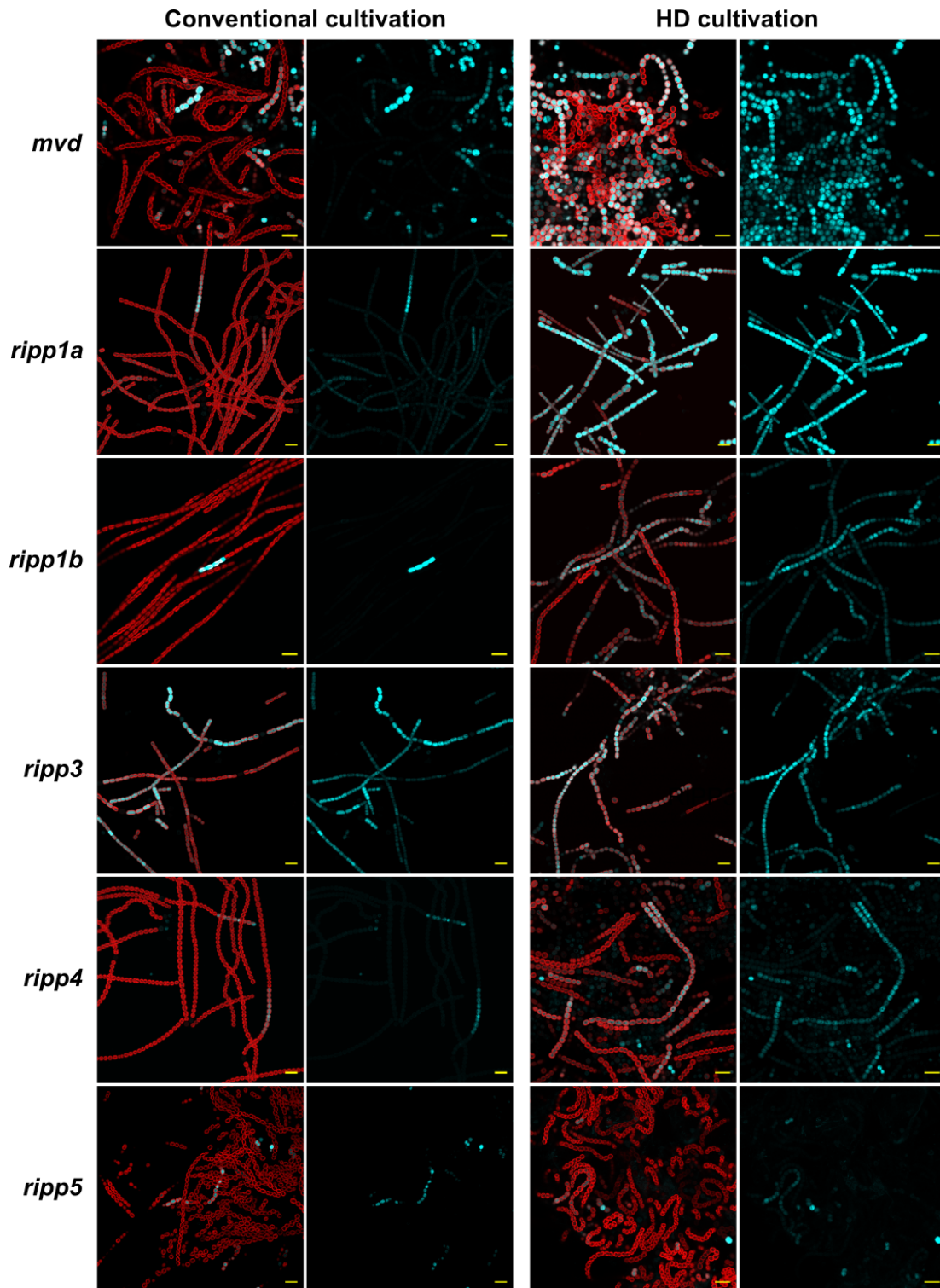
FIGURE 3.11: **Fluorescence micrographs of RiPP BGC reporter strains cultivated conventionally and under HD conditions**
Cultures were grown for 30 days under both cultivation conditions. CFP fluorescence signal (blue) indicates promoter activity of the respective BGCs. Chlorophyll-α autofluorescence (red) indicates living vegetative cells. Respective left images show merged CFP/Chlα channels. Respective right images show only the CFP channels. Yellow scale bars indicate 10 µm.

In total, eight out of 15 BGCs that were predicted by AntiSMASH showed an upregulated expression, indicated by an increased fluorescence signal of the corresponding reporter strains, after 30 days of HD cultivation. Most interestingly, even *pks1* and *pks2*, which reporter strains showed nearly no CFP signal under conventional cultivation conditions, could be induced by HD cultivation. The strongest increase of CFP signal was observed from *mvd*, *ripp1a* and *ripp1b*. Although, the reporter strain assays provided additional information on which BGCs were affected by HD cultivation conditions, further and more specific mass spectrometric analysis of the HD cultivation samples (described in **Section 3.2.1**) did not identify any additional BGC products. This might have been caused by the complexity of the extracts or potential inaccuracies in product prediction.

To investigate if a secreted chemical mediator, accumulating in the supernatant during high density cultivation, is inducing the expression of the eight HD influenced BGCs, another reporter strain assay was conducted. Therefore, reporter strains that were positively influenced upon HD cultivation were cultivated conventionally in 20 days old cell-free HD supernatant from a *N. punctiforme* WT culture (see **Section 2.2.1.3.3**). After 7 days of cultivation, reporter strains were again analyzed by fluorescence microscopy.

From the eight treated strains, four showed an increased CFP signal when compared to the respective non-treated culture (see **Figure 3.12**). Besides the expression of the BGCs *ripp1b* and *pks4*, also the expression of the formerly silent gene clusters of *pks1* and *pks2* could be induced by cultivation with HD supernatant. Apart from a slightly weaker CFP signal in general, no differences could be observed compared to high density cultivated reporter strains. This clearly indicates that factors, secreted during HD cultivation, are able to trigger the expression of certain BGCs, which could be a hint for the presence of a signaling network.
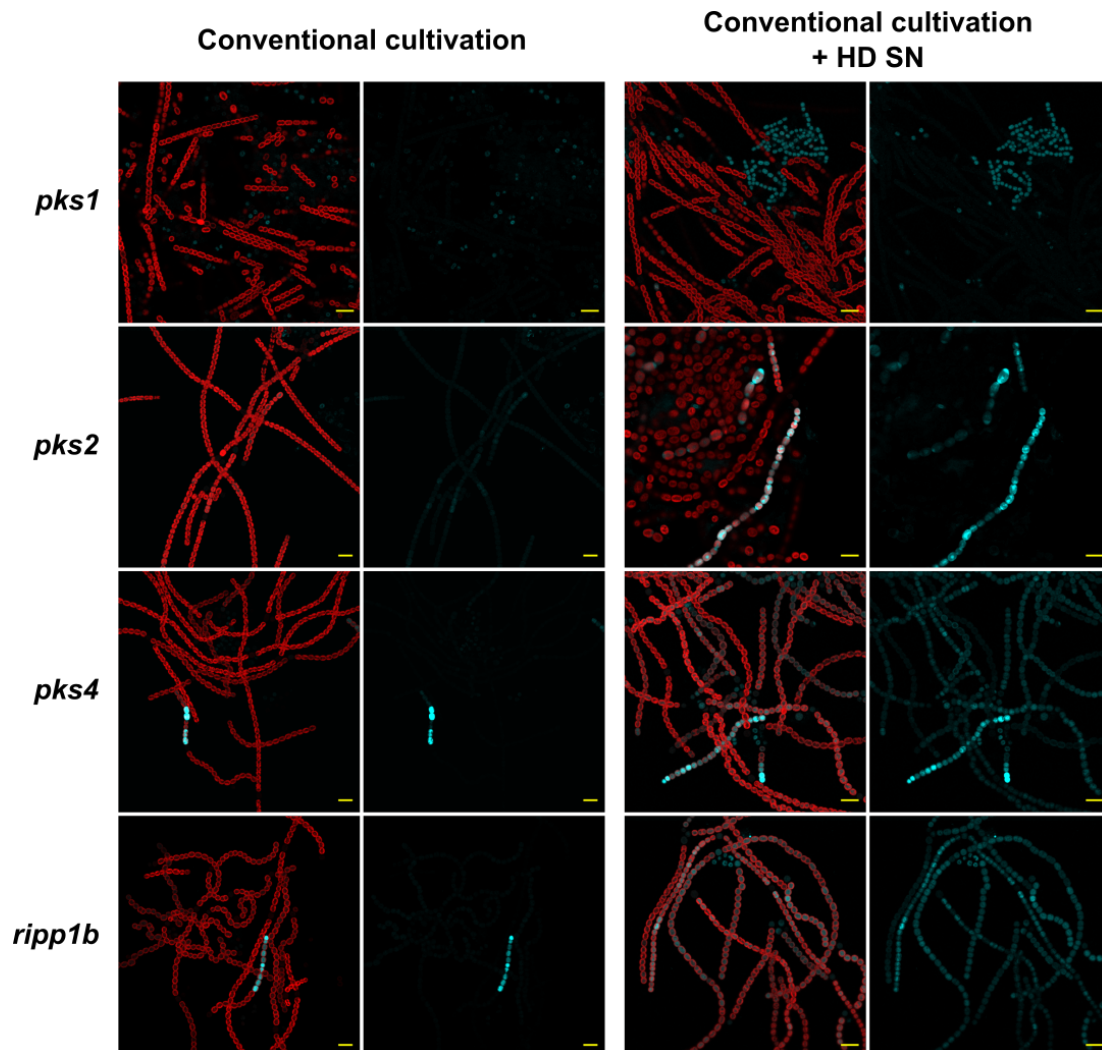
FIGURE 3.12: **Fluorescence micrographs of BGC reporter strains influenced by HD supernatant**

Cultures were grown for 7 days conventionally in HD supernatant (HD SN). CFP fluorescence signal (blue) indicates promoter activity of the respective BGCs. Chlorophyll-α autofluorescence (red) indicates living vegetative cells. Respective left images show merged CFP/Chlα channels. Respective right images show only the CFP channels. Yellow scale bars indicate 10 µm.

3.3 Generation and Analysis of *N. punctiforme* Regulatory Overexpression Mutant Strains

Although the analysis of high density (HD) cultivated *N. punctiforme* WT and reporter strains revealed that several BGCs are upregulated, the identification of gene cluster products was hampered by the complexity of the HD extracts. Additionally, for the characterization by NMR spectroscopy, large amounts of a desired compound are required. Therefore, another more specific approach for the targeted activation of cryptic gene clusters should be developed to facilitate the identification and enable high-titer production of the corresponding products. A commonly used approach to address these problems is the manipulation of pathway-specific regulatory genes. By this approach BGCs that encode potential cell density dependent chemical mediators should be prioritized.

A closer look on the BGCs that are upregulated at high cell densities revealed that only three of these BGCs, namely *pks1*, *pks2* and *ripp4*, encode putative transcription factors within or in close proximity to their respective gene clusters. The BGCs of *pks1* and *pks2* were especially interesting, because both gene clusters were only expressed under high density cultivation conditions. Additionally, *ripp3* BGC whose expression appeared to be independent from cell density, encodes a putative LuxR type transcription factor that is commonly involved in the regulation of cell density dependent mechanisms. The presence of these transcription factors led to the idea of constructing *N. punctiforme* mutants that overexpress one of the transcription factors to possibly influence the expression of the associated gene cluster. To provide further evidence of an existing signaling network, it should be tested whether additional BGCs are affected. The construction of overexpression mutants was planed for the regulatory genes of *pks1*, *pks2*, *ripp4* and *ripp3*.

3.3.1 Characterization of Regulatory Genes

In order to adapt to environmental changes, bacteria use signal transduction systems such as two-component systems. Two-component systems are composed of a histidine kinase, sensing specific environmental changes, and a response regulator, which can be phosphorylated by the histidine kinase [139]. The phosphorylation typically triggers a change in conformation, activating the effector domain of the response regulator, which influences the expression of a target gene [139]. In addition, there are also atypical "two-component" regulators that have a phosphorylation-independent signal

transduction mechanism [140] and one-component systems that consists of a single protein containing input and output domains [141]. The regulatory genes of *pks1*, *pks2*, *ripp4* and *ripp3* were shortly characterized utilizing the NCBI software tool BLAST [132, 133] and the NCBI database [131] to search for conserved domains.

The regulatory gene *RS10525*, located inside the *pks1* BGC (see **Figure 3.13**), encodes a transcriptional regulator of the AraC family. Those typically act as positive regulators and are commonly involved in carbon metabolism, stress response and pathogenesis [142]. The *RS10525*-derived regulator contains two conserved domains, a N-terminal CheY-like receiver domain and an AraC-type DNA-binding domain with a helix-turn-helix motif. Although the CheY prototype is part of a two-component system [143], no gene encoding a histidine kinase could be localized in the immediate proximity of *RS10525*. A comparison of the *RS10525* regulator with the CheY prototype showed the absence of conserved residues, especially of phosphoaccepting aspartate (Asp57 in CheY). This leads to the assumption that the regulator may act independently of its phosphorylation. A bioinformatic search revealed that homologs of the *RS10525*-derived regulator were only found in other cyanobacterial genomes.
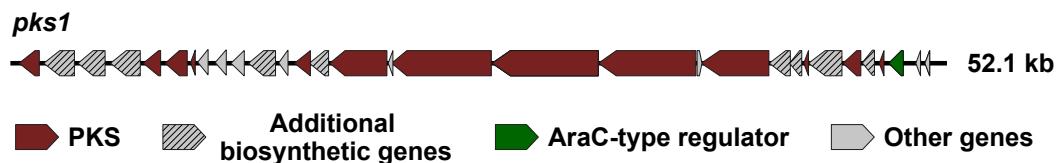
FIGURE 3.13: **Schematic overview of the *pks1* BGC**
The regulatory gene *RS10525* is located inside the *pks1* BGC and is highlighted in green.

The *pks2* response regulator, encoded by the gene *RS16090* that is located at the 3' end of the *pks2* BGC (see **Figure 3.14**), belongs to the TetR/AcrR family of transcriptional regulators. Those are known to act as repressors and can regulate a variety of cellular activities, such as osmotic stress, antibiotic resistance and virulence, or can respond to fluctuations in cell density (quorum sensing) [144, 145]. The regulators of the TetR family are one-component systems that can act independently from a histidine kinase [144]. A bioinformatic search revealed that homologs of the *RS16090*-derived regulator were only found in other cyanobacterial strains of the order *Nostocales*.

pks2

FIGURE 3.14: **Schematic overview of the *pks2* BGC**
The regulatory gene *RS16090* is located adjacent to the *pks2* BGC and is highlighted in green.

The regulatory gene *RS16765* is located at the 5' end of the *ripp3* BGC (see **Figure 3.15**). The encoded regulator consists of a N-terminal receiver domain and a LuxR-like C-terminal helix-turn-helix DNA-binding domain. Those regulators can act as activators or repressors. LuxR-like regulators can be, for example, involved in quorum sensing related mechanisms, such as biofilm formation, bioluminescence, antibiotic biosynthesis or mobility [146] They can be activated as part of a two-component system, by binding of an autoinducer or ligand, or by autonomous activation [147]. Homologs of the *RS16765* regulator were found only in strains of the cyanobacterial order *Nostocales*.
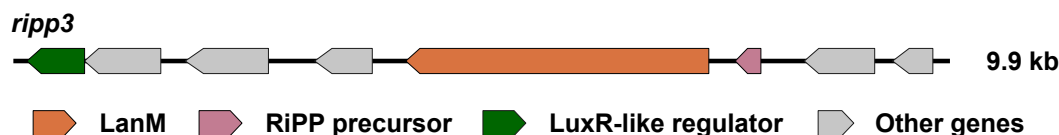
ripp3

FIGURE 3.15: **Schematic overview of the *ripp3* BGC**
The regulatory gene *RS16765* is located adjacent to the *ripp3* BGC and is highlighted in green.

The regulatory gene *RS25505*, located at the 5' end of the *ripp4* BGC (see **Figure 3.16**), encodes a regulator belonging to the OmpR family. Only a receiver domain containing a phosphorylation site was localized inside the regulator. Regulators of the OmpR family can have positive or negative effects on the expression of target genes and can influence e.g. motility, virulence, osmotic stress or membrane production [148]. The gene *RS25500* encoding a histidine kinase is located in 5' direction, directly beside the *RS25505* gene. This leads to the assumption that both regulators work together as part of a two-component system. Again, only other cyanobacterial strains contained homologs of both regulators.
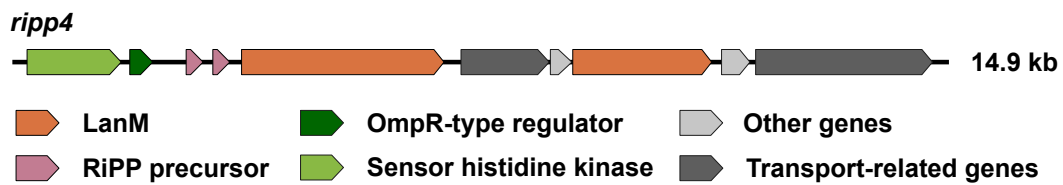
FIGURE 3.16: **Schematic overview of the *ripp4* BGC**
The regulatory genes *RS25500* and *RS25505* are located adjacent to the *ripp4* BGC
and are highlighted in green.

3.3.2 Construction of Overexpression Mutants

For the generation of *N. punctiforme* mutants that overexpress the desired
regulatory genes, cyanobacterial plasmids were constructed. Generally, these
plasmids encode a promoter region, the desired regulatory gene, a resistance
marker, a cyanobacterial origin of replication (ori), as well as an *E. coli* ColE1
ori. All plasmids are based on the pRL1049 vector [118]. First, a precursor
plasmid, named pJK008, was constructed to facilitate the generation of the
desired overexpression plasmids. For this, a promoter region followed by
an EcoRI restriction site was inserted into the pRL1049 vector by NEBuilder®
HiFi mediated homologous recombination, as described in **Section 2.2.2.6**.
As promoter region, the 5' UTR of *RS16340* was chosen, because this region
showed a strong response when analyzed as transcriptional reporter (see
Figure 3.17).
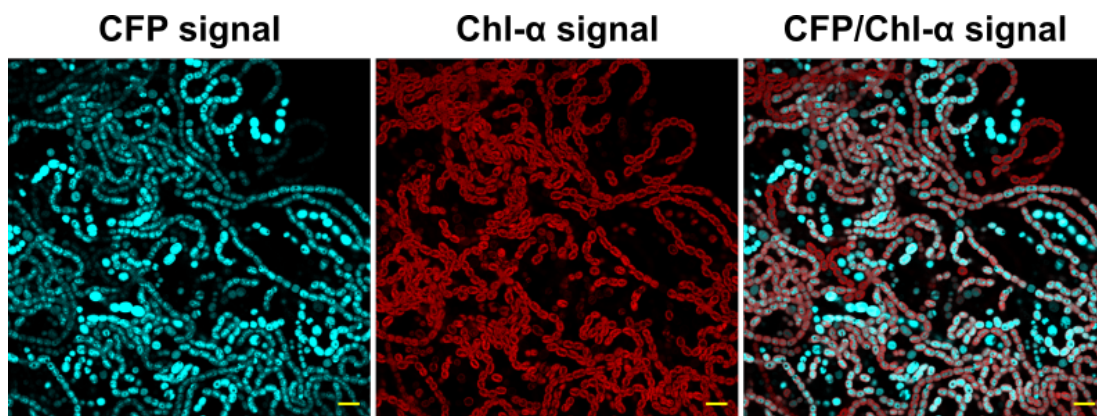
FIGURE 3.17: **Fluorescence micrographs of the *RS16340* reporter strain under
conventional cultivation conditions**
The reporter strain shows a strong CFP fluorescence signal (blue) under
conventional cultivation conditions, which indicates a strong promoter activity.
Chlorophyll-α autofluorescence (red) indicates living vegetative cells. Yellow
scale bars indicate 10 μm. Pictures provided by Daniel Dehm.

The promoter insert was amplified from genomic *N. punctiforme* DNA by PCR with the primer pair J056_FW/J057_RV. The primers attached the necessary homology sequences as well as an EcoRI restriction site to the *RS16340* promoter region. The vector pRL1049 was linearized with the restriction enzyme EcoRI and the promoter insert was incorporated into the vector (see **section 2.2.2.6**). Subsequently, the plasmid was transformed into the *E. coli* strain XL-1 blue and potential positive mutants were identified by colony PCR (see **section 2.2.2.7**). The correct assembly of the plasmid was confirmed by DNA sequencing. A map of the plasmid pJK008 can be seen in **Figure 3.18**.
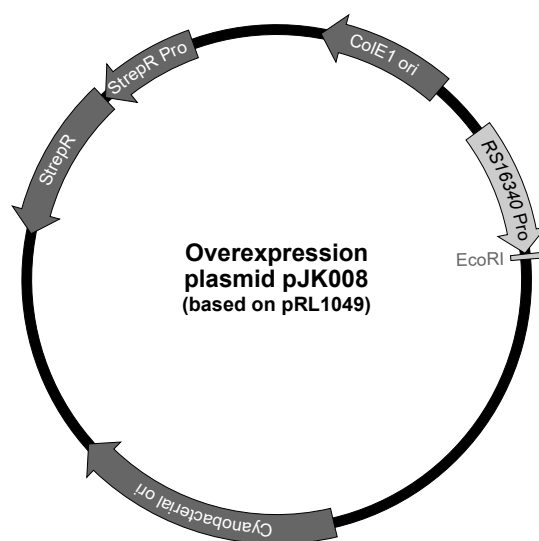
FIGURE 3.18: **Map of overexpression plasmid pJK008**
Features derived from backbone vector pRL1049 are displayed in dark grey.
Separately inserted features are displayed in light grey.
Labels: StrepR: streptomycin resistance cassette, Pro: promoter

The plasmid pJK008 served as vector backbone for the subsequent generation of the actual overexpression plasmids. Therefore, pJK008 was linearized with EcoRI and the desired regulatory genes (see **Table 3.2**), including homologous vector sequences, were amplified from genomic DNA by PCR. Again, the assembly of insert and vector backbone was done by NEBuilder® HiFi mediated homologous recombination. After transformation into *E. coli* XL-1 blue, potential positive mutants were identified by colony PCR and the results were confirmed by DNA sequencing. **Table 3.2** lists the regulatory target genes, their corresponding BGCs and primer pairs, and the final overexpression plasmid names.

TABLE 3.2: **Regulatory genes and corresponding primers used for generation of overexpression plasmids**

BGC	Regulatory gene	Primer	Final plasmid
pks1	*RS10525*	J072_FW/J073_RV	pJK015
pks2	*RS16090*	J074_FW/J075_RV	pJK016
ripp3	*RS16765*	J063_FW/J064_RV	pJK012
ripp4	*RS25500-RS25505*	J058_FW/J059_RV	pJK009
ripp4	*RS25505*	J092_FW/J059_RV	pJK023

Final overexpression plasmids were transformed into *N. punctiforme* WT by electroporation (see **Section 2.2.2.11.1**). Potential mutants were selected on BG11$_0$ plates containing 2 µg/ml streptomycin (see **Figure 3.19**) and the presence of the desired plasmids was confirmed by PCR.

3 days
2 µg/ml streptomycin

30 days
2 µg/ml streptomycin

14 days in liquid culture
2 µg/ml streptomycin
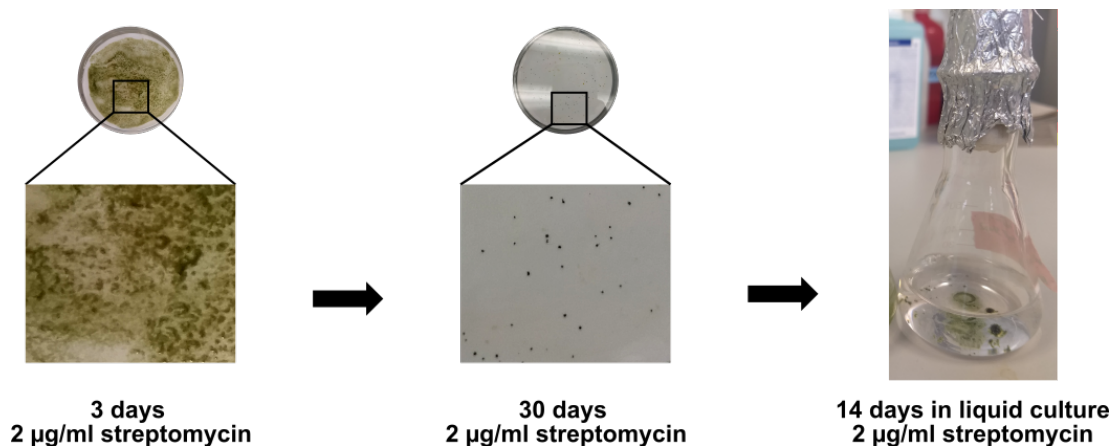
FIGURE 3.19: **Selection process for *N. punctiforme* mutants**
After transformation and a short recovery period on plain BG11$_0$ plates, filters were transferred to BG11$_0$ plates containing 2 µg/ml streptomycin for mutant selection. Potential mutant colonies were transferred to liquid media for further growth.

The *N. punctiforme* mutant containing plasmid pJK015 was named AraC_PKS1, the mutant containing plasmid pJK016 was named TetR_PKS2 and the mutant containing plasmid pJK012 was named LuxR_RiPP3.

Unfortunately, no viable mutant colonies were obtained when the regulatory genes of the *ripp4* BGC (pJK009) were transformed into *N. punctiforme*. Another approach which only focused on the overexpression of the response regulator *RS25505* was also unsuccessful.

To confirm that the generated mutants indeed overexpress the desired regulatory genes, RT-qPCR was performed (see **Section 2.2.2.16**). For that, RNA was isolated from the respective mutant cultures and from a *N. punctiforme* WT culture (see **Section 2.2.2.12**). From the RNA samples, cDNA was synthesized and RT-qPCR was performed to determine the relative transcription levels of the respective regulatory genes in the mutant strains in comparison to the WT. From this data, $\log_2$ fold changes between WT and mutant strains were calculated as described in **Section 2.2.2.18**. The $\log_2$ fold changes of the regulatory genes are visualized in **Figure 3.20**. The data shows that in all three mutant strains the transcription of the respective regulatory gene was strongly upregulated when compared to transcription in the *N. punctiforme* WT. Although the same promoter was used for all three mutants, differences in the expression of the respective regulatory genes were observed. The strongest increase with a $\log_2$ fold change of 15.5 was found for *RS16765* in LuxR_RiPP3. The regulatory gene *RS10525* in AraC_PKS1 showed the second strongest increase of transcription with a $\log_2$ fold change of 12.6. In the strain TetR_PKS2, the respective regulatory gene *RS16090* showed the least strongest increase with a $\log_2$ fold change of 9.5. Overall, the overexpression of the respective regulatory genes was confirmed by the RT-qPCR analysis.
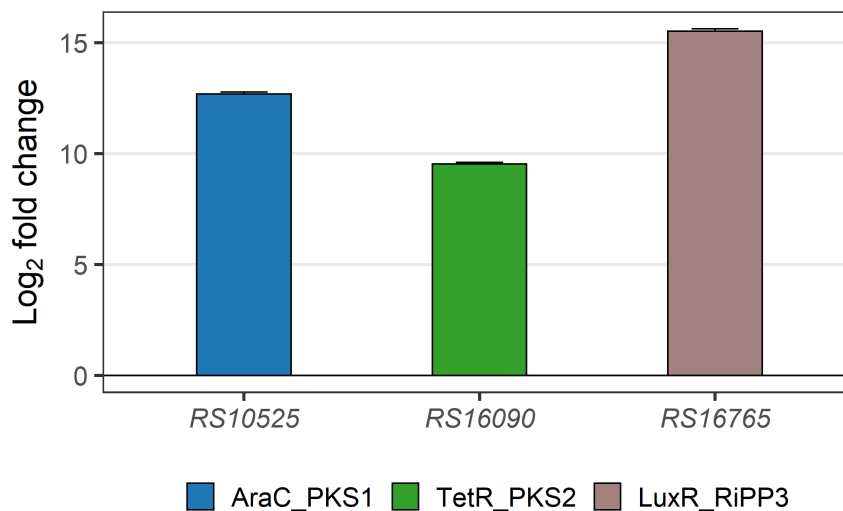
FIGURE 3.20: **Upregulation of *RS10525*, *RS16090* and *RS16765* in their respective *N. punctiforme* overexpression strains**
$\log_2$ fold changes calculated from transcription levels of overexpression strains (AraC_PKS1, TetR_PKS2 and LuxR_RiPP3) relative to transcription levels of the *N. punctiforme* WT.

3.3.3 Metabolomic and Transcriptomic Analysis of Overexpression Mutant Strains

To evaluate whether the overexpressed regulatory genes are able to affect the transcription of their associated BGC and to test whether additional BGCs are also affected, all three mutant strains were further analyzed by RT-qPCR. For that, a representative gene for each BGC was chosen and appropriate primers for RT-qPCR were designed. The list of primers and corresponding genes used for RT-qPCR can be found in **Section 2.1.5**. RT-qPCR was performed as described above and in **Section 2.2.2.16**. Log$_2$ fold changes were calculated from RT-qPCR data using the *N. punctiforme* WT strain as a reference. For visualization of changes at the metabolic level, the mutant strains were also analyzed by HPLC.

The overexpression of the gene *RS10525* in the AraC_PKS1 mutant led to a strong increase of *pks1* transcripts (log$_2$ fold change = 5.2). This confirms a positive regulatory effect of the overexpressed *RS10525* gene on the transcription of its associated BGC *pks1*. In addition, the BGCs *ripp3* (log$_2$ fold change = 4.3) and *ripp4* (log$_2$ fold change = 5.2) also showed a strong increase of transcription in the AraC_PKS1 mutant. In contrast, the BGCs of *mvd*, *nos*, *nrps1* and *nrps2* showed a clear decrease in transcription (log$_2$ fold change < -1). The remaining eight BGCs were not significantly influenced in the AraC_PKS1 mutant strain. The RT-qPCR results are depicted in **Figure 3.21**.
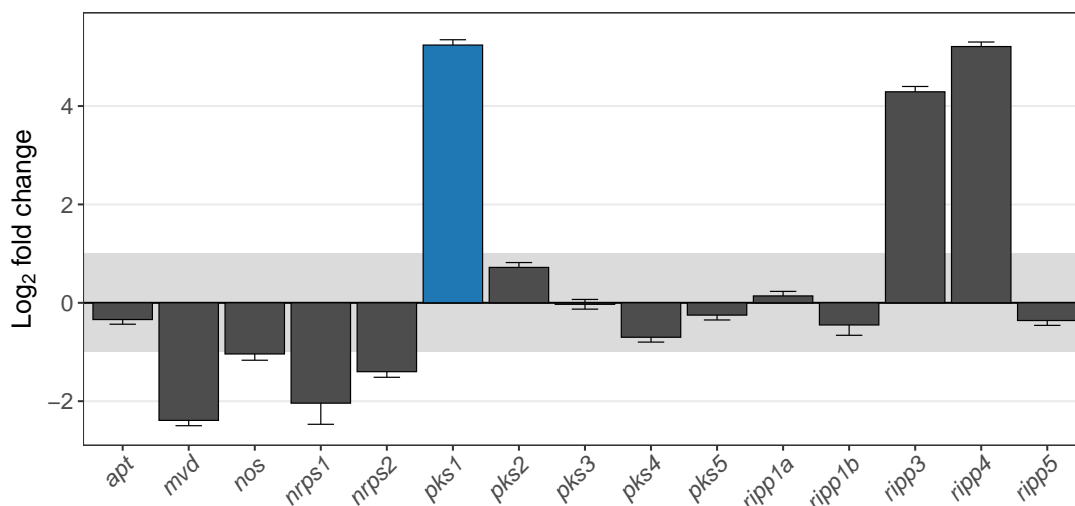
FIGURE 3.21: **Changes of BGC transcription in the AraC_PKS1 mutant**
Log$_2$ fold changes calculated from transcription levels of the AraC_PKS1 mutant
strain relative to transcription levels of the *N. punctiforme* WT strain.   The
transcript level range between -1 and 1 is shaded in grey, indicating the range
of non-significant transcriptional differences between mutant and WT. The *pks1*
BGC is highlighted in blue.

Further analysis of the AraC_PKS1 mutant strain by HPLC revealed a number
of additional peaks in the supernatant (see **Figure 3.22B**), which are not present
in the *N. punctiforme* WT strain. Whereas, the HPLC chromatograms of the cell
pellet from the mutant and the WT strain looked rather similar (see **Figure
3.22A**). These metabolic and transcriptomic data support the idea that the *pks1*
product may be part of a signaling network, with an impact on the expression
of other BGCs like *ripp4* and *ripp3*.
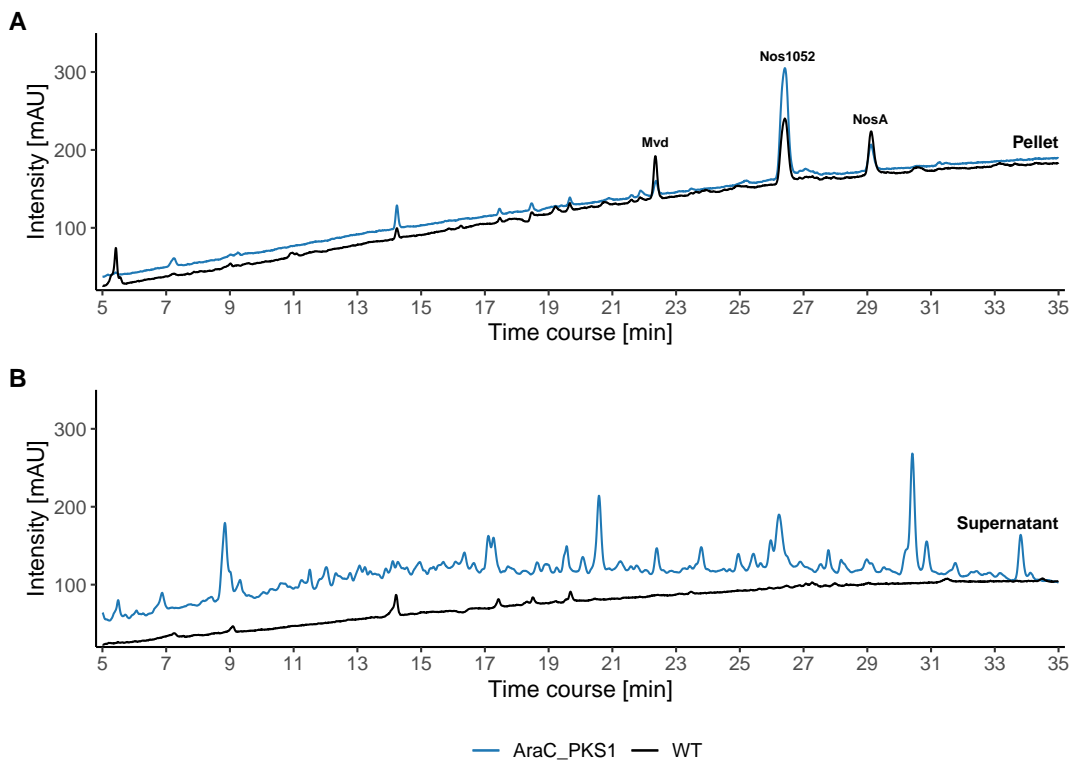
FIGURE 3.22: **Comparative HPLC analysis of *N. punctiforme* AraC_PKS1 and WT**

(A) HPLC profiles of cell pellet extracts. **(B)** HPLC profiles of supernatant extracts. Cultures were grown under conventional cultivation conditions for 25 days. HPLC profiles are shown at a wavelength of 199 nm. Known metabolite peaks are labeled (Mvd: microviridin, Nos1052: nostopeptolide 1052, NosA: nostopeptolide A).

The overexpression of the regulatory gene *RS16090* in the TetR_PKS2 mutant did not affect the transcription of its associated gene cluster *pks2* (see **Figure 3.21**). However, the transcription of several other BGCs was affected in the mutant strain. The BGCs *pks3* ($\log_2$ fold change = 2.4) and *pks4* ($\log_2$ fold change = 3.3) showed the greatest increase in their transcript number. Other positively influenced BGCs (*apt, mvd, nrps1, ripp1a, ripp4*) slightly exceeded the transcription levels of the WT. The only BGC that showed a clear decrease in transcription was *ripp5* ($\log_2$ fold change = -2.38). The transcription of the remaining BGCs was not significantly affected in the TetR_PKS2 mutant. The results of the RT-qPCR analysis of TetR_PKS2 are visualized in **Figure 3.21**.
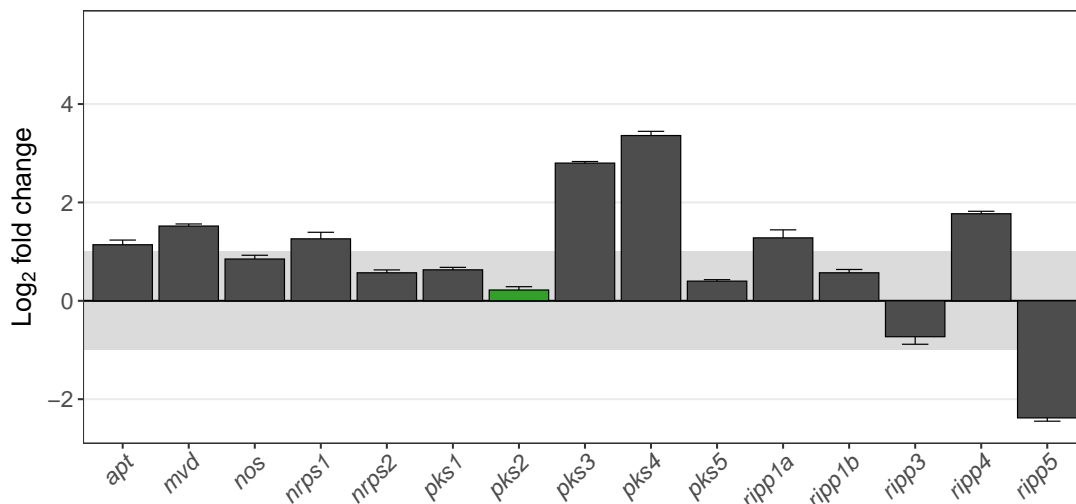
FIGURE 3.23: **Changes of BGC transcription in the TetR_PKS2 mutant**
Log_2 fold changes calculated from transcription levels of the TetR_PKS2 mutant strain relative to transcription levels of the *N. punctiforme* WT strain. The transcript level range between -1 and 1 is shaded in grey, indicating the range of non-significant transcriptional differences between mutant and WT. The *pks2* BGC is highlighted in green.

HPLC analysis of the supernatant of the TetR_PKS2 mutant detected only small additional peaks in comparison to the wild type (see **Figure 3.24B**). One of the peaks, which was also present in the WT (at 9 min, see **Figure 3.24B**), was strongly increased in the mutant strain. Similar to AraC_PKS1, the metabolic pattern in the cell pellet of the TetR_PKS2 mutant remained nearly unchanged compared to the WT control (see **Figure 3.24A**).
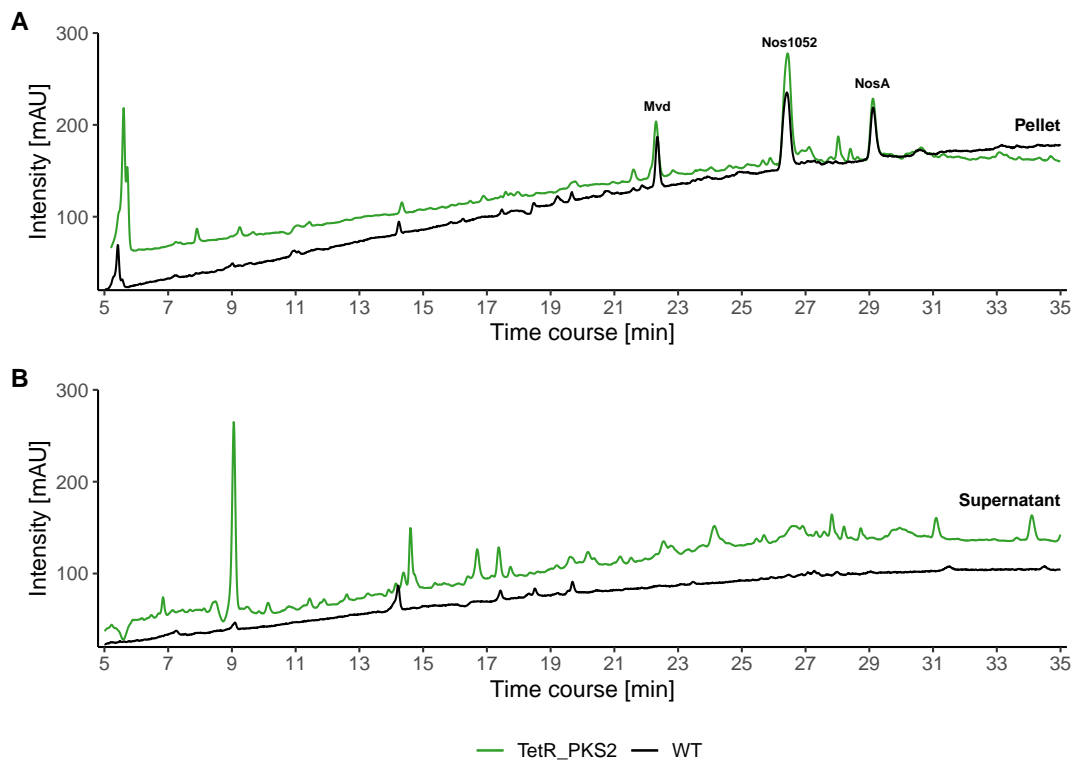
FIGURE 3.24: **Comparative HPLC analysis of *N. punctiforme* TetR_PKS2 and WT**
(A) HPLC profiles of cell pellet extracts. **(B)** HPLC profiles of supernatant extracts. Cultures were grown under conventional cultivation conditions for 25 days. HPLC profiles are shown at a wavelength of 199 nm. Known metabolite peaks are labeled (Mvd: microviridin, Nos1052: nostopeptolide 1052, NosA: nostopeptolide A).

The mutant strain LuxR_RiPP3 did not show a clear influence on the transcription of its associated BGC *ripp3*. However, the transcription levels of five other BGCs were slightly affected in the mutant strain. Again, the BGCs *pks3* and *pks4* were increased in their number of transcripts, with $\log_2$ fold changes of 2.4 and 1.92, respectively. The transcription levels of the other affected BGCs (*nrps2, pks5* and *ripp5*) were clearly decreased, when compared to the transcription levels in the WT ($\log_2$ fold changes = -1.45, -1.58 and -1.54, respectively). All results of the RT-qPCR analysis of LuxR_RiPP3 are shown in **Figure 3.25**.
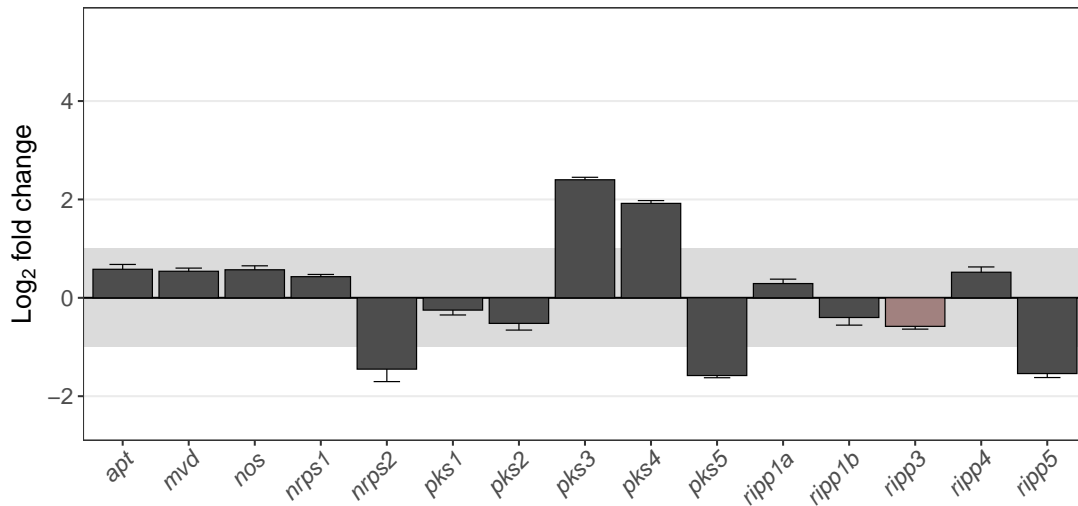
FIGURE 3.25: **Changes of BGC transcription in the LuxR_RiPP3 mutant**
Log_2 fold changes calculated from transcription levels of LuxR_RiPP3 relative to
transcription levels of *N. punctiforme* WT. The transcript level range between -1
and 1 is shaded in grey, indicating the range of non-significant transcriptional
differences between mutant and WT. *ripp3* BGC is highlighted in brown.

Analysis of the LuxR_RiPP3 mutant strain by HPLC showed several additional
peaks in the supernatant that are not present in the supernatant of the WT.
Similar to the other two mutant strains, the metabolic pattern of the cell pellet
appeared almost unchanged compared to the *N. punctiforme* WT control (see
Figure 3.26).
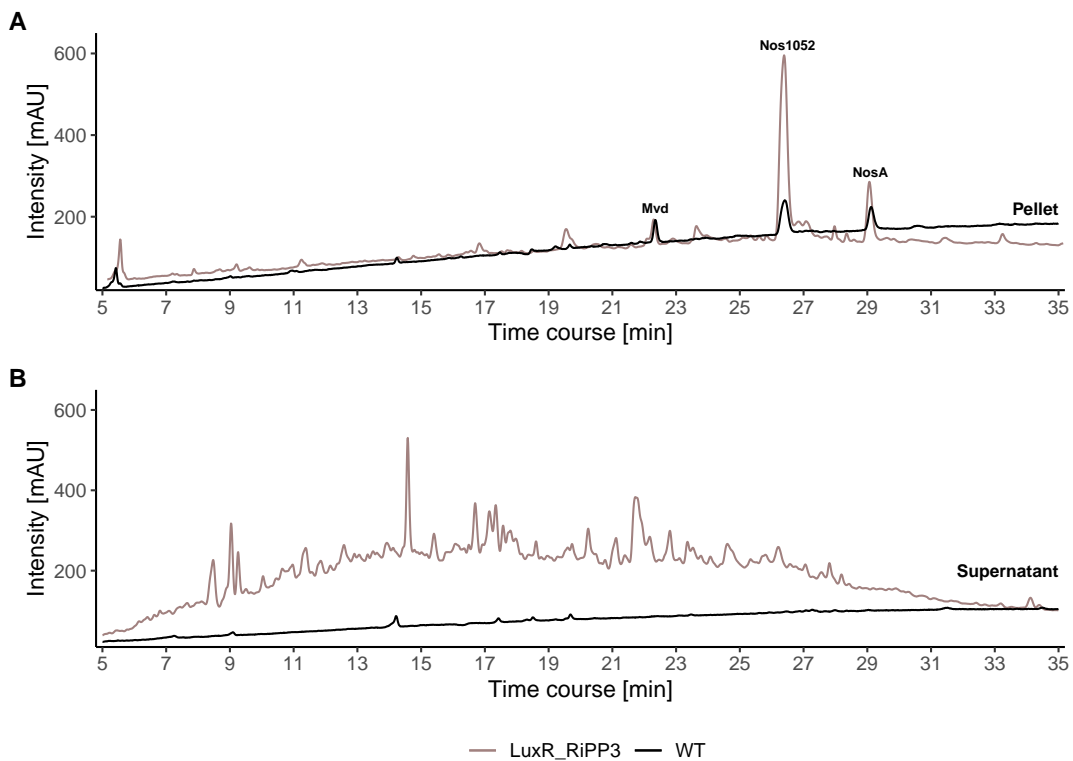
FIGURE 3.26: **Comparative HPLC analysis of *N. punctiforme* LuxR_RiPP3 and WT**

(A) HPLC profiles of cell pellet extracts. **(B)** HPLC profiles of supernatant extracts. Cultures were grown under conventional cultivation conditions for 25 days. HPLC profiles are shown at a wavelength of 199 nm. Known metabolite peaks are labeled (Mvd: microviridin, Nos1052: nostopeptolide 1052, NosA: nostopeptolide A).

In general, the most striking changes in BGC transcription were observed in the AraC_PKS1 mutant strain, which was the only mutant strain that showed a strong increase in transcription of its potentially associated gene cluster. Due to this and the observed metabolic differences compared to the WT, it was decided to focus on the analysis of the AraC_PKS1 mutant.

Further bioinformatic analysis of the *RS10525*-derived regulator and its cyanobacterial homologs revealed that the genes of the homologs were located in close proximity to BGCs of different subtypes including RiPP, NRPS and NRPS-PKS hybrid gene clusters (see **Figure 3.27**).
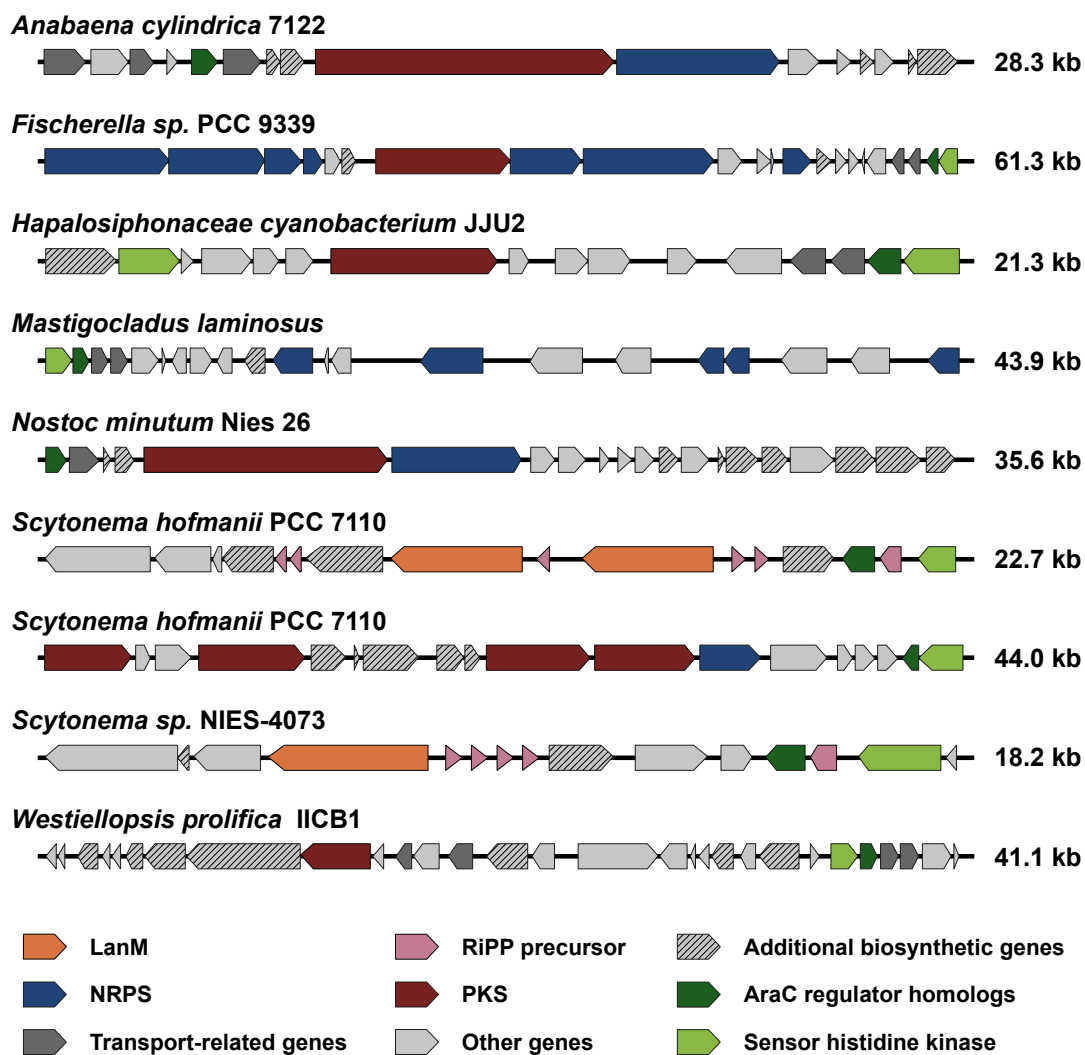
FIGURE 3.27: **Cyanobacterial BGCs with included or adjacent homologs of the**
RS10525-derived AraC-type regulator
Homologs of the *RS10525*-derived AraC regulator are highlighted in dark green.
Sensor histidine kinases are highlighted in light green. BGCs were detected by
AntiSMASH.

3.4 Identification of the *pks1* BGC Compounds

Unfortunately, the growth of the AraC_PKS1 mutant was relatively slow under conventional cultivation conditions. In order to get sufficient amounts of the potential *pks1* compounds for further analysis, the growth conditions were optimized towards medium cell density. It was found that cultivation under high light and high CO_2 conditions (HL/HC conditions), as described in **Section 2.2.1.3.2**, improved the growth of the mutant strain. Compared to conventional cultivation ($\log_2$ fold change = 12.68), the optimized conditions increased the transcription of the overexpressed regulatory gene *RS10525* in the AraC_PKS1 mutant strain even further ($\log_2$ fold change = 14.19) (see **Figure 3.28A**). Similar to the conventionally grown mutant strain, the transcription levels of *pks1, ripp3* and *ripp4* were increased and the transcription levels of *nrps1* and *nrps2* were decreased in the HL/HC grown mutant. However, the transcription of the *pks1* BGC showed a stronger upregulation than under conventional cultivation conditions ($\log_2$ fold change$_{HL/HC}$ = 6.99, $\log_2$ fold change$_{conv}$ = 5.2). Due to the fact that also the regulatory gene showed an increase in transcription, these findings are another hint that the activity of *pks1* is linked to the expression of *RS10525*. In case of other BGCs, the HL/HC cultivation conditions resulted in a different transcription behavior. The transcription of the BGCs *apt*, *nos* and *pks5* was slightly increased ($\log_2$ fold changes = 1.97, 1.35 and 1.35) compared to the WT. In addition, a strong decrease in transcription was observed for *pks4* ($\log_2$ fold change = -4.35). An overview of the BGC transcription levels in the AraC_PKS1 mutant that was grown under HL/HC conditions is shown in **Figure 3.28B**.
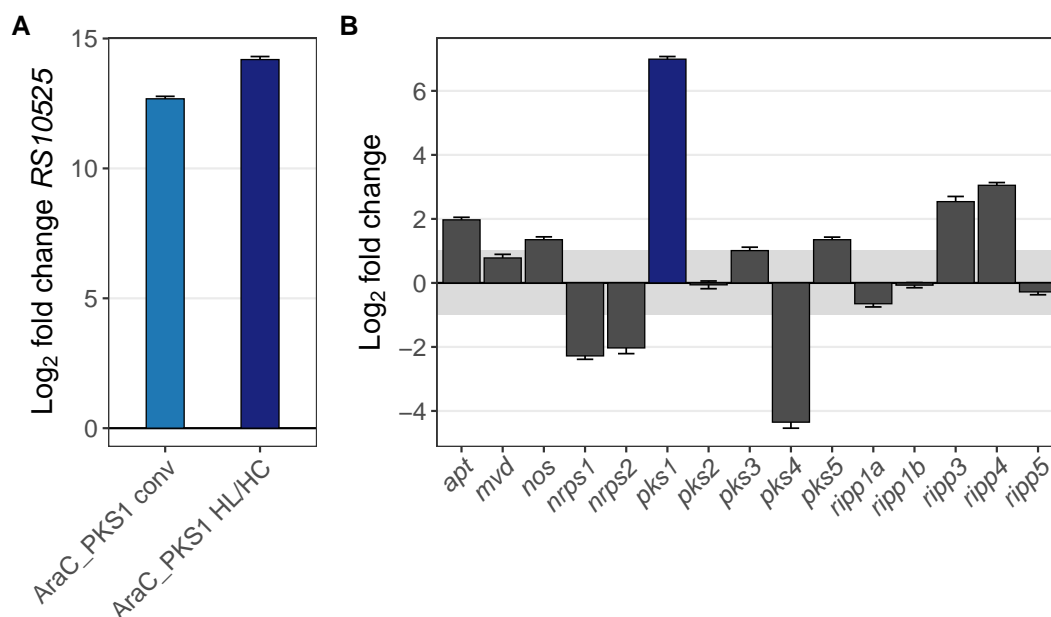
FIGURE 3.28: **Transcriptional changes in the AraC_PKS1 mutant cultivated under HL/HC conditions**

(A) Log_2 fold changes calculated from transcription levels of AraC_PKS1, cultivated under HL/HC or conventional conditions, relative to transcription levels of conventionally grown *N. punctiforme* WT. **(B)** Log_2 fold changes calculated from transcription levels of AraC_PKS1, cultivated under HL/HC conditions, relative to transcription levels of conventionally grown *N. punctiforme* WT. The transcript level range between -1 and 1 is shaded in grey, indicating the range of non-significant transcriptional differences between mutant and WT. The *pks1* BGC is highlighted in blue.

3.4.1   Bioactivity-Guided Purification of Signaling Factors

In order to identify a potential compound of the *pks1* BGC, the AraC_PKS1 mutant strain grown under HL/HC conditions was analyzed by HPLC. The HPLC analysis was conducted by Keishi Ishida (Leibniz Institute for Natural Product Research and Infection Biology, Hans Knöll Institute, Jena, Germany) as described in **Section 2.2.4.1**. Several prominent peaks in the supernatant and the cell pellet were revealed by this HPLC approach (see **Figure 3.29**). All major compound peaks (I–V, see **Figure 3.29**) found in the supernatant were fractionated for further analysis.
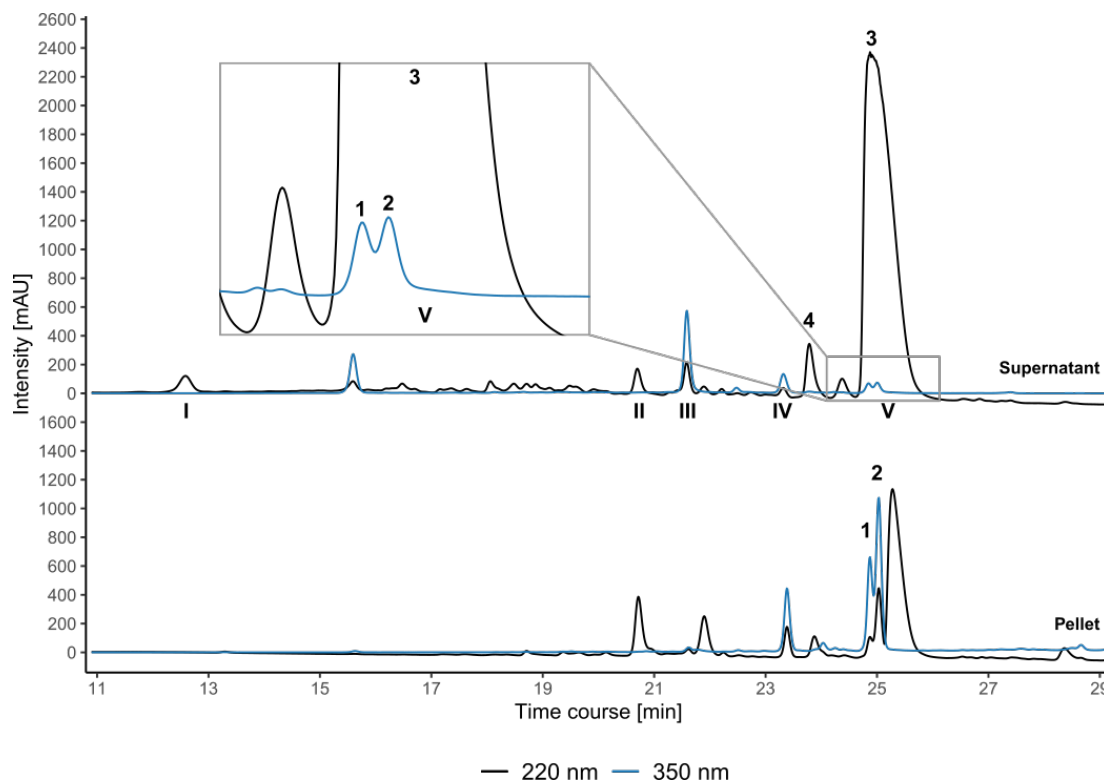
FIGURE 3.29: **HPLC profiles of AraC_PKS1 cultivated under HL/HC conditions**
The culture was grown for 20 days under HL/HC conditions. Preparative HPLC
was conducted by Keishi Ishida as described in **Section 2.2.4.1**. Major supernatant
peaks were labeled with I–V. Labels 1–4 representing the separate compound
peaks.

Since the transcriptomic and metabolic data of the AraC_PKS1 mutant strain
strongly suggested that the transcription of the orphan *ripp4* BGC might be
positively influenced by a *pks1*-derived signaling factor, a bioactivity guided
approach for the identification of the *pks1* compound was designed. For
that, the fractionated compounds (I–V) from the supernatant were added
separately to *ripp4* reporter mutant cultures and the cultures were analyzed
by fluorescence microscopy, as described in **Section 2.2.1.3.4**. After 24 h
of cultivation, the reporter culture treated with fraction V showed a strong
reaction. In contrast to the control culture, where the fluorescence was spatially
restricted, a bright and widely distributed fluorescence signal was observed
after treatment with fraction V (see **Figure 3.30**). Fraction V was the only
fraction which was able to trigger a visible reaction in the *ripp4* reporter strain.
Extended incubation times of 2, 3 and 7 days had no effect on the fluorescence
pattern of the reporter strain when treated separately with the fractions I–IV.
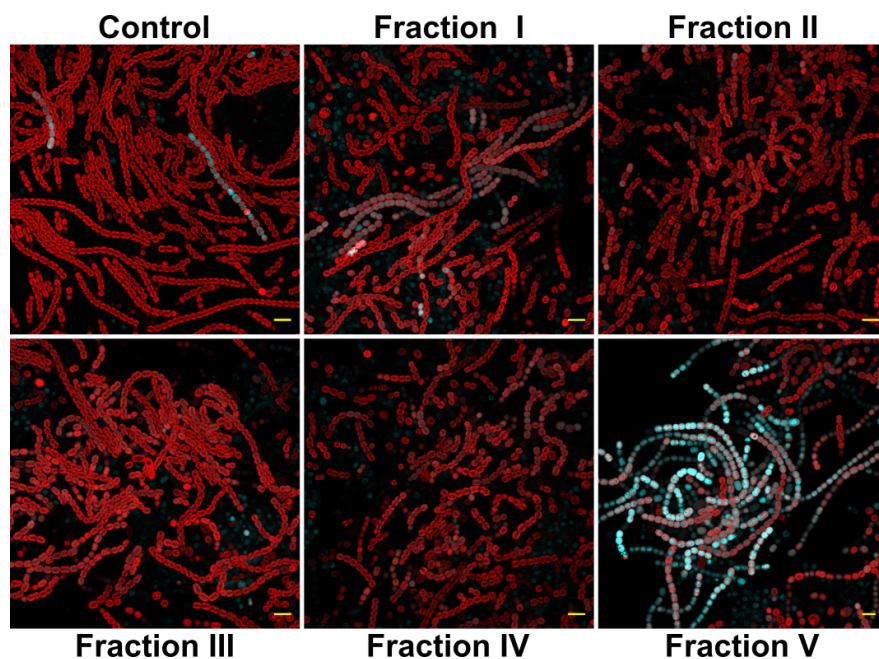
FIGURE 3.30: **Fluorescence micrographs of *ripp4* reporter strain treated with HPLC fractions from the AraC_PKS1 mutant strain**

Cultures of *ripp4* reporter strains were treated separately with the fractions I–V. An untreated *ripp4* reporter culture was used as a control. All cultures were grown conventionally for 24 h. The CFP fluorescence signal (blue) indicates promoter activity of the *ripp4* BGC. The Chlorophyll-α autofluorescence (red) indicates living vegetative cells. The images show merged CFP/Chlα channels. Yellow scale bars indicate 10 μm.

These findings suggest that the compound(s), represented by fraction V, are presumably the product(s) of the *pks1* BGC and are able to induce the expression of the *ripp4* gene cluster.

3.4.2   Structural Elucidation of PKS1 Compounds

The isolation and structural elucidation of the *pks1* compounds was done in cooperation with Keishi Ishida (Leibniz Institute for Natural Product Research and Infection Biology, Hans Knöll Institute, Jena, Germany).

Three potential *pks1* BGC compounds (**1–3**, see **Figure 3.29**) were identified by mass spectrometric analysis of the active fraction V. The compounds were isolated and purified from either the cell pellet or the supernatant, as described in **Section 2.2.4.3**. The purified compounds were further analyzed by a combination of LC-HRMS and NMR spectroscopy (see **Section 2.2.4.5**) to elucidate their structure.

Compound 1 ($C_{19}H_{16}O_3$, *m/z* 293.1166 [M+H]$^+$) and 2 ($C_{20}H_{18}O_4$, *m/z* 323.1278 [M+H]$^+$) were found to be derivatives of each other. They were identified

as new congeners, which are chemical substances sharing the same structural origin, of the nostoclide I and II metabolites that were previously found in a symbiotic *Nostoc* sp. strain of the lichen *Peltigera canina* [149]. Due to their characteristic core structure, nostoclides belong to the family of furanolide natural products. The newly found nostoclides were named N1 and N2. The chemical structures of N1 and N2 are shown in **Figure 3.31**.
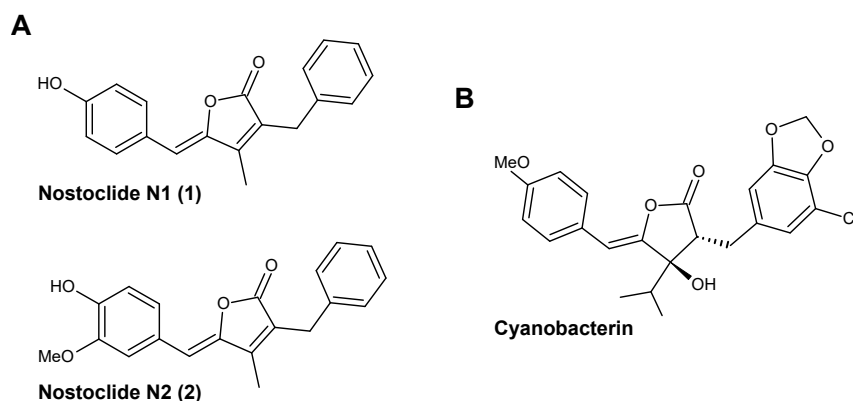
FIGURE 3.31: **Chemical structures of nostoclides (N1, N2) and cyanobacterin** **(A)** Chemical structures of nostoclide N1 (**1**) and N2 (**2**). Data provided by Keishi Ishida. **(B)** Chemical structure of cyanobacterin.

Compound 3 ($C_{20}H_{26}O_7$, *m/z* 377.1605 [M+H]$^-$) was identified as a novel polyketide with an unique bicyclic structure consisting of an oxepane-like moiety and a δ-valerolactone moiety. It was named nostovalerolactone (Nvl). In addition, a congener of Nvl, named 9-dehydronostovalerolactone, was found during the analysis (**4**, see **Figure 3.29**). The structures of these compounds are shown in **Figure 3.32**.

A

Nostovalerolactone (3)

9-Dehydronostovalerolactone (4)

B
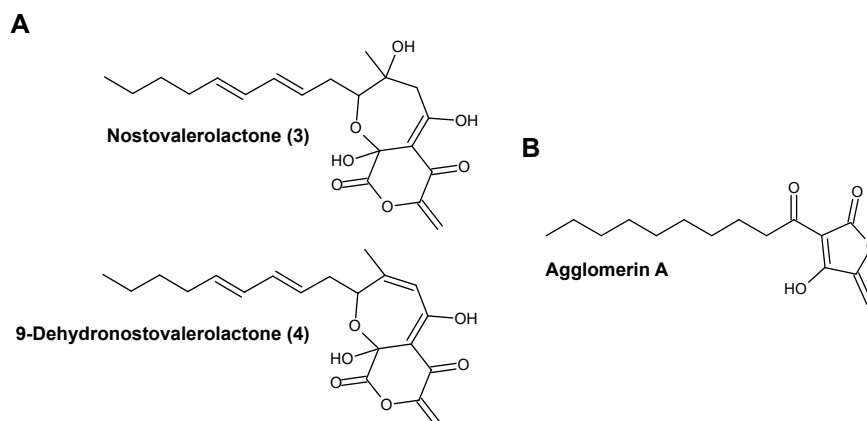
Agglomerin A

FIGURE 3.32: **Chemical structures of nostovalerolactone variants (3, 4) and agglomerin A**
(A) Chemical structures of nostovalerolactone (**3**) and 9-dehydronostovalerolactone (**4**). Data provided by Keishi Ishida. **(B)** Chemical structure of agglomerin A. Nostovalerolactone shares structural features with the linear tetronate agglomerin A.

3.4.2.1   Biosynthesis Proposal for Nostovalerolactone

In cooperation with Martin Baunach (University of Potsdam, Potsdam, Germany), a possible biosynthesis pathway for the newly found compounds was developed. Since the production of nostovalerlactone and nostoclide was clearly affected by the expression of the regulatory gene *RS10525*, it was assumed that the *pks1* BGC is involved in the biosynthesis of both compound types. Analysis of the *pks1* BGC sequence in comparison to other already characterized BGCs revealed that the *pks1* BGC can be split into two subclusters (see **Figure 3.33** and **Appendix Tables B.7–B.8**). A larger part of the gene cluster (*RS10430–RS10535*) is thought to be responsible for the production of nostovalerolactone and a smaller part (*RS10390–RS10425*) for the production of the two nostoclides.

FIGURE 3.33: **Segmentation of the *pks1* BGC**
The *pks1* BGC can be divided into two subclusters, one responsible for the production of nostovalerolactone and one for the production of nostoclides. The assignment is based on protein sequence homology to already characterized tetronate BGCs [150] and the BGC of cyanobacterin [151].

The nostovalerolactone (*nvl*) subcluster has a high number of gene products that show a homology to enzymes that are associated in already characterized tetronate biosynthetic pathways [150]. In addition, linear tetronate antibiotics like agglomerin A share several structural features with nostovalerolactone, such as a terminal lactone ring and a linear hydrocarbon tail [150] (see **Figure 3.32**). The homology that was found on structural and genetic levels was used to propose a biosynthesis model for nostovalerolactone. This model is shown in **Figure 3.34**.

The biosynthesis is initiated by NvlI, which acts as a loading module. Its fatty acyl-AMP ligase (FAAL) domain loads octanoic acid as a starter unit. By an acyl-CoA dehydrogenase (ACAD) domain the octanoic acid gets oxidized, before it is bound to the ACP domain of the NvlI module. Four elongation modules (Nvl J–M) belonging to the type I PKSs, are responsible for the extension of the PKS intermediate by several acyl-CoA substrates. Then, the formation of the bicyclic ring is initiated. For that, a glyceryl residue is transferred from a 1,3-bisphosphoglycerate by the glyceryl-S-ACP synthase NvlE to the ACP domain of NvlF. Then, the glyceryl residue is incorporated into the extended PKS intermediate and the bicyclic ring is formed with involvement of NvlD. Although, NvlD, NvlE, and NvlF are homologs of the enzymes RkD, E, and F that catalyze tetronate ring formation during the biosynthesis of the protein phosphatase inhibitor RK-682 in *Streptomyces* sp. 88–682 [152], an unusual bicyclic structure combining a δ-valerolactone ring with an oxepane-like moiety is formed instead of a tetronate ring. Notably, there is a difference in the number of oxygen atoms before (O_3+O_3) and after (O_7) ring formation. This led to the assumption that an oxygenation reaction is occurring during the ring formation process. After the ring formation has finished, two steps are necessary for the establishment of an exocyclic double bound. First, an oxygen is acetylated by NvlG, then acetic acid is eliminated by NvlN. NvlG and NvlN are homologs of the enzymes Agg4 and Agg5, which are able to catalyze a similar acetylation-elimination reaction during the biosynthesis of agglomerin [153]. The activities of NvlG and NvlN are responsible for the formation of 9-dehydronostovalerolactone. Afterwards, a hydroxylation reaction, catalyzed by the hydroxylase NvlH, yields the final compound nostovalerolactone. The structure was confirmed by feeding studies of the AraC_PKS1 mutant strain with 1-^{13}C and 1,2-^{13}C$_2$ labeled sodium acetate, as described in **Section 2.2.4.4**. The labeled substrates were incorporated into nostovalerolactone (see **Figure 3.34**), verifying its polyketide structure. However, the involvement of putative proteins, with no proposed
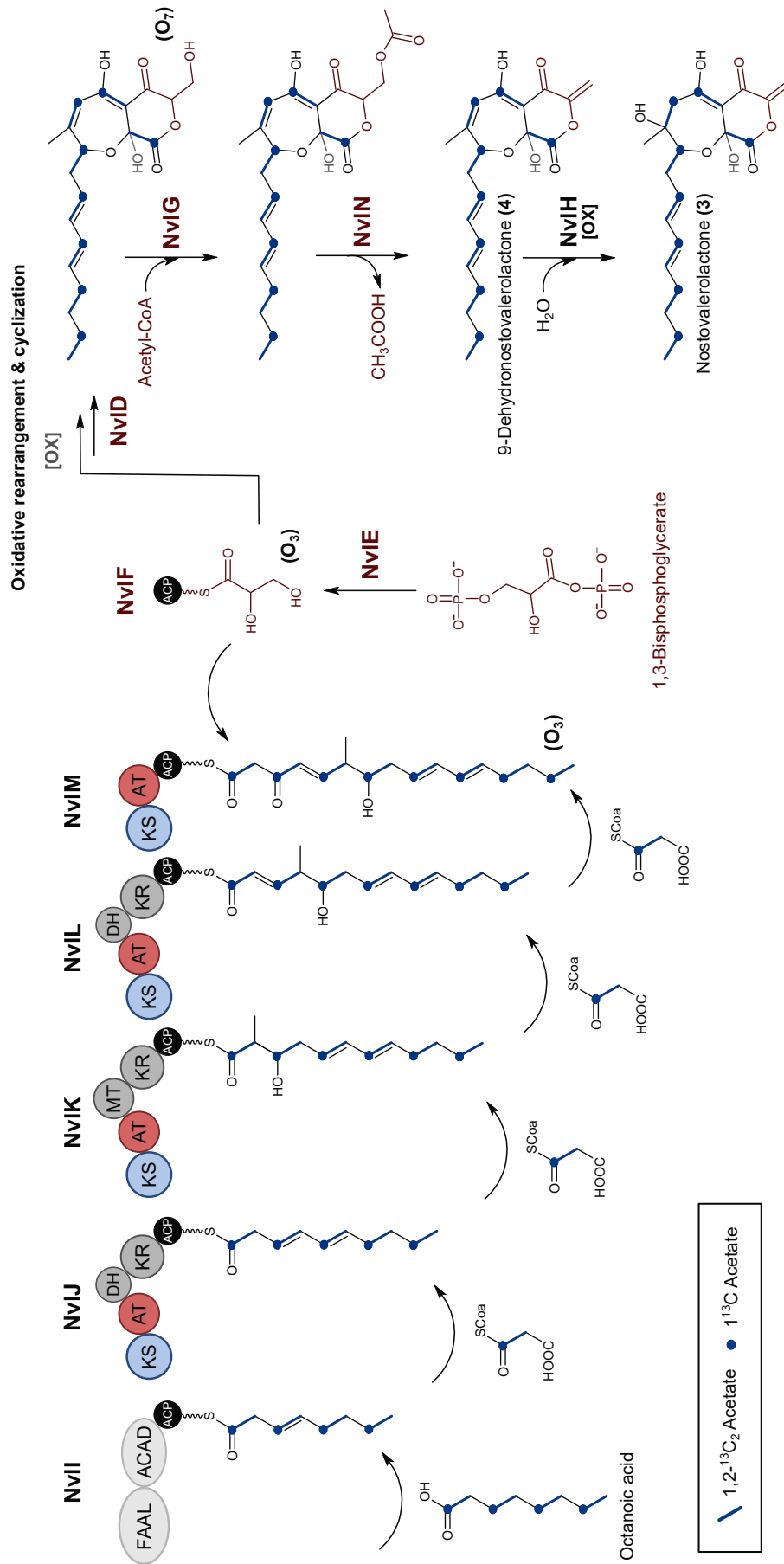
FIGURE 3.34: **Proposed biosynthesis model for nostovalerolactone**
Results of the feeding studies with 1-^{13}C and 1,2-^{13}C$_2$ labeled sodium acetate are indicated in blue. Data provided by Martin Baunach and Keishi Ishida.

FAAL: fatty acyl-AMP ligase, ACAD: acyl-CoA dehydrogenase, ACP: acyl carrier protein, KS: ketoacylsynthase, AT: acyl transferase, DH: dehydratase, KR: ketoreductase, MT: C-methyltransferase.

or confirmed function, and further details on the formation of the unusual bicyclic ring and the oxygenation remain unclear.

The nostoclide (*ncl*) subcluster shows similarity to the recently described BGC of cyanobacterin [151], a known photosynthesis inhibitor [154]. By having a furanolide core structure, the nostoclides also have a similarity to cyanobacterin on the structural level (see **Figure 3.31**). A recent study by D'Agostino et. al [151] revealed that four of the proteins encoded in the cyanobacterin BGC are necessary for the synthesis of the furanolide core structure. This includes the proteins CybB, an aromatic amino acid ammonia lyase, CybC, a long-chain acyl-CoA synthetase, CybE, a thiamine pyrophosphate-binding protein and CybF, a 3-oxoacyl-ACP synthase. Homologs of all four proteins were also found in the *ncl* subcluster, encoded by the genes *nclD*, *nclE*, *nclF* and *nclG* (see **Appendix Table B.8**). Therefore, it is assumed that the biosynthesis of the newly found nostoclides (N1, N2) is strongly related to the recently described biosynthesis of cyanobacterin.

3.5   Elucidation of a Signaling Pathway in *N. punctiforme*

To find additional evidence about a potential signaling pathway involving the regulatory gene *RS10525* and the *pks1* BGC compounds, RNA sequencing studies were conducted. These studies provided more insights into the transcriptional changes in the AraC_PKS1 mutant strain, the involvement of abiotic factors and the role of the *pks1* BGC compounds. In allelopathy assays, the influence of secreted factors, especially nostoclides, on different cyanobacteria and the eukaryotic alga *Chlamydomonas reinhardtii* (*C. reinhardtii*) was analyzed.

3.5.1   RNA Sequencing Studies

For the first RNA sequencing study, AraC_PKS1 and *N. punctiforme* WT were cultivated under conventional cultivation conditions and under HL/HC cultivation conditions for 20 days. The different samples are referred to as AraC_PKS1 conv, AraC_PKS1 HL/HC, WT conv and WT HL/HC. The RNA was extracted (see **Section 2.2.2.12**) and RNA sequencing and subsequent raw data processing was conducted as described in **Section 2.2.2.14**. For the calculation of $\log_2$ fold changes, the transcription levels of the conventionally grown WT strain served as reference. Furthermore, a $\log_2$ fold change of $\pm$ 1 and a p-value ≤ 0.01 were used as threshold values to indicate meaningful transcriptional changes.

The analysis revealed that from a total set of 7522 genes, predicted for the genome of *N. punctiforme*, 588 genes ($\sim$8%) were upregulated and 296 genes ($\sim$4%) were downregulated in the conventionally grown AraC_PKS1 mutant. The number of influenced genes can be calculated from the overlapping and non-overlapping areas of the venn diagrams visualized in **Figure 3.35**. For example, the number of upregulated genes in AraC_PKS1 conv is reflected by the sum of uniquely upregulated genes (310), genes upregulated in AraC_PKS1 conv and AraC_PKS1 HL/HC (127), genes upregulated in AraC_PKS1 conv and WT HL/HC (55) and genes upregulated in all three samples (96).

The HL/HC cultivation conditions led to an upregulation of 768 ($\sim$10%) genes and a downregulation of 642 ($\sim$8.5%) genes in the mutant strain. Only a fraction of the genes that show an altered transcription level is influenced under both cultivation conditions, 223 of the upregulated genes and 110 of the downregulated genes. Remarkably, high light and high CO_2 cultivation

conditions had a much greater impact on the WT strain, with 1412 ($\sim$19%) upregulated genes and 1471 ($\sim$19.5%) downregulated genes. An overview of up- and downregulated genes in all tested samples is visualized in **Figure 3.35**.
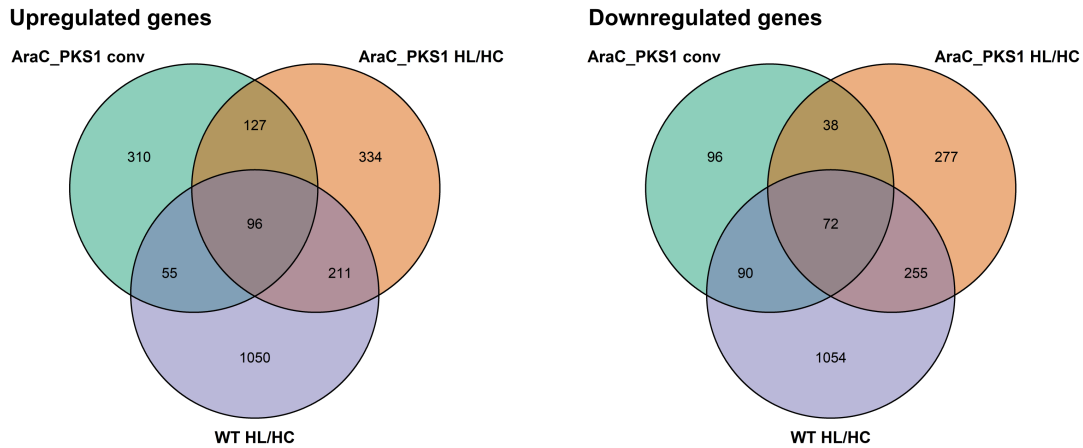
FIGURE 3.35: **Overview of up- and downregulated genes in the AraC_PKS1 mutant and the WT HL/HC sample**
Non-overlapping areas represent the number of genes that are uniquely influenced in one of the samples. Overlapping areas represent the number of genes influenced in multiple samples. The AraC_PKS1 mutant was grown conventionally (AraC_PKS1 conv) and under HL/HC conditions (AraC_PKS1 HL/HC). The WT strain was grown under HL/HC conditions (WT HL/HC). A conventionally grown WT strain was used as a reference.

The affected genes were assigned to functional categories according to the Clusters of Orthologous Groups of protein [COG] database [155, 156] (see **Appendix Figure A.3**). This revealed that in all tested samples, a large fraction of the affected genes are genes of unknown function and genes for which only a general function is known. In the AraC_PKS1 mutant, especially when grown under HL/HC conditions, genes related to the cell wall and membrane were upregulated.

Noticeably, the mutant showed an impact on genes related to secondary metabolite biosynthesis. In the AraC_PKS1 conv sample, 7% of the genes assigned to this COG-category were upregulated and 9% were downregulated. In the AraC_PKS1 HL/HC sample, the effect on secondary metabolite biosynthesis related genes was even higher. Here, 20% of the assigned genes were positively and 11% were negatively influenced. These data confirm the observations from the high cell density (see **Section 3.2.1**) and transcriptional reporter studies (see **Section 3.2.2**) that light, CO_2 and cell-density have a strong impact on specialized metabolite production.

A closer look at the transcriptional data of the genes, belonging to the 15 BGCs that were predicted by AntiSMASH (see **Section 3.1**), showed that the positively influenced BGCs in the AraC_PKS1 mutant can be divided into two categories. Category I includes BGCs that are upregulated independently of the cultivation conditions used, whereas category II only includes BGCs that are upregulated when the mutant is cultivated under HL/HC conditions.

The BGCs *pks1*, *ripp3* and *ripp4* were assigned to category I. Especially, the transcription of the *pks1* BGC was greatly increased (see **Figures 3.36** and **3.37**) in the AraC_PKS1 mutant strain. All genes of the *ncl* subcluster were strongly upregulated, with $\log_2$ fold changes ranging from 6.6 to 12.4. However, when the mutant was grown under HL/HC cultivation conditions the transcription levels of all genes were always slightly higher than in the conventionally grown mutant (see **Figures 3.36**). HPLC analysis of the mutant showed that under both cultivation conditions the amount of nostoclide was higher than in the WT strain. But, in agreement with the transcriptomic data, the amount was higher in the AraC_PKS1 HL/HC sample. The WT HL/HC sample also showed elevated transcription levels ($\log_2$ fold changes = 3–8.5) for the *ncl* subcluster, but these were not as high as in the mutant strain. Still, the expression levels were too low to detect the *ncl* compound by HPLC (see **Figures 3.36**).

FIGURE 3.36: **Transcriptional response of the *ncl* subcluster in the AraC_PKS1 mutant, grown conventionally and under HL/HC conditions, and in the HL/HC cultivated WT**
The heatmap visualizes the $\log_2$ fold changes of the *ncl* subcluster in the samples AraC_PKS1 conv, AraC_PKS1 HL/HC and WT HL/HC in comparison to the reference sample WT conv. The HPLC chromatogram shows the corresponding nostoclide (N1/N2) peak. Culture supernatants were used for HPLC analysis. The chromatogram is shown at a wavelength of 350 nm.

Almost all the genes assigned to the *nvl* subcluster were strongly upregulated in the AraC_PKS1 mutant strain, regardless of the cultivation conditions that

were used ($\log_2$ fold changes$_{conv}$ = 1.9–12.3 and $\log_2$ fold changes$_{HL/HC}$ = 3.1–13). Again, the transcription levels of the single genes were higher when the mutant was grown under HL/HC cultivation conditions. The expression of the *nvl* subcluster was also increased in the WT HL/HC sample ($\log_2$ fold changes = 2.3–12.4). This time, the transcriptions levels were more similar to the mutant strain. The transcriptional differences between all tested samples are also reflected at the metabolic level (see **Figure 3.37**).

nvl	RS10445	RS10450	RS10455	RS10460	RS41710	RS10465	RS10470	RS10475	RS10480	RS10485	RS10490	RS10495	RS10500	RS10505	RS10510	RS10515	RS37470	RS10525	RS10530	RS10535
WT HL/HC	2.7	6.7	5.6	6.4	8.1	6	7.3	7.2	2.3	7.6	9	10.5	8.8	10.5	10.4	12.4	11.2	11.4	9.1	7.8
AraC_PKS1 conv	4.5	8.6	7.4	5.6	7.3	5.1	6.2	5.6	0.3	5.9	7.7	8.6	6.9	8.1	8.4	2.4	1.9	12.3	2	0.8
AraC_PKS1 HL/HC	5.4	10	8.2	8.7	9.7	8.1	8.9	8.4	3.1	8.6	9.6	11	8.7	10.3	10.7	6.4	5.2	13	3.1	3.9

$\log_2$ fold change
-10 -5 0 5 10

FIGURE 3.37: **Transcriptional response of the *nvl* subcluster in the AraC_PKS1 mutant, grown conventionally and under HL/HC conditions, and in the HL/HC cultivated WT**
The heatmap visualizes the $\log_2$ fold changes of the *nvl* subcluster in the samples AraC_PKS1 conv, AraC_PKS1 HL/HC and WT HL/HC compared to the reference sample WT conv. The HPLC chromatogram shows the corresponding nostovalerolactone (Nvl) peak. Culture supernatants were used for HPLC analysis. The chromatogram is shown at a wavelength of 350 nm.

A check on all precursor genes of the different RiPP BGCs revealed that the precursor genes of the orphan BGCs *ripp3* and *ripp4* had an upregulated transcription level in the AraC_PKS1 mutant strain ($\log_2$ fold changes = 3.5–4.8). In this case, the WT HL/HC sample did not show any similar transcriptional changes (see **Figure 3.38**). Beside the precursor genes, not all the genes that were assigned to the BGCs *ripp3* and *ripp4* were upregulated in the mutant strain (see **Figure 3.38**). For the *ripp3* BGC, the AraC_PKS1 conv sample showed slightly increased transcript levels only for the genes *RS16800* ($\log_2$ fold change = 1.5) and *RS16790* ($\log_2$ fold change = 1.2), which are located adjacent to the precursor gene *RS16795*. The gene *RS16800* encodes a hypothetical protein and *RS16790* a lanthibiotic biosynthesis protein (LanM). In the AraC_PKS1 HL/HC sample, only the precursor gene of the *ripp3* BGC showed an increased transcription level ($\log_2$ fold change = 4.7). Noticeably, the transcript level of the gene *RS16765*, encoding the response regulator, was not affected in any of the analyzed samples. In case of the *ripp4* BGC, the samples AraC_PKS1 conv and AraC_PKS1 HL/HC showed an upregulated

transcript level for the genes *RS25520* ($\log_2$ fold change = 2.7 and 2.2) and *RS25525* ($\log_2$ fold change = 3.7 and 2.2) in addition to the two precursor genes *RS25510* and *RS25515*. *RS25520* encodes a lanthibiotic biosynthesis protein (LanM) and *RS25525* a secretion protein. Again, the transcription of the regulatory genes (*RS25500*, *RS25505*) was not affected in the mutant strain.

RiPP precursor genes

	RS16230 (ripp1a)	RS16235 (ripp1a)	RS16240 (ripp1a)	RS16245 (ripp1a)	RS16250 (ripp1a)	RS16255 (ripp1a)	RS16310 (ripp1b)	RS16315 (ripp1b)	RS16320 (ripp1b)	RS16795 (ripp3)	RS25510 (ripp4)	RS25515 (ripp4)	RS38030 (ripp5)	RS38845 (mvd)
WT HL/HC	-1.6	-2.6	-1.4	-0.7	-2.4	-2	1.7	0.5	0.6	0.1	-1.3	-1.4	-2.1	-0.1
AraC_PKS1 conv	0.4	0.2	-0.5	0	-0.4	0.7	0.5	0.7	-0.3	4.8	3.7	3.5	0.3	0.1
AraC_PKS1 HL/HC	0.8	0.8	0.5	0	0.5	0.9	0.6	-0.5	0.7	4.7	3.7	4.4	0.6	2

Log$_2$ fold change −5.0 −2.5 0.0 2.5 5.0

ripp3

	RS16765	RS16770	RS16780	RS16785	RS16790	RS16795	RS16800	RS40840
WT HL/HC	0.5	0.7	0	-0.2	0.3	0.1	4.4	0.8
AraC_PKS1 conv	-0.1	0.1	-0.5	0.4	1.2	4.8	1.5	0.2
AraC_PKS1 HL/HC	0.3	0.3	0.6	-0.6	-0.1	4.7	0.7	-0.3

ripp4

	RS25500	RS25505	RS25510	RS25515	RS25520	RS25525	RS25530	RS25535	RS25540	RS25545	
-2.4	-1.8	-1.3	-1.4	-1	-0.7	-0.1	-0.5	1.5	0.4	WT HL/HC
-0.5	0.6	3.7	3.5	2.7	3.7	1.2	0.9	0.4	-0.1	AraC_PKS1 conv
-0.5	-0.4	3.7	4.4	2.2	2.2	0.5	0.6	0.7	0	AraC_PKS1 HL/HC

FIGURE 3.38: **Transcriptional response of RiPP BGCs in theAraC_PKS1 mutant, grown conventionally and under HL/HC conditions, and in the HL/HC cultivated WT**
The heatmaps visualize the $\log_2$ fold changes of all RiPP precursor genes and of the orphan BGCs *ripp3* and *ripp4* in the samples AraC_PKS1 conv, AraC_PKS1 HL/HC and WT HL/HC compared to the reference sample WT conv.

The BGCs *apt*, *mvd*, *nos* and the orphan gene clusters *pks2* and *pks3* were assigned to category II BGCs, because they were only upregulated in the AraC_PKS1 HL/HC sample (see **Figures 3.39–3.42**). Since the genes associated with the production of scytonemin, a photoprotective metabolite, showed a similar behavior (see **Figure 3.43**), the scytonemin (*scy*) cluster was also assigned to the category II BGCs.

All the genes assigned to the *apt* BGC showed a slightly elevated transcript level in the AraC_PKS1 HL/HC sample compared to the WT conv reference sample, with $\log_2$ fold changes ranging from 1.3 to 2.9. Consistent with this, HPLC analysis of the AraC_PKS1 HL/HC sample detected a distinct peak representing anabaenopeptin. Although the transcription of *apt* remained almost unchanged in the WT HL/HC sample compared to the reference, a compound peak was detectable by HPLC analysis.

FIGURE 3.39: **Transcriptional response of the *apt* BGC in the AraC_PKS1 mutant, grown conventionally and under HL/HC conditions, and in the HL/HC cultivated WT**
The heatmap visualizes the $\log_2$ fold changes of the *apt* BGC in the samples AraC_PKS1 conv, AraC_PKS1 HL/HC and WT HL/HC compared to the reference sample WT conv. The HPLC chromatogram shows the corresponding anabaenopeptin (Apt) peak. Cell pellets were used for HPLC analysis. The chromatogram is shown at a wavelength of 199 nm.

Similar to the genes of the *apt* BGC, all the genes belonging to the *mvd* BGC were slightly upregulated in the AraC_PKS1 HL/HC sample ($\log_2$ fold changes = 1.8–3.7). Due to the fact that also a conventionally grown *N. punctiforme* culture is capable to produce small amounts of microviridin, it was not surprising that all WT and mutant samples showed a respective compound peak in the HPLC analysis (see **Figure 3.40**).

FIGURE 3.40: **Transcriptional response of the *mvd* BGC in the AraC_PKS1 mutant, grown conventionally and under HL/HC conditions, and in the HL/HC cultivated WT**
The heatmap visualizes the $\log_2$ fold changes of the *mvd* BGC in the samples AraC_PKS1 conv, AraC_PKS1 HL/HC and WT HL/HC compared to the reference sample WT conv. The HPLC chromatogram shows the corresponding microviridin peak. Cell pellets were used for HPLC analysis. The chromatogram is shown at a wavelength of 199 nm.

In case of the *nos* BGC, the majority of the assigned genes showed an upregulated transcription in the AraC_PKS1 HL/HC samples ($\log_2$ fold

changes = 2.1–3.4). Only three genes, encoding hypothetical proteins, located at the 5′ end of the gene cluster were not positively influenced (see **Figure 3.41**). These findings are reflected on the metabolic level by two distinct compound peaks in the HPLC analysis representing the two nostopeptolide variants, Nos1052 and NosA. Although, the transcription of *nos* was slightly negatively influenced in the WT HL/HC sample, a clear peak, which was greater than the peak found for the conventional sample, was detected by HPLC analysis.
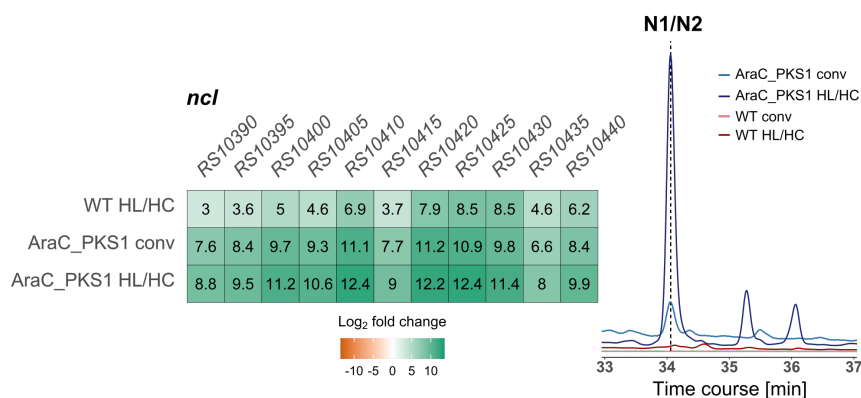

FIGURE 3.41: **Transcriptional response of the *nos* BGC in the AraC_PKS1 mutant, grown conventionally and under HL/HC conditions, and in the HL/HC cultivated WT**
The heatmap visualizes the log$_2$ fold changes of the *nos* BGC in the samples AraC_PKS1 conv, AraC_PKS1 HL/HC and WT HL/HC compared to the reference sample WT conv. The HPLC chromatogram shows the corresponding nostopeptolide peaks (Nos1052, NosA). Cell pellets were used for HPLC analysis. The chromatogram is shown at a wavelength of 199 nm.

The transcriptomic data of the orphan gene clusters *pks2* and *pks3* revealed that all genes, except the transporter-related gene *RS17080* in the *pks3* BGC, had an increased transcript level in the AraC_PKS1 HL/HC sample (see **Figure 3.42**). The WT HL/HC sample did not show a similar effect on the transcription of the two BGCs (see **Figure 3.42**).

pks2

	RS15970	RS15975	RS15980	RS15985	RS15990	RS15995	RS15600	RS37680	RS16005	RS16010	RS16015	RS16020	RS16025	RS16030	RS37685	RS16045	RS16050	RS16055	RS16060	RS37690	RS16070	RS16075	RS16080	RS37695	RS16090
WT HL/HC	0	-0.7	1	-0.9	0	-0.1	0.6	2	0.4	0.5	-0.5	-0.8	0.2	-0.4	0.3	-0.9	-0.3	-0.9	-1.5	-2.4	0.5	0.8	2.8	2.7	1.3
AraC_PKS1 conv	-0.6	-0.9	-0.5	0.3	0	-0.4	-0.8	0.1	0.5	-0.2	-0.7	-0.7	0.6	1	-0.5	-0.8	-0.6	-1.1	-1.7	-3.3	0	-0.2	1.5	1.8	1.3
AraC_PKS1 HL/HC	5.4	1.6	4.6	4.7	5	3.5	3.8	4.6	4.3	3.6	2.4	1.8	2.8	1.8	1.5	2.4	1.4	2.1	2.9	3.8	1.9	2.6	3.9	4.1	1.7

pks3

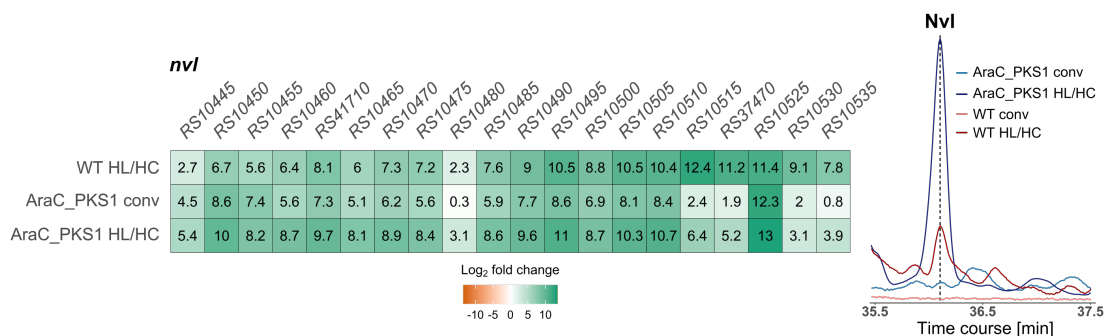|	RS17005	RS40855	RS17010	RS17015	RS17020	RS17025	RS17030	RS17035	RS17040	RS17045	RS17050	RS17055	RS17060	RS17065	RS17070	RS17075	RS17080	RS17085
WT HL/HC	-0.6	-0.8	-1.3	-2.4	-1.3	0.2	-0.7	-0.6	-0.2	-0.7	-0.1	-0.6	-0.6	0.4	-0.8	-1.3	0.7	-0.5
AraC_PKS1 conv	-0.2	-0.3	0.5	0.4	0.2	0.1	-0.2	0.1	0.5	0.3	0.2	0.6	0.6	0.1	-0.4	0.2	-0.6	-0.1
AraC_PKS1 HL/HC	1.7	1.7	3.5	3.6	2.6	2.8	3.1	3.2	4	3.9	3.4	3.8	4.1	2.1	3	2	0.4	1.4

Log$_2$ fold change

-5.0 -2.5 0.0 2.5 5.0

FIGURE 3.42: **Transcriptional response of the *pks2* and *pks3* BGCs in the AraC_PKS1 mutant, grown conventionally and under HL/HC conditions, and in the HL/HC cultivated WT**
The heatmaps visualize the log$_2$ fold changes of the orphan BGCs *pks2* and *pks3* in the samples AraC_PKS1 conv, AraC_PKS1 HL/HC and WT HL/HC compared to the reference sample WT conv.

The genes associated with the production of scytonemin had strongly elevated transcription levels in the AraC_PKS1 HL/HC sample, with log$_2$ fold changes ranging from 4.0 to 10.5 (see **Figure 3.43**). In the WT HL/HC sample, only a few genes showed an upregulated transcript level, but not as high as in the mutant strain. Only in the AraC_PKS1 HL/HC sample, the regulatory genes (*RS06505* – sensor histidine kinase, *RS06510* – OmpR/AraC-type response regulator) that were assigned to the *scy* gene cluster [157] showed an increased transcript level. Despite the increased transcription, scytonemin could not be detected in the mutant strain. Instead, a scytonemin monomer, also referred to as prescytonemin, was found in the supernatant of the HL/HC cultivated AraC_PKS1 mutant strain.
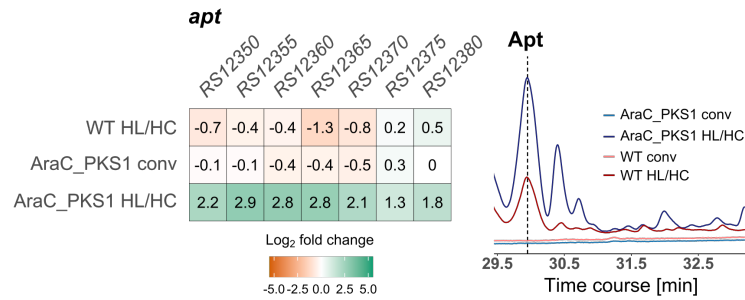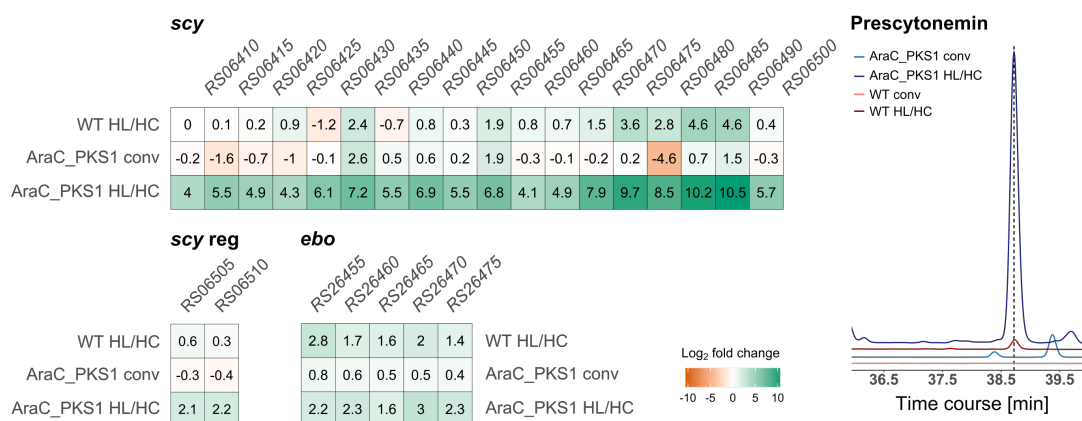
FIGURE 3.43: **Transcriptional response of the *scy* and *ebo* cluster in the AraC_PKS1 mutant, grown conventionally and under HL/HC conditions, and in the HL/HC cultivated WT**
The heatmaps visualize the $\log_2$ fold changes of the genes assigned to the production of scytonemin (*scy, ebo* and regulatory genes (*scy* reg)) in the samples AraC_PKS1 conv, AraC_PKS1 HL/HC and WT HL/HC compared to the reference sample WT conv. The HPLC chromatogram shows the prescytonemin peak. Culture supernatants were used for HPLC analysis. The chromatogram is shown at a wavelength of 410 nm.

The isolation and structural elucidation of this scytonemin monomer was again done in cooperation with Keishi Ishida (Leibniz Institute for Natural Product Research and Infection Biology, Hans Knöll Institute, Jena, Germany) as described in **Section 2.2.4.3** and **2.2.4.5**. The obtained structure of the monomer is shown in **Figure 3.44A**. In a recent study by Klicki et al. [158], this monomer was described as a scytonemin precursor. They figured out that the scytonemin monomers are usually transported to the periplasm, where the final product (see **Figure 3.44B**) is formed by oxidative dimerization. A cluster of five conserved genes, called *ebo* cluster, is involved in the export of the monomers from the cytoplasm to the periplasm. A look into the transcriptional data of the *ebo* cluster showed that these genes had an upregulated transcription ($\log_2$ fold changes = 2.2–3.0) in the AraC_PKS1 HL/HC sample, but the transcription was not as much increased as the transcription of the genes belonging to the *scy* cluster (see **Figure 3.43**).
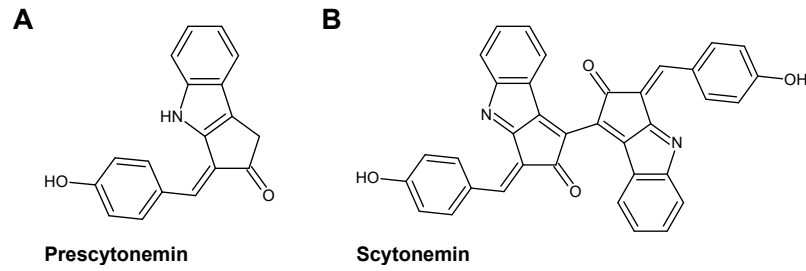
FIGURE 3.44: **Chemical structures of prescytonemin and scytonemin**
(A) Chemical structure of the scytonemin monomer, also referred to as prescytonemin. **(B)** Chemical structure of scytonemin.

The transcriptome analysis further revealed two BGCs, *pks4* and *pks5*, that seem to be modifiable by HL/HC cultivation conditions (see **Figure 3.45**). The majority of the *pks4* BGC genes was negatively influenced in the WT HL/HC and the AraC_PKS1 HL/HC samples. In contrast to that, the majority of the *pks5* BGC genes showed an upregulated transcript level. Here, the observed effect was stronger in the WT HL/HC ($\log_2$ fold changes = 2.0–4.3) than in the AraC_PKS1 HL/HC sample ($\log_2$ fold changes = 1.6–2.0).

pks4

	RS17290	RS17295	RS17300	RS17305	RS17310	RS17315	RS17320	RS37760	RS17330	RS17335	RS17340	RS17345	RS17350	RS17355	RS17360	RS17365	RS17370	RS17375	RS17380	RS17385	RS17390	RS17395	RS17400	RS17405	RS17410	RS17415	RS17420	RS17425	RS17430	RS17435	RS17440	RS17445	RS17450	RS17455
WT HL/HC	-1.8	-1.7	-0.2	-1.6	-0.1	0.5	-1.6	-1.5	-1.7	-3.3	-2.6	-0.6	-1	-0.3	-1.6	-1.2	-1.6	-0.5	-2.3	-2.5	-1.6	-2.2	-2.8	-2.1	-0.7	-2.8	-1.4	0.5	0.4	-0.5	-1.5	-1	-1.7	-3.1
AraC_PKS1 conv	-0.3	0.4	-0.5	-0.5	-0.7	-0.5	-1	-0.7	-0.8	-0.3	-0.7	-1	-0.8	-0.7	-0.6	-0.7	-1.1	-1.2	-0.9	-0.8	-0.6	-0.3	0.1	0	-0.3	-2.6	-1.3	0.5	-0.3	-0.3	-1.3	-1.2	0.4	-0.2
AraC_PKS1 HL/HC	0.8	-0.4	0.6	0.1	-0.3	-0.6	-1.6	-2.3	-1.6	-1.3	-2.1	-1.7	-1.7	-1.2	-1.5	-1.9	-2.1	-2.5	-1.5	-1.8	-2.4	-1.8	-2.5	-2.5	-3.5	-1.8	-1.2	0.1	-0.7	-0.9	-2.1	-2.5	-1.3	-2.7

pks5

	RS33505	RS33510	RS38005	RS33525	RS33530	RS33535	RS33540	RS40215
WT HL/HC	-1.6	-2.2	-1.9	2	2.4	4.3	3.3	4.3
AraC_PKS1 conv	-0.3	-1	-0.2	0.5	0.1	0.8	0	0.5
AraC_PKS1 HL/HC	0.4	-0.3	-0.6	1.6	2	1.9	1.9	1.7

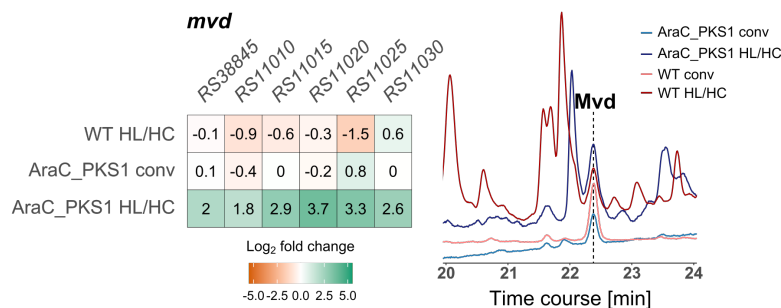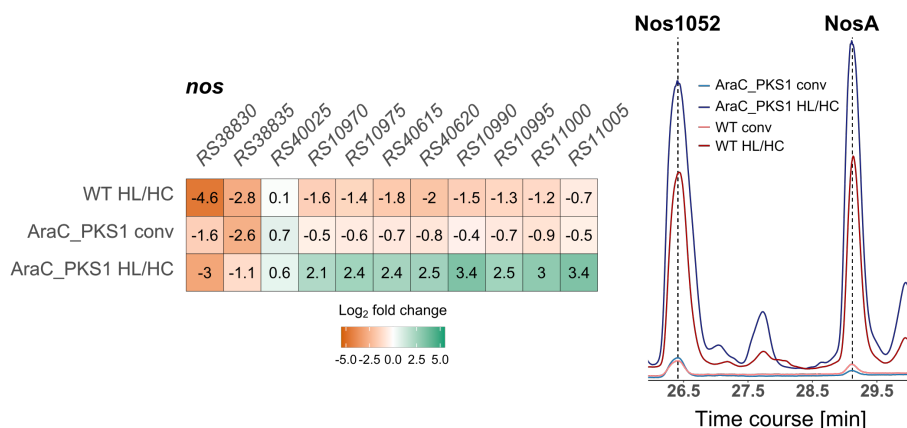$\log_2$ fold change

-5.0 -2.5 0.0 2.5 5.0

FIGURE 3.45: **Transcriptional response of the *pks4* and *pks5* BGCs in the AraC_PKS1 mutant, grown conventionally and under HL/HC conditions, and in the HL/HC cultivated WT**
The heatmaps visualize the $\log_2$ fold changes of the orphan BGCs *pks4* and *pks5* in the samples AraC_PKS1 conv, AraC_PKS1 HL/HC and WT HL/HC compared to the reference sample WT conv.

Apart from genes assigned to BGCs, the list of upregulated genes in the AraC_PKS1 mutant strain also includes genes encoding proteins involved in secretion and chemotaxis (PilA, PilB, PilC, PilT). In addition, several regulatory key genes were upregulated as well, including the genes, which encode the sigma factors B, C and J and the RNA chaperone Hfq (see **Figure 3.46**). Only sigma factor B was strongly positively affected by HL/HC cultivation conditions.
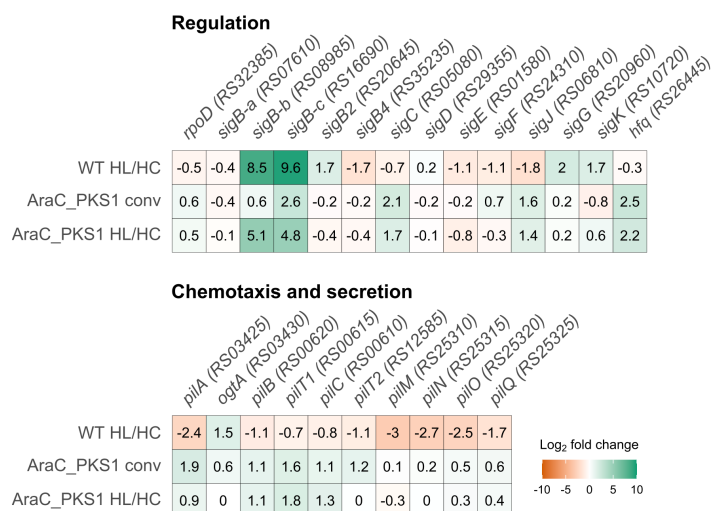
FIGURE 3.46: **Transcriptional response of genes typically involved in chemotaxis, secretion or regulation in the AraC_PKS1 mutant, grown conventionally and under HL/HC conditions, and in the HL/HC cultivated WT** The heatmaps visualize the $\log_2$ fold changes of genes typically involved in chemotaxis, secretion or regulation in the samples AraC_PKS1 conv, AraC_PKS1 HL/HC and WT HL/HC compared to the reference sample WT conv.

This initial RNA sequencing study has revealed that specialized metabolite production is strongly upregulated in the AraC_PKS1 mutant strain and can be even further enhanced, when combined with HL/HC cultivation conditions. This shows that the regulatory gene *RS10525* and thus the presence of the *pks1*-derived compounds could play an important role in a signaling pathway. To gain further insights into the role that the two *pks1* BGC products might play for the transcriptional changes in the AraC_PKS1 mutant strain, a second RNA sequencing study was planned and conducted. For this, two-day-old cultures of *N. punctiforme* WT were treated with N1, N2, both nostoclides or nostovalerolactone (final concentration: 15 µM). The cells were harvested after 24 h and the RNA was extracted. The different samples are referred to as WT N1, WT N2, WT N1 + N2 and WT Nvl. The transcription was analyzed in a preliminary RT-qPCR. Here, it was found that N1 showed a lower effect on the transcription of category I BGCs than N2 or the combination of both nostoclides (see **Figure 3.47**). Consequently, RNA sequencing was only carried out for the WT N2, WT N1 + N2 and WT Nvl samples.
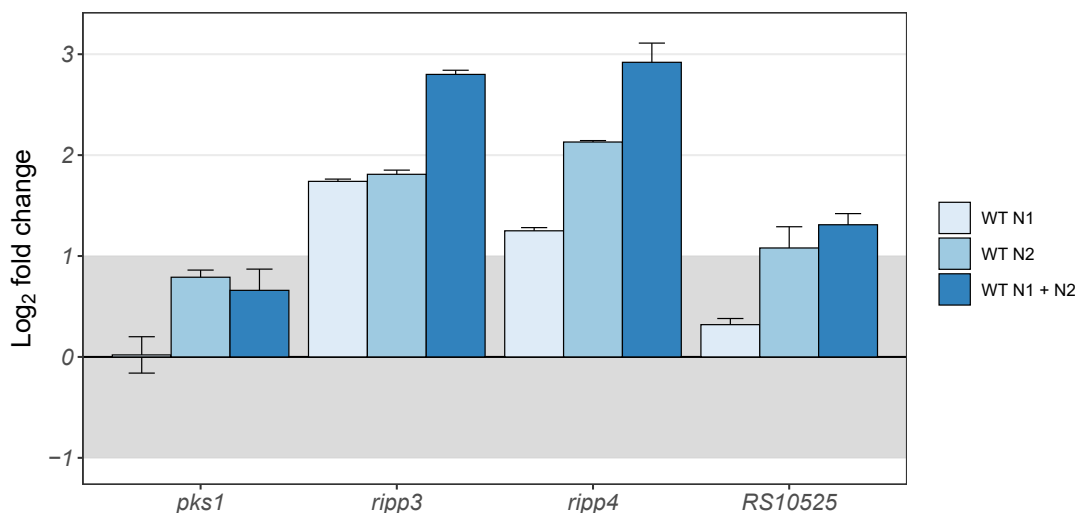
FIGURE 3.47: **Transcriptional changes of category I BGCs after nostoclide treatment in the *N. punctiforme* WT**
Log$_2$ fold changes were calculated from transcription levels of a *N. punctiforme* WT culture treated with nostoclides (N1, N2 or a combination) relative to transcription levels of an untreated WT culture. The transcript level range between -1 and 1 is shaded in grey, indicating the range of non-significant transcriptional differences between treated and untreated sample. *pks1*, *ripp3* and *ripp4* represent the category I BGCs. *RS10525*: regulatory gene of the *pks1* BGC

Similar to the first RNA sequencing study, the transcription levels of an untreated conventionally grown WT strain served as the reference for the calculation of log$_2$ fold changes. As threshold values, log$_2$ fold changes ± 1 and a p-value ≤ 0.01 were used.

Analysis of transcriptomic data revealed that the addition of N2 to a *N. punctiforme* WT culture led to an upregulation of 258 genes and a downregulation of 554 genes (see **Figure 3.48**). The addition of both nostoclides led to an upregulation of 244 genes and a downregulation of 464 genes. From the upregulated genes, 176 were upregulated in both nostoclide samples and from the downregulated genes, 366 were downregulated in the two nostoclide samples. Thus, the majority of the affected genes are the same. When Nvl was added to the WT, 253 genes were upregulated and 499 genes were downregulated. From the upregulated genes, 97 were also upregulated in one or both nostoclide samples and from the downregulated genes, 293 were also downregulated in one or both nostoclide samples. The treatment with the *pks1* compounds was capable of reproducing 15.1% of the upregulated genes found in the conventionally grown AraC_PKS1 mutant strain. The WT N2 sample reproduced 6.2% (37 out of 588 genes), the WT N1 + N2 sample reproduced 6.6% (39 out of 588 genes) and the WT Nvl

sample reproduced 9.6% (57 out of 588 genes) of the upregulated genes found in the AraC_PKS1 conv sample. In contrast, treatment with the *pks1* BGC compounds replicated a total of 55.7% of the negatively affected genes present in the mutant. The WT N2 sample reproduced 40.8% (121 out of 296 genes), the WT N1 + N2 sample reproduced 36.4% (108 out of 296 genes) and the WT Nvl sample reproduced 37.5% (111 out of 296 genes) of the downregulated genes found in the AraC_PKS1 conv sample.
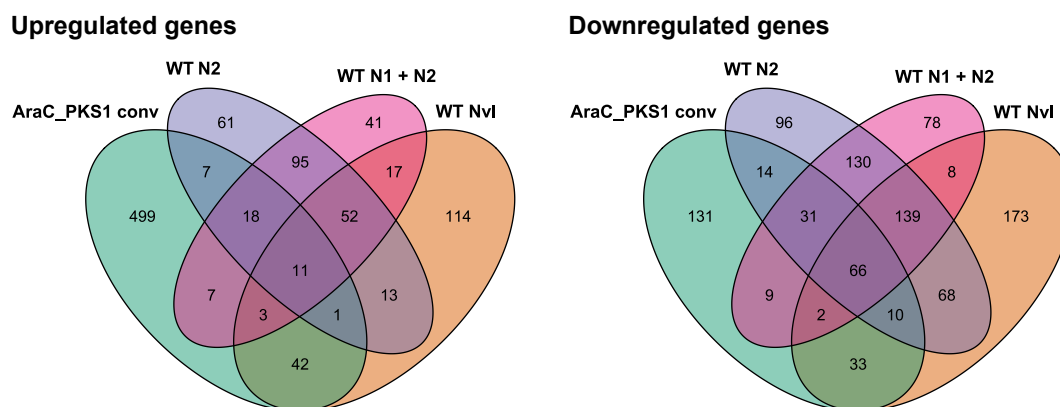
FIGURE 3.48: **Overview of up- and downregulated genes in the *N. punctiforme* WT treated with *pks1* compounds and in the AraC_PKS1 conv sample** Non-overlapping regions represent the number of genes uniquely influenced in one of the samples. Overlapping regions represent the number of genes influenced in multiple samples. All cultures were grown conventionally. The WT was treated either with N2, both nostoclides (N1 + N2) or with nostovalerolactone (Nvl). Data of the AraC_PKS1 conv sample is shown as a comparison. An untreated WT conv sample was used as reference.

These results suggest that the *pks1* metabolites are capable of triggering a part of the transcriptional effects that occur in the AraC_PKS1 mutant. However, the effects are more pronounced in downregulated genes.

Similar to the first RNA seqeuencing study, the affected genes were assigned to functional categories according to the COG database [155] (see **Appendix Figure A.5**). A large fraction of the affected genes, especially downregulated genes, are genes with unknown function and genes, for which only a general function is known. This suggests that nostovalerolactone and nostoclides are involved in the regulation of currently uncharacterized gene clusters or regulons.

Further analysis of the transcriptomic data, focusing on changes in BGC expression, showed that treatment with the *pks1*-derived metabolites can reproduce a majority of the BGC effects, observed in the AraC_PKS1 mutant

(see **Figures 3.50–3.51**). Interestingly, none of the *pks1*-derived metabolites was able to induce the strong upregulation of the *pks1* BGC itself (see **Figure 3.49**), as observed in the AraC_PKS1 mutant strain. The transcript levels of the majority of the *pks1* genes were not affected. Only a few genes showed a very slight up- or downregulation upon the treatment with nostoclide(s) or Nvl. Notably, the regulatory gene *RS10525*, which was overexpressed in the mutant, was not influenced in the WT Nvl sample ($\log_2$ fold change = 0.2) and showed a very slight downregulation in both nostoclide samples ($\log_2$ fold change = -1.2). These findings indicate that another, yet unknown, factor is required to induce the *pks1* BGC expression.
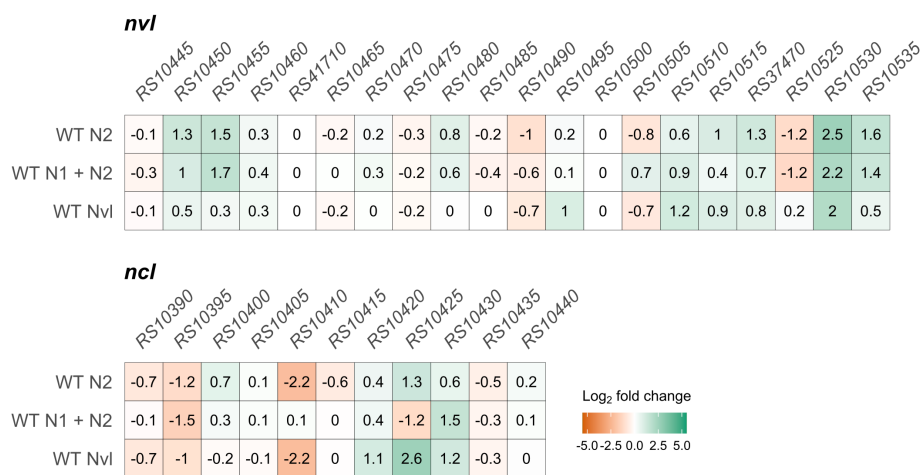
FIGURE 3.49: **Transcriptional response of the *pks1* BGC in the WT treated with nostoclide(s) or nostovalerolactone**
The heatmaps visualize the $\log_2$ fold changes of the two subclusters of the *pks1* BGC, *nvl* and *ncl*, in a WT culture treated with N2, N1 + N2 or Nvl compared to an untreated WT culture. All cultures were grown conventionally.

The remaining category I BGCs, *ripp3* and *ripp4*, were affected similarly to the AraC_PKS1 mutant when Nvl was added to the WT (see **Figure 3.50**). In case of the *ripp3* BGC, especially the precursor gene (*RS16795*) showed an elevated transcript level ($\log_2$ fold change = 4.2) compared to the untreated WT. Nearly all the genes, which are assigned to the *ripp4* BGC, showed an upregulated transcription. In contrast, the treatment with both nostoclides (N1 + N2) was only able to slightly increase the transcription of some genes of the *ripp3* and *ripp4* BGCs. The addition of N2 alone did not trigger this effect. Here, the transcript levels of the *ripp3* and *ripp4* genes remained mostly unchanged compared to the untreated WT control sample.
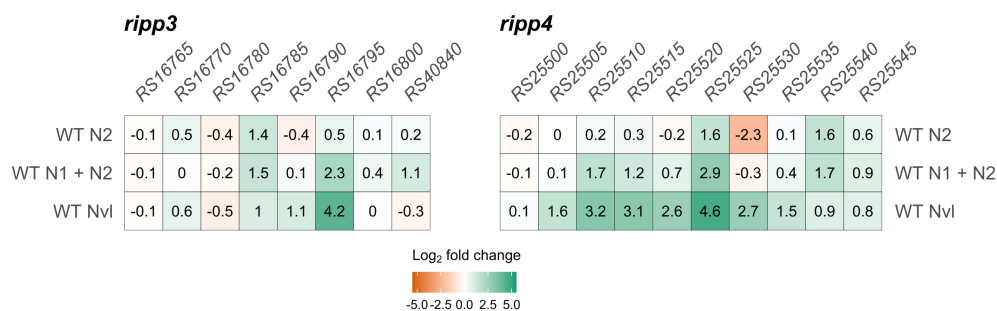
FIGURE 3.50: **Transcriptional response of the *ripp3* and *ripp4* BGCs in the WT treated with nostoclide(s) or nostovalerolactone**
The heatmaps visualize the $\log_2$ fold changes of the orphan BGCs *ripp3* and *ripp4* in a WT culture treated with N2, N1 + N2 or Nvl compared to an untreated WT culture. All cultures were grown conventionally.

Upon nostovalerlactone or nostoclide addition, the category II BGCs, *apt*, *mvd* and *nos* showed a similarly upregulated transcription as observed in the AraC_PKS1 HL/HC sample (see **Figure 3.51**). Here, nearly all the genes of the respective gene clusters showed an increased transcription. The upregulated transcript levels of the orphan BGCs *pks2* and *pks3*, and of the genes assigned to the production of scytonemin, were not reproducible by addition of the *pks1* BGC products (see **Appendix Figure A.6 and A.7**).
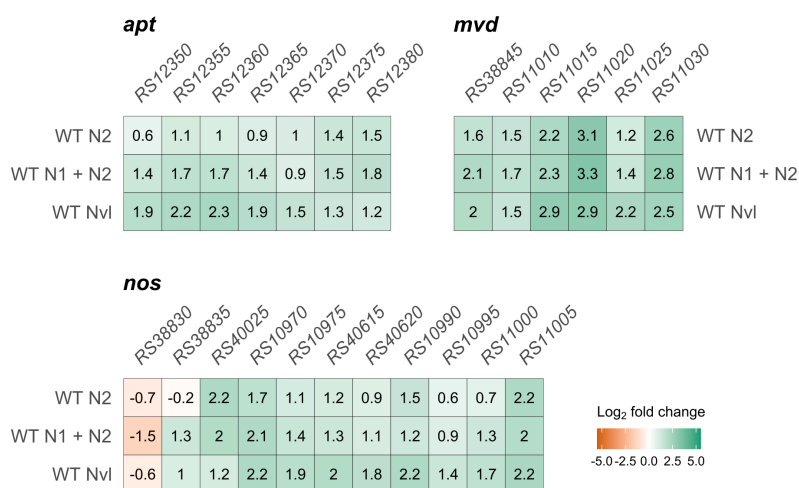
FIGURE 3.51: **Transcriptional response of the *apt*, *mvd* and *nos* BGCs in the WT treated with nostoclide(s) or nostovalerolactone**
The heatmaps visualize the $\log_2$ fold changes of the BGCs *apt*, *mvd* and *nos* in a WT culture treated with N2, N1 + N2 or Nvl compared to an untreated WT culture. All cultures were grown conventionally.

The effects observed in the AraC_PKS1 mutant on genes involved in regulation, chemotaxis and secretion were also not reproducible by addition

of the *pks1* BGC products (see **Figure 3.52**). Most of the genes were slightly downregulated or not affected.
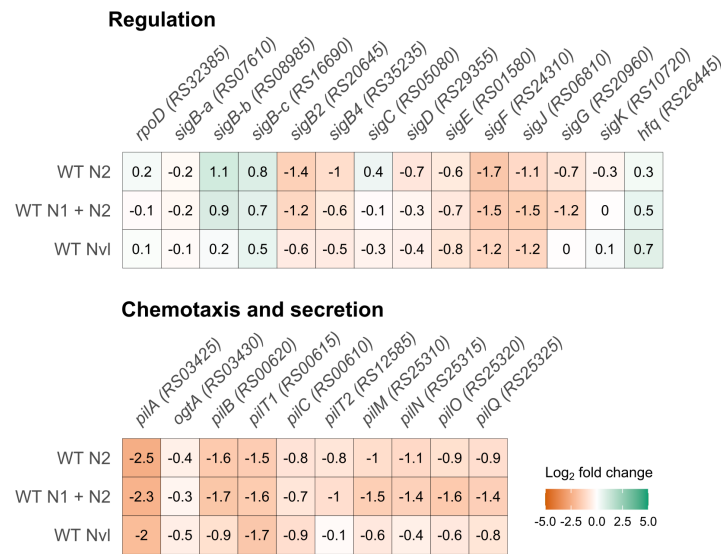
FIGURE 3.52: **Transcriptional response of genes typically involved in chemotaxis, secretion or regulation in the WT treated with nostoclide(s) or nostovalerolactone**
The heatmaps visualize the log$_2$ fold changes of genes typically involved in chemotaxis, secretion or regulation in a WT culture treated with N2, N1 + N2 or Nvl compared to an untreated WT culture. All cultures were grown conventionally.

In summary, by addition of the purified *pks1* BGC products it is possible to reproduce a large part of the BGC expression effects that have been found in the AraC_PKS1 mutant. A cumulative effect of the treatments was found for the upregulated transcription of the BGCs *apt*, *mvd* and *nos*. In contrast, the upregulated transcription of the BGCs *ripp3* and *ripp4* was particularly dependent on the presence of Nvl. However, none of the treatments was able to trigger an autoinduction of the *pks1* pathway.

Based on the data from both RNA sequencing studies, it could be demonstrated that in the mutant strain, the upregulated transcription of the BGCs *ripp3* and *ripp4* occurs independently of the cultivation conditions used. It seems that this effect is linked to the presence of nostovalerolactone. The transcript levels of the BGCs *apt*, *mvd* and *nos* are only upregulated when the AraC_PKS1 culture is cultivated under HL/HC conditions. The observed upregulation appeared to be triggered by both nostoclides and nostovalerolactone. Additionally, the expression of the gene clusters of *pks2*, *pks3* and *scy* was only positively affected when the mutant strain was grown

under HL/HC cultivation conditions, but no association with the presence of nostoclide or nostovalerolactone was found.

3.5.2 Influence of Nostoclides on Photosynthetic Organisms

The newly discovered nostoclide congeners, N1 and N2, show a distinct structurally resemblance to cyanobacterin (see **Figure 3.31**). This compound is able to inhibit the growth of cyanobacteria, algae and several angiosperms by blocking photosynthetic electron transport in photosystem II [159, 160]. Due to their structural similarity, it has been assumed that nostoclides may also function as allelopathic agents against photosynthetic organisms [161].

Closer examination of the cells of *N. punctiforme* WT and the AraC_PKS1 mutant strain by microscopy showed that compared with the WT, the mutant strain had an increased number of broken cells (see **Figure 3.53**), indicating cell stress. Probably, one of the metabolites that is produced in increased amounts in the AraC_PKS1 mutant, like nostoclide, is the reason for this observation.
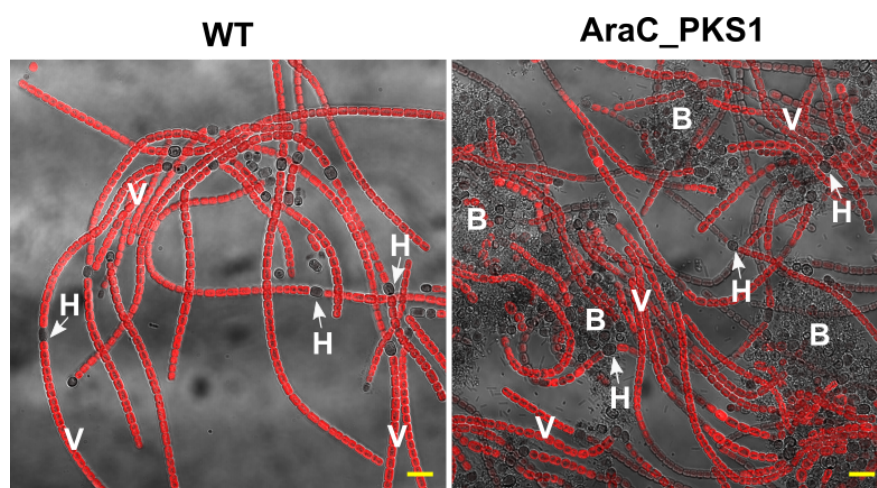
FIGURE 3.53: **Cell morphology of the *N. punctiforme* WT and the AraC_PKS1 mutant strain**
The WT and AraC_PKS1 mutant strains were grown conventionally for 20d. The mutant strain shows an increased number of broken cells compared to the WT. Labels: V, vegetative cells; H, heterocysts, B, broken cells.

To find evidence that the growth deficiencies found in the AraC_PKS1 mutant are caused by nostoclide production and a possible impact on photosynthesis related genes, the transcriptomic data was inspected to find corresponding effects. It was found that most of the photosynthesis-related genes were not affected in the WT N2 and WT N1 + N2 samples. Interestingly, one copy of the photosystem I related gene *psaB* was clearly downregulated in both

nostoclide samples ($\log_2$ fold changes = -4.5 and -3.8, respectivly; see **Figure 3.54**). Furthermore, four of the five copies of the photosystem II related gene *psbA* showed an altered transcription upon nostoclide treatment. Here, the transcription of one copy (*psbA1*) was downregulated ($\log_2$ fold changes = -2.6 and -1.5, respectively) and three of the *psbA* copies (psbA2–psbA4) showed an increased transcription ($\log_2$ fold changes = 1.6–3.3).

Photosystem

	psaB1	psaB2	psbA1	psbA2	psbA3	psbA4	psbA5
WT N2	-4.5	-0.6	-2.6	2.3	2.6	1.6	-0.5
WT N1 + N2	-3.8	-1.2	-1.5	3.3	2.8	2.1	-0.4
WT Nvl	-0.4	1	0.1	-0.3	-0.6	-1.4	-1.8

Log$_2$fold change

-5.0 -2.5 0.0 2.5 5.0
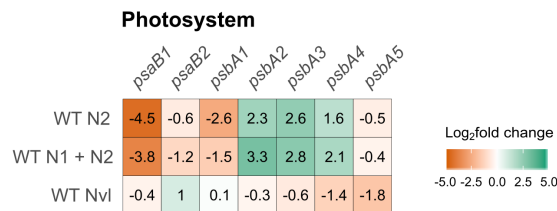
FIGURE 3.54: **Transcriptional response of the photosystem-related genes *psaB* and *psbA* in the WT treated with noctoclide(s) or nostovalerolactone**
The heatmap visualizes the $\log_2$ fold changes of the photosystem-related genes *psaB* and *psbA* in a WT culture treated with N2, N1 + N2 or Nvl, compared to an untreated WT culture. All cultures were grown conventionally.

In addition, the purified nostoclides (N1, N2) were used in a growth assay together with *N. punctiforme*, *Anabaena sp.* PCC 7120 and the green alga *Chlamydomonas reinhardtii* (*C. reinhardtii*) to determine the nostoclide's potential allelopathic activity. The assays were conducted as described in **Sections 2.2.1.5.1** and **2.2.1.5.2**. The growth assay of *C. reinhardtii* was conducted by the group of Severin Sasso (University of Leipzig, Institute for Biology, Department of Plant Physiology, Leipzig, Germany). None of the nostoclides was able to trigger a visible effect on any of the tested organisms (see **Figure 3.55**).
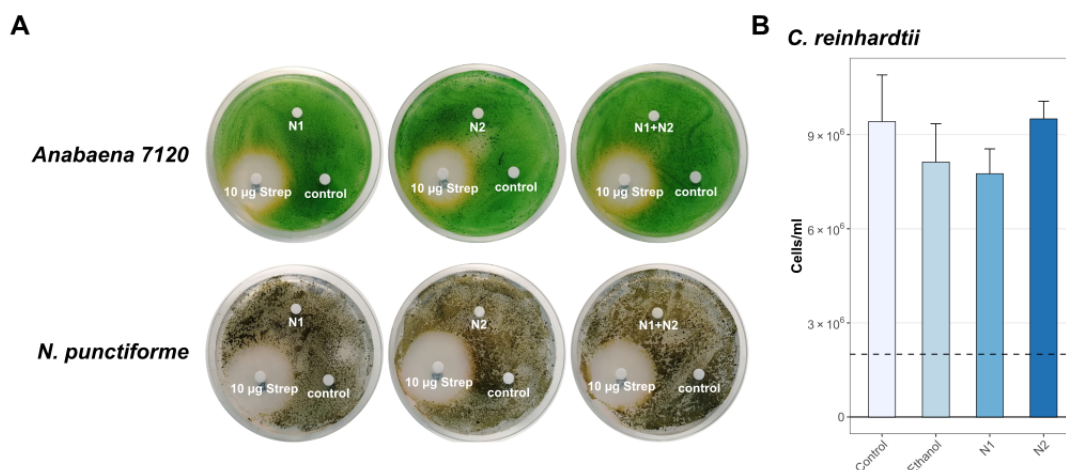
FIGURE 3.55:   **Influence of nostoclides on the growth of *N. punctiforme*,** ***Anabaena sp.*** **PCC 7120 and *C. reinhardtii***

(A) Influence of nostoclides on *N. punctiforme* and *Anabaena sp.* PCC 7120. Plated cyanobacterial cultures were treated with 25 µg N1, N2 or N1 + N2 and grew for 14 d. Streptomycin (10µg) was used as an antibiotic control and 60% methanol as a negative control. **(B)** Influence of nostoclides on the growth of *C. reinhardtii*. The column chart visualizes the cell density of *C. reinhardtii*, 24 h after treatment with 10 µM N1 or N2. The dashed line indicates the initial cell density of 2×10^6 cells. An ethanol-treated sample and an untreated sample served as controls. Data provided by the group of Severin Sasso.

To determine possible effects of the nostoclides on photosystem II, similar to the effects known from cyanobacterin, chlorophyll fluorescence measurements were conducted for nostoclide-treated *N. punctiforme* and *C. reinhardtii* cultures. The analysis was performed by the group of Severin Sasso as described in **Section 2.2.1.6**. By measuring chlorophyll fluorescence, the photosystem II quantum yield (YPSII) was determined, which is an indicator for photosystem II activity. No meaningful changes were oberserved in the nostoclide-treated organisms in comparison to the controls (see **Figure 3.56**). Thus, in contrast to cyanobacterin, the newly found nostoclides N1 and N2 do not seem to inhibit photosystem II activity, at least not in the organisms that were tested.
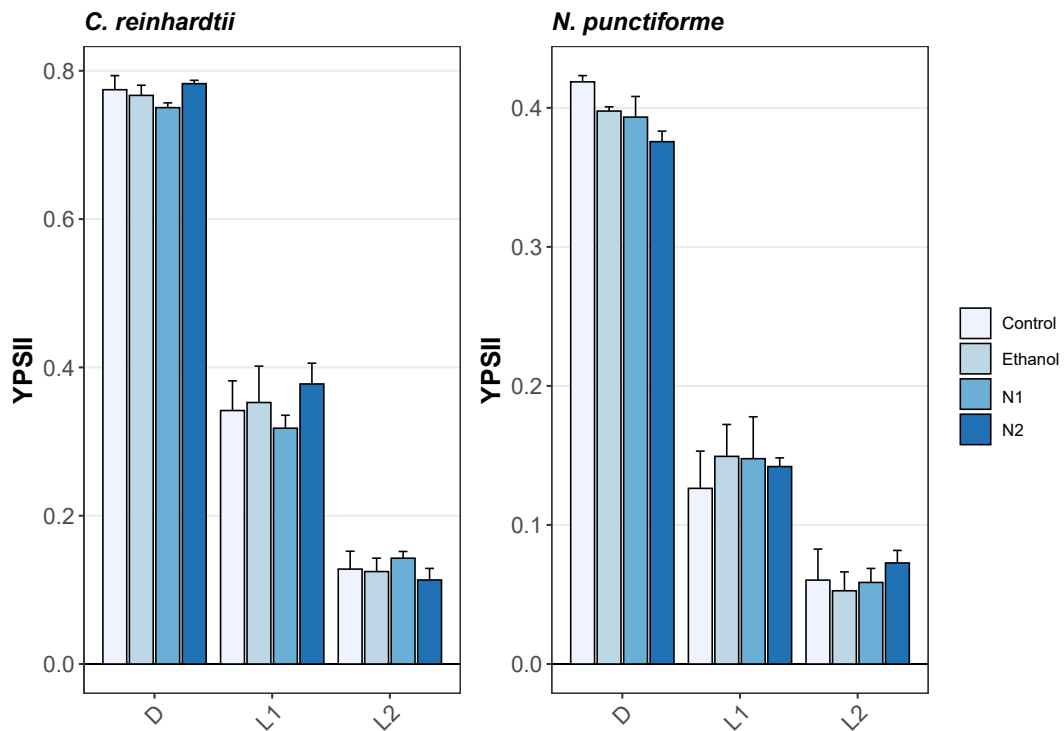
FIGURE 3.56: **Influence of nostoclides on photosystem II quantum yields in**
N. punctiforme **and** *C. reinhardtii*

Photosystem II quantum yields (YPSII) were measured 24 h after addition of
10 μM N1 or N2. YPSII was measured after adaptation to darkness for 5 min (D),
after subsequent actinic illumination with 700 μmol photons m^{-2} s^{-1} for 3 min
(L1) and after subsequent illumination with 2000 μmol photons m^{-2} s^{-1} for 3 min
(L2). Ethanol-treated samples and untreated samples served as controls. The error
bars indicate standard deviations. Data provided by the group of Severin Sasso.

3.6 Attempts to Identify the *ripp4* BGC Product

Although, the lanthipeptide BGCs *ripp3* and *ripp4* showed an increased transcription in the AraC_PKS1 mutant strain, the products of both gene clusters could not be identified by mass spectrometry. Furthermore, the transcriptional reporter study (see **Section 3.2.2**) showed that the *ripp4* BGC was also upregulated in *N. punctiforme* WT when grown under HD cultivation conditions (see **Figure 3.11**). But from the variety of potentially new compounds found in the HD cultures by HPLC analysis, the product of the *ripp4* BGC could not be identified. Focused on the *ripp4* BGC, targeted expression and knockout experiments were planned to facilitate compound identification.

By knocking-out an important gene of a gene cluster, the production of the corresponding compound is disturbed. This results in an absent or altered compound peak in HPLC analysis. By comparison of HPLC chromatograms of WT and mutant strains, potential corresponding compounds can be traced. Additionally, further insights on gene and gene cluster function can be gained from knockout experiments.

To interrupt the *ripp4* BGC, the gene *RS25520* was selected for knockout. This gene encodes the lanthibiotic biosynthesis protein LanM, which is typically involved in posttranslational modifications such as cyclization and dehydration of the amino acids serine and threonine [162, 163].

For the generation of a *N. punctiforme* mutant, which lacks a functional *RS25520* gene, an according suicide plasmid was constructed. A suicide plasmid does not have an ori of the final target organism and therefore does not replicate in the target cells. Consequently, such a plasmid is only used when the mutation needs to be integrated into the genome. For plasmid construction, the pRL271 vector-based plasmid pDD012, provided by Daniel Dehm (University of Potsdam, Potsdam, Germany) [138], was utilized. The vector pRL271 [164] already supplied the plasmid with the following features: an *E. coli* ori (pBR322), a chloramphenicol resistance gene for antibiotic selection, a *sacB* gene for negative selection and a basis of mobility region (bom), which is necessary for triparental conjugation. In addition, the plasmid pDD012 contained a streptomycin resistance cassette with unique restriction sites on each end (5′ AfeI, 3′ EheI). Two homology sequences targeting the *RS25520* were amplified by PCR using the primer pairs J013_FW/J014_RV and J015_FW/J016_RV. To built the final plasmid, the sequences were introduced into the pDD012 plasmid by two consecutive NEBuilder® HiFi mediated

cloning steps as described in **Section 2.2.2.6** utilizing the two unique restriction sites. The final plasmid was referred to as pJK004. A schematic overview of pJK004 is depicted in **Figure 3.57**.
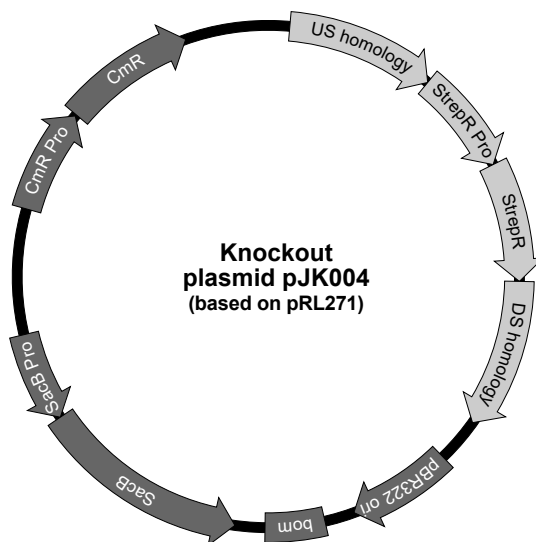
FIGURE 3.57: **Map of the knockout plasmid pJK004**
The streptomycin resistance cassette is flanked by homologous sequences of the target gene *RS25520* to enable disruption of the target gene. Features derived from vector pRL271 are displayed in dark grey. Separately inserted features are displayed in light grey.
Labels: US: upstream, DS: downstream, StrepR: streptomycin resistance cassette, Pro: promoter, bom: basis of mobility, CmR: Chloramphenicol resistance cassette

After successful assembly of the knockout plasmid, the *E. coli* strain harboring pJK004 was used to transfer the plasmid into *N. punctiforme* by triparental conjugation, as described in **Section 2.2.2.11.2**. In case of success, the streptomycin resistance cassette, flanked by the homologous sequences, would be integrated by homologous recombination into the *RS25520* gene and thereby interrupting it. Unfortunately, all attempts to integrate the streptomycin resistance cassette into the *ripp4* BGC were unsuccessful, as no viable clones were obtained.

A second approach to find the *ripp4* BGC product was to express one of the precursor genes from a separate plasmid in *N. punctiforme*. To facilitate the identification of the BGC product, the precursor was to be fused to a Polyhistidine-Tag (His-Tag). After expression, the His-Tag should enable specific purification of the precursor peptide. For this approach the precursor gene *RS25510* was chosen. Since the core peptide alone would be rather small (1.98 kDa, without potential posttranlational modifications) after cleavage from the leader peptide, it was decided to exchange the double-glycin

cleavage motif with a double-isoleucine, thereby the leader peptide should remain linked to the core peptide. This allows the attachment of the His-Tag to the leader peptide, so that it possibly not interferes with any potential posttranslational modifications of the core peptide. A schematic overview of the modified precursor peptide can be seen in **Figure 3.58**. The His-Tag together with a start codon and a short linker sequence is attached N-terminally to the modified leader peptide followed by the core peptide.
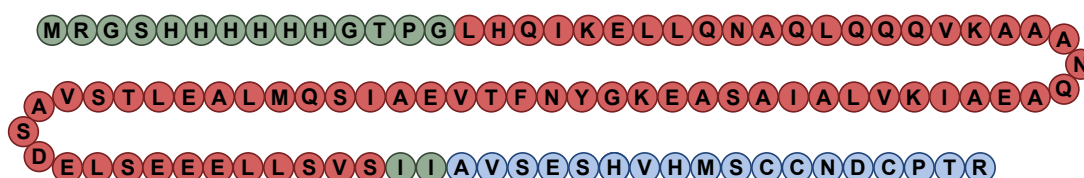
FIGURE 3.58: **Schematic overview of modified the *ripp4* BGC precursor peptide** The spheres represent the amino acid chain of the modified precursor peptide. A His-Tag with a start codon (methionine) was attached N-terminally to the leader peptide. To avoid cleavage of the leader peptide (orange) from the core peptide (blue), the double-glycin motif of the leader peptide was exchanged with double-isoleucine. All additions and modifications are highlighted in green. The plain amino acid sequence has a size of 11.3 kDa.

The modified precursor sequence together with its native promoter region was synthesized and cloned into the pRL1049 vector by the ProteoGenix company (Schiltigheim, France), as described in **Section 2.2.2.19**. The final plasmid is referred to as pJK028. A schematic overview of pJK028 is depicted in **Figure 3.59**.
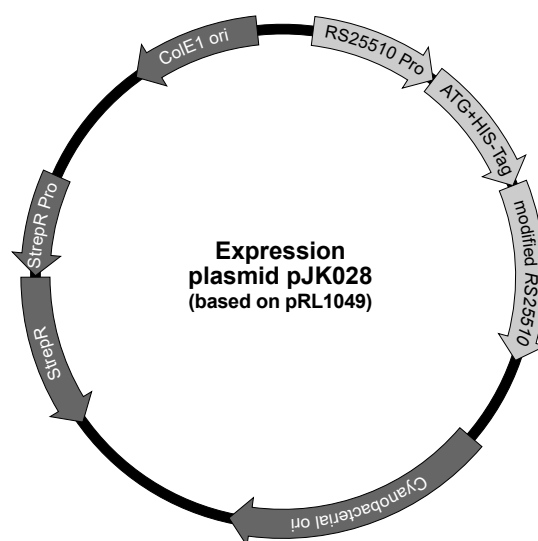
FIGURE 3.59: **Map of the expression plasmid pJK028**
The modified precursor gene *RS25510* was fused to a His-tag. For HD mediated
expression, the native promoter was placed in front of the precursor gene.
Features derived from the vector pRL1049 are displayed in dark grey. Separately
inserted features are displayed in light grey.
Labels: Pro: promoter, StrepR: streptomycin resistance cassette

The final plasmid was transformed into *N. punctiforme* by electroporation, as
described in **Section 2.2.2.11.1**. Potential mutants were selected on $BG11_0$
plates containing 2 µg/ml streptomycin. The presence of pJK028 was
confirmed by PCR. The *N. punctiforme* mutant was named RiPP4_His.

The RiPP4_His strain was cultivated for 20 days under HD cultivation
conditions. According to the transcriptomic reporter study (see **Section
3.2.2**), the *ripp4* promoter should be active under these conditions. The
cells were harvested and proteins were extracted as described in **Section
2.2.3.2**. The gathered extracts were analzyed by SDS-page (see **Section 2.2.3.3**)
and subsequent western blotting (see **Section 2.2.3.4**) utilizing a primary
His-Tag antibody. Unfortunately, the His-tagged precursor peptide could
not be detected. Even after several attempts with prolonged cultivation and
incubation times, the His-tagged precursor peptide was not traceable.

The RNA sequencing study (see **Section 3.5.1**) revealed that the transcription
of the *ripp4* precursor gene (*RS25510*) is positively influenced by the presence
of the *pks1* BGC compounds, especially by Nvl. Therefore, the fractionated
peak V (see **Figure 3.29**) from the AraC_PKS1 mutant strain, containing the
pks1 compounds, was added to the RiPP4_His mutant strain to activate the
expression of the modified precursor gene. Cells were harvested two days
after the addition of the *pks1*-derived compounds. Proteins were extracted and

analyzed by SDS-Page and western blotting. Unfortunately, the His-tagged precursor peptide could not be detected either.

Another approach to express the modified precursor gene *RS25510* in *N. punctiforme* was to exchange the native promoter by an inducible promoter system. For this purpose, the P_{rha} rhamnose-inducible promoter system, which was recently established in *Synechocystis* sp. PCC 6803 [165], was chosen. The plasmid construction was based on the pRL1049-derived plasmids pSK008 and pSK009, provided by Stella Scholz (University of Potsdam, Potsdam, Germany). Besides the features derived from the pRL1049 vector, including the *E. coli* ori ColE1, a cyanobacterial ori and a streptomycin resistance cassette, the plasmids contained the sequence of the rhamnose inducible promoter P_{rha} with a C-terminal AscI restriction site and the *rhaS* gene encoding the transcriptional activator of P_{rha}. The activator protein was either controlled by the strong promoter P_{J2319} [165] (pSK009) or the promoter P_{J23111} (pSK008), which has a half as strong promoter activity as P_{J2319} [165]. Utilizing the primer pairs J110_FW/J111_RV and J110_FW/J111_RV, the modified precursor gene was amplified from the pJK028 plasmid by PCR. The AscI restriction site was used to linearize the pSK008 and pSK009 plasmids. Subsequently, the precursor peptide sequence was introduced into both vectors by NEBuilder® HiFi mediated homologous recombination. The assembled plasmids were named pJK031 (based on pSK008) and pJK032 (based on pSK009). A corresponding plasmid map can be seen in **Figure 3.60A**. Two additional plasmids were constructed on the basis of pSK008 and pSK009, containing the unmodified sequence of the precursor gene *RS25510* for later analysis by HPLC. For that purpose, the precursor sequence was amplified from genomic DNA by PCR, utilizing the primer pair J113_FW/J111_RV. Again, the incorporation was done by homologous recombination. The resulting plasmids were named pJK035 (based on pSK008) and pJK036 (based on pSK009). A schematic overview of the plasmids is depicted in **Figure 3.60B**.
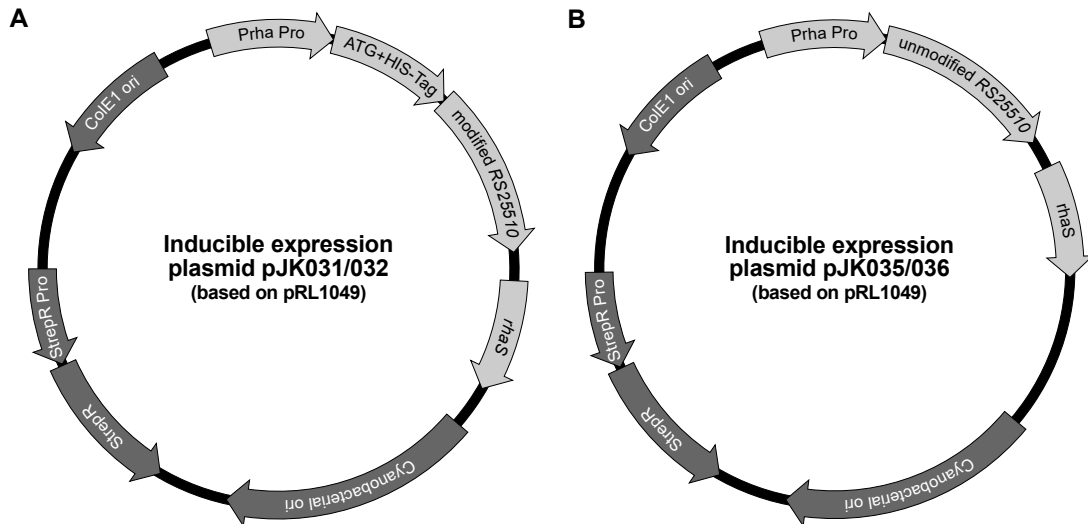
FIGURE 3.60: **Maps of the inducible expression plasmids for targeted peptide purification and HPLC analysis**
(A) For targeted peptide purification, the His-tagged precursor gene *RS10525* was placed downstream of a rhamnose-inducible promoter. **(B)** For HPLC analysis, the unmodified precursor gene *RS10525* was placed downstream of a rhamnose-inducible promoter.
Features derived from vector pRL1049 are displayed in dark grey. Separately inserted features are displayed in light grey. Labels: Prha Pro: rhamnose-inducible promoter, StrepR: streptomycin resistance cassette, Pro: promoter

The final plasmids were transformed into *N. punctiforme* by electroporation. Even after several attempts, no viable mutants were obtained after transformation.

Unfortunately, all attempts to find and identify the *ripp4* BGC product failed at some point. Next steps could include, the heterologous expression of the whole *ripp4* BGC in *E. coli* or in a closer related host organism, like *Anabaena* sp. 7120.

Chapter 4

Discussion

4.1 Developing New Strategies for Natural Product Discovery in Cyanobacteria

Comprehensive genomic studies [102, 103] on cyanobacteria have already uncovered a strong biosynthetic potential that is inherent in their genomes. Still, this potential is to a large extent unexplored, as the majority of BGCs found by genome mining approaches are orphan clusters [102, 103]. New strategies for systematic exploration of cyanobacterial natural products are necessary to identify new compounds and to make them accessible for potential biotechnological applications, such as drug development.

For the design of new approaches for natural product discovery in cyanobacteria, *N. punctiforme* PCC 73102 was chosen, due to its promising characteristics, including a large setup of orphan BGCs and an amenability to genetic manipulation.

A setup of different approaches, including cultivation-based analysis with transcriptional reporter studies, and the generation and analysis of overexpression mutant strains, was utilized to influence BGC expression. The combination of these approaches led to the discovery of new polyketides, i.e. two nostoclides (N1, N2) and a nostovalerolactone, which acting as chemical mediators. Besides the detection of the new compounds, the study also gave first-time insights into a complex signaling network regulating a specialized metabolism in *N. punctiforme*.

This study demonstrated that the regulatory framework already present in the native organism can be exploited for the activation of silent BGCs. The insights gained on the regulatory mechanisms that activate the specialized metabolism of *N. punctiforme* can guide the design of systematic screening strategies for novel natural products in other cyanobacteria. The findings of this study also

provide inspiration for the engineering of sustainable production platforms for cyanobacterial natural products.

4.1.1 High Density Cultivation Alters Specialized Metabolite Production

Low amounts of biomass combined with low secondary metabolite concentrations strongly hamper the exploration of the biosynthetic potential of cyanobacteria. To overcome the problem of low cell densities and to increase the growth rate, a high density (HD) cultivation system for photoautotrophic organisms was recently developed [137]. By turbulent mixing of the culture combined with sufficient supply of CO_2 and light, this system enables a rapid production of biomass [137]. Furthermore, it has been demonstrated that this system can improve the production of natural products, such as cyanophycin [120] and sesquiterpenoids [166]. A recent study by Guljamow et al. [110] revealed that HD cultivation of the *Nostoc* strains *N. punctiforme* PCC 73102 and *Nostoc* sp. KVJ2 alters the secondary metabolome of both strains. This led to the discovery of novel anabaenopeptin variants in *Nostoc* sp. KVJ20. In addition, they demonstrated that secreted factors are presumably involved in altering the secondary metabolome of *N. punctiforme*.

Following up on the findings of Guljamow et al. [110], cell density dependent BGC expression was further investigated in *N. punctiforme* utilizing HD cultivation. The different HD cultivation approaches that were performed in the course of this study confirmed an increase in specialized metabolite production, but the extent of the observed effects was very variable. In case the cultivation media was regularly replaced by fresh media, the *N. punctiforme* culture grew more densely than without regular exchange of the media. This is likely due to the increased nutrient supply from the regular media exchange. Furthermore, it was discovered that regular exchange of the cultivation media, although leading to higher cell-densities, resulted in a less pronounced activation of metabolite production, which was particularly evident in the cell-free supernatant fraction. This hints that secreted chemical mediators influence BGC expression. Without media exchange these factors can accumulate in the culture supernatant and presumably activate the expression of other BGCs as part of a cell density dependent signaling network. However, one should also consider that without regular exchange of the cultivation media, degradation products, by-products or intermediate compounds may also accumulate in the supernatant in addition to the secreted

metabolites. Presumably, not all of the additional HPLC peaks that were present in the HD extracts represent new and final processed metabolites. Furthermore, without regularly replacement of the media also continuously produced stable metabolites that are already produced during conventional cultivation, like nostopeptolide, accumulate in the supernatant. In cases were this metabolite is an undiscovered compound, this type of cultivation can be advantageous, otherwise it can make the metabolites extracts overly complex and complicating the detection of other metabolites.

Additionally, the utilized light intensities altered the metabolite production. In case the media was not exchanged during cultivation, light intensities of up to 350 μmol photons m^{-2} s^{-1} resulted in a different HPLC profile than using higher light intensities with up to 800 μmol photons m^{-2} s^{-1}. Only a fraction of the observed metabolite peaks that were observed by HPLC overlapped.
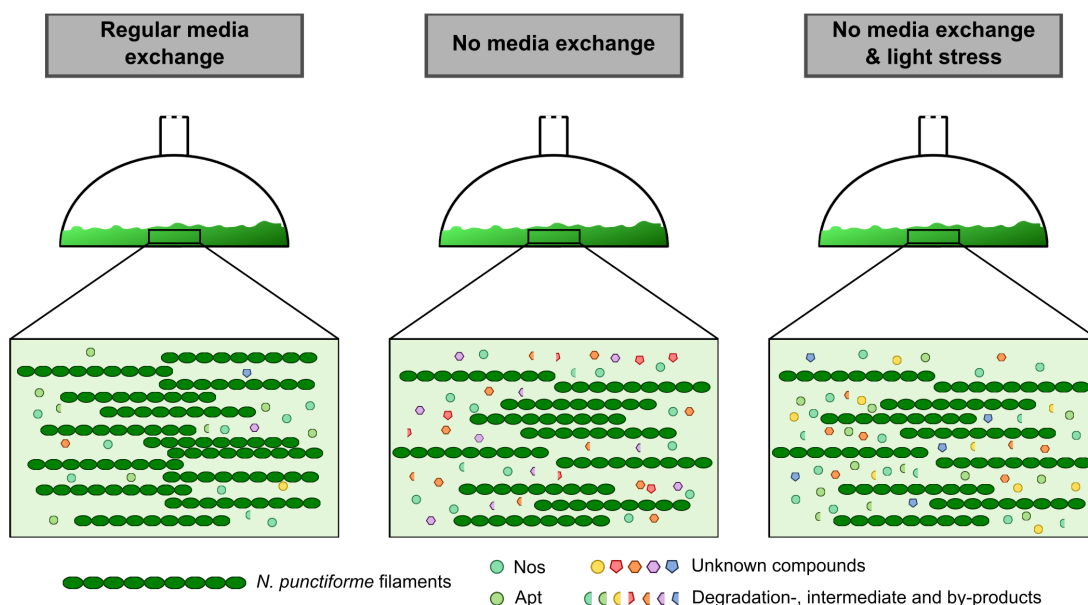
FIGURE 4.1: **Effects of cell density, media exchange and light intensity on specialized metabolite production during HD cultivation of *N. punctiforme*** Regular media exchange during HD cultivation led to higher cell densities, but the activation of metabolite production was less pronounced than without media exchange. The metabolite production can be altered by using very high light intensities (light stress). Without regular media exchange degradation-, intermediate and by-products presumably accumulating in the cultivation media in addition to the secreted metabolites.

This indicates that not only the cell density itself, but also other factors like light intensity are able to alter metabolite production. Some of the HPLC peaks observed from the HD cultures are presumably produced as a side effect of the cultivation procedure and are not directly related to cell density. Instead, the

activity of the corresponding BGCs are possibly related to abiotic factors, like light intensity, CO_2 concentration or stress. To evaluate the impact of these factors on metabolite production in detail, systematic cultivation approaches would be necessary.

BGCs, which were influenced by high cell densities, were identified by utilization of a fluorescence reporter strain library [115, 138]. This library contained a transcriptional CFP reporter strain for each of the 15 predicted BGCs of *N. punctiforme*. Analysis of the reporter strains growing under HD cultivation conditions revealed that eight out of 15 BGCs (*apt*, *mvd*, *pks1*, *pks2*, *pks4*, *ripp1a*, *ripp1b*, *ripp4*) had an increased expression when compared to the conventionally grown reporter strains. Moreover, four of the influenced BGCs (*pks1*, *pks2*, *pks4*, *ripp1b*) also showed an increased fluorescence signal when grown conventionally in HD supernatant, which hints towards an influence of secreted chemical mediators.

A reporter strain-based approach has the advantage that changes in BGC activity, e.g. induced by different cultivation conditions, can be easily tracked by fluorescence microscopy *in vivo*. Furthermore, the BGC activity can be tracked at the single-cell level, which can provide information about the distribution of BGC expression within the culture. Another advantage is the quick and easy preparation, as one can directly screen the living cells of the reporter strains for BGC activity. However, it should be considered that genetic modification, in the form of the introduction of an additional plasmid including an antibiotic selection marker into the organism, can cause unwanted side effects. This includes for example antibiotic stress and the increase of the metabolic burden, which can cause growth deficiencies and the development of altered phenotypes. Furthermore, variations in the plasmid copy number between cells may occur and influence the expression level. Due to that it is not possible to exactly quantify the relative expression levels by CFP fluorescence [167]. In comparison to appropriate control samples, it is nevertheless possible to evaluate changes of gene expression qualitatively [167]. Therefore, the reporter plasmid-based approach was a useful tool for rapid assessment of BGC activity in response to different cultivation conditions and thereby guided the identification of potential cell-density depending BGCs.

In summary, the HD cultivation approach effectively activated the secondary metabolome. In combination with the reporter strain-based approach, influenced BGCs were identified and first hints about a signaling pathway

were gained, in which secreted chemical mediators initiate BGC expression. Even though several upregulated BGCs were identified, only one new compound, a new microviridin variant, was identified [115] from the HD extracts. Due to the fact that the expression of several other BGC could be demonstrated, the expression itself did not seem to be the main reason for problems regarding the detection of the corresponding products. Certainly, the activation of multiple BGCs, which is the case when *N. punctiforme* is cultivated under HD cultivation conditions, leads to very complex metabolite extracts, complicating the compound identification process. The isolation of a single compound becomes more elaborate due to the presence of other metabolites, intermediate- and degradation-products. The complexity is especially problematic when the compound prediction by genome mining tools is inaccurate, leading to a biased and potentially wrong understanding of the compounds. Prediction inaccuracies may appear due to the limited knowledge about potential modifications that can occur during the maturation process of the natural product. Particularly, the identification of new and unusual post-translational modifications of RiPPs is an ongoing field of research. Although there is already an extensive list of potential modifications, still previously unknown modifications of RiPPs are being found [168], including the incorporation of β-amino acids [169], D-amino acids [170] or unnatural amino acids [171], as well as new variants of thioether cross-links [172]. To overcome the detection problems, a targeted approach increasing the production of a specific target compound is necessary.

Although the HD cultivation of *N. punctiforme* did not lead to product identification of all the influenced BGC, it was still a suitable approach to get first insights into a potential regulatory network. In addition, it aided the prioritization of BGCs of interest, encoding potential signaling factors involved in this network.

4.1.2   Overexpression of Pathway-Specific Regulatory Genes

Targeted or pathway-specific approaches are used as an alternative to untargeted BGC activation approaches, like cultivation-based strategies. Targeted approaches aim to activate a specific BGC. A promising strategy for targeted BGC activation is the manipulation of pathway-specific regulatory genes, as the activity of many natural compound BGCs is under control of pathway-specific transcriptional activators or repressors [173]. Usually, these regulators are encoded within their associated gene cluster. Therefore, they

can be easily found by bioinformatical analysis of the BGC [173]. For fungi and *streptomycetes*, several regulator families have been described that are typically acting as cluster-situated and pathway-specific regulators, but also novel families are still being discovered [174]. However, no typical families of pathway-specific regulators are currently known for cyanobacteria.

Manipulation of pathway-specific regulatory genes have already led to the discovery of new natural compounds in bacteria and fungi. For example, overexpression of the regulatory gene *afoA* in *Aspergillus nidulans* triggered the production of the formerly unknown polyketide asperfuranone [175], in *Streptomyces ambofaciens* the overexpression of a LAL (large ATP-binding regulators of the LuxR family) family regulatory gene led to the discovery of stambomycins, a new class of macrolides with antiproliferative activities [176], and the deletion of the pathway-specific repressor gene *alpW* led to the identification of *Streptomyces ambofaciens* as producer of kinamycin antibiotics [177].

In *N. punctiforme*, four putative pathway-specific regulators, belonging to the BGCs *pks1*, *pks2*, *ripp3* and *ripp4*, were chosen to be used in a targeted BGC activation approach, utilizing a native constitutive promoter for the overexpression of the regulatory genes in *N. punctiforme*. Unfortunately, the number of well-characterized promoters for cyanobacteria is rather limited, especially for filamentous strains. Most of the promoters that are commonly used in biotechnological approaches were evaluated only for unicellular strains, such as *Synechococcus* and *Synechocystis* [104]. Therefore, the promoter that was used in this study was chosen based on *N. punctiforme* reporter strain data. The 5′ UTR region of *RS16340* proved to be a strong constitutive promoter, since it successfully overexpressed the chosen regulatory genes ($\log_2$ fold changes = 9.5–15.5). However, the promoter strength varied in the different mutant strains. It is presumed that the promoter region is stimulated by environmental factors like light or cell-density.

Unfortunately, in case of the *N. punctiforme ripp4* regulator mutant no viable clones have been obtained. Since the generation of the three other overexpression mutants was successful, a methodical problem seems to be unlikely. It is speculated that an upregulation of *RS25505* expression may lead to the production of a compound, which is potentially toxic to *N. punctiforme* at high concentrations. As it has not been proven that *RS25505* has an impact on *ripp4* BGC expression, it is not clear if the potential *ripp4* BGC product represents the potentially toxic compound.

In case of the TetR_PKS2 and the LuxR_Ripp3 mutant strains, the assumed

pathway specific effect of the overexpressed regulatory genes was not observed. Here, the respective potentially associated BGCs were neither negatively nor positively affected. Interestingly, the RNA sequencing data of the AraC_PKS1 mutant revealed that although the BGCs *ripp3*, *ripp4* and *pks2* showed an increased transcription, the proposed associated regulatory genes were not affected, or in case of *pks2* only slightly affected.

The AraC_PKS1 mutant strain showed a pathway-specific effect, as an increased transcription ($\log_2$ fold change$_{RT-qPCR}$ = 5.2) of the *pks1* BGC was observed in the mutant. After optimizing the growth conditions (HL/HC cultivation conditions) of the mutant, two new polyketides, nostoclide (Ncl) and nostovalerolactone (Nvl), were discovered. Both are encoded by the *pks1* BGC. Besides the *pks1* BGC, also other BGCs were influenced upon overexpression of the regulatory gene *RS10525*, especially when the mutant strain was cultivated under HL/HC conditions. This included further orphan BGCs, such as *ripp3*, *ripp4*, *pks2* and *pks3*. However, the corresponding products could not be identified. Again, analytical limitations due to insufficient knowledge about the potential compounds, as mentioned in the context of HD cultivation, could be a reason.

In conclusion, the overexpression of putative pathway-specific regulatory genes proved to be a powerful approach to specifically activate gene cluster expression and detect new natural products in the native producer. But, the findings of the study also showed that the outcome of such an approach can be unpredictable, as two of the regulators did not show the anticipated effect on their associated BGC, one could not be overexpressed at all and the only regulator which had an effect on its corresponding BGC seemed to have an additional global effect on gene expression (see **Section 4.2.1**).

4.1.3 Lanthipeptide detection

The detection and identification of the product of the lanthipeptide BGC *ripp4* proved to be problematic throughout the whole study. Although the *ripp4* BGC was upregulated by HD cultivation of the WT and also in the AraC_PKS1 mutant strain, a potential product could not be detected by mass-spectrometric analyses. Also the approaches targeting the *ripp4* BGC did not lead to the detection of the corresponding peptide.

Gene-knockouts are an established method in *N. punctiforme* and several successful examples can be found in the literature [109, 158, 178, 179]. To gather further information about the *ripp4* BGC, it was planed to interrupt the

gene cluster by knocking out the *lanM* gene (*RS25520*), but no viable mutant were obtained. Possibly, the BGC product, although being a specialized metabolite, is important for the viability of *N. punctiforme*, at least under laboratory conditions. Moreover, several approaches of expression and detection of the His-tagged *ripp4* precursor peptide failed. This could be caused by peptide degradation, His-tag degradation, a solubility problem or the His-tag could be hidden inside the peptide due to folding events. In the end, none of the approaches, no matter if they were targeted or untargeted, could aid in the identification of the *ripp4* BGC compound. Possibly, there is a systematic problem hampering the detection of the *ripp4* lanthipeptide. Furthermore, it is conspicuous that lanthipeptide BGCs are widespread in the genomes of cyanobacteria, but only very few cyanobacterial lanthipeptide natural products have been detected so far. One of those natural products are prochlorosins, which have been first detected after heterologous expression in *E. coli* rather than in their native producer *Prochlorococcus* [180]. Therefore, it is assumed that there is a general problem of lanthipeptide detection in cyanobacteria. Maybe, the lanthipeptides are covalently bound to a cellular structure, which would complicate their detection. Possibly heterologous expression in *E. coli*, like it was done for the prochlorosins, is a suitable alternative for the production in the native organism.

4.2 Specialized Metabolism in *N. punctiforme*

4.2.1 The *RS10525*-derived Regulator NvlA is Part of a Signaling Network

This study identified the *RS10525*-derived regulator NvlA as a transcriptional activator that plays an important role in a cell density dependent signaling network in *N. punctiforme*. NvlA belongs to the AraC family of transcriptional regulators. It is not accompanied by a sensor histidine kinase, therefore NvlA is a so-called orphan response regulator. Since it lacks a conserved phosphoaccepting aspartate in the receiver domain, it is further assumed that the regulator has an atypical phosphorylation-independent activation mechanism. Multiple ways to achieve this kind of activation are described in the literature, including other post-translational modifications, like acetylations and the binding of small molecules or proteins to the response regulator [181, 182]. In this context, an autoregulatory mechanism in

Streptomyctes has also been transcribed. Hereby, RedZ and JadR1 are atypical response regulators of two antibiotic biosynthetic pathways that are in turn also controlled by their respective pathway end products [183, 184]. However, in case of the *RS10525*-derived regulator, this type of activation can be excluded, since neither of the compounds of the *pks1* pathway, Ncl or Nvl, were able to regulate the activity of the response regulator. So the activation mechanism remains elusive. The induced expression of the *pks1* BGC under high-density cultivation suggested that abiotic factors, like high light and CO_2 concentrations, cell density or a combination of these factors trigger the activity of the related signaling network. Due to the fact that AraC-type regulators are often involved in carbon metabolism [142], it could be possible that the activation is directly triggered by an environmental factor like carbon availability.

Based on the RNA sequencing data of the AraC_PKS1 mutant, the overexpression of *nvlA* directly or indirectly influenced the transcription of 884 genes (11.7% of all predicted genes of the *N. punctiforme* genome). The addition of the *pks1* compounds to the WT strain was only able to reproduce a fraction of the observed global effects on gene expression. For example, the influence on other regulatory factors, such as sigma factors and the global RNA chaperone Hfq was not induced by any of the *pks1*-derived signaling factors. Obviously, the observed transcriptional effects were not mediated solely by the identified signaling factors. This indicates that NvlA may act as a global regulator and is not exclusively specific for a single biosynthetic pathway. Similar findings were already described for *Streptomyces avermitilis*. Here, the pathway-specific regulator PteF does not only control the expression of the BGC it is located in, but also the expression of other BGCs. PteF seemed to be additionally involved in other cellular processes beside secondary metabolite biosynthesis, such as morphological differentiation, transcriptional regulation or energy metabolism [185]. However, further analyses are needed to gain more insights into the regulatory mechanisms of NvlA. Direct targets of the regulator could be identified by using electrophoretic mobility shift assays or ChIP-seq-based experiments. Cyanobacterial homologs of the NvlA regulator were found to be mostly located inside various types of BGCs. Due to this, it can be speculated that this family of AraC regulators is commonly cluster-situated in cyanobacteria and controls diverse types of downstream mediators.

It is assumed that NvlA is part of a hierarchical signaling network with Ncl and Nvl acting as downstream chemical mediators, influencing the

expression of additional BGCs. A similar hierarchical network was already described to regulate a quorum sensing signaling system in the model organism *Pseudomonas aeruginosa*. Here, the global AraC-type regulator VqsM is controlling the production of two kinds of quorum sensing AHL signals (*las* and *rhl*) directly and indirectly by influencing other quorum sensing related regulators [186, 187].

As it was found that the transcriptional effects observed in the AraC_PKS1 mutant strain could be extended by cultivation under HL/HC conditions, it can be speculated that these conditions induce a mutual interaction, a so-called cross-talk, between NvlA and other regulatory factors. A potential interaction partner could be a sensor histidine kinase that interacts with the regulator in a phosphorylation-independent manner. Interestingly, most of the NvlA homologs that were found in cyanobacteria were accompanied by a sensor histidine kinase. The sensor kinase regulating the *scy* gene cluster is a possible candidate for an interaction with the *RS10525*-derived response regulator. Its cognate response regulator shows a homology to NvlA and both regulatory genes of the *scy* gene cluster showed an increased transcription in the AraC_PKS1 HL/HC sample. However, the specific regulatory circuit, which is induced upon HL/HC cultivation conditions in the AraC_PKS1 mutant strain, remains to be clarified.

Unfortunately, the specific effector increasing the production of the NvlA regulator in *N. punctiforme* could not be identified during this study. To identify which of the biotic and abiotic factors that are changed during HL/HC cultivation compared to conventional cultivation, comprising cell density, CO_2 concentration and light intensity, is the major trigger of gene expression, their effects need to be analyzed separately. The impact of altered light intensities, CO_2 levels and cell densities, could either be verified by analyzing the activity of the original promoter of *nvlA* utilizing a respective reporter strain or by monitoring the transcription levels of *nvlA* by RT-qPCR. With the identification of the specific triggering factor, conclusions might be drawn about the ecological or biological function of the activated regulatory circuit.

4.2.2   Ncl and Nvl as Chemical Mediators

Although Ncl and Nvl were not able to reproduce all the transcriptional effects found in the AraC_PKS1 mutant strain, they still demonstrated that they act as extracellular chemical mediators as part of a regulatory circuit. They were

able to upregulate the expression of several BGCs, comprising the orphan lanthipeptide BGCs *ripp3* and *ripp4*, as well as the BGCs *apt*, *nos* and *mvd*. In the AraC_PKS1 mutant, the BGCs *apt*, *nos* and *mvd* were only upregulated upon HL/HC cultivation conditions. Therefore, it is assumed that a higher amount of the *pks1* compounds is needed to induce the expression of these three BGCs, than for the orphan BGCs *ripp3* and *ripp4*, which were also upregulated under conventional cultivation conditions. Additionally, the two orphan BGCs seemed to be especially effected by the presence of Nvl, whereas the BGCs *apt*, *nos* and *mvd* are triggered by both *pks1*-derived compounds. For the orphan BGCs *pks2* and *pks3*, which showed an upregulated transcription in the AraC_PKS1 HL/HC sample, no association to Nvl and Ncl was found. The found effects of Ncl and Nvl are illustrated in a putative signaling model in **Figure 4.2**.
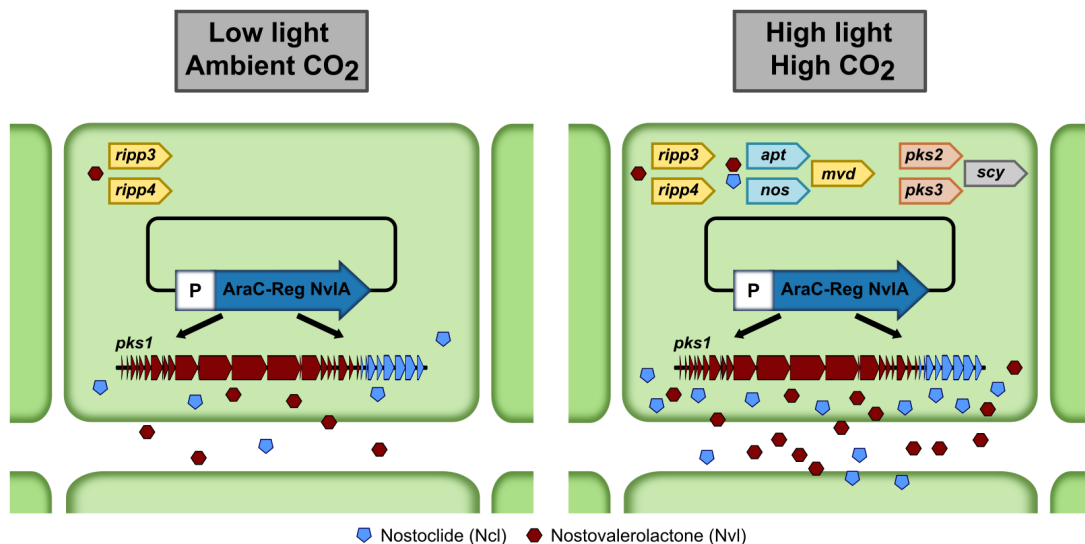
FIGURE 4.2: **Signaling model illustrating the effects found in the AraC_PKS1 mutant strain and the influence of the *pks1*-derived compounds**
Under low light and ambient CO_2 (conventional) conditions and under HL/HC conditions Nvl is able to trigger *ripp3* and *ripp4* BGC expression in the AraC_PKS1 mutant strain. The upregulated expression of *apt*, *mvd* and *nos* BGCs in the mutant is restricted to HL/HC cultivation conditions and stimulated by Ncl and Nvl. The upregulated transcription of the BGCs *pks2*, *pks3* and *scy*, found in the AraC_PKS1 HL/HC sample, is not associated with Ncl or Nvl.

The already characterized compounds anabaenopeptin and nostopeptolide are involved in intra- and interspecific interactions of *N. punctiforme* [110, 116]. For anabaenopeptin, it was demonstrated that it can have an allelopathic effect against other *Nostoc* strains [110]. Nostopeptolide is a hormogonium-repressing factor, typically downregulated in the presence

of potential symbiotic partners, such as *Blasia pusilla* [116]. The enhanced transcription of *apt* and *nos*, observed upon Ncl and Nvl addition, indicates an involvement of both compounds in inter- and intraspecific interaction of *N. punctiforme* with other organisms.

Ncl and Nvl share structural features with other natural compounds that typically act as bacterial chemical mediators.
Nostoclides belong to the butenolide-based natural products, which are characterized by their typical furanone ring core structure [188]. Butenolides are known to act as signaling molecules in gram-positive bacteria, like *Streptomyces* [189]. For example, the butenolide-based chemical mediator avenolide controls the production of the antibiotic avermectin in *Streptomyces avermitilis* [190]. A recent study by Klapper et al. [191] provided evidence that butenolides could potentially act as signaling factors in the gram-negative bacterium *Pseudomonas*. In regards to its chemical structure, butenolides are related to γ-butyrolactones (GBLs) and linear tetronates. In *Streptomyces*, GBLs are typical signaling factors that are involved in quorum sensing mechanisms. In many streptomyces strains, the GBLs thereby regulate the secondary metabolism, including for example the production of antibiotics [75]. Linear tetronates are often found to interfere with phosphorylation-dependent signaling pathways by inhibiting phosphatase enzymes [150].
In contrast to Ncl, Nvl shares only a few similarities to already known bacterial signaling factors. Like Ncl, it is structurally related to linear tetronates. Additionally, the γ-valerolactone ring resembles an α-pyrone ring. In *Photorhabdus luminescens*, α-pyrones were recently identified as signaling molecules, which are involved in a cell-to-cell communication circuit [77].

The findings of this study clearly indicate that complex regulatory circuits, involving several chemical mediators, control the BGC expression in *N. punctiforme*. Although the two newly found polyketides are obviously acting as chemical mediators, more investigation is needed to fully understand their physiological role and how they are involved in the activation of BGC expression. Understanding the regulatory circuits is necessary to develop a systematic approach for the activation of orphan BGCs and the detection of the corresponding natural products in the native producer.

4.2.3   Nostoclides as Alleopathic Agents

Although the biological activities of the nostoclide family have not been fully explored so far, it is commonly considered that nostoclides have

allelopathic properties [161, 192]. This is based on their structural similarities with the alleopathic agent cyanobacterin, which is able to inhibit the growth of photosynthetic organisms [192]. Moreover, this assumption is supported by findings from an analysis of the symbiotic relationship between nostoclide-producing *Nostoc* sp. strains and the lichen *Peltigera canina* [149]. Here, it was observed that the cultures were unusually clean and free of contaminating microorganisms [149]. Nostoclides have been identified as potential phytotoxins that can be used for the development of new environmentally friendly herbicides for crop protection in agriculture [192]. Given the emerging resistance of weeds against commonly used herbicides and the environmental pollution caused by these compounds there is a constant need to develop new environmentally friendly herbicides [193]. Since the inhibitory properties of nostoclides are structure-dependent and can vary depending on the substituent of the benzylidene moiety, they are a promising compound family for the design of novel herbicides with a high specificity [192, 193].

In case of the newly discovered nostoclides N1 and N2 the anticipated phytotoxic activity was not observed during this study. However, this was only determined for three organisms, *Anabaena* sp. 7120, *C. reinhardtii* and *N. punctiforme* itself. Therefore, it could be possible that N1 and N2 have a more specific allelopathic effect on a certain group of photosynthetic organisms, which were not tested in this study.

Although, no change in photosystem II activity was detected in photosystem II quantum yield measurements after treatment of *N. punctiforme* WT with N1 or N2, a change in transcription of the photosystem II related gene family *psbA* was found to be connected to the presence of the nostoclides. For cyanobacteria, it is typical to have several copies (2–6 copies) of the *psbA* gene [194]. All *psbA* genes encode the D1 protein, which is an essential part of the photosystem II protein complex [195]. The different gene copies are responsible for the production of different D1 isoforms in response to changing environmental conditions [195]. However, the regulatory mechanism controlling the transcription of the different *psbA* copies seemed to be rather strain-specific [195]. When *N. punctiforme* WT was treated with nostoclide, three out of five *psbA* copies showed an increased transcription, which indicates an increased turnover of the D1 protein and a possible reorganization of photosystem II. Unfortunately, little is known about the roles of the alternative *psbA* copies in *N. punctiforme*. Therefore, it is difficult to speculate about the impact of the observed transcriptional effects on

photosystem II.

Nevertheless, the study demonstrated that *N. punctiforme* is a suitable host for high-titer production of nostoclides and could therefore be used as a sustainable production platform for these compounds. Nostoclides can potentially be applied as herbicides for weed control in agriculture, highlighting *N. punctiforme* as a promising host for the development of green biotechnology approaches.

4.3 Implications for Other Cyanobacteria

Heterologous expression is a frequently used strategy for the activation of silent BGCs due to its many advantages, including established genetic manipulation techniques, targeted production of the desired compound and facilitated compound detection and isolation. Although some examples of successful heterologous expression of cyanobacterial metabolites have been described in the literature, like for lyngbyatoxin A [196, 197] and microcystin [198], a robust heterologous host for cyanobacteria is missing. Even cyanobacterial hosts like *Synechococcus elongatus* PCC 7942 are often not able to express BGCs from other cyanobacteria due to missing biosynthetic precursors or enzymes, or an incompatible regulatory system. In that case, extensive metabolic engineering would be necessary or finding a better, more compatible host, like it was shown in a recent study by Arnaud et al. [199]. Here, the PKS/NRPS BGC of cryptomaldamide from *Moorena producens* could be heterologously expressed in *Anabaena* PCC 7120, but not in *Synechococcus elongatus* PCC 7942. Activation of BGC expression in the native producers does not have the problems mentioned above, because all requirements for the biosynthesis of the compound of interest, like biosynthetic precursors and enzymes, and factors for regulation and transport, are available [200]. Here, the major challenge is to identify a required trigger or a regulatory element that controls BGC expression.

The findings of this study can guide the activation of silent BGCs in native cyanobacterial producers. High density cultivation is a sustainable approach that can be easily transferred to other cyanobacteria to induce BGC activation, even if they are not amenable to genetic manipulation. A drawback of this approach is its unpredictability. One can not tell in advance which and how many BGCs might be influenced upon this type of cultivation. Depending on the amount of activated BGCs, the complexity of the cultivation extracts

could hamper the metabolite detection, similar as it has been shown for *N. punctiforme* in this study.

Furthermore, optimizing the growth conditions of a cyanobacterial mutant strain by alteration of light intensities and CO_2 concentrations proved to be an appropriate method for high-titer production of a desired compound. Especially for slow-growing cyanobacteria and if the strain needs to grow in the presence of antibiotics, which can also hamper growth, optimized growth conditions are important for the production of compound levels high enough for further analysis aiming for structural elucidation.

Searching and manipulating putative pathway-specific regulatory genes proved to be a successful strategy for BGC activation in this study. This could be also the case in other cyanobacteria. Since homologs of the AraC regulator NvlA in various other cyanobacteria were encoded by genes located inside predicted BGCs, this type of regulator could generally be related to specialized metabolite biosynthesis in cyanobacteria. In order to verify this hypothesis, an increased expression of the respective genes is needed. In case of genetically modifiable cyanobacteria like *Anabaena*, a similar overexpression approach like described in this study could be used. Due to the observation that the NvlA regulator has an increased production upon HL/HC cultivation conditions (see **Figure 3.37**), a cultivation-based approach utilizing cyanobacterial WT strains could be a suitable method to induce regulator gene expression. Hereby, a genetical manipulation wouldn't be necessary.

The insights gained for the regulatory circuit of the specialized metabolism in *N. punctiforme* can guide the design of screening strategies for bioactive compounds in other cyanobacteria. From the homologous regulators found in other cyanobacterial strains, one can implicate that these regulators might have a similar function and may control a similar pathway in their producing strain. Therefore, the findings of this study may aid in the discovery of novel natural products in other cyanobacteria and in the development of high-titer production strategies of bioactive compounds in the native producer.

Appendix A

Supplementary Figures
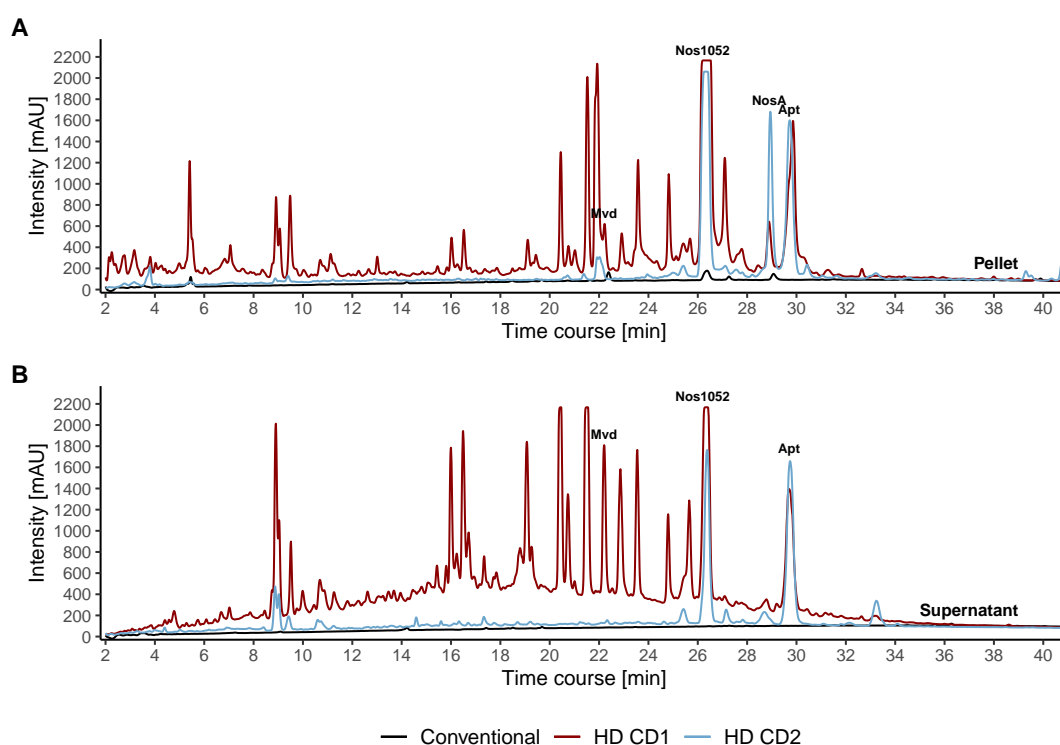
FIGURE A.1: **HPLC analysis of high density cultivation approaches of** *N. punctiforme* **conducted by the CellDeg company**
(A) HPLC profiles of cell pellet extracts; **(B)** HPLC profiles of supernatant extracts; Light intensities of up to 620 µmol photons m^{-2} s^{-1} were established earlier in HD CD1 than in HD CD2. A conventionally grown *N. punctiforme* culture was used as a control. HPLC profiles are shown at a wavelength of 199 nm. Known metabolite peaks are labeled (Mvd: microviridin, Nos1052: nostopeptolide 1052, NosA: nostopeptolide A, Apt: Nostamid A).
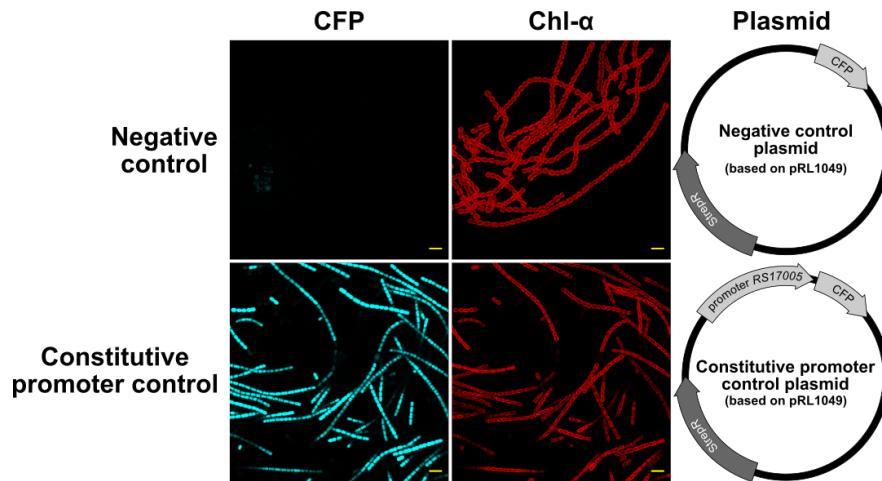
FIGURE A.2: **Fluorescence micrographs of *N. punctiforme* transcriptional CFP reporter controls**

The upper row shows the negative control strain, carrying the reporter plasmid without any promoter region. The lower row shows a positive control strain, which carries a reporter plasmid with a constitutive promoter region (5′ UTR of *RS17005*). The CFP fluorescence signal (blue) indicates promoter activity. Chlorophyll-α autofluorescence (red) indicates living vegetative cells. Yellow scale bars indicate 10 μm. The corresponding plasmid maps of both control strains are shown on the right.
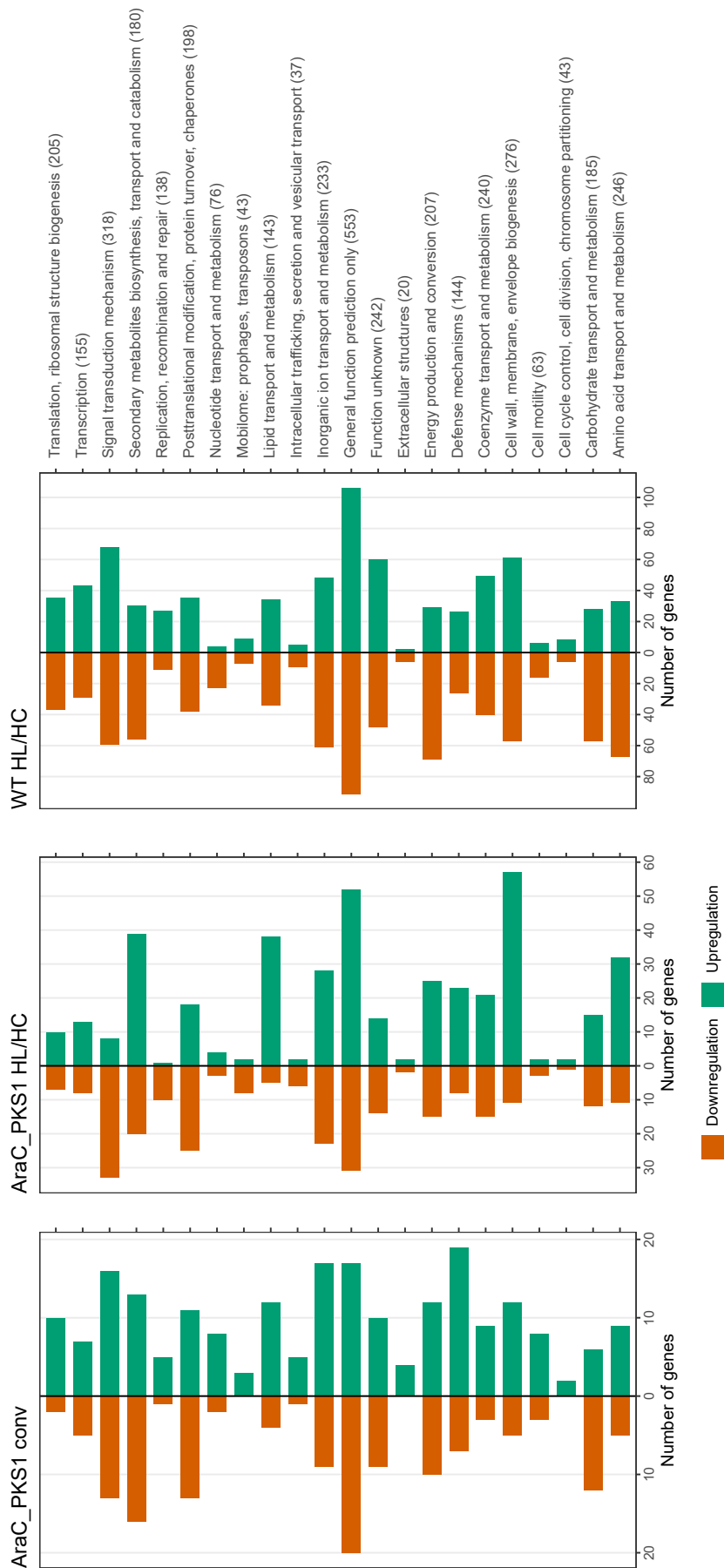
FIGURE A.3: **Assignment of up- and downregulated genes in AraC_PKS1 conv, AraC_PKS1 HL/HC and WT HL/HC to functional categories**

The allocation was based on the Cluster of Orthologous Groups (COG) database [155]

Upregulated genes

Downregulated genes
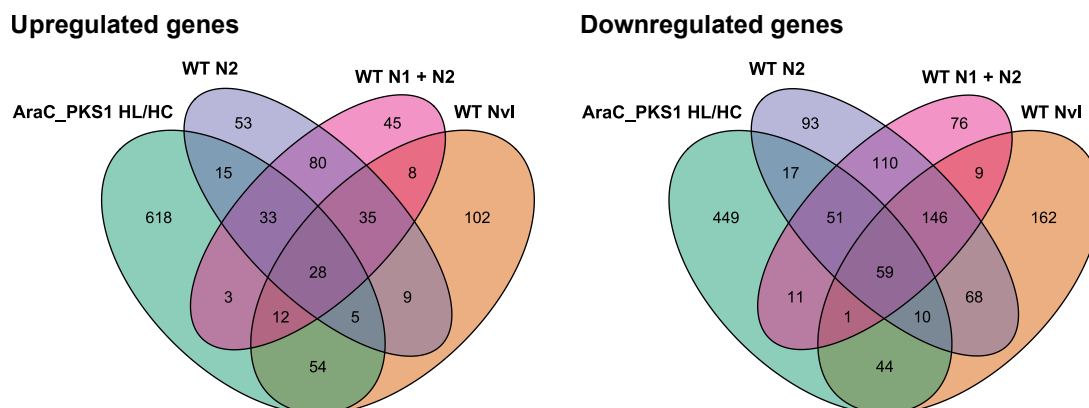
FIGURE A.4: **Overview of up- and downregulated genes in the *N. punctiforme* WT treated with *pks1* compounds and in the AraC_PKS HL/HC sample**
Non-overlapping regions represent the number of genes uniquely influenced in one of the samples. Overlapping regions represent the number of genes influenced in multiple samples. All cultures were grown conventionally. The WT was treated either with N2, both nostoclides (N1 + N2) or with nostovalerolactone (Nvl). Data of the AraC_PKS1 HL/HC sample is shown as a comparison. An untreated WT conv sample was used as the reference.

Compared to the AraC_PKS1 HL/HC sample, the treatment with the *pks1* BGC compounds was able to reproduce 19.5% of the upregulated genes found in the AraC_PKS1 sample. The WT N2 sample reproduced 10.5% (81 out of 768 genes), the WT N1 + N2 sample reproduced 9.9% (76 out of 768 genes) and the WT Nvl sample reproduced 12.8% (out of 768 genes) of the positively influenced genes in the AraC_PKS1 HL/HC sample. From the negatively affected genes observed in the HL/HC cultivated mutant, a total of 30% was reproduced by the treatment with the *pks1* BGC compounds. The WT N2 sample reproduced 21.3% (137 out of 642 genes), the WT N1 + N2 sample reproduced 19% (122 out of 642 genes) and the WT Nvl sample reproduced 17.7% (114 out of 642 genes) of the downregulated genes found in the AraC_PKS HL/HC sample.
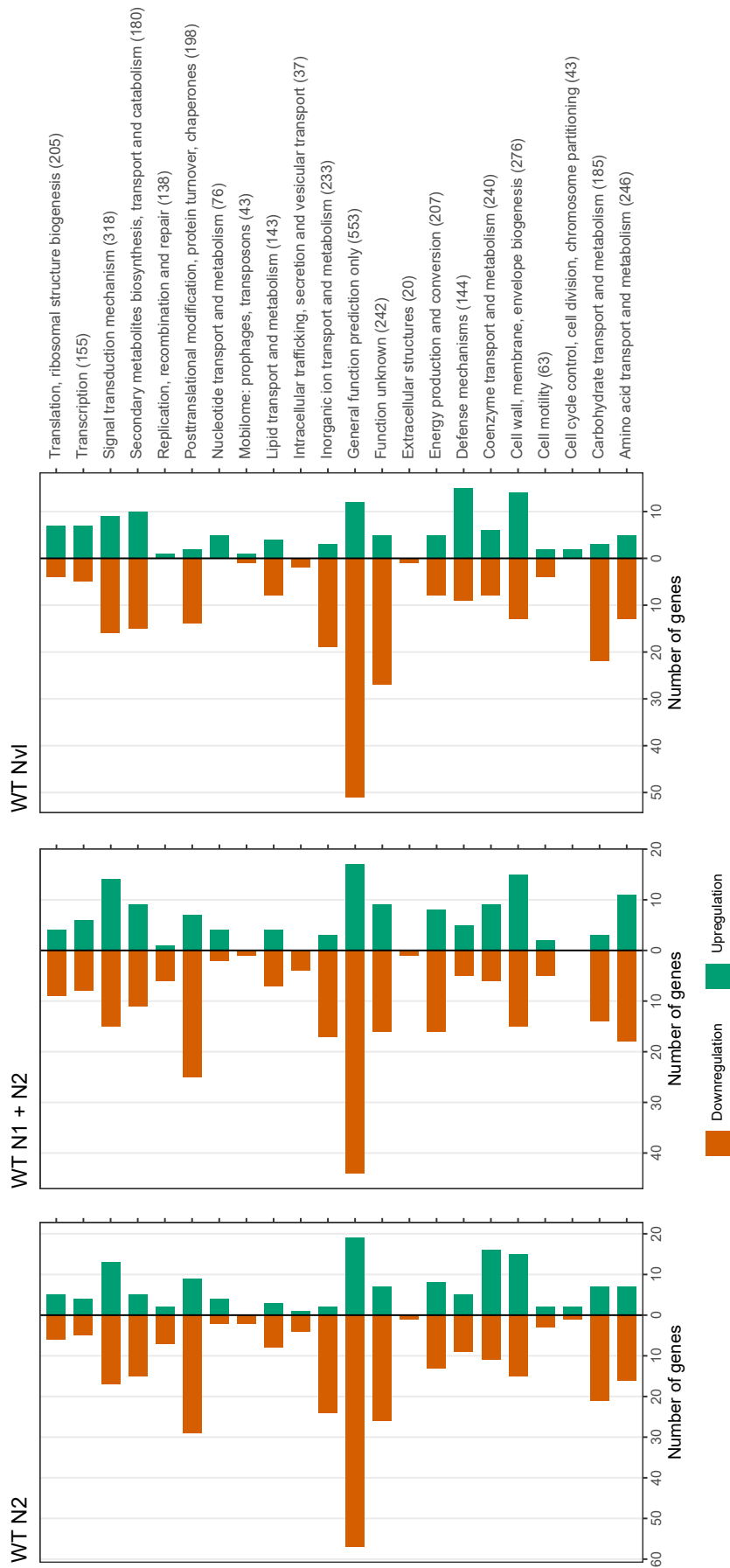
FIGURE A.5: **Assignment of up- and downregulated genes in WT N2, WT N1 + N2 and WT Nvl to functional categories**
The allocation was based on the Cluster of Orthologous Groups (COG) database [155]
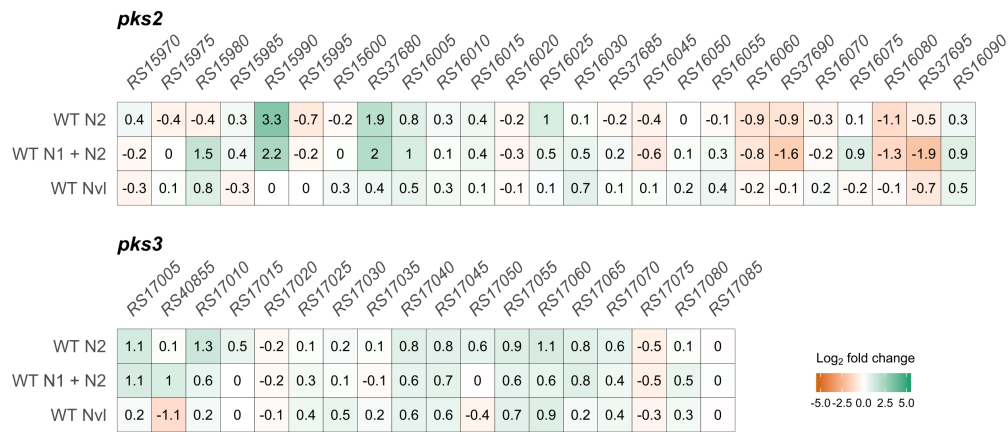
FIGURE A.6: **Transcriptional response of the *pks2* and *pks3* BGCs in the WT treated with nostoclide(s) or nostovalerolactone**
The heatmaps visualizes the $\log_2$ fold changes of the orphan BGCs, *pks2* and *pks3*, in a WT culture treated with N2, N1 + N2 or Nvl, compared to an untreated WT culture. All culture were grown conventionally.
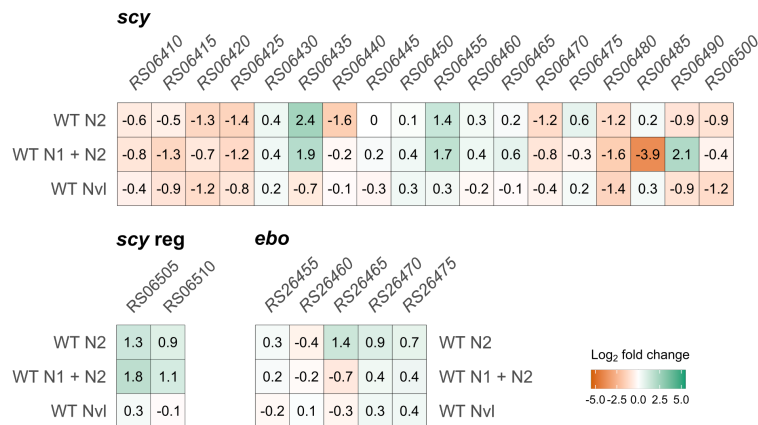
FIGURE A.7: **Transcriptional response of the *scy* and *ebo* BGCs in the WT treated with nostoclide(s) or nostovalerolactone**
The heatmaps visualizes the $\log_2$ fold changes of the genes assigned to the production of scytonemin (*scy*, *ebo* and regulatory genes (*scy* reg)) in a WT culture treated with N2, N1 + N2 or Nvl, compared to an untreated WT culture. All culture were grown conventionally.

Appendix B

Supplementary Tables

TABLE B.1: **HD cultivation conditions of the HD1 sample**
The culture was harvested on day 69.

Days	Light intensity [μmol photons m^{-2} s^{-1}]	CO$_2$ exchange buffer [mbar]
0	60	32
5	60	32
9	60	32
14	60	32
19	100	32
23	100	32
28	100	32
33	150	90
37	150	90
42	150	90
47	200	90
49	200	90
54	350	90
59	350	90
63	600	90
66	800	90

TABLE B.2: **HD cultivation conditions of the HD2 sample**
The culture was harvested on day 55.

Days	Light intensity [μmol photons m^{-2} s^{-1}]	CO$_2$ exchange buffer [mbar]
0	60	5
3	60	32
8	100	32
13	100	32
17	100	32
22	150	90
27	150	90
31	150	90
34	200	90
36	200	90
41	350	90
45	350	90
49	600	90
52	800	90

TABLE B.3: **HD cultivation conditions of the HD CD1 sample**
The culture was harvested on day 24.

Days	Light intensity [μmol photons m^{-2} s^{-1}]	CO$_2$ concentration
0	50	0%
3	135	8%
8	100	8%
9	100–620 (in 18 h)	8%
15	620	8%
16	620	10%
17	310	10%
20	400	10%
22	620	10%
23	620	12%

TABLE B.4: **HD cultivation conditions of the HD CD2 sample**
The culture was harvested on day 18.

Days	Light intensity [μmol photons m^{-2} s^{-1}]	CO_2 concentration
0	40	4%
3	80	4%
7	40	4%
9	40–300 (in 24 h)	4–8% (in 24 h)
13	300–600 (in 24 h)	8%
15	160	8.5%
16	300–500 (in 48 h)	8%

TABLE B.5: **HD cultivation conditions of the HD noME sample**
The culture was harvested on day 27.

Days	Light intensity [μmol photons m^{-2} s^{-1}]	CO_2 exchange buffer [mbar]
0	60	32
3	60	32
7	100	32
10	150	32
12	150	32
14	150	90
17	150	90
19	200	90
21	250	90
24	350	90

TABLE B.6: **HD cultivation conditions of the HD noME + LS sample**
The culture was harvested on day 56.

Days	Light intensity [μmol photons m^{-2} s^{-1}]	CO$_2$ exchange buffer [mbar]
0	100	32
3	100	32
7	100	32
11	100	90
15	200	90
18	300	90
22	400	90
26	500	90
29	600	90
35	700	90
38	800	90
43	800	90
46	800	90
50	800	90
53	800	90

TABLE B.7: **Proposed function of *nvl* subcluster genes based on sequence homology**

Gene	Annotation	Size [aa]	Characterized homolog(s)	Identities/ Positives [%/%]	Proposed/confirmed function
RS10535	Nitrogenase	88	-	-	Unknown
RS10530	Hypothetical protein	105	-	-	Unknown
RS10525 (*nvlA*)	Response regulator, transcription factor	256	BacR	32/56	Response regulator [201]
RS37470 (*nvlB*)	Phosphopantetheine- binding protein	153	-	-	Unknown
RS10515 (*nvlC*)	4'-Phosphopante- theinyl transferase superfamily protein	251	PPT_{NS}	43/60	*Sfp*-type phosphopantetheinylase [202]
RS10510 (*nvlD*)	3-Oxoacyl-ACP synthase III family protein	344	AbmA1, RkD	46/56, 52/67	Ketoacyl-S-ACP synthase [203], 3-Oxoacyl-ACP synthase III [152]
RS10505 (*nvlE*)	HAD-IIIC family phosphatase	638	AbmA2, RkE	41/62, 38/60	Glyceryl-S-ACP synthase [203], [152]
RS10500 (*nvlF*)	Acyl carrier protein	73	AbmA3, RkF	38/66, 33/64	Acyl carrier protein (ACP) [203], [152]
RS10495 (*nvlG*)	Dehydrogenase catalytic domain containing protein	253	AbmA4, Agg4	42/64, 28/51	Acetyltransferase [203], [153]
RS10490 (*nvlH*)	FAD-dependent oxidoreductase	406	OxyE	30/52	FAD-dependent hydroxylase [204]
RS10485 (*nvlI*)	AMP-binding protein	1284	FAAL domain: PuwC ACAD domain: Bcd	63/73, 29/47	Fatty acyl-AMP ligase [205], Buturyl-CoA dehydrogenase [206]
RS10475 (*nvlJ*)	Type I PKS	1850	MgiI	53/70	Type I PKS [207]
RS10470 (*nvlK*)	Type I PKS	2016	HctD	51/67	Type I PKS [208]
RS10465 (*nvlL*)	SDR family oxidoreductase	1872	MgiI	53/71	Type I PKS [207]
RS10460 (*nvlM*)	Type I PKS	1080	CurI	52/67	Type I PKS [209]
RS10455 (*nvlN*)	α/β Hydrolase	366	AbmA5, Agg5	40/59, 30/52	α/β Hydrolase [203], [153]
RS10450 (*nvlO*)	Thioesterase	264	AbmT	37/52	Type II thioesterase [203]
RS10445 (*nvlP*)	SRPBCC domain-containing protein	149	-	-	Unknown
RS10440 (*nvlQ*)	NAD(P)/FAD-dependent oxidoreductase	514	CHMO	25/40	Cyclohexanone monooxygenase [210]
RS10435 (*nvlR*)	Hypothetical protein	253	-	-	Unknown
RS10430 (*nvlS*)	Hypothetical protein	253	-	-	Unknown

TABLE B.8: **Proposed function of *ncl* subcluster genes based on sequence homology**

Gene	Annotation	Size [aa]	Characterized homolog(s)	Identities/ Positives [%/%]	Proposed/confirmed function
RS10425	IS630 family transposase	143	-	-	Unknown
RS10420 (nclA)	Acyl carrier protein	81	ACP_BORBU	35/65	Acyl carrier protein [211]
RS10415 (nclB)	β-ketoacyl-ACP synthase II	422	RedR	44/61	3-Ketoacyl-ACP-synthase II [212]
RS10410 (nclC)	Ketoacyl-ACP synthase III	333	RedP	41/59	3-Ketoacyl-ACP-synthase III [212]
RS10405 (nclD)	Aromatic amino acid ammonia-lyase	569	FevV, CybB	34/50, 71/82	Tyrosine ammonia lyase [213], Aromatic amino acid ammonia-lyase [151]
RS10400 (nclE)	Long-chain fatty acid CoA ligase	512	MoeA4, CybC	39/55, 69/84	Acyl-CoA ligase [214], Long-chain acyl-CoA-synthetase [151]
RS10395 (nclF)	Thiamine pyrophosphate-binding protein	586	ScyA, CybE	61/75, 67/77	Acyloin Synthase [215], Thiamine pyrophosphate-binding protein [151]
RS10390 (nclG)	3-Oxoacyl-ACP synthase	386	RedP, CybF	26/44, 70/86	3-Ketoacyl-ACP synthase [212], Furanolide synthase [151]

Bibliography

1. All natural. *Nature chemical biology* **3,** 351. doi:`10.1038/nchembio0707-351` (2007).

2. Demain, A. L. & Fang, A. in *History of modern biotechnology* (eds Fiechter, A., Scheper, T. & Beppu, T.) 1–39 (Springer, Berlin, 2000). doi:`10.1007/3-540-44964-7_1`.

3. Dittmann, E., Gugger, M., Sivonen, K. & Fewer, D. P. Natural Product Biosynthetic Diversity and Comparative Genomics of the Cyanobacteria. *Trends in Microbiology* **23,** 642–652. doi:`10.1016/j.tim.2015.07.008` (2015).

4. Medema, M. H., Kottmann, R., Yilmaz, P., Cummings, M., Biggins, J. B., *et al.* Minimum Information about a Biosynthetic Gene cluster. *Nature chemical biology* **11,** 625–631. doi:`10.1038/nchembio.1890` (2015).

5. Keller, N. P. Fungal secondary metabolism: regulation, function and drug discovery. *Nature reviews. Microbiology* **17,** 167–180. doi:`10.1038/s41579-018-0121-1` (2019).

6. Soule, T., Garcia-Pichel, F. & Stout, V. Gene Expression Patterns Associated with the Biosynthesis of the Sunscreen Scytonemin in *Nostoc punctiforme* ATCC 29133 in Response to UVA Radiation. *Journal of Bacteriology* **191,** 4639–4646. doi:`10.1128/JB.00134-09` (2009).

7. Spraker, J. E., Wiemann, P., Baccile, J. A., Venkatesh, N., Schumacher, J., *et al.* Conserved Responses in a War of Small Molecules between a Plant-Pathogenic Bacterium and Fungi. *mBio* **9.** doi:`10.1128/mBio.00820-18` (2018).

8. Arnison, P. G., Bibb, M. J., Bierbaum, G., Bowers, A. A., Bugni, T. S., *et al.* Ribosomally synthesized and post-translationally modified peptide natural products: overview and recommendations for a universal nomenclature. *Natural Product Reports* **30,** 108–160. doi:`10.1039/c2np20085f` (2013).

9. Ligon, B. L. Penicillin: its discovery and early development. *Seminars in pediatric infectious diseases* **15,** 52–57. doi:`10.1053/j.spid.2004.02.001` (2004).

10. Survase, S. A., Kagliwal, L. D., Annapure, U. S. & Singhal, R. S. Cyclosporin A - a review on fermentative production, downstream processing and pharmacological applications. *Biotechnology advances* **29,** 418–435. doi:`10.1016/j.biotechadv.2011.03.004` (2011).

11. Feng, Y., Huang, Y., Zhan, H., Bhatt, P. & Chen, S. An Overview of Strobilurin Fungicide Degradation:Current Status and Future Perspective. *Frontiers in Microbiology* **11,** 389. doi:`10.3389/fmicb.2020.00389` (2020).

12. Singh, A. K., Rana, H. K. & Pandey, A. K. in *Recent Advancement in White Biotechnology Through Fungi* (eds Yadav, A. N., Singh, S., Mishra, S. & Gupta, A.) 229–248 (Springer International Publishing, Cham, 2019). doi:`10.1007/978-3-030-14846-1_8`.

13. Pham, J. V., Yilma, M. A., Feliz, A., Majid, M. T., Maffetone, N., *et al.* A Review of the Microbial Production of Bioactive Natural Products and Biologics. *Frontiers in microbiology* **10,** 1404. doi:`10.3389/fmicb.2019.01404` (2019).

14. Yagüe, P., Lopez-Garcia, M. T., Rioseras, B., Sanchez, J. & Manteca, A. New insights on the development of *Streptomyces* and their relationships with secondary metabolite production. *Current trends in microbiology* **8,** 65–73 (2012).

15. Harris, D. M., Diderich, J. A., van der Krogt, Z. A., Luttik, M. A. H., Raamsdonk, L. M., *et al.* Enzymic analysis of NADPH metabolism in beta-lactam-producing *Penicillium chrysogenum*: presence of a mitochondrial NADPH dehydrogenase. *Metabolic engineering* **8,** 91–101. doi:`10.1016/j.ymben.2005.09.004` (2006).

16. Singh, N. & Rai, V. Optimization of cultural parameters for antifungal and antibacterial metabolite from microbial isolate; *streptomyces rimosus* MTCC 10792 from soil of Chhattisgarh. *International Journal of Pharmacy and Pharmaceutical Sciences* **4** (2012).

17. da Silva, O. S., Prado, G. R., da Silva, J. L. R., Silva, C. E., da Costa, M., *et al.* Oral toxicity of *Photorhabdus luminescens* and *Xenorhabdus nematophila* (Enterobacteriaceae) against *Aedes aegypti* (Diptera: Culicidae). *Parasitology Research* **112,** 2891–2896. doi:`10.1007/s00436-013-3460-x` (2013).

18. Baltz, R. H. Natural product drug discovery in the genomic era: realities, conjectures, misconceptions, and opportunities. *Journal of industrial microbiology & biotechnology* **46,** 281–299. doi:`10.1007/s10295-018-2115-4` (2019).

19. Imai, Y., Meyer, K. J., Iinishi, A., Favre-Godal, Q., Green, R., *et al.* A new antibiotic selectively kills Gram-negative pathogens. *Nature* **576,** 459–464. doi:`10.1038/s41586-019-1791-1` (2019).

20. Ortega, M. A. & van der Donk, W. A. New Insights into the Biosynthetic Logic of Ribosomally Synthesized and Post-translationally Modified Peptide Natural Products. *Cell chemical biology* **23,** 31–44. doi:`10.1016/j.chembiol.2015.11.012` (2016).

21. McIntosh, J. A., Donia, M. S. & Schmidt, E. W. Ribosomal peptide natural products: bridging the ribosomal and nonribosomal worlds. *Natural Product Reports* **26,** 537–559. doi:`10.1039/b714132g` (2009).

22. Russell, A. H. & Truman, A. W. Genome mining strategies for ribosomally synthesised and post-translationally modified peptides. *Computational and Structural Biotechnology Journal* **18,** 1838–1851. doi:`10.1016/j.csbj.2020.06.032` (2020).

23. Knerr, P. J. & van der Donk, W. A. Discovery, Biosynthesis, and Engineering of Lantipeptides. *Annual review of biochemistry* **81,** 479–505. doi:`10.1146/annurev-biochem-060110-113521` (2012).

24. Sivonen, K., Leikoski, N., Fewer, D. P. & Jokela, J. Cyanobactins-ribosomal cyclic peptides produced by cyanobacteria. *Applied microbiology and biotechnology* **86,** 1213–1225. doi:`10.1007/s00253-010-2482-x` (2010).

25. Hegemann, J. D., Zimmermann, M., Xie, X. & Marahiel, M. A. Lasso Peptides: An Intriguing Class of Bacterial Natural Products. *Accounts of chemical research* **48,** 1909–1919. doi:`10.1021/acs.accounts.5b00156` (2015).

26. Liao, R., Duan, L., Lei, C., Pan, H., Ding, Y., *et al.* Thiopeptide Biosynthesis Featuring Ribosomally Synthesized Precursor Peptides and Conserved Posttranslational Modifications. *Chemistry & biology* **16,** 141–147. doi:`10.1016/j.chembiol.2009.01.007` (2009).

27. Oman, T. J. & van der Donk, W. A. Follow the leader: the use of leader peptides to guide natural product biosynthesis. *Nature chemical biology* **6,** 9–18. doi:`10.1038/nchembio.286` (2010).

28. Wang, H., Fewer, D. P., Holm, L., Rouhiainen, L. & Sivonen, K. Atlas of nonribosomal peptide and polyketide biosynthetic pathways reveals common occurrence of nonmodular enzymes. *Proceedings of the National Academy of Sciences of the United States of America* **111,** 9259–9264. doi:`10.1073/pnas.1401734111` (2014).

29. Walsh, C. T. The Chemical Versatility of Natural-Product Assembly Lines. *Accounts of chemical research* **41,** 4–10. doi:`10.1021/ar7000414` (2008).

30. Shen, B. Polyketide biosynthesis beyond the type I, II and III polyketide synthase paradigms. *Current Opinion in Chemical Biology* **7,** 285–295. doi:`10.1016/S1367-5931(03)00020-6` (2003).

31. Süssmuth, R. D. & Mainz, A. Nonribosomal Peptide Synthesis-Principles and Prospects. *Angewandte Chemie (International ed. in English)* **56,** 3770–3821. doi:`10.1002/anie.201609079` (2017).

32. Marahiel, M. A. A structural model for multimodular NRPS assembly lines. *Natural Product Reports* **33,** 136–140. doi:`10.1039/c5np00082c` (2016).

33. Marahiel, M. A. Working outside the protein-synthesis rules: insights into non-ribosomal peptide synthesis. *Journal of peptide science : an official publication of the European Peptide Society* **15,** 799–807. doi:`10.1002/psc.1183` (2009).

34. Grünewald, J. & Marahiel, M. A. Chemoenzymatic and Template-Directed Synthesis of Bioactive Macrocyclic Peptides. *Microbiology and Molecular Biology Reviews* **70,** 121–146. doi:`10.1128/MMBR.70.1.121-146.2006` (2006).

35. Du, L. & Shen, B. Identification and characterization of a type II peptidyl carrier protein from the bleomycin producer *Streptomyces verticillus* ATCC 15003. *Chemistry & biology* **6,** 507–517. doi:`10.1016/S1074-5521(99)80083-0` (1999).

36. Crosa, J. H. & Walsh, C. T. Genetics and Assembly Line Enzymology of Siderophore Biosynthesis in Bacteria. *Microbiology and Molecular Biology Reviews* **66,** 223–249. doi:`10.1128/MMBR.66.2.223-249.2002` (2002).

37. Cheng, Y.-Q., Tang, G.-L. & Shen, B. Type I polyketide synthase requiring a discrete acyltransferase for polyketide biosynthesis. *Proceedings of the National Academy of Sciences* **100,** 3149–3154. doi:`10.1073/pnas.0537286100` (2003).

38. Kehr, J.-C., Gatte Picchi, D. & Dittmann, E. Natural product biosyntheses in cyanobacteria: A treasure trove of unique enzymes. *Beilstein journal of organic chemistry* **7,** 1622–1635. doi:`10.3762/bjoc.7.191` (2011).

39. Doroghazi, J. R., Albright, J. C., Goering, A. W., Ju, K.-S., Haines, R. R., *et al.* A roadmap for natural product discovery based on large-scale

genomics and metabolomics. *Nature chemical biology* **10,** 963–968. doi:`10.1038/nchembio.1659` (2014).

40. Demain, A. L. Importance of microbial natural products and the need to revitalize their discovery. *Journal of industrial microbiology & biotechnology* **41,** 185–201. doi:`10.1007/s10295-013-1325-z` (2014).

41. Rigali, S., Anderssen, S., Naômé, A. & van Wezel, G. P. Cracking the Regulatory Code of Biosynthetic Gene Clusters as a Strategy for Natural Product Discovery. *Biochemical pharmacology* **153,** 24–34. doi:`10.1016/j.bcp.2018.01.007` (2018).

42. World Health Organization. *World Health Statistics 2020: Monitoring Health for the SDGs* (World Health Organization, 2020).

43. Ren, H., Wang, B. & Zhao, H. Breaking the silence: new strategies for discovering novel natural products. *Current opinion in biotechnology* **48,** 21–27. doi:`10.1016/j.copbio.2017.02.008` (2017).

44. Katz, L. & Baltz, R. H. Natural product discovery: past, present, and future. *Journal of industrial microbiology & biotechnology* **43,** 155–176. doi:`10.1007/s10295-015-1723-5` (2016).

45. Harvey, C. J. B., Puglisi, J. D., Pande, V. S., Cane, D. E. & Khosla, C. Precursor Directed Biosynthesis of an Orthogonally Functional Erythromycin Analogue: Selectivity in the Ribosome Macrolide Binding Pocket. *Journal of the American Chemical Society* **134,** 12259–12265. doi:`10.1021/ja304682q` (2012).

46. Fjaervik, E. & Zotchev, S. B. Biosynthesis of the polyene macrolide antibiotic nystatin in *Streptomyces noursei*. *Applied microbiology and biotechnology* **67,** 436–443. doi:`10.1007/s00253-004-1802-4` (2005).

47. Hutchings, M. I., Truman, A. W. & Wilkinson, B. Antibiotics: past, present and future. *Current opinion in microbiology* **51,** 72–80. doi:`10.1016/j.mib.2019.10.008` (2019).

48. Bachmann, B. O., van Lanen, S. G. & Baltz, R. H. Microbial genome mining for accelerated natural products discovery: is a renaissance in the making? *Journal of industrial microbiology & biotechnology* **41,** 175–184. doi:`10.1007/s10295-013-1389-9` (2014).

49. Ziemert, N., Alanjary, M. & Weber, T. The evolution of genome mining in microbes - a review. *Natural Product Reports* **33,** 988–1005. doi:`10.1039/c6np00025h` (2016).

50. Bentley, S. D., Chater, K. F., Cerdeño-Tárraga, A.-M., Challis, G. L., Thomson, N. R., *et al.* Complete genome sequence of the model

actinomycete *Streptomyces coelicolor* A3(2). *Nature* **417,** 141–147. doi:`10.1038/417141a` (2002).

51. Ikeda, H., Ishikawa, J., Hanamoto, A., Shinose, M., Kikuchi, H., *et al.* Complete genome sequence and comparative analysis of the industrial microorganism *Streptomyces avermitilis*. *Nature biotechnology* **21,** 526–531. doi:`10.1038/nbt820` (2003).

52. van Heel, A. J., de Jong, A., Song, C., Viel, J. H., Kok, J., *et al.* BAGEL4: a user-friendly web server to thoroughly mine RiPPs and bacteriocins. *Nucleic acids research* **46,** W278–W281. doi:`10.1093/nar/gky383` (2018).

53. Weber, T., Rausch, C., Lopez, P., Hoof, I., Gaykova, V., *et al.* CLUSEAN: a computer-based framework for the automated analysis of bacterial secondary metabolite biosynthetic gene clusters. *Journal of biotechnology* **140,** 13–17. doi:`10.1016/j.jbiotec.2009.01.007` (2009).

54. Blin, K., Shaw, S., Steinke, K., Villebro, R., Ziemert, N., *et al.* antiSMASH 5.0: updates to the secondary metabolite genome mining pipeline. *Nucleic acids research* **47,** W81–W87. doi:`10.1093/nar/gkz310` (2019).

55. Medema, M. H. & Fischbach, M. A. Computational approaches to natural product discovery. *Nature chemical biology* **11,** 639–648. doi:`10.1038/nchembio.1884` (2015).

56. Cimermancic, P., Medema, M. H., Claesen, J., Kurita, K., Wieland Brown, L. C., *et al.* Insights into secondary metabolism from a global analysis of prokaryotic biosynthetic gene clusters. *Cell* **158,** 412–421. doi:`10.1016/j.cell.2014.06.034` (2014).

57. Hannigan, G. D., Prihoda, D., Palicka, A., Soukup, J., Klempir, O., *et al.* A deep learning genome-mining strategy for biosynthetic gene cluster prediction. *Nucleic acids research* **47,** e110. doi:`10.1093/nar/gkz654` (2019).

58. Sélem-Mojica, N., Aguilar, C., Gutiérrez-García, K., Martínez-Guerrero, C. E. & Barona-Gómez, F. EvoMining reveals the origin and fate of natural product biosynthetic enzymes. *Microbial Genomics* **5.** doi:`10.1099/mgen.0.000260` (2019).

59. Kenshole, E., Herisse, M., Michael, M. & Pidot, S. J. Natural product discovery through microbial genome mining. *Current Opinion in Chemical Biology* **60,** 47–54. doi:`10.1016/j.cbpa.2020.07.010` (2020).

60. Albarano, L., Esposito, R., Ruocco, N. & Costantini, M. Genome Mining as New Challenge in Natural Products Discovery. *Marine drugs* **18.** doi:`10.3390/md18040199` (2020).

61. Bilyk, O. & Luzhetskyy, A. Metabolic engineering of natural product biosynthesis in actinobacteria. *Current opinion in biotechnology* **42,** 98–107. doi:`10.1016/j.copbio.2016.03.008` (2016).

62. Li, L., Jiang, W. & Lu, Y. New strategies and approaches for engineering biosynthetic gene clusters of microbial natural products. *Biotechnology advances* **35,** 936–949. doi:`10.1016/j.biotechadv.2017.03.007` (2017).

63. Ochi, K. Insights into microbial cryptic gene activation and strain improvement: principle, application and technical aspects. *The Journal of Antibiotics* **70,** 25–40. doi:`10.1038/ja.2016.82` (2017).

64. Mingyar, E., Mühling, L., Kulik, A., Winkler, A., Wibberg, D., *et al.* A Regulator Based "Semi-Targeted" Approach to Activate Silent Biosynthetic Gene Clusters. *International Journal of Molecular Sciences* **22,** 7567. doi:`10.3390/ijms22147567` (2021).

65. Bode, H. B., Bethe, B., Höfs, R. & Zeeck, A. Big Effects from Small Changes: Possible Ways to Explore Nature's Chemical Diversity. *ChemBioChem* **3,** 619. doi:`10.1002/1439-7633(20020703)3:7<619::AID-CBIC619>3.0.CO;2-9` (2002).

66. Romano, S., Jackson, S. A., Patry, S. & Dobson, A. D. W. Extending the "One Strain Many Compounds" (OSMAC) Principle to Marine Microorganisms. *Marine drugs* **16.** doi:`10.3390/md16070244` (2018).

67. Pan, R., Bai, X., Chen, J., Zhang, H. & Wang, H. Exploring Structural Diversity of Microbe Secondary Metabolites Using OSMAC Strategy: A Literature Review. *Frontiers in Microbiology* **10,** 294. doi:`10.3389/fmicb.2019.00294` (2019).

68. Kouprina, N. & Larionov, V. Transformation-associated recombination (TAR) cloning for genomics studies and synthetic biology. *Chromosoma* **125,** 621–632. doi:`10.1007/s00412-016-0588-3` (2016).

69. Kim, J. H., Feng, Z., Bauer, J. D., Kallifidas, D., Calle, P. Y., *et al.* Cloning Large Natural Product Gene Clusters from the Environment: Piecing Environmental DNA Gene Clusters Back Together with TAR. *Biopolymers* **93,** 833–844. doi:`10.1002/bip.21450` (2010).

70. Wang, H., Li, Z., Jia, R., Hou, Y., Yin, J., *et al.* RecET direct cloning and Red-alphabeta recombineering of biosynthetic gene clusters, large

operons or single genes for heterologous expression. *Nature protocols* **11,** 1175–1190. doi:`10.1038/nprot.2016.054` (2016).

71. Gibson, D. G., Young, L., Chuang, R.-Y., Venter, J. C., Hutchison, C. A., *et al.* Enzymatic assembly of DNA molecules up to several hundred kilobases. *Nature Methods* **6,** 343–345. doi:`10.1038/nmeth.1318` (2009).

72. Jiang, W., Zhao, X., Gabrieli, T., Lou, C., Ebenstein, Y., *et al.* Cas9-Assisted Targeting of CHromosome segments CATCH enables one-step targeted cloning of large gene clusters. *Nature Communications* **6,** 8101. doi:`10.1038/ncomms9101` (2015).

73. Huo, L., Hug, J. J., Fu, C., Bian, X., Zhang, Y., *et al.* Heterologous expression of bacterial natural product biosynthetic pathways. *Natural Product Reports* **36,** 1412–1436. doi:`10.1039/c8np00091c` (2019).

74. Verbeke, F., de Craemer, S., Debunne, N., Janssens, Y., Wynendaele, E., *et al.* Peptides as Quorum Sensing Molecules: Measurement Techniques and Obtained Levels In vitro and In vivo. *Frontiers in Neuroscience* **11,** 183. doi:`10.3389/fnins.2017.00183` (2017).

75. Biarnes-Carrera, M., Breitling, R. & Takano, E. Butyrolactone signalling circuits for synthetic biology. *Current Opinion in Chemical Biology* **28,** 91–98. doi:`10.1016/j.cbpa.2015.06.024` (2015).

76. Brameyer, S., Kresovic, D., Bode, H. B. & Heermann, R. Dialkylresorcinols as bacterial signaling molecules. *Proceedings of the National Academy of Sciences* **112,** 572–577. doi:`10.1073/pnas.1417685112` (2015).

77. Brachmann, A. O., Brameyer, S., Kresovic, D., Hitkova, I., Kopp, Y., *et al.* Pyrones as bacterial signaling molecules. *Nature Chemical Biology* **9,** 573–578. doi:`10.1038/nchembio.1295` (2013).

78. Papenfort, K. & Bassler, B. L. Quorum sensing signal-response systems in Gram-negative bacteria. *Nature Reviews Microbiology* **14,** 576–588. doi:`10.1038/nrmicro.2016.89` (2016).

79. Kleerebezem, M. Quorum sensing control of lantibiotic production; nisin and subtilin autoregulate their own biosynthesis. *Peptides* **25,** 1405–1414. doi:`10.1016/j.peptides.2003.10.021` (2004).

80. Schmidt, S., Blom, J. F., Pernthaler, J., Berg, G., Baldwin, A., *et al.* Production of the antifungal compound pyrrolnitrin is quorum sensing-regulated in members of the *Burkholderia cepacia* complex. *Environmental microbiology* **11,** 1422–1437. doi:`10.1111/j.1462-2920.2009.01870.x` (2009).

81. El-Sayed, A. K., Hothersall, J. & Thomas, C. M. Quorum-sensing-dependent regulation of biosynthesis of the polyketide antibiotic mupirocin in *Pseudomonas fluorescens* NCIMB 10586. *Microbiology* **147,** 2127–2139. doi:`10.1099/00221287-147-8-2127` (2001).

82. Ishida, K., Lincke, T., Behnken, S. & Hertweck, C. Induced biosynthesis of cryptic polyketide metabolites in a *Burkholderia thailandensis* quorum sensing mutant. *Journal of the American Chemical Society* **132,** 13966–13968. doi:`10.1021/ja105003g` (2010).

83. Hoiczyk, E. & Hansel, A. Cyanobacterial Cell Walls: News from an Unusual Prokaryotic Envelope. *Journal of Bacteriology* **182,** 1191–1199. doi:`10.1128/jb.182.5.1191-1199.2000` (2000).

84. Rasmussen, B., Fletcher, I. R., Brocks, J. J. & Kilburn, M. R. Reassessing the first appearance of eukaryotes and cyanobacteria. *Nature* **455,** 1101–1104. doi:`10.1038/nature07381` (2008).

85. Madigan, M. T., Martinko, J. M., Bender, K. S., Buckley, D. H. & Stahl, D. A. *Brock Biology of Microorganisms* Fourteenth edition (Pearson, Boston, 2015).

86. Zakhia, F., Jungblut, A.-D., Taton, A., Vincent, W. F. & Wilmotte, A. in *Psychrophiles* (ed Margesin, R.) 121–135 (Springer, Berlin, 2008). doi:`10.1007/978-3-540-74335-4`.

87. Stanier, R. Y., Trüper, H. G., Gorlenko, V. N., Hansen, T. A., Gherna, R. L., *et al.* Proposal to Place the Nomenclature of the Cyanobacteria (Blue-Green Algae) Under the Rules of the International Code of Nomenclature of Bacteria. *International Journal of Systematic and Evolutionary Microbiology* **28,** 335–336. doi:`10.1099/00207713-28-2-335` (1978).

88. Mazard, S., Penesyan, A., Ostrowski, M., Paulsen, I. T. & Egan, S. Tiny Microbes with a Big Impact: The Role of Cyanobacteria and Their Metabolites in Shaping Our Future. *Marine drugs* **14.** doi:`10.3390/md14050097` (2016).

89. Dixit, R. B. & Suseela, M. R. Cyanobacteria: potential candidates for drug discovery. *Antonie van Leeuwenhoek* **103,** 947–961. doi:`10.1007/s10482-013-9898-0` (2013).

90. Oren, A. Cyanobacteria in hypersaline environments: biodiversity and physiological properties. *Biodiversity and Conservation* **24,** 781–798. doi:`10.1007/s10531-015-0882-z` (2015).

91. Dadheech, P. K., Glöckner, G., Casper, P., Kotut, K., Mazzoni, C. J., *et al.* Cyanobacterial diversity in the hot spring, pelagic and benthic habitats

of a tropical soda lake. *FEMS microbiology ecology* **85,** 389–401. doi:`10.1111/1574-6941.12128` (2013).

92. Amarouche-Yala, S., Benouadah, A., El Ouahab Bentabet, A. & López-García, P. Morphological and phylogenetic diversity of thermophilic cyanobacteria in Algerian hot springs. *Extremophiles* **18,** 1035–1047. doi:`10.1007/s00792-014-0680-7` (2014).

93. Adams, D. G., Bergman, B., Nierzwicki-Bauer, S. A., Duggan, P. S., Rai, A. N., *et al.* in *The Prokaryotes* (eds DeLong, E. F. & Rosenberg, E.) 359–400 (Springer Reference, Berlin, 2013). doi:`10.1007/978-3-642-30194-0`.

94. Zanchett, G. & Oliveira-Filho, E. C. Cyanobacteria and Cyanotoxins: From Impacts on Aquatic Ecosystems and Human Health to Anticarcinogenic Effects. *Toxins* **5,** 1896–1917. doi:`10.3390/toxins5101896` (2013).

95. Mandal, S. & Rath, J. *Extremophilic Cyanobacteria for Novel Drug Development* doi:`10.1007/978-3-319-12009-6` (Springer, Cham, 2015).

96. Demay, J., Bernard, C., Reinhardt, A. & Marie, B. Natural Products from Cyanobacteria: Focus on Beneficial Activities. *Marine drugs* **17.** doi:`10.3390/md17060320` (2019).

97. Zahra, Z., Choo, D. H., Lee, H. & Parveen, A. Cyanobacteria: Review of Current Potentials and Applications. *Environments* **7,** 13. doi:`10.3390/environments7020013` (2020).

98. Kounnis, V., Chondrogiannis, G., Mantzaris, M. D., Tzakos, A. G., Fokas, D., *et al.* Microcystin LR Shows Cytotoxic Activity Against Pancreatic Cancer Cells Expressing the Membrane OATP1B1 and OATP1B3 Transporters. *Anticancer research* **35,** 5857–5865 (2015).

99. Singh, R. K., Tiwari, S. P., Rai, A. K. & Mohapatra, T. M. Cyanobacteria: An emerging source for drug discovery. *The Journal of antibiotics* **64,** 401–412. doi:`10.1038/ja.2011.21` (2011).

100. Rastogi, R. P. & Incharoensakdi, A. Characterization of UV-screening compounds, mycosporine-like amino acids, and scytonemin in the cyanobacterium *Lyngbya* sp. CU2555. *FEMS microbiology ecology* **87,** 244–256. doi:`10.1111/1574-6941.12220` (2014).

101. Stevenson, C. S., Capper, E. A., Roshak, A. K., Marquez, B., Grace, K., *et al.* Scytonemin–a marine natural product inhibitor of kinases key in hyperproliferative inflammatory diseases. *Inflammation Research* **51,** 112–114. doi:`10.1007/BF02684014` (2002).

102. Calteau, A., Fewer, D. P., Latifi, A., Coursin, T., Laurent, T., *et al.* Phylum-wide comparative genomics unravel the diversity of secondary metabolism in Cyanobacteria. *BMC genomics* **15,** 977. doi:`10.1186/1471-2164-15-977` (2014).

103. Shih, P. M., Wu, D., Latifi, A., Axen, S. D., Fewer, D. P., *et al.* Improving the coverage of the cyanobacterial phylum using diversity-driven genome sequencing. *Proceedings of the National Academy of Sciences* **110,** 1053–1058. doi:`10.1073/pnas.1217107110` (2013).

104. Santos-Merino, M., Singh, A. K. & Ducat, D. C. New Applications of Synthetic Biology Tools for Cyanobacterial Metabolic Engineering. *Frontiers in bioengineering and biotechnology* **7,** 33. doi:`10.3389/fbioe.2019.00033` (2019).

105. Meeks, J. C., Elhai, J., Thiel, T., Potts, M., Larimer, F., *et al.* An overview of the genome of *Nostoc punctiforme*, a multicellular, symbiotic cyanobacterium. *Photosynthesis research* **70,** 85–106. doi:`10.1023/A:1013840025518` (2001).

106. Campbell, E. L., Summers, M. L., Christman, H., Martin, M. E. & Meeks, J. C. Global Gene Expression Patterns of *Nostoc punctiforme* in Steady-State Dinitrogen-Grown Heterocyst-Containing Cultures and at Single Time Points during the Differentiation of Akinetes and Hormogonia. *Journal of Bacteriology* **189,** 5247–5256. doi:`10.1128/JB.00360-07` (2007).

107. Liaimer, A., Jensen, J. B. & Dittmann, E. A Genetic and Chemical Perspective on Symbiotic Recruitment of Cyanobacteria of the Genus *Nostoc* into the Host Plant *Blasia pusilla* L. *Frontiers in microbiology* **7,** 1693. doi:`10.3389/fmicb.2016.01693` (2016).

108. Ekman, M., Picossi, S., Campbell, E. L., Meeks, J. C. & Flores, E. A *Nostoc punctiforme* Sugar Transporter Necessary to Establish a Cyanobacterium-Plant Symbiosis. *Plant physiology* **161,** 1984–1992. doi:`10.1104/pp.112.213116` (2013).

109. Liaimer, A., Jenke-Kodama, H., Ishida, K., Hinrichs, K., Stangeland, J., *et al.* A polyketide interferes with cellular differentiation in the symbiotic cyanobacterium *Nostoc punctiforme*. *Environmental Microbiology Reports* **3,** 550–558. doi:`10.1111/j.1758-2229.2011.00258.x` (2011).

110. Guljamow, A., Kreische, M., Ishida, K., Liaimer, A., Altermark, B., *et al.* High-Density Cultivation of Terrestrial *Nostoc* Strains Leads to Reprogramming of Secondary Metabolome. *Applied and environmental microbiology* **83.** doi:`10.1128/AEM.01510-17` (2017).

111. Campbell, E. L., Cohen, M. F. & Meeks, J. C. A polyketide-synthase-like gene is involved in the synthesis of heterocyst glycolipids in *Nostoc punctiforme* strain ATCC 29133. *Archives of microbiology* **167,** 251–258. doi:`10.1007/s002030050440` (1997).

112. Giglio, S., Jiang, J., Saint, C. P., Cane, D. E. & Monis, P. T. Isolation and Characterization of the Gene Associated with Geosmin Production in Cyanobacteria. *Environmental science & technology* **42,** 8027–8032. doi:`10.1021/es801465w` (2008).

113. Rouhiainen, L., Jokela, J., Fewer, D. P., Urmann, M. & Sivonen, K. Two Alternative Starter Modules for the Non-Ribosomal Biosynthesis of Specific Anabaenopeptin Variants in *Anabaena* (Cyanobacteria). *Chemistry & biology* **17,** 265–273. doi:`10.1016/j.chembiol.2010.01.017` (2010).

114. Hunsucker, S. W., Klage, K., Slaughter, S. M., Potts, M. & Helm, R. F. A preliminary investigation of the *Nostoc punctiforme* proteome. *Biochemical and biophysical research communications* **317,** 1121–1127. doi:`10.1016/j.bbrc.2004.03.173` (2004).

115. Dehm, D., Krumbholz, J., Baunach, M., Wiebach, V., Hinrichs, K., *et al.* Unlocking the Spatial Control of Secondary Metabolism Uncovers Hidden Natural Product Diversity in *Nostoc punctiforme. ACS chemical biology,* 1271–1279. doi:`10.1021/acschembio.9b00240` (2019).

116. Liaimer, A., Helfrich, E. J. N., Hinrichs, K., Guljamow, A., Ishida, K., *et al.* Nostopeptolide plays a governing role during cellular differentiation of the symbiotic cyanobacterium *Nostoc punctiforme. Proceedings of the National Academy of Sciences of the United States of America* **112,** 1862–1867. doi:`10.1073/pnas.1419543112` (2015).

117. Rippka, R., Deruelles, J., Waterbury, J. B., Herdman, M. & Stanier, R. Y. Generic Assignments, Strain Histories and Properties of Pure Cultures of Cyanobacteria. *Microbiology* **111,** 1–61. doi:`10.1099/00221287-111-1-1` (1979).

118. Black, T. A. & Wolk, C. P. Analysis of a Het⁻ Mutation in *Anabaena* sp. Strain PCC 7120 Implicates a Secondary Metabolite in the Regulation of Heterocyst Spacing. *Journal of Bacteriology* **176,** 2282–2292. doi:`10.1128/jb.176.8.2282-2292.1994` (1994).

119. Cai, Y. P. & Wolk, C. P. Use of a Conditionally Lethal Gene in *Anabaena* sp. Strain PCC 7120 to Select for Double Recombinants and To Entrap Insertion Sequences. *Journal of Bacteriology* **172,** 3138–3145. doi:`10.1128/jb.172.6.3138-3145.1990` (1990).

120. Lippi, L., Bähr, L., Wüstenberg, A., Wilde, A. & Steuer, R. Exploring the potential of high-density cultivation of cyanobacteria for the production of cyanophycin. *Algal Research* **31,** 363–366. doi:`10.1016/j.algal.2018.02.028` (2018).

121. Harris, E. H., Stern, D. B. & Witman, G. in *The Chlamydomonas Sourcebook* (eds Harris, E. H., Stern, D. B. & Witman, G.) 241–302 (Academic Press, Amsterdam and Boston, 2009). doi:`10.1016/B978-0-12-370873-1.00008-3`.

122. Schreiber, U. in *Chlorophyll a Fluorescence* (ed Papageorgiou, G. C.) 279–319 (Springer, Dordrecht, 2004). doi:`10.1007/978-1-4020-3218-9`.

123. Fu, C., Donovan, W. P., Shikapwashya-Hasser, O., Ye, X. & Cole, R. H. Hot Fusion: an Efficient Method to Clone Multiple DNA Fragments as Well as Inverted Repeats without Ligase. *PloS one* **9,** e115318. doi:`10.1371/journal.pone.0115318` (2014).

124. Untergasser, A., Cutcutache, I., Koressaar, T., Ye, J., Faircloth, B. C., *et al.* Primer3–new capabilities and interfaces. *Nucleic acids research* **40,** e115. doi:`10.1093/nar/gks596` (2012).

125. Afgan, E., Baker, D., Batut, B., van den Beek, M., Bouvier, D., *et al.* The Galaxy platform for accessible, reproducible and collaborative biomedical analyses: 2018 update. *Nucleic acids research* **46,** W537–W544. doi:`10.1093/nar/gky379` (2018).

126. Kim, D., Langmead, B. & Salzberg, S. L. HISAT: a fast spliced aligner with low memory requirements. *Nature methods* **12,** 357–360. doi:`10.1038/nmeth.3317` (2015).

127. Anders, S., Pyl, P. T. & Huber, W. HTSeq–a Python framework to work with high-throughput sequencing data. *Bioinformatics (Oxford, England)* **31,** 166–169. doi:`10.1093/bioinformatics/btu638` (2015).

128. R. Core Team. *R: A Language and Environment for Statistical Computing* Vienna, Austria, 2020.

129. Love, M. I., Huber, W. & Anders, S. Moderated estimation of fold change and dispersion for RNA-seq data with DESeq2. *Genome biology* **15,** 550. doi:`10.1186/s13059-014-0550-8` (2014).

130. Strohalm, M., Hassman, M., Kosata, B. & Kodíček, M. mMass data miner: an open source alternative for mass spectrometric data analysis. *Rapid communications in mass spectrometry : RCM* **22,** 905–908. doi:`10.1002/rcm.3444` (2008).

131. Database resources of the National Center for Biotechnology Information. *Nucleic acids research* **44,** D7–19. doi:`10.1093/nar/gkv1290` (2016).

132. Altschul, S. F., Gish, W., Miller, W., Myers, E. W. & Lipman, D. J. Basic Local Alignment Search Tool. *Journal of molecular biology* **215,** 403–410. doi:`10.1016/S0022-2836(05)80360-2` (1990).

133. Boratyn, G. M., Camacho, C., Cooper, P. S., Coulouris, G., Fong, A., *et al.* BLAST: a more efficient report with usability improvements. *Nucleic acids research* **41,** W29–33. doi:`10.1093/nar/gkt282` (2013).

134. Medema, M. H., Blin, K., Cimermancic, P., de Jager, V., Zakrzewski, P., *et al.* antiSMASH: rapid identification, annotation and analysis of secondary metabolite biosynthesis gene clusters in bacterial and fungal genome sequences. *Nucleic acids research* **39,** W339–46. doi:`10.1093/nar/gkr466` (2011).

135. Blin, K., Wolf, T., Chevrette, M. G., Lu, X., Schwalen, C. J., *et al.* antiSMASH 4.0-improvements in chemistry prediction and gene cluster boundary identification. *Nucleic acids research* **45,** W36–W41. doi:`10.1093/nar/gkx319` (2017).

136. Yu, J., Liberton, M., Cliften, P. F., Head, R. D., Jacobs, J. M., *et al. Synechococcus elongatus* UTEX 2973, a fast growing cyanobacterial chassis for biosynthesis using light and CO_2. *Scientific reports* **5,** 8132. doi:`10.1038/srep08132` (2015).

137. Bähr, L., Wüstenberg, A. & Ehwald, R. Two-tier vessel for photoautotrophic high-density cultures. *Journal of Applied Phycology* **28,** 783–793. doi:`10.1007/s10811-015-0614-5` (2016).

138. Dehm, D. *Development of Concepts for the Genomic Mining of Novel Secondary Metabolites in Symbiotic Cyanobacteria* PhD thesis (Universität Potsdam, 2020). doi:`10.25932/PUBLISHUP-47834`.

139. Capra, E. J. & Laub, M. T. Evolution of Two-Component Signal Transduction Systems. *Annual review of microbiology* **66,** 325–347. doi:`10.1146/annurev-micro-092611-150039` (2012).

140. Ruiz, D., Salinas, P., Lopez-Redondo, M. L., Cayuela, M. L., Marina, A., *et al.* Phosphorylation-independent activation of the atypical response regulator NblR. *Microbiology* **154,** 3002–3015. doi:`10.1099/mic.0.2008/020677-0` (2008).

141. Ulrich, L. E., Koonin, E. V. & Zhulin, I. B. One-component systems dominate signal transduction in prokaryotes. *Trends in Microbiology* **13,** 52–56. doi:`10.1016/j.tim.2004.12.006` (2005).

142. Gallegos, M. T., Schleif, R., Bairoch, A., Hofmann, K. & Ramos, J. L. Arac/XylS family of Transcriptional Regulators. *Microbiology and Molecular Biology Reviews* **61,** 393–410 (1997).

143. Mo, G., Zhou, H., Kawamura, T. & Dahlquist, F. W. Solution structure of a complex of the histidine autokinase CheA with its substrate CheY. *Biochemistry* **51,** 3786–3798. doi:`10.1021/bi300147m` (2012).

144. Cuthbertson, L. & Nodwell, J. R. The TetR Family of Regulators. *Microbiology and Molecular Biology Reviews* **77,** 440–475. doi:`10.1128/MMBR.00018-13` (2013).

145. Deng, W., Li, C. & Xie, J. The underling mechanism of bacterial TetR/AcrR family transcriptional repressors. *Cellular signalling* **25,** 1608–1613. doi:`10.1016/j.cellsig.2013.04.003` (2013).

146. Chen, J. & Xie, J. Role and Regulation of Bacterial LuxR-Like Regulators. *Journal of cellular biochemistry* **112,** 2694–2702. doi:`10.1002/jcb.23219` (2011).

147. De Bruijn, I. & Raaijmakers, J. M. Diversity and Functional Analysis of LuxR-Type Transcriptional Regulators of Cyclic Lipopeptide Biosynthesis in *Pseudomonas fluorescens*. *Applied and environmental microbiology* **75,** 4753–4761. doi:`10.1128/AEM.00575-09` (2009).

148. Zhao, Z., Peng, T., Oh, J.-I., Glaeser, J., Weber, L., *et al.* A response regulator of the OmpR family is part of the regulatory network controlling the oxidative stress response of *Rhodobacter sphaeroides*. *Environmental Microbiology Reports,* 1–11. doi:`10.1111/1758-2229.12718` (2018).

149. Yang, X., Shimizu, Y., Steiner, J. R. & Clardy, J. Nostoclide I and II, Extracellular Metabolites from a Symbiotic Cyanobacterium, *Nostoc* sp., from the Lichen *Peltigera canina*. *Tetrahedron Letters* **34,** 761–764. doi:`10.1016/0040-4039(93)89005-B` (1993).

150. Vieweg, L., Reichau, S., Schobert, R., Leadlay, P. F. & Süssmuth, R. D. Recent advances in the field of bioactive tetronates. *Natural Product Reports* **31,** 1554–1584. doi:`10.1039/c4np00015c` (2014).

151. D'Agostino, P. M., Seel, C. J., Gulder, T. & Gulder, T. *(Bio-)Synthesis of the Aquatic Phytotoxin Cyanobacterin – A Paradigm for Furanolide Core Structure Assembly* 2021. doi:`10.26434/chemrxiv.14625774.v1`.

152. Sun, Y., Hahn, F., Demydchuk, Y., Chettle, J., Tosin, M., *et al. In vitro* reconstruction of tetronate RK-682 biosynthesis. *Nature Chemical Biology* **6,** 99–101. doi:`10.1038/nchembio.285` (2010).

153. Kanchanabanca, C., Tao, W., Hong, H., Liu, Y., Hahn, F., *et al.* Unusual Acetylation-Elimination in the Formation of Tetronate Antibiotics. *Angewandte Chemie (International ed. in English)* **52,** 5785–5788. doi:`10.1002/anie.201301680` (2013).

154. Gagunashvili, A. N. & Andrésson, Ó. S. Distinctive characters of *Nostoc* genomes in cyanolichens. *BMC Genomics* **19,** 434. doi:`10.1186/s12864-018-4743-5` (2018).

155. Chen, I.-M. A., Chu, K., Palaniappan, K., Ratner, A., Huang, J., *et al.* The IMG/M data management and analysis system v.6.0: new tools and advanced capabilities. *Nucleic acids research* **49,** D751–D763. doi:`10.1093/nar/gkaa939` (2021).

156. Galperin, M. Y., Wolf, Y. I., Makarova, K. S., Vera Alvarez, R., Landsman, D., *et al.* COG database update: focus on microbial diversity, model organisms, and widespread pathogens. *Nucleic acids research* **49,** D274–D281. doi:`10.1093/nar/gkaa1018` (2021).

157. Janssen, J. & Soule, T. Gene expression of a two-component regulatory system associated with sunscreen biosynthesis in the cyanobacterium *Nostoc punctiforme* ATCC 29133. *FEMS microbiology letters* **363,** fnv235. doi:`10.1093/femsle/fnv235` (2016).

158. Klicki, K., Ferreira, D., Hamill, D., Dirks, B., Mitchell, N., *et al.* The Widely Conserved *ebo* Cluster Is Involved in Precursor Transport to the Periplasm during Scytonemin Synthesis in *Nostoc punctiforme. mBio* **9.** doi:`10.1128/mBio.02266-18` (2018).

159. Gleason, F. K. & Case, D. E. Activity of the Natural Algicide, Cyanobacterin, on Angiosperms. *Plant physiology* **80,** 834–837. doi:`10.1104/pp.80.4.834` (1986).

160. Gleason, F. K., Case, D. E., Sipprell, K. D. & Magnuson, T. S. Effect of the Natural Algicide, Cyanobacterin, on a Herbicide-Resistant Mutant of *Anacystis nidulans* R2. *Plant Science* **46,** 5–10. doi:`10.1016/0168-9452(86)90124-X` (1986).

161. Barbosa, L. C., Demuner, A. J., de Alvarenga, E. S., Oliveira, A., King-Diaz, B., *et al.* Phytogrowth- and photosynthesis-inhibiting properties of nostoclide analogues. *Pest management science* **62,** 214–222. doi:`10.1002/ps.1147` (2006).

162. Repka, L. M., Chekan, J. R., Nair, S. K. & van der Donk, W. A. Mechanistic Understanding of Lanthipeptide Biosynthetic Enzymes. *Chemical reviews* **117,** 5457–5520. doi:`10.1021/acs.chemrev.6b00591` (2017).

163. Zhang, Q., Yu, Y., Vélasquez, J. E. & van der Donk, W. A. Evolution of lanthipeptide synthetases. *Proceedings of the National Academy of Sciences* **109,** 18361–18366. doi:`10.1073/pnas.1210393109` (2012).

164. Black, T. A., Cai, Y. & Wolk, C. P. Spatial expression and autoregulation of hetR, a gene involved in the control of heterocyst development in *Anabaena*. *Molecular microbiology* **9,** 77–84. doi:`10.1111/j.1365-2958.1993.tb01670.x` (1993).

165. Behle, A., Saake, P., Germann, A. T., Dienst, D. & Axmann, I. M. Comparative Dose-Response Analysis of Inducible Promoters in Cyanobacteria. *ACS synthetic biology* **9,** 843–855. doi:`10.1021/acssynbio.9b00505` (2020).

166. Dienst, D., Wichmann, J., Mantovani, O., Rodrigues, J. S. & Lindberg, P. High density cultivation for efficient sesquiterpenoid biosynthesis in *Synechocystis* sp. PCC 6803. *Scientific reports* **10,** 5932. doi:`10.1038/s41598-020-62681-w` (2020).

167. Argueta, C., Yuksek, K. & Summers, M. Construction and use of GFP reporter vectors for analysis of cell-type-specific gene expression in Nostoc punctiforme. *Journal of Microbiological Methods* **59,** 181–188. doi:`10.1016/j.mimet.2004.06.009` (2004).

168. Kloosterman, A. M., Cimermancic, P., Elsayed, S. S., Du, C., Hadjithomas, M., *et al.* Expansion of RiPP biosynthetic space through integration of pan-genomics and machine learning uncovers a novel class of lanthipeptides. *PLOS Biology* **18,** e3001026. doi:`10.1371/journal.pbio.3001026` (2020).

169. Morinaka, B. I., Lakis, E., Verest, M., Helf, M. J., Scalvenzi, T., *et al.* Natural noncanonical protein splicing yields products with diverse beta-amino acid residues. *Science (New York, N.Y.)* **359,** 779–782. doi:`10.1126/science.aao0157` (2018).

170. Yang, X. & van der Donk, W. A. Post-translational Introduction of D-Alanine into Ribosomally Synthesized Peptides by the Dehydroalanine Reductase NpnJ. *Journal of the American Chemical Society* **137,** 12426–12429. doi:`10.1021/jacs.5b05207` (2015).

171. Ogasawara, Y., Kawata, J., Noike, M., Satoh, Y., Furihata, K., *et al.* Exploring Peptide Ligase Orthologs in Actinobacteria-Discovery of Pseudopeptide Natural Products, Ketomemicins. *ACS chemical biology* **11,** 1686–1692. doi:`10.1021/acschembio.6b00046` (2016).

172. Caruso, A., Bushin, L. B., Clark, K. A., Martinie, R. J. & Seyedsayamdost, M. R. Radical Approach to Enzymatic beta-Thioether Bond Formation.

Journal of the American Chemical Society **141,** 990–997. doi:`10.1021/jacs.8b11060` (2019).

173. Rutledge, P. J. & Challis, G. L. Discovery of microbial natural products by activation of silent biosynthetic gene clusters. *Nature reviews. Microbiology* **13,** 509–523. doi:`10.1038/nrmicro3496` (2015).

174. Zhang, X., Hindra & Elliot, M. A. Unlocking the trove of metabolic treasures: activating silent biosynthetic gene clusters in bacteria and fungi. *Current opinion in microbiology* **51,** 9–15. doi:`10.1016/j.mib.2019.03.003` (2019).

175. Chiang, Y.-M., Szewczyk, E., Davidson, A. D., Keller, N., Oakley, B. R., *et al.* A gene cluster containing two fungal polyketide synthases encodes the biosynthetic pathway for a polyketide, asperfuranone, in *Aspergillus nidulans. Journal of the American Chemical Society* **131,** 2965–2970. doi:`10.1021/ja8088185` (2009).

176. Laureti, L., Song, L., Huang, S., Corre, C., Leblond, P., *et al.* Identification of a bioactive 51-membered macrolide complex by activation of a silent polyketide synthase in *Streptomyces ambofaciens. Proceedings of the National Academy of Sciences* **108,** 6258–6263. doi:`10.1073/pnas.1019077108` (2011).

177. Bunet, R., Song, L., Mendes, M. V., Corre, C., Hotel, L., *et al.* Characterization and manipulation of the pathway-specific late regulator AlpW reveals *Streptomyces ambofaciens* as a new producer of Kinamycins. *Journal of Bacteriology* **193,** 1142–1153. doi:`10.1128/JB.01269-10` (2011).

178. Garby, T. J., Matys, E. D., Ongley, S. E., Salih, A., Larkum, A. W. D., *et al.* Lack of Methylated Hopanoids Renders the Cyanobacterium *Nostoc punctiforme* Sensitive to Osmotic and pH Stress. *Applied and Environmental Microbiology* **83.** doi:`10.1128/AEM.00777-17` (2017).

179. Ferreira, D. & Garcia-Pichel, F. Mutational Studies of Putative Biosynthetic Genes for the Cyanobacterial Sunscreen Scytonemin in *Nostoc punctiforme* ATCC 29133. *Frontiers in Microbiology* **7,** 735. doi:`10.3389/fmicb.2016.00735` (2016).

180. Li, B., Sher, D., Kelly, L., Shi, Y., Huang, K., *et al.* Catalytic promiscuity in the biosynthesis of cyclic peptide secondary metabolites in planktonic marine cyanobacteria. *Proceedings of the National Academy of Sciences* **107,** 10430–10435. doi:`10.1073/pnas.0913677107` (2010).

181. Desai, S. K. & Kenney, L. J. To ~P or Not to ~P? Non-canonical activation by two-component response regulators. *Molecular microbiology* **103,** 203–213. doi:`10.1111/mmi.13532` (2017).

182. Gao, R., Bouillet, S. & Stock, A. M. Structural Basis of Response Regulator Function. *Annual review of microbiology* **73,** 175–197. doi:`10.1146/annurev-micro-020518-115931` (2019).

183. Guthrie, E. P., Flaxman, C. S., White, J., Hodgson, D. A., Bibb, M. J., *et al.* A response-regulator-like activator of antibiotic synthesis from *Streptomyces coelicolor* A3(2) with an amino-terminal domain that lacks a phosphorylation pocket. *Microbiology* **144 (Pt 3),** 727–738. doi:`10.1099/00221287-144-3-727` (1998).

184. Wang, L., Tian, X., Wang, J., Yang, H., Fan, K., *et al.* Autoregulation of antibiotic biosynthesis by binding of the end product to an atypical response regulator. *Proceedings of the National Academy of Sciences* **106,** 8617–8622. doi:`10.1073/pnas.0900592106` (2009).

185. Vicente, C. M., Payero, T. D., Santos-Aberturas, J., Barreales, E. G., de Pedro, A., *et al.* Pathway-specific regulation revisited: cross-regulation of multiple disparate gene clusters by PAS-LuxR transcriptional regulators. *Applied Microbiology and Biotechnology* **99,** 5123–5135. doi:`10.1007/s00253-015-6472-x` (2015).

186. Dong, Y.-H., Zhang, X.-F., Xu, J.-L., Tan, A.-T. & Zhang, L.-H. VqsM, a novel AraC-type global regulator of quorum-sensing signalling and virulence in *Pseudomonas aeruginosa*. *Molecular microbiology* **58,** 552–564. doi:`10.1111/j.1365-2958.2005.04851.x` (2005).

187. Liang, H., Deng, X., Li, X., Ye, Y. & Wu, M. Molecular mechanisms of master regulator VqsM mediating quorum-sensing and antibiotic resistance in *Pseudomonas aeruginosa*. *Nucleic acids research* **42,** 10307–10320. doi:`10.1093/nar/gku586` (2014).

188. Chatterjee, S., Sahoo, R. & Nanda, S. Recent reports on the synthesis of gamma-butenolide, gamma-alkylidenebutenolide frameworks, and related natural products. *Organic & Biomolecular Chemistry.* doi:`10.1039/d1ob00875g` (2021).

189. Wang, W., Zhang, J., Liu, X., Li, D., Li, Y., *et al.* Identification of a butenolide signaling system that regulates nikkomycin biosynthesis in *Streptomyces*. *The Journal of biological chemistry* **293,** 20029–20040. doi:`10.1074/jbc.RA118.005667` (2018).

190. Kitani, S., Miyamoto, K. T., Takamatsu, S., Herawati, E., Iguchi, H., *et al.* Avenolide, a *Streptomyces* hormone controlling antibiotic production

in *Streptomyces avermitilis*. *Proceedings of the National Academy of Sciences* **108,** 16410–16415. doi:`10.1073/pnas.1113908108` (2011).

191. Klapper, M., Schlabach, K., Paschold, A., Zhang, S., Chowdhury, S., *et al.* Biosynthesis of Pseudomonas-Derived Butenolides. *Angewandte Chemie (International ed. in English)* **59,** 5607–5610. doi:`10.1002/anie.201914154` (2020).

192. Teixeira, R. R., Barbosa, L. C. A., Forlani, G., Piló-Veloso, D. & Walkimar de Mesquita Carneiro, J. Synthesis of Photosynthesis-Inhibiting Nostoclide Analogues. *Journal of agricultural and food chemistry* **56,** 2321–2329. doi:`10.1021/jf072964g` (2008).

193. Teixeira, R. R., Pinheiro, P. F., Barbosa, L. C. d. A., Carneiro, J. W. d. M. & Forlani, G. QSAR modeling of photosynthesis-inhibiting nostoclide derivatives. *Pest management science* **66,** 196–202. doi:`10.1002/ps.1855` (2010).

194. Mulo, P., Sakurai, I. & Aro, E.-M. Strategies for psbA gene expression in cyanobacteria, green algae and higher plants: from transcription to PSII repair. *Biochimica et biophysica acta* **1817,** 247–257. doi:`10.1016/j.bbabio.2011.04.011` (2012).

195. Mulo, P., Sicora, C. & Aro, E.-M. Cyanobacterial psbA gene family: optimization of oxygenic photosynthesis. *Cellular and Molecular Life Sciences* **66,** 3697–3710. doi:`10.1007/s00018-009-0103-6` (2009).

196. Ongley, S. E., Bian, X., Zhang, Y., Chau, R., Gerwick, W. H., *et al.* High-titer heterologous production in *E. coli* of lyngbyatoxin, a protein kinase C activator from an uncultured marine cyanobacterium. *ACS Chemical Biology* **8,** 1888–1893. doi:`10.1021/cb400189j` (2013).

197. Videau, P., Wells, K. N., Singh, A. J., Gerwick, W. H. & Philmus, B. Assessment of *Anabaena* sp. Strain PCC 7120 as a Heterologous Expression Host for Cyanobacterial Natural Products: Production of Lyngbyatoxin A. *ACS synthetic biology* **5,** 978–988. doi:`10.1021/acssynbio.6b00038` (2016).

198. Liu, T., Mazmouz, R., Ongley, S. E., Chau, R., Pickford, R., *et al.* Directing the Heterologous Production of Specific Cyanobacterial Toxin Variants. *ACS Chemical Biology* **12,** 2021–2029. doi:`10.1021/acschembio.7b00181` (2017).

199. Taton, A., Ecker, A., Diaz, B., Moss, N. A., Anderson, B., *et al.* Heterologous Expression of Cryptomaldamide in a Cyanobacterial Host. *ACS synthetic biology* **9,** 3364–3376. doi:`10.1021/acssynbio.0c00431` (2020).

200. Zhang, M. M., Wang, Y., Ang, E. L. & Zhao, H. Engineering microbial hosts for production of bacterial natural products. *Natural Product Reports* **33,** 963–987. doi:`10.1039/c6np00017g` (2016).

201. Neumüller, A. M., Konz, D. & Marahiel, M. A. The two-component regulatory system BacRS is associated with bacitracin 'self-resistance' of *Bacillus licheniformis* ATCC 10716. *European journal of biochemistry* **268,** 3180–3189. doi:`10.1046/j.1432-1327.2001.02203.x` (2001).

202. Copp, J. N., Roberts, A. A., Marahiel, M. A. & Neilan, B. A. Characterization of PPTNs, a Cyanobacterial Phosphopantetheinyl Transferase from *Nodularia spumigena* NSOR10. *Journal of Bacteriology* **189,** 3133–3139. doi:`10.1128/JB.01850-06` (2007).

203. Tu, J., Li, S., Chen, J., Song, Y., Fu, S., *et al.* Characterization and heterologous expression of the neoabyssomicin/abyssomicin biosynthetic gene cluster from *Streptomyces koyangensis* SCSIO 5802. *Microbial cell factories* **17,** 28. doi:`10.1186/s12934-018-0875-1` (2018).

204. Wang, P., Zhang, W., Zhan, J. & Tang, Y. Identification of OxyE as an Ancillary Oxygenase during Tetracycline Biosynthesis. *ChemBioChem* **10,** 1544–1550. doi:`10.1002/cbic.200900122` (2009).

205. Mareš, J., Hájek, J., Urajová, P., Kopecký, J. & Hrouzek, P. A Hybrid Non-Ribosomal Peptide/Polyketide Synthetase Containing Fatty-Acyl Ligase (FAAL) Synthesizes the beta-Amino Fatty Acid Lipopeptides Puwainaphycins in the Cyanobacterium *Cylindrospermum alatosporum*. *PloS one* **9,** e111904. doi:`10.1371/journal.pone.0111904` (2014).

206. Demmer, J. K., Pal Chowdhury, N., Selmer, T., Ermler, U. & Buckel, W. The semiquinone swing in the bifurcating electron transferring flavoprotein/butyryl-CoA dehydrogenase complex from *Clostridium difficile*. *Nature Communications* **8,** 1577. doi:`10.1038/s41467-017-01746-3` (2017).

207. Moss, N. A., Leão, T., Rankin, M. R., McCullough, T. M., Qu, P., *et al.* Ketoreductase Domain Dysfunction Expands Chemodiversity: Malyngamide Biosynthesis in the Cyanobacterium *Okeania hirsuta*. *ACS chemical biology* **13,** 3385–3395. doi:`10.1021/acschembio.8b00910` (2018).

208. Ramaswamy, A. V., Sorrels, C. M. & Gerwick, W. H. Cloning and Biochemical Characterization of the Hectochlorin Biosynthetic Gene Cluster from the Marine Cyanobacterium *Lyngbya majuscula*. *Journal of Natural Products* **70,** 1977–1986. doi:`10.1021/np0704250` (2007).

209. Chang, Z., Sitachitta, N., Rossi, J. V., Roberts, M. A., Flatt, P. M., *et al.* Biosynthetic Pathway and Gene Cluster Analysis of Curacin A, an Antitubulin Natural Product from the Tropical Marine Cyanobacterium *Lyngbya majuscula*. *Journal of Natural Products* **67,** 1356–1367. doi:`10 . 1021/np0499261` (2004).

210. Mirza, I. A., Yachnin, B. J., Wang, S., Grosse, S., Bergeron, H., *et al.* Crystal Structures of Cyclohexanone Monooxygenase Reveal Complex Domain Movements and a Sliding Cofactor. *Journal of the American Chemical Society* **131,** 8848–8854. doi:`10.1021/ja9010578` (2009).

211. Barnwal, R. P., van Voorhis, W. C. & Varani, G. NMR structure of an acyl-carrier protein from *Borrelia burgdorferi*. *Acta Crystallographica Section F: Structural Biology and Crystallization Communications* **67,** 1137–1140. doi:`10.1107/S1744309111004386` (2011).

212. Mo, S., Sydor, P. K., Corre, C., Alhamadsheh, M. M., Stanley, A. E., *et al.* Elucidation of the *Streptomyces coelicolor* Pathway to 2-Undecylpyrrole, a Key Intermediate in Undecylprodiginine and Streptorubin B Biosynthesis. *Chemistry & biology* **15,** 137–148. doi:`10 . 1016 / j . chembiol.2007.11.015` (2008).

213. Martinet, L., Naômé, A., Deflandre, B., Maciejewska, M., Tellatin, D., *et al.* A Single Biosynthetic Gene Cluster Is Responsible for the Production of Bagremycin Antibiotics and Ferroverdin Iron Chelators. *mBio* **10.** doi:`10.1128/mBio.01230-19` (2019).

214. Ostash, B., Saghatelian, A. & Walker, S. A Streamlined Metabolic Pathway for the Biosynthesis of Moenomycin A. *Chemistry & biology* **14,** 257–267. doi:`10.1016/j.chembiol.2007.01.008` (2007).

215. Balskus, E. P. & Walsh, C. T. An enzymatic cyclopentylbindole formation involved in scytonemin biosynthesis. *Journal of the American Chemical Society* **131,** 14648–14649. doi:`10.1021/ja906752u` (2009).

Publications and Conferences

Publications

Parts of this thesis are already published in:

Dehm, D., Krumbholz, J., Baunach, M., Wiebach, V., Hinrichs, K., et al. Unlocking the Spatial Control of Secondary Metabolism Uncovers Hidden Natural Product Diversity in *Nostoc punctiforme*. *ACS chemical biology* 14, 1271–1279 (2019).

Under review:

Krumbholz, J., Ishida, K., Baunach, M.,Teikari, J., Rose, M. M., et al. Deciphering chemical mediators regulating the specialized metabolism in the symbiotic cyanobacterium *Nostoc punctiforme*.

Conferences

March 2021

"Elucidation of a quorum sensing like regulatory network in *Nostoc punctiforme* PCC 73102" *oral presentation* at the Annual Conference of the Association for General and Applied Microbiology (VAAM 2021, online)

September 2019

"Elucidation of a quorum sensing like regulatory network in *Nostoc punctiforme* PCC 73102" *oral presentation* at the International VAAM Workshop 2019: Biology of Microorganisms Producing Natural Products, Jena, Germany

"Elucidation of a quorum sensing like regulatory network in *Nostoc punctiforme* PCC 73102" *oral presentation* at the Early Career Researcher Symposium on Cyanobacteria (Cyano2019), Tübingen, Germany

September 2018

"Ultra High Density Cultivation Enables Capturing of the Secondary Metabolite Diversities in *Nostoc punctiforme* PCC 73102" *poster presentation* at the 3rd Early Career Researcher Symposium on Cyanobacteria (Cyano2018), Freiburg, Germany

August 2018

"Ultra High Density Cultivation Enables Capturing of the Secondary Metabolite Diversities in *Nostoc punctiforme* PCC 73102" *poster presentation* at the International VAAM Workshop 2018: Biology of Microorganisms Producing Natural Products, Frankfurt, Germany

September 2017

"Characterization of a hybrid RiPP/NRPS Gene Cluster from *Nostoc punctiforme*" *poster presentation* at the International VAAM Workshop 2017: Biology of Microorganisms Producing Natural Products, Tübingen, Germany

Acknowledgements

Many people have contributed in their own way to bring this study to a successful conclusion and have supported me during this time.

First and foremost, I would like to thank Prof. Dr. Elke Dittmann, not only for providing me the opportunity to work on this interesting topic, but also for her scientific guidance and support, her numerous and creative ideas and her steadfast optimism.

Additionally, I want to thank Prof. Dr. Vera Meyer and apl. Prof. Dr. Evi Stegmann for taking over the review of this thesis.

I also want to express my appreciation to all the external cooperation partners, including Vincent Wiebach and the group of Prof. Dr. Severin Sasso. In this context, I want to especially thank Dr. Keishi Ishida for his endurance and persistence during the long and arduous process of structural elucidation.

Furthermore, I want to thank all my collaborating colleagues: Daniel Dehm for being a great help in learning how to handle *Nostoc*, Jonna Teikari for introducing me into the fine details of RNA-Sequencing analysis and Martin Baunach for being a great support regarding biosynthetical and chemical details.

I want to extend my thanks to all my colleagues, sharing with me the daily struggles in the lab. You provided a pleasant working atmosphere, made the life in the lab easier and funnier. You were a great support when the frustration began to set in as an experiment didn't worked out as it should. I want to thank all of you for the great time together!

I also want to thank my whole family, especially my parents, for the support they gave me throughout my studies.

Finally, my love and gratefulness goes to my boyfriend Robin. Thank you for your understanding and for your invaluable support and encouragement during the preparation of this thesis and beyond. I'm glad to have you by my side.

Eidesstattliche Erklärung

Gemäß §9 sowie §12 der Promotionsordnung der Mathematisch-Naturwissenschaftlichen Fakultät I der Universität Potsdam in der Fassung vom 18. September 2013, erkläre ich,

Julia KRUMBHOLZ,

dass ich die vorliegende Arbeit mit dem Titel "Identification of Chemical Mediators that Regulate the Specialized Metabolism in *Nostoc punctiforme*" selbständig angefertigt und ohne fremde Hilfe verfasst habe, keine außer den angegebenen Hilfsmitteln und Quellen dazu verwendet habe, die den verwendeten Werken wörtlich oder inhaltlich entnommenen Stellen als solche kenntlich gemacht habe und die Arbeit in der vorliegenden Fassung bisher an keiner anderen Hochschule eingereicht habe.

Ort, Datum:

_____

Unterschrift:

_____